The role of GFAP mutation in Alexander disease

by

Shu-Fang Wen

A thesis submitted at the University of Durham for the

degree of Doctor of Philosophy

School of Biological and Biomedical Sciences

University of Durham

DECLARATIONS

I declare that the experiments described in this thesis were carried out by myself in the School of Biological and Biomedical Sciences, University of Durham, under the supervision of Prof. Roy A. Quinlan. This thesis has been composed by myself and in a record of work that has not been submitted previously for a higher degree. All references have been consulted by myself unless stated otherwise.

Shu-Fang Wen

I certify that the work reported in this thesis has been performed by Shu-Fang Wen, who, during the period of study, has fulfilled the conditions of the Ordinance and Regulations governing the Degree of Doctor of Philosophy.

Roy A. Quinlan

Acknowledgements

Contents

List of Tables

List of Figures

Abbreviation

Aβ	amyloid β peptide
AIDS	acquired immune disease syndrome
α-MEM	α-minimum essential medium
ANOVA	analysis of variance
AP-1	activator protein-1
APC	adenomatous polyposis coli
APC	anaphase-promoting complex
ARE	antioxidant response element
ASK	apoptosis signal-regulating kinase
ASPK	stress-activated protein kinase
ATc	anhydrotetracycline
ATF	activating transcription factor
ATP	adenosine triphosphate
AxD	Alexander disease
BCA	bicinchonic acid assay
BFGF	basic fibroblast growth factor
bfsp	beaded filament structural protein
Bip	immunoglobulin heavy chain-binding protein
BMK1	big-mitogen activated kinase 1
BSA	bovine serum albumin
CBB	Coomassie Brilliant Blue
cdc	cyclin D1-dependent kinase
CFTR	cystic fibrosis transmembrane conductance regulator
CJD	Creutzfeld-Jakob disease
CKs	cytokeratins
CMV	cytomegalovirus
CNS	central nervous system
Cox-2	Cyclooxygenase-2
CP115	cytoskeletal protein 115
CP49	cytoskeletal protein 49

cPLA2	cytosolic phospholipase A2
CREB	camp response element-binding protein
CT	computed tomography
DCC	deleted in colorectal cancer
DAPI	4,6-diamidino-2-phenylindole
DBT	delayed brain tumor
DEDD	the death effector domain containing DNA binding domain
DEPC	diethyl pyrocarbonate
DISC	death-inducing signalling complex
DMEM	Dulbecco's modified eagle's medium
Dox	doxycycline
DTT	dithiothreitol
DUBs	deubiquitinating enzymes
E1	ubiquitin-activating enzyme
E2s	ubiquitin-conjugating enzymes
E3s	ubiquitin-protein ligases
EBS	epidermolysis bullosa simplex
ECL	enhanced chemiluminescence reagent
E. coli	Escherichia coli
EDTA	ethylene diamine tetra-acidic acid
EGF	epidermal growth factor
EGTA	ethylene glycol tetra-acetic acid
eIF-4e	eukaryotic initiation factor-4e
ER	endoplasmic reticulum
ERK	extracellular-signal-regulated protein kinase
FADD	Fas receptor-associated death domain protein
FCS	fetal calf serum
FRAP	fluorescence recovery after photobleaching
G418	geneticin
GAPDH	glyceraldehyde 3-phosphate dehydrogenase
GFAP	glial fibrillary acidic protein
GPS	L-glutamine, penicillin, streptomycin

GSS	Gerstmann-Straussler syndrome
H2B	histone 2B
HBPl	high mobility group-box protein l
HEB	harsher extraction buffer
HECT	homologous to the E6-AP C-terminus
HRP	horseradish peroxidase
HSP	heat shock protein
HSV	herpes simplex virus
IAPs	inhibitor of apoptosis proteins
IFAPs	intermediate filament associated proteins
IFs	intermediate filaments
IGFl	insulin-like grow factor l
ILM	inner limiting membrane
IPTG	isopropyl-l-thio-β-D-galactopyranoside
IREl	inosito-requiring enzyme l
JASPl	JNK/SAPK activating protein l
JIP	JNK interacting protein
JNK	c-Jun N-terminal kinase
Keapl	Kelch-like ECH-associated protein l
KSR	kinase suppressor of ras
LB	Luria Bertain
LPS	lipopolysaccharide
LSP-l	lymphocyte-specific protein l
MAPK	mitogen-activated protein kinase
MAPKK	MAP kinase kinase
MAP2K	
MEK	
MKK	
MAPKKK	MAP kinase kinase kinases
MAP3Ks	
MEKK	
MKKK	

MAPKKKK	MAP kinase kinase kinase kinases
MAP4Ks	
MKKKK	
MCS	multiple cloning site
MEB	mild extraction buffer
MEF2C	myocyte enhance factor 2C
α-MEM	α-minimum essential medium
MFs	microfilaments
MG-132	carbobenzoxy-L-leucyl-L-leucyl-L-leucinal
MKPs	MAPK phosphatases
MKs	MAPK-activated protein kinases
MLKs	mix-lineage kinases
MRI	magnetic resonance imaging
MSK1	mitogen- and stress-activated protein kinase-1
MTs	microtubules
MTS	3-(4,5-dimethyl-thiazol-2yl)-5-(3-carboxymethoxyphenyp)-2-(4-sulfophenyl)-2H-tetrazolium
NA	numerical aperture
NF	neurofilament
NFAT4	nuclear factor of activated T cells
NF-H	neurofilament-heavy chain
NFH-GFP	neurofilament heavy chain-green fluorescence protein
NF-κB	nuclear factor kappa B
NF-L	neurofilament-light chain
NF-M	neurofilament-medium chain
NGF	nerve growth factor
NHE-1	Na+/H+ exchanger isoform-1
NP-40	Nonidet P-40
Nrf2	nuclear factor erythroid-2 related factor 2
OD	optical density
PBS	phosphate buffered saline
PDGF	platelet-derived growth factor

PERK	PKR-like ER kinase
p-JNK	phosphorylated JNK
PminCMV	human cytomegalovirus immediate early gene IE1 promoter
PMSF	phenylmethylsulfonyl fluoride
PNS	peripheral nervous system
Pol II	RNA polymerase II
polyQ diseases	polyglutamine diseases
p-p38	phosphorylated p38
PRAK	p38 regulated/activated kinase
Rb	retinoblastoma
RFs	Rosenthal fibres
RING	really interesting new gene
RIPA	radioimmunoprecitation assay
ROI	reactive oxygen intermediates
ROS	reactive oxygen species
RSK	90 Kda ribosomal S6 kinase
rtetR	reverse tetracycline repressor
RT-PCR	reverse transcriptase polymerase chain reaction
RVI	regulatory volume increase
RVD	regulatory volume decrease
tTA	reverse tetracycline-controlled transactivator
SAP1	serum response factor accessory protein 1
SAPKs	stress activated protein kinases
SCF-Box	Skp-Cullin-F-Box
SD	standard deviation
SDS-PAGE	sodium dodecyl sulphate-polyacrylamide gel electrophoresis
sHSP	small heat shock protein
SOS	son of sevenless
SRF	serum response factor
TBS	Tris-buffered saline
TCF	Ternary Complex Factor
Tet	tetracyclinet

*tet*R	tetracycline repressor
*tet*O	tetracycline operator
TEN buffer	Tris-HCl, EDTA and NaCl buffer
TEY	Thr-Glu-Tyr motif
Tn10	transposon 10
TNF-α	tumor necrosis factor-α
TRADD	TNF receptor-type 1-associated death domain protein
TRE	Tet response element
tTA	tetracycline-controlled transactivator
TTBS	TBS containing 0.2% (v/v) Tween 20
TTP	tristetraprolin
TXY	Thr-Xaa-Tyr motif
Ub	ubiquitin
UCH	ubiquitin carboxy terminal hydrolase
ULF	unit-length filament
UPR	unfolded protein response
UPS	ubiquitin-proteasome system
VHL	von Hippel-Lindau protein
VP16	virion protein 16
XBP1	X-box binding protein 1
Z-VAD-FMK	benzyloxycarbonyl-Val-Ala-Asp-Fluoromethyloketone

Abstract

Alexaneder disease (AxD) is a primary genetic disorder of astrocyte caused by mutations in the type III intermediate filament (IF) glial fibrillary acidic protein (GFAP). The pathological hallmark of this disease is the presence of Rosenthal fibres (RF), ubiquitinated protein aggregates with GFAP being the primary constituent. On the basis of age at onset, the disease has been divided into three subtypes: infantile, juvenile and adult. Whilst one of the common mutations R416W is reported in AxD with a wide range in disease severity and age of onset, the mechanisms by which this mutation leads to AxD remain unknown. To investigate the role of mutated protein in the disease process, I have developed a cell model system in which the expression of GFAP can be regulated by doxycycline. Expression of R416W GFAP leads to aggregate formation, which increases small heat shock protein (sHSP) expression, activates stress-activated protein kinase (SAPK) pathways and partially impairs proteosome function. This is accompanied by the sequestration of sHSPs and activated SAPK into GFAP-containing aggregates, which make cells more susceptible to stress. However, R416W mutation was found to not always disrupt the endogenous IFs, but to incorporate into GFAP networks when expressed at low levels. The potential functional impact of incorporating low level of the disease-causing GFAP mutant into the pre-exiting GFAP networks is that cells respond poorly to stressful conditions. These data provide direct evidence to suggest that astrocyte dysfunction play a key role in the development of AxD and stress is likely to have the most influence on the presence and progression of the disease.

Chapter 1

Introduction

Intermediate filaments are the major cytoskeletal component comprising a family of highly heterogeneous proteins whose main function is to provide structure support in the cytoplasm and nucleus of higher eukaryotes. This chapter documents the general structural features and functional aspects of intermediate filaments. In particular, a number of novel functions have recently been discovered for intermediate filament proteins. Most of the functions are related to the capacity of intermediate filaments to act as signalling scaffolds that translate changes of environmental conditions into alterations of gene expression at the cellular level. Intermediate filaments also provide a biochemically versatile interface that can be tailored by individual cells to serve as a dynamic platform for the binding of associated proteins, such as protein chaperones. Some of these functions are altered by genetic mutations that cause cell dysfunction and account for a variety of genetic diseases in humans. For instance, Alexander disease, a primary genetic disorder of astrocyte, is caused by mutations in a type III intermediate filament protein, glial fibrillary acidic protein (GFAP). Whilst the genetic basis for Alexander disease has been firmly established, little is known about the mechanisms resulting in its devastating consequences. Here I review recent progress on elucidating the role of GFAP mutations in Alexander disease, particularly focusing on observations made by the cell and animal model systems. These literatures cover: 1) structure and functions of intermediate filaments involving in mechanical, metabolic, regulatory and cell signalling processes, and a wide range of diseases; 2) the role of GFAP in the cell biology of astrocytes and the function of astrocytes in the central nervous system; 3) GFAP mutation and its involvement in astrocyte stress response; 4) details of Alexander disease and possible mechanisms leading to its pathogenesis.

1.1 The cytoskeleton

The cytoskeleton is a complex network of interconnected filaments that extends throughout the cytosol, from the nucleus to the inner surface of the plasma membrane. This elaborate internal framework forms highly structured yet very dynamic matrix that not only gives cells their distinctive shape and high level of internal organisation but also plays important roles in cell movement and division. In addition, the cytoskeleton serves as a framework for anchoring and transport membrane-bound organelles within the cell. The three major structural elements of the cytoskeleton are microtubules, microfilaments and intermediate filaments, each of which has a characteristic size, structure and intracellular distribution. Each structural element is formed by the polymerisation of a different kind of protein subunit. The main structural features of the three major components of the cytoskeleton are summarised in Table 1.1.

Table 1.1 An overview of the cytoskeleton

	Microtubules	Intermediate filaments	Microfilaments
Structural feature	Hollow tubes with polar structure	Biopolymers of fibrous proteins	Thin and flexible filaments
Diameter	25 nm	10-12 nm	6-8 nm
Components	α-tubulin β-tubulin	A superfamily of at least 70 intermediate filament proteins	α-actin β-actin γ-actin
Functions	Maintenance of cell shape, mobility, cell division, and organelle movement	Mechanical support, formation of nuclear lamina and scaffolding, stabilising muscle fibres	Cell division and locomotion, cell shape maintenance, and muscle contraction

1.2 Intermediate filaments

1.2.1 General features of intermediate filaments

Intermediate filaments (IFs) derive their name from the observation by electron microscopy (Ishikawa et al., 1968) that their apparent 10-nm diameter is intermediate in size between microtubules (~25 nm) and microfilaments (~6 nm). Whilst the tubulins and actin are highly conserved globular proteins with nucleotide-binding and hydrolyzing activity, IF proteins are fibrous proteins with no known enzymatic activity. In further contrast to microtubules and microfilaments, IFs are the most stable and least soluble constituents of the cytoskeleton (Osborn and Weber, 1989), which are resistant against extraction with buffers containing high concentrations of salt and non-ionic detergents (Zackroff and Goldman, 1979). This feature enables their isolation and characterisation from various cells and tissues.

1.2.2 The superfamily of IF proteins

One remarkable feature of IF proteins is their diversity both in terms of number and expression pattern. In the human genome, at least 70 functional genes encode IF proteins (Hesse et al., 2001) making them one of the largest gene families in humans. IFs genes can be classified according to various criteria (Herrmann and Aebi, 2000), as exemplified in Table 1.2. Based on the primary gene structure and sequence homology, IF genes are grouped into five distinct types.

1.2.2.1 Type I and Type II IFs

Keratins are IF-forming proteins that provide mechanical support and fulfil a variety of additional functions in epithelial cells. According to new nomenclature for keratin by Schweizer et al. (2006), type I keratins consist of K9-28 epithelial keratin, K31-40 hair keratins and K41-70 nonhuman epithelial and hair keratins. Type II keratins include K1-8 and

3

K71-80 epithelial keratins, K81-86 hair keratins and K87-120 nonhuman epithelial and hair keratins. The members of both types of keratins are unusual in that they assemble *in vitro* as obligatory heteropolymers in a 1:1 ratio of any combination of at least one type I and one type II keratin (Hofmann and Franke, 1997; Steinert et al., 1976).

Table 1.2 The IF proteins multigene family

Member Name	No. of Gene(s)	Sequence Type	Assembly Group	Protein Size (kDa)	Cell/Tissue Distribution
Keratin	60	I	A	40-64	Epithelial
Keratin	58	II	A	52-68	cells
Vimentin	1	III	B	55	Heterogeneous
Dsemin	1	III	B	53	Muscles
GFAP	1	III	B	50	Astrocyte/glia
Peripherin	1	III	B	52	PNS* neuron
NF-H	1	IV	B	110	CNS[#]/PNS neuron
NF-M	1	IV	B	102	CNS/PNS neuron
NF-L	1	IV	B	62	CNS/PNS neuron
α-internexin	1	IV	B	66	CNS neuron
Nestin	1	?	B	240	Heterogeneous
Synemin	1	?	B	182	Muscles
Paranemin	1	?	B	178	Muscles
Lamin A/C	1	V	C	72/62	All cell types
Lamin β1	1	V	C	65	All cell types
Lamin β2	1	V	C	78	All cell types
BFSP/CP49/Phakanin	1	?	Orphan	46	Lens
BFSP2/CP115/Filensin	1	?	Orphan	83	Lens

* PNS, peripheral nervous system.

[#] CNS, central nervous system.

1.2.2.2 Type III IFs

Type III IF proteins include vimentin, desmin, GFAP, and peripherin. Vimentin is the most widely expressed IF protein in a number of cells of endothelial, fibroblastic and hematopoietic origin (Lane et al., 1983; Virtanen et al., 1981), as well as in the eye lens (Bloemendal et al., 1981). Desmin represents the major IF protein in all muscle tissues. It is one of the earliest marker protein specifically expressed in skeletal muscle where it becomes detectable in somites and myoblasts (Kaufman and Foster, 1988). GFAP is the main protein constituent of glial filaments in mature astrocytes and glial cells associated with central nervous system (CNS) (Eng, 1982). Peripherin is predominantly expressed in peripheral neurons (Portier et al., 1983) or neurons whose axon lies at least partially outside the CNS (Escurat et al., 1990). Unlike the keratins, type III IF proteins can form both homopolymers (Steinert et al., 1981) and heteropolymers with other type III or type IV IF proteins (Eliasson et al., 1999; Monteiro and Cleveland, 1989).

1.2.2.3 Type IV IFs

Type IV IF proteins comprise neurofilament (NF) triplet proteins and α-internexin. The core of mature axons of both central and peripheral nervous system (PNS) is filled with NFs. This heteropolymer is composed of three subunits, NF-H (heavy chain), NF-M (medium chain) and NF-L (light chain), which differ greatly in molecular weight (Lee and Cleveland, 1996). An additional type IV IF protein α-internexin was first isolated from optic nerve and spinal cord, and was found particularly abundant in the developing nervous system (Pachter and Liem, 1985).

1.2.2.4 Type V IFs

Type V IF proteins are nuclear lamins that are the main structural constituents of nuclear lamina, a filamentous scaffold that supports inner nuclear membrane (Aebi et al., 1986; Stuurman et al., 1998), and are also present in the nucleoplasm (Goldman et al., 2002). Lamins are divided into A and B types on the basis of their expression patterns and protein structure. A-type lamins are derived through alternative splicing of a single gene *LMNA*, and are expressed only in differentiated cells and more complex organisms. B-type lamins are encoded by two separate genes (*LMNB1* and *LMNB2*), and are present in all metazoan cells. Lamins differ from other IF proteins by an insertion of 42 amino acids within 1B subdomain (Fig. 1.1). This feature is also found in cytoplasmic IF proteins of invertebrates, whereby it is very likely that lamins were the first IF protein to occur in evolution.

1.2.2.5 Type VI IFs

Several recently identified proteins are clearly members of IF protein superfamily based on the gene structure and sequence identity, but they do not fit easily into either of the established types of IF proteins. To reflect this current indecision, they are tentatively grouped as type VI IFs (Table 1.2). For instance, nestin is a novel IF protein expressed in neuroepithelial stem cells of mammalian CNS (Lendahl et al., 1990). It is also expressed early in cardiac and skeletal muscles, but is only retained in adult skeletal muscle at the neuromuscular and myotendinous junctions (Carlsson et al., 1999). *In vitro* assembly studies suggested that whilst nestin is unable to self-assemble into typical 10-nm IFs, it could form heteropolymeric filaments when co-assembled with purified vimentin or α-internexin (Steinert et al., 1999). Two additional high-molecular-weight IF proteins, synemin

6
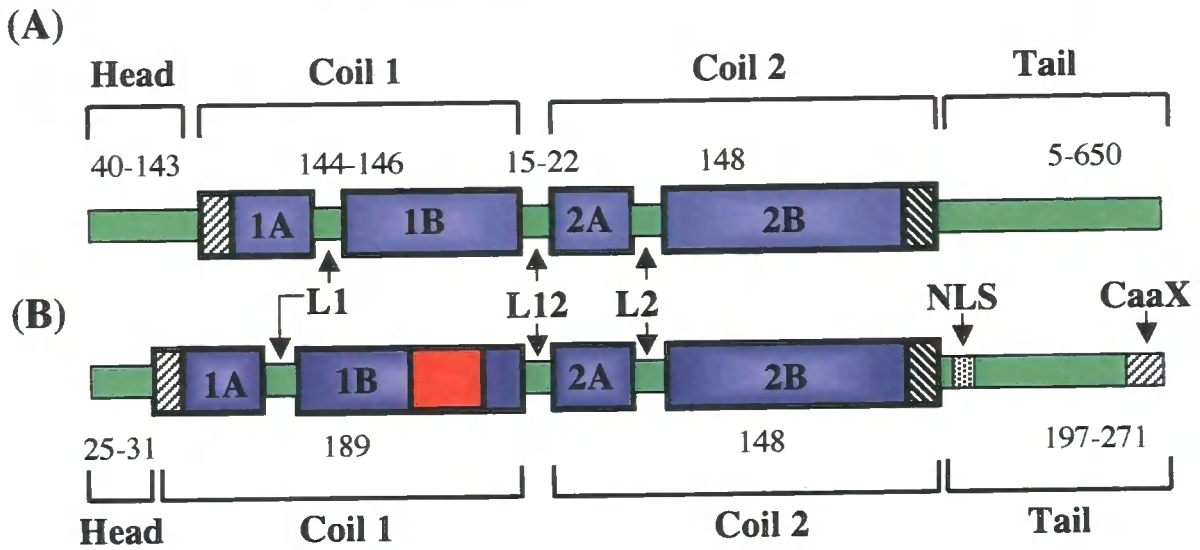
Figure 1.1 Schematic representation of the domain structure common to cytoplasmic (A) and nuclear (B) IF proteins. A central rod-forming domain, consisting of α-helical subdomains coil 1 and coil 2, is flanked by non-α-helical amino-terminal head and carboxy-terminal 'tail' domains. Helical regions are boxed and are connected by non-helical 'linker' (L) regions. The numbers of amino acids found with the individual domains is indicated. The hatched area in the coil 1 of (B) represents the 42-amino acid insertion found in general in nuclear IF proteins, but also in cytoplasmic IFs of lower vertebrates. Note that the heptad substructure is maintained in L1 of nuclear IF proteins, suggesting that lamins have a continuous helix 1 segment. The darkened regions at both ends of coil 1A and coil 2B indicate the evolutionarily highly conserved regions. The light grey marking at the end of the tail domain of nuclear IF proteins (B) represents the so-called 'CaaX' box, in which post-translational modification occurs. NLS, nuclear location sequence.

(Bilak et al., 1998; Granger and Lazarides, 1980) (also called desmuslin (Mizuno et al., 2001)) and paranemin (Hemken et al., 1997; Price and Lazarides, 1983), are coexpressed in muscle and form heteropolymers with desmin (Schweitzer et al., 2001). A recently discovered IF protein syncoilin is also present in skeletal muscle (Newey et al., 2001), where it colocalises with desmin but does not co-assemble with desmin to form heteropolymers (Poon et al., 2002). Furthermore, two other IF proteins found exclusively in the eye lens comprise a unique cytoskeletal structure called beaded filaments (Maisel and Perry, 1972). The two structural components initially isolated from urea-soluble extract of chicken lens were termed cytoskeletal protein 49 (CP49) and cytoskeletal protein 95 (CP95) according to the molecular weight by SDS-PAGE (Ireland and Maisel, 1983; Ireland and Maisel, 1984). CP95 was later renamed filensin (Merdes et al., 1991) to avoid confusion due to different apparent molecular weight in the different species. These two lens-specific IF proteins filensin and CP49 have acquired a number of unique structural features and distinct assembly properties (Perng and Quinlan, 2005), which mark them out from the other cytoplasmic IF proteins.

1.2.3 Structure features of cytoplasmic IF proteins

Although IF proteins differ remarkably in size and amino acid compositions, they all share a common structural organisation, a schematic version of which is shown in Fig. 1.1. A centrally located α-helical rod domain of about 310 amino acids that is flanked by non-α-helical domains of different size and sequence (Fuchs and Weber, 1994; Geisler and Weber, 1982). Variations in these so-called "head" and "tail" domains contribute significantly to the marked heterogeneity of members of this protein family. The rod domain features a heptad repeat pattern, which mediates coiled-coil dimer formation and represents the major driving force for IF self-assembly (Strelkov et al., 2003). The heptad periodicity with hydrophobic residues usually being in the first and fourth of every seven residues is interrupted by short

8
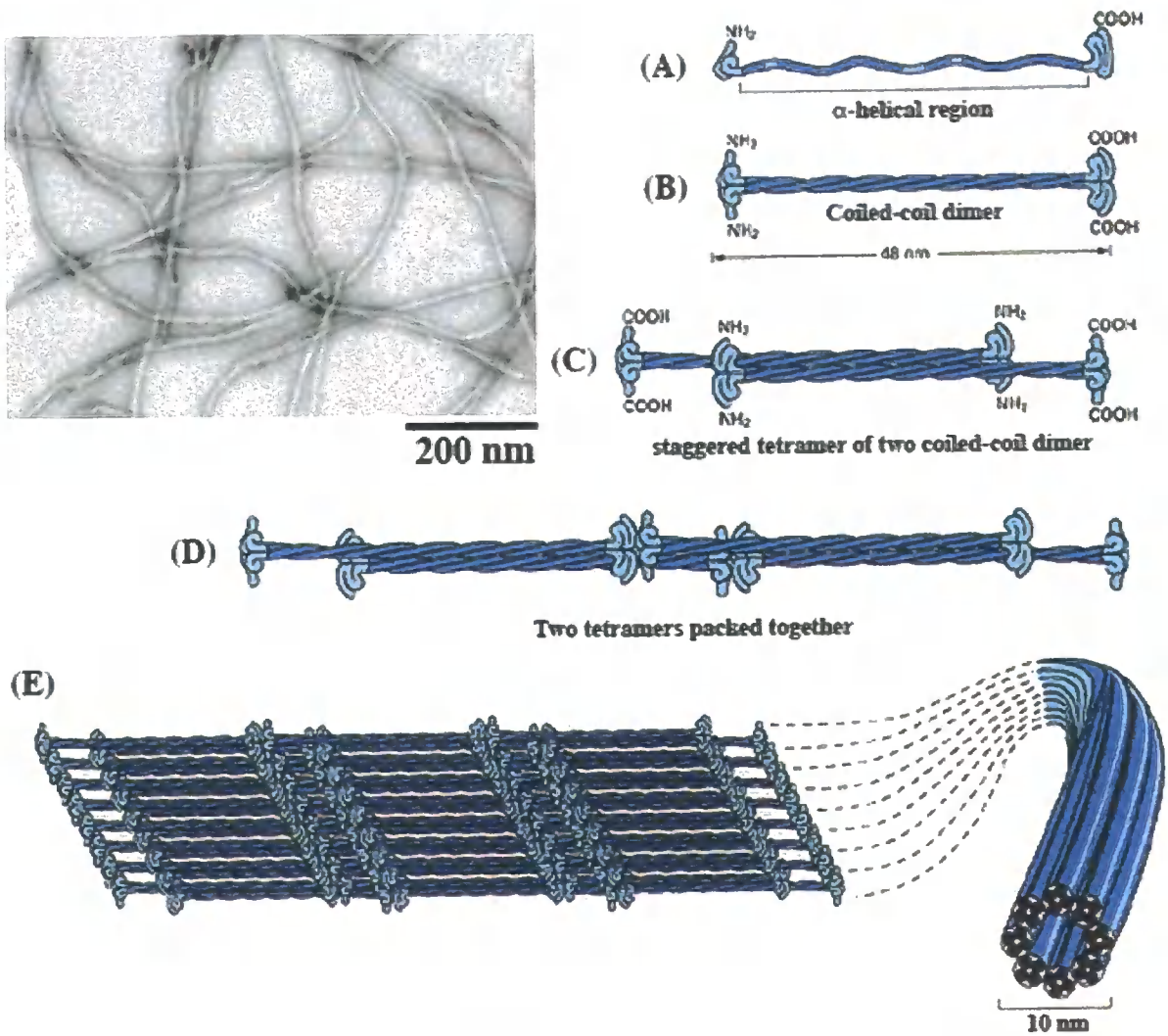
Figure 1.2. A textbook view of the IF assembly. Two monomers (A) paired together to form dimers (B) in which the conserved central rod domains are aligned in parallel to form a coiled–coil. Two dimers then lined up side by side to form an anti-parallel tetramer (C). Within each tetramer the dimers are staggered with respect to one another, thereby allowing it to associate with another tetramer, as shown in (D). In the final step of assembly, tetramers are packed together to form a typical 10-nm filaments (E). An electron micrograph of the final filament is shown upper left (courtesy of Dr. Ming-Der Perng). This figure is modified from Figure 16.14 in the Molecular Biology of the Cell 3rd edition, 1994.

linkers L1, L12 and L2, resulting in four consecutive segments 1A, 1B, 2A and 2B. With the exception of nuclear lamins, filensin and invertebrate IF proteins, the size of the rod domains and the position of the linker regions are well conserved throughout all cytoplasmic IF proteins (Fuchs and Weber, 1994; Parry and Steinert, 1999). Another highly conserved feature of the rod domain is a discontinuity in the heptad repeat pattern within the 2B subdomain, a so-called "stutter". The stutter is equivalent to an insertion of extra four amino acids into a continuous heptad repeat, which is located at exactly the same position despite a considerable sequence variation in this region (Weber and Geisler, 1985).

1.2.4 *In vitro* assembly of IFs

IF proteins are remarkable in that they can self-assemble into 10-nm filaments in a complex and hierarchical fashion in the absence of accessory proteins or cofactors. Owing to the presence of heptad repeats within the rod domain, IF proteins readily form stable coiled-coil dimer (Burkhard et al., 2001), which is the molecular building block of IFs. Whilst most IF proteins assemble into homodimers, keratins are obligatory heterodimers formed by one acidic chain and one basic/neutral chain (Hatzfeld and Franke, 1985). Despite the heteropolymeric nature of keratin dimers, they do not dimerise with other IF proteins. In addition, certain IF proteins, even those belonging to different types can form heterodimers with each other. Accordingly, IF proteins can be divided into three assembly groups (Table 1.2). The first assembly group (Group A) consists of keratins and the most other cytoplasmic IF proteins are assigned to the second group (Group B). The third group (Group C) includes nuclear lamins. IFs from members of the three assembly groups do not copolymerise with each other but can co-exist as distinct filament systems in one cell type.

IF assembly begins with a pair of monomers (Fig. 1.2A) associated in parallel into a coiled-coil dimer (Fig. 1.2B). In the next stage of assembly, two dimers associate laterally in

an anti-parallel fashion to form a tetramer (Fig. 1.2C). Soluble tetramers are found in small amounts in cells (Soellner et al., 1985), indicating that they are fundamental subunits from which IFs are assembled. The anti-parallel arrangement of dimers implies that IF formed from tetramer is a nonpolarised structure (Herrmann and Aebi, 1998). This feature distinguishes IFs from microtubules and actin microfilaments, which are polarized and whose functions depend on this polarity (Table 1.1). Microtubules and microfilaments polymerize non-covalently from a slow-growing end (minus end) and a fast-growing end (plus end). At steady state, the shrinkage at the minus end and the growth at the plus end give rise to an effect known as treadmilling (Akhmanova and Steinmetz, 2008; Carballido-López, 2006). IF assembly beyond tetramer is less well characterised, because IF proteins have been difficult to crystallise owing to their notorious insolubility, lack of specific assembly inhibitors and polymerisation-prone character (Strelkov et al., 2003). Current models proposed that *in vitro* assembly of cytoplasmic IF proteins takes place in a three-step process (Fig.1.3I), in which first tetramers rapidly associate laterally to form the so-called "unit-length filament" (ULF). These ULFs are approximately 16 nm in diameter and 60 nm in length (Herrmann et al., 1999; Herrmann et al., 2003). Once formed, the ULFs start to anneal into loosely packed filaments that are 200-300 nm long (Fig. 1.3II). On further elongation, these filaments undergo intrafilamentous subunit reorganisation leading to a radial compaction (Fig. 1.3III). The filament diameter decreases to 11 nm in the case of human vimentin and 14 nm in the case of human desmin, without reducing their mass-per-length. With this general scheme, the assembly of vimentin, desmin, keratin 8/18 and NF-L have been described previously (Herrmann et al., 1999; Herrmann et al., 2002).
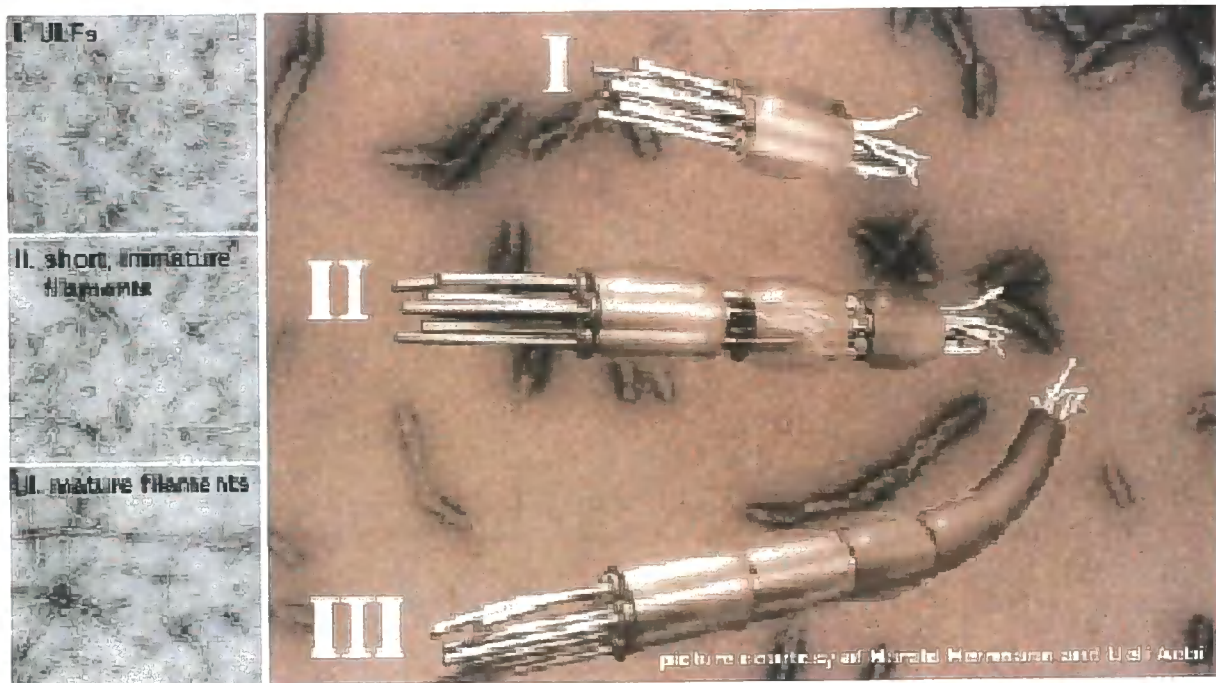
Figure 1.3. Current model of IF assembly *in vitro*. Negatively stained electron micrographs show vimentin assembled in vitro through three-step process. I. Unit-length filaments (ULFs). II. Loosely packed short immature filaments. III. Longer, compact mature filaments. A model shows that ULFs anneal end-to-end to form loosely packed, short IF. These immature filaments undergo internal compaction to produce mature IFs. Images courtesy of Drs. H. Herrmann (German Cancer Research Centre, Heidelberg) and U. Aebi (Maurice E. Muller Institute for structural biology, Biocentrun Basel, Switzerland). Reproduced from (Herrmann, H. and Aebi, U., Cur. Opin. Struct. Biol. 8, 177-185, 1998) with permission.

1.2.5 The role of end domains on IF assembly

Previous studies on the specific inter-molecular interactions involved in IF assembly are based upon examining the effect of certain truncated or mutated IF protein. On one hand, such studies have revealed that two highly conserved segments in the rod domain, the helix-initiation segment located at the beginning of 1A subdomain and helix-termination segment situated at the very end of the 2B subdomain, are critical for the correct IF assembly (Herrmann and Aebi, 1998). On the other hand, whilst *in vitro* and *in vivo* studies have often led to contradictory conclusions, there seems to be a general agreement that the highly conserved rod ends play essential roles in IF assembly. In particular, the head domain seems to control both end-to-end and lateral associations (Hatzfeld et al., 1992; Herrmann et al., 1996; Raats et al., 1990), whereas the tail domain plays an important role both in controlling filament width *in vitro* (Herrmann et al., 1996; Kaufmann et al., 1985; Kouklis et al., 1991) and establishing proper IF networks *in vivo* (Chen and Liem, 1994; Eckelt et al., 1992; Makarova et al., 1994; McCormick et al., 1993). Furthermore, given their exposure at the filament surface, the end domains could mediate coordinated interactions of IFs with other cytoskeletal components and a host of cellular proteins (Green et al., 2005), as well as serve as substrates for post-translational modifications (Izawa and Inagaki, 2006; Omary et al., 2006) that regulate IF structure, organisation, and function.

1.2.6 Organisation of IFs in living cells

The assembly of IF in cells was first investigated by microinjecion experiments (Kreis et al., 1983). When keratin mRNA was injected into cultured cells, the first structure observed by immunfluorescence microscopy was dots that with time elongated into short fibres and eventually giving rise to extended filaments. Such a scenario is entirely compatible with recent studies by live cell imaging using GFP-tagged vimentin (Ho et al., 1998; Prahlad et al.,

13

1998; Yoon et al., 1998). These studies have shown vimentin exists in several assembly intermediates, including non-filamentous particles and short filaments that are known as "squiggles". Individual particles are frequently converted into squiggles, which might be precursors in the assembly of long IFs. The exact structures of these IF precursors are currently unknown, but they are assembled in a highly regulated process to form typical IF networks. Interestingly, keratin filaments appear to be formed following a similar multistep process (Windoffer et al., 2004; Yoon et al., 2001).

1.2.7 IF dynamics and motile properties

Studies of variable types of live cells have revealed that IFs and their precursors are remarkably dynamic and exhibit highly motile properties (Helfand et al., 2003; Liovic et al., 2003; Windoffer et al., 2004). Initial studies using fluorophore-tagged IF proteins showed that when microinjected into cells, they form discrete particles that are subsequently incorporated into the endogenous IF networks in a dose-dependent manner (Miller et al., 1993; Miller et al., 1991). These observations provide direct evidence that a dynamic equilibrium exists between soluble subunit and polymerised filaments. Subsequent studies using fluorescence recovery after photobleaching (FRAP) following microinjection of fluorophore-tagged vimentin (Vikstrom et al., 1992) or in cells expressing GFP-tagged vimentin (Yoon et al., 1998) have confirmed that IF subunit exchange is apolar and exists along the entire length of polymerised IFs. Whilst the mechanisms responsible for the steady-state dynamics remain to be defined, variable dynamics between soluble subunits and polymerised filaments may allow cells to continuously rearrange IF structure in a gradual manner, which is important for many cellular processes during cell division and differentiation.

Recent time-lapse studies of live cells expressing GFP-tagged IF proteins clearly show that many types of IF engage in a complex array of movements that are closely associated with

14

assembly, disassembly and subcellular organisations (Martys et al., 1999; Yoon et al., 1998). However, not all IFs move in the same way. For instance, the motile properties of keratin tonofibrils and squiggles are dramatically different from those of vimentin fibrils and squiggles within the same cytoplasmic regions (Liovic et al., 2003; Yoon et al., 2001). The difference in motility may be related to their interactions with IF-associated proteins or molecular motors, such as conventional kinesin, cytoplasmic dynein and myosin. These associations are not only responsible for many of the motile properties of IFs, but also appear to be involved in regulating the subunit exchange that is critical for the maintenance of IF structure and organisation within cells. When considered together, the evidence supporting the dynamic and motile properties of IFs has overturned the long-standing view that IFs simply form static space-filling cytoskeletal networks that serve nothing but structural support.

1.2.8 Regulation of IF dynamics and functions

IF dynamics is reflected not only by their steady-state equilibrium between a soluble and an insoluble pool but also by their reorganisation in response to a spectrum of stimuli including mitosis, apoptosis and other cellular stresses. These dynamic properties are regulated by post-translational modifications particularly on the non-helical head and tail domains of IF proteins.

Phosphorylation is the best-studied IF post-translational modification given its prevalence and functional implications (Ku et al., 1996a). IF phosphorylation is essential for the regulation of IF dynamics by modulating IF solubility, conformation, turnover and filament organisation (for recent review see (Omary et al., 2006)). Moreover, IF-phosphorylation provides a key point for the regulation of other IF post-translational modifications, such as

ubiquitination (e.g. (Ku and Omary, 2000)). These phosphorylation-regulated properties determine generalised and unique IF functions that reflect their tissue-specific expression.

Identification of phosphorylation sites on IF proteins is, therefore, of great importance in order to understand the mechanism by which cellular IF reorganisation is regulated. A variety of tools have been used to characterize *in vivo* IF phosphorylation sites. In particular, generation of phosphorylation site-specific antibodies allows visualisation of spatiotemporal distribution of intracellular IF phosphorylation sites (Izawa and Inagaki, 2006). These antibodies can also monitor localised kinase activity responsible for a specific IF phosphorylation. IF phosphorylation sites are clustered in the head and tail domains and primarily at serine and threonine residues, although tyrosine phosphorylation can also be detected in some IF proteins (Ku et al., 1996a). Whilst tyrosine phosphorylation occurs on IF proteins, such as vimentin (Valgeirsdóttir et al., 1998; Meriane et al., 2000), peripherin (Angelastro et al., 1998), and keratins (Feng et al., 1999), it appears to be less common compared to serine/threonine phosphorylation.

IF phosphorylation is regulated by many *in vivo* kinases (see Appendix 1), most of which dramatically alter the network configuration and induce filament disruption. For many of the identified *in vivo* kinases, direct or indirect interaction of the kinase with its IF substrate has also been demonstrated. However, it is important to keep in mind that although IF can be phosphorylated by purified kinases, the *in vitro* phosphorylation sites may not necessarily reflect *in vivo* situations.

Cellular processes that are controlled by phosphorylation require not only kinases, but also phosphatases. The serine/threonine phosphatases and tyrosine phosphatases (Mumby and Walter, 1993) comprise two major groups of protein phosphatases in eukaryotes. The importance of protein phosphatases in IF phosphorylation is highlighted by the dramatic hyperphosphorylation of IFs upon phosphatase inhibition as demonstrated for vimentin

(Eriksson et al., 1992), keratins (Toivola et al., 1997), NFs (Sacher et al., 1992), and lamins (Almazan et al., 1993). Furthermore, the inhibition of tyrosine phosphatase by pervanate and orthovanadate resulting in hyperphosphorylation of keratins implies the significance of tyrosine phosphatases on the regulation of phosphate turnover on IF proteins (Feng et al., 1999). Finally, recent studies have provided evidence that IFs may potentially serve as a "phosphate sponge" that absorbs excessive kinase activity (Ku and Omary, 2006). Upon apoptotic stimulation, the hepatocytes extracted from mice with a human disease associated keratin 8 mutation (G61C) or its phosphorylation site (S73) have shown increased nonkeratin proapoptotic substrates phosphorylated by stress-activated kinases, compared with wild-type hepatocytes. Hence, keratin 8 with conserved S73 containing phosphoepitope can protect tissue from injury by acting as a phosphate sponge for stress-activated kinases. Other than keratin, the tail domain of NF-H, can also provide such a molecular sink for preventing untoward phosphorylation of other kinase substrates in neurons (Nguyen et al., 2001), indicating that this type of phosphate buffering could be a general phenomenon for IFs.

1.2.9 Ubiquitination of IFs

1.2.9.1 Ubiquitin-proteasome system

Ubiquitination is another type of post-translational modification that is essential for selective degradation of many short-lived proteins in eukaryotic cells. Indeed, as many as 30% of newly synthesized proteins in eukaryotes are degraded by the ubiquitin-proteasome system (UPS) within minutes of synthesis (Schubert et al., 2000), as well as the aberrant proteins resulted from mutation or translational damage (Sherman and Goldberg, 2001). The ubiquitin-mediated degradation of proteins plays important roles in the control of myriad cellular processes, including cell cycle progression, differentiation, apoptosis, transcription

regulation, DNA repair, signal transduction, endocytosis, immune response and quality control of protein folding (see Appendix 2).

In the UPS pathway, proteins are targeted for degradation by covalent ligation to ubiquitin, a 76-amino-acid globular protein that is highly conserved throughout eukaryotes. Ubiquitination is a multistep process (Fig. 1.4), involving three types of enzymes. First, an ubiquitin-activating enzyme (also known as E1) forms a thiol-ester bond with the carboxy-terminal glycine of ubiquitin in an ATP-dependent process. Then, an ubiquitin-conjugating enzyme or ubiquitin-carrier enzyme (also known as E2) accepts the carboxyl terminus of ubiquitin from the E1 by a transthiolation reaction to the active cysteine residue of the E2. Finally, an ubiquitin protein ligase (E3) catalyses the transfer of ubiquitin from the E2 enzyme to the lysine residue in the substrate that is selected exquisitely by the E3.

Ubiquitinated proteins are recognised and degraded by the 26S proteasome, an ATP dependent proteolytic complex. The catalytic component of this remarkable and highly complex structure is a cylindrical chamber of 28 subunits (the 20S core) that includes two copies of subunits with trypsin, chymotrypsin, and peptidylglutamyl peptidase-like activities (Kierszenbaum, 2000; Mochida et al., 2000). The 20S core is capped at each end by a multisubunit regulatory complex, the 19S cap. Protein recognition and ATP-dependent unfolding occur in the 19S cap and subsequent proteolysis takes place in the 20S core. At the proteosome, deubiquitinating enzymes (DUBs) cleave multi-ubiquitin chains from residue peptides (Papa and Hochstrasser, 1993) and shorten protein-bound multi-ubiquitin chains by removing the terminal ubiquityl group (Lam et al., 1997). The ubiquitin released from the proteosome can be reused for additional ubiquitination.

(A) Protein ubiquitination

(B) Proteasomal degradation
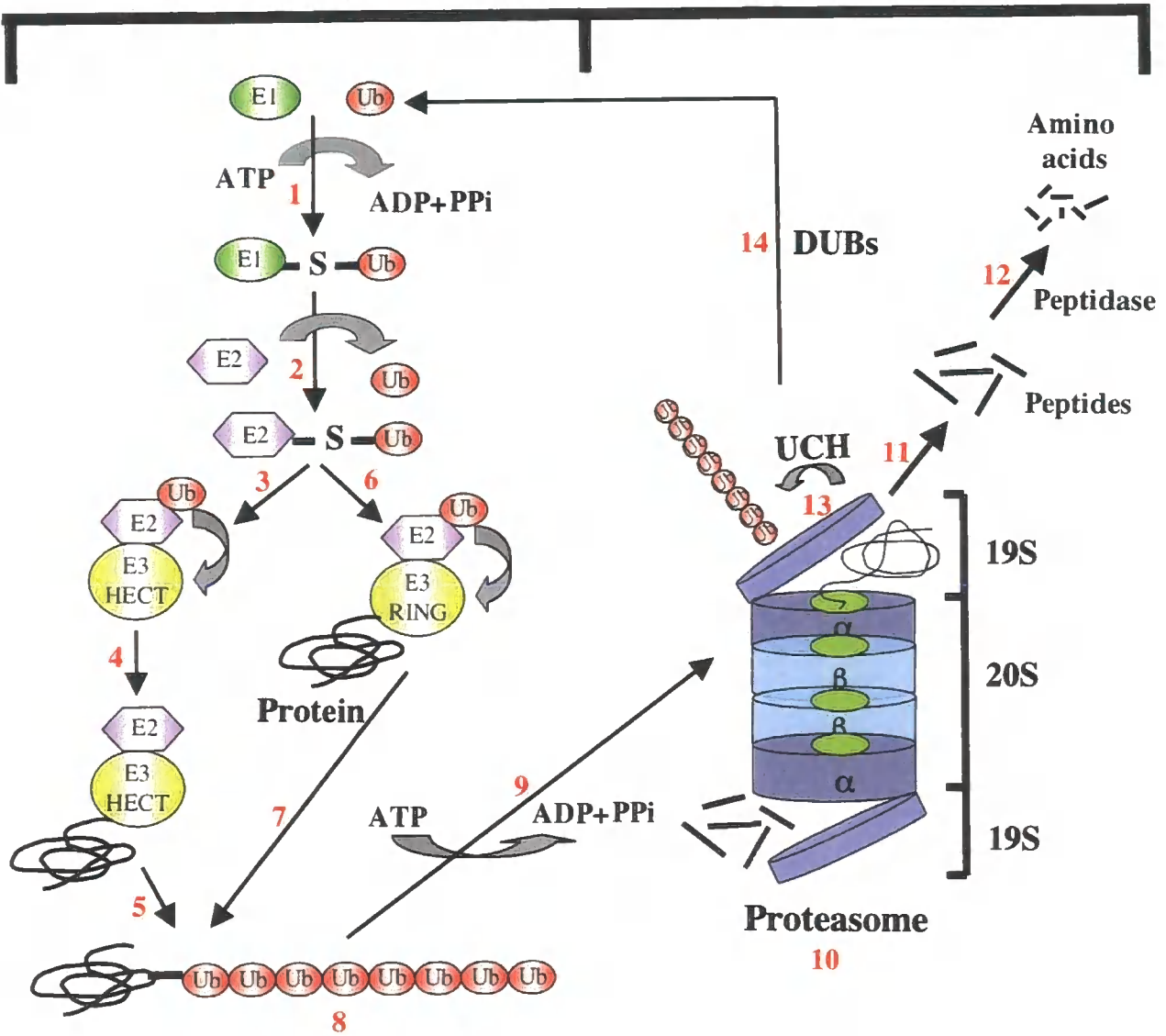
Figure 1.4. The ubiquitin-proteasome system. Proteolysis of a target substrate by the ubiquitin-proteasome system involves two steps— first, conjugation of ubiquitin moieties to the protein substrate (A); second, degradation of the ubiquitin-marked substrate by the 26S proteasome (B). Protein ubiquitination is catalyzed by three enzymes: E1 (ubiquitin-activating enzyme) hydrolyses ATP (adenosine triphosphate) and forms a thioester-linked conjugate with ubiquitin |1|; E2 (ubiquitin-conjugating enzyme) receives ubiquitin from E1 and forms a similar thioester linkage with ubiquitin |2|; E3 (ubiquitin-protein ligase) binds both E2 and the substrate, and transfers the ubiquitin that is bound to E2 to the substrate. |3-7|. Two major classes of E3 are identified: the HECT (homologous to the E6-AP C-terminus) |3| directly catalyses the attachment of ubiquitin |4| to substrate proteins |5| or the RING (really interesting new gene) finger domain |6| promotes target protein ubiquitylation or autoubiquitylation |7|. Successive conjugation of ubiquitin molecules to one another generates a polyubiquitin chain |8| that serves as a binding and degradation signal for the 26S proteasome. The substrate tagged with a polyubiquitin chain is shuttled to the proteasome, in a process requires ATP |9|. The 26S proteasome contains two 19S cap regulatory complex and 20S cylindric catalytic core complex |10|. Each outer ring of the 20S comprises seven α subunits for the entrance of the substrate, while each inner ring of the 20S encompasses seven β subunits with proteolytically active sites. The target protein is degraded to short peptides |11| and then hydrolysed to amino acids by cytosolic peptidases |12|. The polyubiquitin chain is cleaved away from the substrate by the UCH (ubiquitin carboxy-terminal hydrolase) |13|, and can be recycled by deubiquitinating enzymes (DUBs) |14|.

1.2.9.2 Substrates of the ubiquitin-proteasome system

1.2.9.2.1 Nrf2

Nrf2 (nuclear factor erythroid-2 related factor 2) is a redox-sensitive transcription factor that regulates the expression of genes encoding antioxidants, xenobiotic detoxification enzymes and drug efflux pumps, and confers cytoprotection against oxidative stress and xenobiotics in normal cells. Under homeostatic conditions, Nrf2 is normally localised in the cytoplasm via its Neh2 domain tethered with an actin-binding protein homologous to the Drosophila actin-binding protein Kelch called Keap1 (Kelch-like ECH-associated protein 1; Li et al., 2005; Itoh et al., 1999; Dhakshinamoorthy and Jaiswal, 2001). Keap1 functions as an adaptor protein for redox-regulated substrate to a Cul3-dependent ubiquitin ligase, and negatively regulates Nrf2 activity by targeting it to proteasomal degradation (Zhang et al., 2004). Upon exposure to oxidative stress, Nrf2 is released for nuclear translocation (Dinkova-Kostova et al., 2002; Motohashi and Yamamoto, 2004) by modification of the sulfhydryl group interactions in the Keap1-Nrf2 complex. Whilst translocated into the nucleus, Nrf2 specifically binds the antioxidant response element (ARE) found in the promoters of phase 2 and antioxidant defense enzymes, such as NAD(P)H:quinone oxidoreductase, glutathione-S-transferase, glutathione peroxidase and heme oxygenase-1 (Venugopal and Jaiswal, 1996).

Nrf2 has a short half-life, $T_{1/2} = 15$ minutes (Nguyen et al., 2003) to 3 hours (Stewart et al., 2003). The fast turnover of Nrf2 is a result of degradation through the UPS, and it can be inhibited by Keap1 (Sekhar et al., 2002). Since several protein kinase pathways including mitogen activated protein kinase and protein kinase C have been implicated in transducing signals that control Nrf2 dependent gene expression (Huang et al., 2002; Kong et al., 2001; Lee et al., 2001), a link between Nrf2 phosphorylation, Nrf2 stability, and mitogen activated protein kinase pathway is proposed by Nguyen and coworkers (Nguyen et al., 2003). Recently, antioxidant stress response including increased gene expression regulated by Nrf2

had been found in mice overexpressing wild-type GFAP along with Rosenthal Fibres formation (Hagemann et al., 2005).

1.2.9.2.2 Cyclin D1

Cyclin D1, D2, and D3 make up the cyclin D family. Cyclin D proteins and their associated kinases are uniquely positioned to regulate the cell cycle as they link mitogenic signals to the cell cycle machinery (Ekholm and Reed, 2000). For instance, cyclin D1 accumulation is necessary for G1-S phase cell cycle transition. Phosphorylation of retinoblastoma (Rb) protein by active cyclin D1-dependent kinase 4/6 (cdc4/6) complexes leads to release of sequestered E2F transcription factors that activate expression of genes required for progression into S phase (Sherr and Roberts, 1999).

Cyclin D1 degradation occurs at the end of G1 phase, where turnover of cyclin D1 is rapid (T$_{1/2}$ = ~20-30 minutes) (Diehl et al., 1998). This degradation is critical for progression into S phase, and inability to degrade cyclin D1 results in G1 arrest (Sherr and Roberts, 1999). Levels of cyclin D1 elevate in response to mitogen following S phase, which is essential for continued cell cycling (Baldin et al., 1993). Ubiquitin-dependent cyclin D1 degradation requires cyclin D1 phosphorylated by GSK3β at threonine residue (Thr^{286}) near the carboxyl terminus, triggering polyubiquitination of cyclin D1 and its subsequent degradation by the 26S proteasome (Diehl et al., 1998; Diehl et al., 1997). Besides, cyclin D1 can also be ubiquitylated by alternative mechanisms independent of Thr^{286} phosphorylation (Germain et al., 2000). Ras-activated pathways increase cyclin D1 stability by inhibiting GSK3β activity in proliferating cells (Diehl et al., 1998). Conversely, activated p38 kinase promotes the transcriptional down-regulation of cyclin D1 that is enhanced by the specific p38 inhibitor SB203580 upon exposure to a variety of stresses (Lavoie et al., 1996; Casanovas et al., 2000). Aggregates resulted from overexpression of mutant keratin 14 have shown to suppress 20S

21

proteasome function, as judged by the inhibited turnover of cyclin D1 that is under the regulated control of the UPS in normal circumstances (Diehl et al., 1997).

1.2.9.3 Ubiquitination of IFs

IF proteins are also targets for ubiquitination, but little is known about the role of ubiquitination on IFs. A direct evidence of *in vivo* ubiquitination of IFs comes from studies with keratin 8/18 (Ku and Omary, 2000). When cotransfected with ubiquitin followed by proteosome inhibition or overexpression of each keratin individually, keratin 8 and keratin 18 are significantly ubiquitinated. Keratin ubiquitination is associated with its degradation as evidenced by decreased keratin degradation after proteosome inhibition. Furthermore, keratin ubiquitination seems to be cross-regulated by phosphorylation. Similar modes of ubiquitination and degradation are likely to involve other IF proteins. Thus proper ubiquitination and subsequent degradation of IF proteins may be required for their turnover. Uncoupling of ubiquitination and degradation may lead to aberrant accumulation of ubiquitin in IF-enriched cytoplasmic inclusions in a number of diseases, such as Mallory bodies in liver diseases, intrasarcoplasmic inclusions in desmin-related myopathies and Rosenthal fibres in Alexander disease. One potential explanation is that the formation of inclusions results in the proteosome capacity being exceeded or inhibited, with subsequent accumulation of ubiquitinated proteins within aggresome (Johnson and Englund, 1998). In the case of Rosenthal fibres, ubiquitinated protein inclusions containing GFAP and the small stress proteins HSP27 and αB-crystallin occur as an early event during their formation (Perng et al., 2006).

1.2.10 IF associated proteins

IF dynamics and functions can be regulated by interactions with binding partners, such as IF-associated proteins (IFAPs). IFAPs coordinate interactions of IFs with a variety of cellular proteins and other cytoskeletal elements, which provide a dynamic platform for the organisation of the cytoplasm on a structural and functional level. The number of known IFAPs is increasing steadily. Appendix 3 summarises a range of IFAPs that interact with various cytoplasmic IF proteins. This appendix is not intended to be comprehensive, but rather is to provide a general overview that cytoplasmic IFs interact with a number of cellular proteins.

In particular, proteins of plakin family are cytoskeletal linkers that feature a long α-helical rod domain, flanked by globular end domains that mediate binding to IFs and other cytoskeletal proteins (Jefferson et al., 2004). This type of IFAPs thus serves as critical connecting links in the IF scaffolding that organise the cytoplasm and confers mechanical stability to cells and tissues. However, IFAPs are not limited to crosslinkers but also include chaperones, kinases, phosphatases, adapters and receptors, which function in signalling networks that regulate cell cycle, programmed cell death and the cellular response to stress (Pallari and Eriksson, 2006). Whilst the role of IF, particularly keratin IFs, in resisting mechanical stresses has been well established (Ku et al., 1995; Loranger et al., 1997), evidence that IFs exert a cytoprotective role in countering non-mechanical stress is emerging. Probably, the best example is provided by the simple epithelial keratins 8/18 in protecting liver hepatocytes from non-mechanical stress (Ku et al., 1996b; Toivola et al., 1998; Zatloukal et al., 2000). The role of IFs in protection from mechanical and non-mechanical stresses may involve their interactions with stress proteins. For instance, keratins interact with a broad range of stress proteins, including HSP70, GRP78 and Mrj, a DnaJ/HSP40 family protein (Appendix 3). Stress proteins not only associate with keratins but also reside

abundantly in other IFs (Quinlan, 2001). All type III IF proteins and the lens-specific IF proteins CP49 and filensin have been shown to associate with the small heat shock proteins (sHSP) αB-crystallin and HSP27 (Appendix 3).

1.2.11 IFs and apoptosis

Among the more recently recognised IFAPs are enzymes and receptors involved in the apoptosis (Marceau et al., 2007). Apoptosis, or programmed cell death, is a tightly controlled, energy-dependent process mediated by discrete intracellular signals, characterised by cell shrinkage, nuclear condensation and DNA fragmentation. In the later stages, the cell membrane devolves into neatly packaged vesicles, termed apoptotic bodies, which are taken up by neighboring cells. The apoptotic signals are often transduced by two cellular processes, the "extrinsic" and "intrinsic" pathways (Dragovich et al., 1998; Strasser et al., 2000). Whilst the intrinsic apoptosis death pathway is mitochondrial-dependent, the extrinsic apoptosis pathway is activated by two death receptors, tumor necrosis factor-α (TNF-α) and Fas receptors. Following ligand binding, these receptors trimerize and recruit the death domain adaptor molecules, such as TRADD (TNF receptor-type 1-associated death domain protein) and FADD (Fas receptor-associated death domain protein) to form the death-inducing signalling complex (DISC) (Peter and Krammer, 2003; Ozören and El-Deiry, 2002). Both receptor-mediated and mitochondrial-dependent apoptotic pathways are often executed by a group of cysteinyl-aspartate-directed proteases called caspases (Nicholson, 1999; Takahashi and Earnshaw, 1996). Caspases degrade multiple cellular proteins as the apoptotic programme moves into its execution phase.

Several IF proteins are directly cleaved by effector caspases at an early stage of apoptosis (Byun et al., 2001; Chen et al., 2003; Mouser et al., 2006; Oshima, 2002; Ruchaud et al., 2002). Cleavage often occurs at a conserved site within the rod domain of IFs, leading to loss

of filament integrity and destruction of the IF networks. Initial studies suggest that caspase-mediated cleavage of IFs promotes the apoptotic signalling cascade and timely execution of apoptosis (Schietke et al., 2006), as evidenced by the delay incurred when caspase-resistant forms of IFs were overexpressed (Byun et al., 2001; Rao et al., 1996). The cleavage of IF proteins has additional significance. For instance, caspase-cleavage of vimentin releases the filament-bound p53 to the nucleus, where it can enhance TNF-α-induced apoptosis (Yang et al., 2005).

IFs are not only caspase substrates, but they also act as scaffolds in the sequential caspase activation. This regulated process involves an apoptosis-signalling molecule, such as the death effector domain containing DNA binding domain (DEDD) (Schutte et al., 2006; Lee et al., 2002). Recent studies on keratins revealed that DEDD associates with IFs and directs caspases to IFs to facilitate their ordered cleavage during apoptosis (Dinsdale et al., 2004). In addition, keratins 8/18 have also been shown to attenuate TNF-α induced apoptosis by interacting with TRADD (Inada et al., 2001). Keratin mutations associated with epidermolysis bullosa simplex (EBS; e.g. R125C K14) abrogates its interaction with TRADD, making keratinocytes more susceptible to apoptosis (Yoneda et al., 2004).

1.2.12 IF and signalling pathways

IFs serve as signalling platforms for intracellular kinases and phosphatases, which not only regulate phosphorylation and assembly states of IFs, but also modulate kinase/phosphatase activities (Omary et al., 2006; Pallari and Eriksson, 2006; Sihag et al., 2007). With IFs being substrates for many of the estimated 518 human kinases (Johnson and Hunter, 2005), mitogen-activated protein kinases (MAPKs) signalling pathways are evolutionary highly conserved. Cells respond to a variety of stimuli by activating MAPK pathways to regulate a given cellular process, such as gene expression, cellular metabolism, and cellular response to

differentiation, proliferation, apoptosis, inflammation and stress response (Chang and Karin, 2001; Johnson and Lapadat, 2002; Kyriakis and Avruch, 2001; Cowan and Storey, 2003; Xia and Karin, 2004).

1.2.12.1 MAPK family

The MAPK family is composed of three prototype kinases: the extracellular signal-regulated protein kinases (ERKs), c-Jun NH2-terminal kinase (JNK) and p38 kinase (Kyriakis and Avruch, 2001; Cowan and Storey, 2003). Both JNK and p38 are involved in cellular stress, whereas ERKs are activated by growth factors and other mitogens. All MAPK pathways are operated in a three-tiered system (Fig. 1.5). The first component of the system is MAPK kinase kinases (MAPKKKs or MAP3Ks), which are activated by stimuli-activated membrane receptors or by interaction with GTP-binding proteins. This activation leads to phosphorylation of dual-specific MAPK Kinases (MAPKKs or MAP2Ks) on serine/threonine and tyrosine residues within a conserved motif of the MAPKs. MAPKs are serine/threonine kinases that can phosphorylate a number of target proteins ranging from transcription factors to cellular proteins on a consensus sequence Pro-Xaa-Ser/Thr-Pro (Widmann et al., 1999).

1.2.12.1.1. ERK1 and ERK2

ERK1 and ERK2 share 83% amino acid identity, and are expressed to various extents in all tissues (Chen et al., 2001). The ERK pathway responds primarily to growth factors, serum, and phorbol esters (Lewis et al., 1998). Depending on the strength and duration of stimulation, activated ERK often leads to cell proliferation, development, differentiation, meiosis cellular survival and learning and memory in neurons (Marshall, 1995; Xia et al., 1995; Guyton et al., 1996; Wang et al., 1998). ERK1 and ERK2 are activated by MAPKKs MEK1 and MEK2, which phosphorylate ERK at Thr-Glu-Tyr motif. The MEKs are in turn
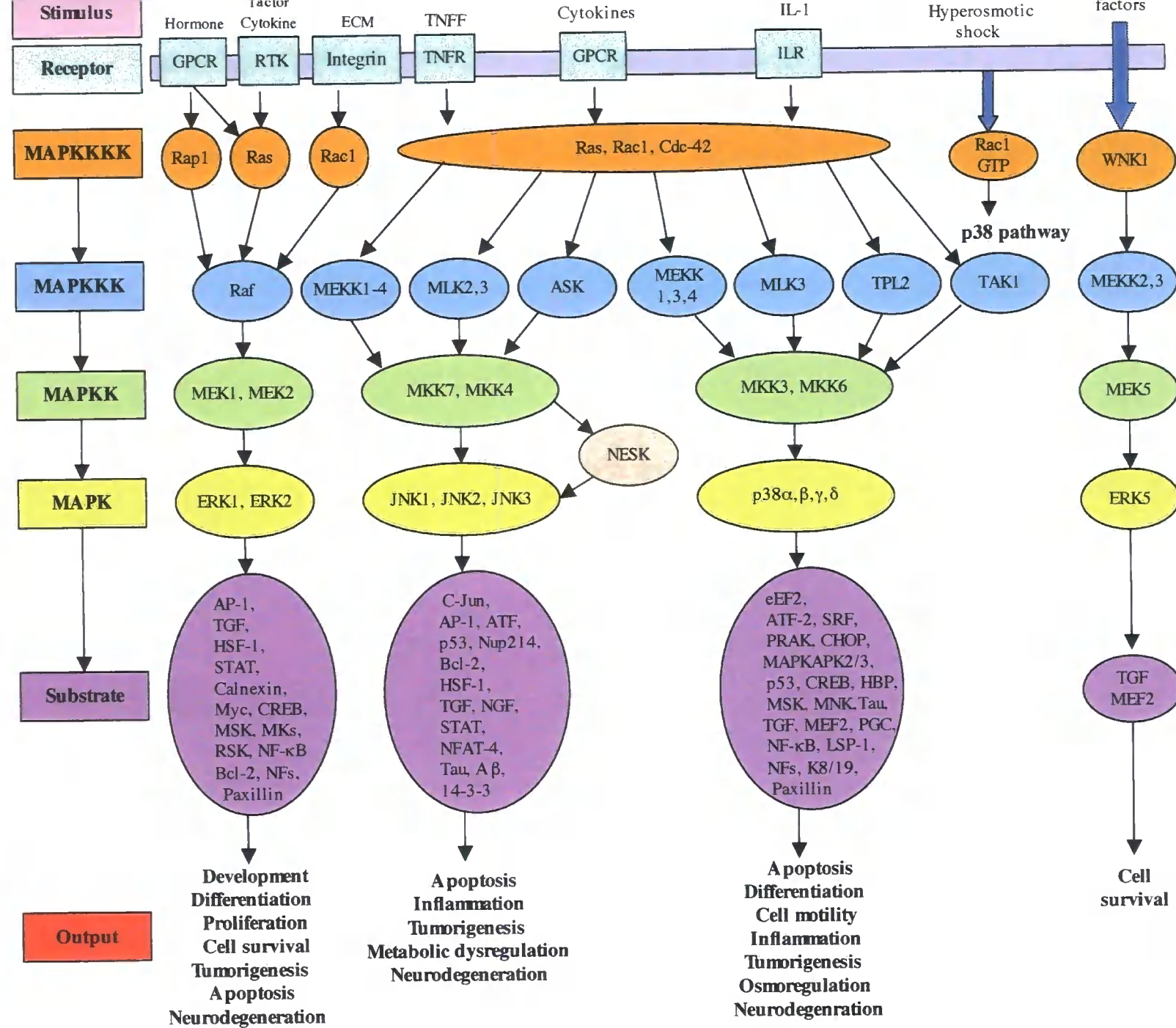
Figure 1.5. Mammalian mitogen-activated protein kinase (MAPK) signalling pathways. In response to stimuli, four subfamilies of MAPK in mammalian cells are activated: ERK1/2, ERK5, JNKs and p38s. MAPK pathways are three-tiered signalling modules comprising MAPK kinase (MAPKKK; MEKK), MAPK kinase (MAPKK; MEK; MKK) and MAPK. Most upstream, MAPKKK is activated by MAPK kinase kinase knase (MAPKKKK). GPCR, G protein-coupled receptor; RTK, receptor tyrosine kinase; ECM, extracellular matrix; TNF, tumor necrosis factor; TNFR, tumor necrosis factor receptor; IL-1, interleukin-1; ILR, Interleukin-1 receptor; NESK, NIK-like embryo-specific kinase; AP-1, activator protein-1; HSF-1, heat shock factor-1; ATF-2, activating transcription factor-2; CREB, camp response element-binding protein; NFAT, nuclear factor of activated T-cells; NF-κB, nuclear factor kappa B; MSK, mitogen- and stress-activated protein kinase; RSK, 90 kDa ribosomal S6 kinase; MK, MAPK-activated kinase; Nup214, nucleoprotein 214; NFs, neurofilaments; Aβ, amyloid β; NGF, nuclear growth factor; PRAK, p38 regulated/activate kinase; CHOP, CCAAT/enhancer-binding protein-homologous protein; SRF, serum response factor; MEF2, myocyte enhancing factor 2; LSP1, lymphocyte-specific protein 1; PGC, peroxisome proliferators activated receptor γ coactivator; SAP, serum response factor accessory protein; HBP, high mobility group-box transcription factor; MAPKAP-K, MAPK-activated protein kinase; MNK, MAPK-interacting protein; TAK, transforming growth factor-β-activated kinase; K8/19, keratins 8 and 19; eEF2, eukaryotic elongation factor 2. This diagram is not intended to be comprehensive, but representative.

activated by the GTPase Ras (Cowan and Storey, 2003). When activated ERKs are translocated to the nucleus, they phosphorylate various transcription factors (AP-1 (activator protein-1), NF-κB (nuclear factor kappa B), Elk-1, c-myc and c-fos) depending on the initial stimuli (Widmann et al., 1999; Cowan and Storey, 2003). In addition, ERKs can also phosphorylate cytoplasmic substrates, such as several MAPK-activated protein kinases (MKs) (Chen et al., 2001; Frodin and Gammeltoft, 1999), cell survival regulator (e.i. Bcl-2, cPL2), epidermal growth factor receptor, paxillin and NFs (Lenormand et al., 1993; Widmann et al., 1999; Cowan and Storey, 2003). Recently, ERK1/2 has been demonstrated in chronic neuronal death *in vitro* and *in vivo* (Colucci-D'Amato et al., 2003), albeit ERK1/2 was mostly regarded as a pro-survival signalling molecule.

1.2.12.1.2 JNKs

Cells are constantly exposed to a variety of stresses, such as metabolic stress, heat and osmotic shocks, UV irradiation, and pro-inflammatory cytokines (Davis, 2000), which lead to the activation of the JNK pathway. The JNKs, also referred to as stress-activated kinases (SAPKs), are encoded by three different genes JNK1, JNK2 and JNK3 (Gupta et al., 1996). JNK1 and JNK2 are expressed ubiquitously, whereas the expression of JNK3 is largely restricted to the brain, heart and testis (Derijard et al., 1994; Kyriakis et al., 1994; Pulverer et al., 1991; Yang et l., 1997). These genes are alternatively spliced to generate as many as 10 different isoforms. Transcripts derived from all three JNKs encode proteins with or without a C-terminal extension to create 46 kDa and 54 kDa isoforms (Pulverer et al., 1991). The JNKs are phosphorylated on the Thr-Pro-Tyr motif by MKK4 and MKK7 (Davis, 2000; Kyriakis and Avruch, 2001). Upstream kinases include MEKK1-4, ASK (apoptosis signal-regulating kinase) and mixed-lineage kinases (MLKs), which are activated by members of the Rho family.

Activated JNKs are translocated to the nucleus, where they phosphorylate trancription factors. c-Jun was the first identified substrate for JNK, which then leads to increased activity of AP-1 (Davis, 2000). Other transcription factors activated by JNK include Jun, Fos, Maf and ATF (activating transcription factor) subunits (Behrens et al., 1999). Since then, a number of other substrates, predominantly transcription factors have been recognised, including ATF-2, Elk-1, p53 and NFAT4 (nuclear factor of activated T-cells 4) (Chen et al., 2001; Kyriakis and Avruch, 2001).

Activation of JNKs often leads to apoptosis, when JNKs function as a proapoptotic protein kinase (Davis, 2000; Lin, 2003). JNKs can also promote cell survival under certain circumstances. For instance, activated JNKs protect neonatal cardiac myocytes after reoxygenation (Dougherty et al, 2002) and JNK upstream kinase MEKK1 suppresses apoptosis induced by hydrogen peroxide in embryonic stem cell-derived cardiac myocytes (Minamino et al., 1999). In addition, JNKs have a significant role in tumorigenesis (Zenz and Wagner, 2006; Yang et al., 2003; Papachristou et al., 2003; Hess et al., 2002), inflammation (Ricci et al., 2004; Sumara et al., 2005; Karin and Gallagher, 2005; Karin et al., 2006), and metabolic disregulation (Hirosumi et al., 2002; Hotamisligil, 2005; Musi and Goodyear, 2006).

1.2.12.1.3 p38

In mammals, p38 MAPKs are identified as four isoforms. Of which, p38α (also called SAPK2a) (Han et al., 1994) is the best characterised. Three additional isoforms were encoded by different genes, p38β (also called SAPK2b) (Jiang et al., 1996), p38γ (also called SAPK3 and ERK6) (Lechner et al., 1996; Mertens et al., 1996), and p38δ (also called SAPK4) (Goedert et al., 1997). Despite all p38 isoforms are widely expressed, p38γ is mainly expressed in skeletal muscle and p38δ is most found in pancreas, kidney, small intestine and

testis (Goedert et al., 1997). Based on the amino-acid sequence identity and the susceptibilities to inhibition by SB203580 (Cuenda et al., 1995) and SB202190 (Davies et al., 2000) compounds, the p38 MAPK subfamily can be further divided into two distinct subsets, p38α and p38β on the one hand and p38γ and p38δ on the other. For amino-acid sequence, the former are 75% identical, whereas the latter share ~70% identity. Furthermore, the p38 inhibitors only affected p38α and p38β, but not p38γ and p38δ (Goedert et al., 1997; Cuenda et al., 1997; Kuma et al., 2005).

Similar to other MAPKs, p38 MAPKs are subject to dual phosphorylation on a Thr-Gly-Tyr motif by MKK3 and MKK6 (Kyriakis and Avruch, 2001), in turn activated by MKKKs. MKKKs including MLKs, MEKK and ASK are activated by GTPase such as Racs and Rhos, which are responsible for signal transmission of the stress stimuli. The p38 kinases are generally activated by heat, osmotic and oxidative stresses, inflammatory cytokines and TNF receptor-mediated signalling, leading to the phosphorylation of diverse substrate proteins ranging from transcription factors (e.g. Elk-1, ATF-2 or SAP1 (serum response factor accessory protein 1)) (Tan et al., 1996; Raingeaud et al., 1995; Janknecht and Hunter, 1997) to cytoplasmic targets (e.g. MAPKAP-2 and -3, HSP25/27) (Rouse et al., 1994; Freshney et al., 1994; Stokoe et al., 1992; Ben-Levy et al., 1998).

1.2.12.2 IF and MAPKs

Besides being important modulators of transcription factors, MAPKs are also involved in the regulation of IF phosphorylation. For instance, keratin 8 is phosphorylated by ERK1/2 *in vitro* on Ser-431, and phosphorylation of this site increases dramatically upon epidermal growth factor (EGF) stimulation and mitotic arrest (Ku and Omary, 1997). In addition, keratin 8 is phosphotylated by and associated with SAPKs p38 (Ku et al., 2002a) and JNK (He et al., 2002) both *in vitro* and in stressed cells. These phosphorylations could play important roles in

30

regulating SAPK signalling and keratin filament reorganisation. The K8 phosphorylation motif is unique among type II keratin and recent studies have shown that keratins 5 and 6 are also phosphorylated by p38 kinase *in vitro* (Toivola et al., 2002). Furthermore, keratinocyte cell lines carrying keratin 14 mutations associated with EBS have higher basal level of activated JNK (D'Alessandro et al., 2002). Upon osmotic shock, the stress-activated response by JNK was induced more rapidly in EBS keratinocytes with severe mutations than those with milder mutations. Interestingly, expression of keratin 10 prevents cell proliferation through the inhibition of Akt kinase activity (Paramio et al., 2001), which impairs NF-κB activity and leads to increased production of TNF-α and concomitant activation of JNK in the epidermis of K10 transgenic mice (Santos et al., 2003).

Recent studies have revealed that MAPKs are also involved in the regulation of other IF protein phosphorylation. For instance, NF-H has been implicated as a JNK substrate, with phosphorylation at repeated Lys-Ser-Pro-X-Glu motif within the C-terminal domain (Giasson and Mushynski, 1996). In addition, expression of the disease-causing GFAP mutant in a range of cell types leads to accumulation of GFAP and induces the activation of JNK and its upstream kinase MLKs and ASK-1 (Tang et al., 2006). Activated JNK is associated with GFAP-enriched protein inclusions both in transfected cells and in samples from Alexander disease brain tissues (Tang et al., 2006). It is hypothesized that GFAP accumulation induced JNK activation could lead to a positive feedback loop that produces further protein accumulation and cellular stress response. Moreover, vimentin was recently implicated in a novel function on preserving the activated states of MAPKs (Perlson et al., 2005). After nerve injury, translation of vimentin and importin-β mRNAs is locally activated in the wound-proximal axoplasm, together with phosphorylation-dependent activation of ERK kinases (Perlson et al., 2005). Newly expressed vimentin appears to act in concert with importin-β and cytoplasmic dynein to mediate the retrograde transport of activated ERKs to the cell body

and nucleus during axonal regeneration. Therefore, vimentin could function as a vehicle to transport long-range kinase signalling. These findings indicate that IF protein may play an active role in transmitting specific signals from the cell periphery to the nucleus in different cell types (Chang and Goldman, 2004; Paramio and Jorcano, 2002).

1.2.13 IF-related diseases

The role of IFs in protection from mechanical and non-mechanical stresses distinguishes them from other cytoskeletal elements. This cytoprotective function is reflected by a broad range of human diseases that are associated with mutations in genes encoding IFs (see http://www.interfil.org). Collectively, these disorders span diverse clinical manifestations that include ectodermal dysplasias, cardiomyopathies, neuropathies, muscular dystrophies, lipodystrophies and premature ageing (Table 1.3). Most mutations behave dominantly and the disease pathogenesis often involves fragility of cells expressing mutant IF proteins (Omary et al., 2004; Porter and Lane, 2003), whereas a minority may predispose to disease. For instance, NFs mutations may predispose to amyotrophic lateral sclerosis (Al-Chalabi and Miller, 2003; Lariviere and Julien, 2004) and keratins 8/18 mutations may predispose to end-stage liver disease (Ku et al., 2003). A significant number of IF-associated diseases are typified by the presence of intracellular aggregates of abnormal IF proteins, such as Mallory bodies in liver disease (Zatloukal et al., 2007), Lewy bodies in Parkinson's diseases (Galloway et al., 1992), NF aggregates in Charcot-Marie-Tooth disease (Perez-Olle et al., 2002) and Rosenthal fibres in Alexander diseae (Quinlan et al., 2007).

Table 1.3 Genetic disorders associated with IF gene mutations

Disorders	IF gene mutated	OMIM**	Main clinical features
Keratin-related disorders			
Epidermolytic hyperkeratosis	Keratins 1, 10	113800 600648 146590 607602	Hyperkeratosis, Skin fragility
Meesman corneal dystrophy	Keratins 3, 12	122100	Fine punctuate opacities in cornea
Oral white-sponge nevus	Keratins 4, 13	193900	Thickened, white, opalescent spongiform mucosa in mouth
Epidermolysis Bullosa Simplex	Keratins 5, 14	131760 131800 131900 131960	Generalised or localised fluid-filled bullous skin lesions
Pachyonichia congenita	Keratins 6a, 6b, 16, 17	167200 167210	Severe nail dystrophy, variable effects on other epithelial appendages
Inflammatory bowel disease	Keratin 8	601458 266600	Ulcerative colitis, Crohn's disease, extra intestinal feature
Chronic pancreatitis	Keratin 8	Not assigned	Malabsorbtion, pain, weight loss
Cirrhosis, Hepatitis	Keratins 8, 18	215600	Variceal bleeding, ascites
Ichthyosis bullosa of Siemens	Keratin 2e	146800	Bullous ichthyosis erythema
Loose-anagen syndrome	Keratin 6hf	600628	Sparse, short hair that falls out easily
Monilethrix	Human-hair keratins1, 6	158000	Alopecia, beaded and fragile hair
Epidermolytic palmoplantar keratoderma	Keratins 1, 9	144200 148700 607654	Diffuse hyperkeratosis of palm and sole
Non-epidermolytic palmoplantar keratoderma	Keratins 1, 16	600962	Focal hyperkeratosis of palm and sole
Steatocystoma multiplex	Keratin 17	184500 184510	Multiple oval cystic tumourson back, anterior trunk, arms and thighs

Table 1.3 (Continued)

Disorders	IF gene mutated	OMIM**	Main clinical features
Lamin-related diseases			
Charcot-Marie-Tooth disease, type 2B1	Lamins A and C	605558	Symmetrical muscle weakness, wasting, foot deformities, reduced tendon reflexes
Dilated cardiomyopathy	Lamins A and C	115200	Conduction defects in the heart
Familial partial lipodystrophy	Lamins A and C	151660	Substantial redistribution of adipose tissue
Lipoatrophy with diabetes	Lamins A/C	608056	General lipoatrophy, liver steatosis, skin alterations
Emery-Dreifuss muscular dystrophy	Lamins A and C	181350 604929	Contractures of elbows and Achilles' tendons, muscle weakness
Limb-girdle muscular dystrophy, type 1B	Lamins A and C	159001	Progressive proximal weakness, cadiac conduction defects
Hutchison-Gilford progeria	Lamins A and C	176670	Prematuring ageing, alopecia, dystrophic nail
Werner's syndrom	Lamins A and C	277700	Prematuring ageing, senescence
Mandibuloacral dysplasia	Lamins A and C	248370	Mandibular and clavicular hypoplasia, joint contractures, lipodystrophy
Atrial fibrillation	Lamins A and C	607554	Atrioventricular conduction defects
Other disorders			
Alexander Disease	Glial fibrillary acidic protein	203450	Megalencephaly, progressive spasticity, dementia
Desmin-related myopathies	Desmin	601419	Peripheral and distal muscle weakness, arrhythmias, restrictive heart failure
Dilated cardiomyopathy	Desmin	604765	Pure cardiomyopahty
Amyotrophic lateral sclerosis	NF-H Peripherin	105400	Rapid loss of motor function
Charcot-Marie-Tooth, type 2E, type 1F	Neurofilament light chain (NF-L)	607684 607734	Motor and sensory neuropathies, demyelination
Cataract	CP49, Filensin	604219	Ocular cataracts

* Information comes from Human Intermediate Filament Database (www.interfil.org)
** Online Mendelian Inheritance in Man

34

1.3 GFAP

1.3.1 General information on GFAP

My study is particularly focused on GFAP and its role in Alexander disease. GFAP is a type III IF protein, first identified from multiple sclerosis plaque in the brain (Eng et al., 1970; Eng et al., 1971). Whilst GFAP is mainly expressed in cells of astroglial origin in the central nervous system (CNS) (Inagaki et al., 1994; Rutka et al., 1997; Tardy et al., 1989), it is also expressed at low levels in a range of other cells, including retinal Müller cells (Guerin et al., 1990; Lewis et al., 1992; Vaughan et al., 1990), non-myelinating Schwann cells (Jessen et al., 1990), enteric glia cells (Jessen and Mirsk, 1980), as well as other tissues, such as liver, testis, kidney and bowel (Galea et al., 1995; Barber and Lindsay, 1982; Feinstein et al., 1992).

During brain development, GFAP progressively replaces vimentin in the asctocytes for IF network until the astrocytes mature, whereby vimentin levels become undetectable (Bovolenta et al., 1984; Pixley and de Vellis, 1984; Eng, 1995). As GFAP is the major IF protein in astrocytes, it has been used as a specific marker to track the development of astrocyte *in vivo* and in primary cultures (Bock et al., 1997; Trimmer et al., 1982). Convincingly, GFAP positive cells are reported to exert normal astrocyte functions, such as modulation of neuronal proliferation (Gomes et al., 1999; Yoshimura et al., 1998).

1.3.2 GFAP gene and isoforms

GFAP has been isolated and characterised in a number of species, including human, mouse, and rat (Lewis et al., 1984; Balcarek and Cowan, 1985; Reeves et al., 1989; Brenner et al., 1990; Feinstein et al., 1992). Human GFAP gene is located on chromosome 17q21.1-q25 (Bongcam-Rudloff et al., 1991) and comprises nine exons extending over 10 kb. Whilst most IF genes are not alternatively spliced, GFAP is known to generate several splice variants (Quinlan et al., 2007). Previously, three GFAP isoforms were identified. The major isoform

α-GFAP is predominantly expressed in subependymal astrocytes adjacent to the cerebral ventricles of the central nervous system, protoplasmic astrocytes of the gray matter, fibrous astorcytes in the white matter and radial Bergmann glia in the cerebellum (Eng et al., 2000). Accordingly, α-GFAP is widely employed as a marker of astrocytes, especially in astrogliosis or astrocytoma. Compared to the most common GFAP isoform, α-GFAP (Reeves et al., 1989; Bongcam-Rudloff et al., 1991), the mRNAs of the β- and γ-GFAP splice variants are produced by transcription from different start sites of the GFAP gene. The β-GFAP transcription starts upstream of α-GFAP and is found predominantly in Schwann cells of the peripheral nervous system (Feinstein et al., 1992; Galea et al., 1995). The γ-GFAP mRNA lacks exon 1, but contains a part of the intron 1 and is expressed in mouse bone marrow and spleen as well as in human and mouse CNS (Zelenika et al., 1995). Whilst the β- and γ-GFAP mRNAs are expected to produce translation products differing in the N-terminal head domain, alternative splicing of the 3'-end of the GFAP gene produces two new products ε- and κ-GFAP that differ in their C-terminal tail domains to α-GFAP.

In the case of ε-GFAP, a splicing event replaces the last two exons of the α-GFAP gene with an alternative terminal exon located within intron 7 (Nielsen et al., 2002). This resulting spliced form has initially been found in rat and was called δ-GFAP (Condorelli et al., 1999). ε-GFAP is specifically expressed in the subpial zone of the cerebral cortex, the subgranular zone of the hippocampus, and, most intensely, by a ribbon of astrocytes following the ependymal layer of the cerebral ventricles. Unlike α-GFAP, ε-GFAP is not upregulated by astrogliosis, and overexpression of ε-GFAP in transfected cells has a negative effect on filament formation (Roelofs et al., 2005). Furthermore, it has been shown that ε-GFAP is able to bind to presenilin proteins (Nielesen et al., 2002), whose mutations are associated with familial Alzheimer's disease (Cruts et al., 1996). Intriguingly, three novel out-of frame GFAP splice forms. Δ135nt, exon 6 and Δ164nt, have been reported in patients with Alzheimer's

disease and Down's syndrome (Hol et al., 2003), and in these situation they are expressed mainly in neurons. Periphery nerve injury also increases GFAP levels in Schwann cells (Triolo et al., 2006). Indeed, increased GFAP expression is one of the hallmarks of astrogliosis (Pekny and Pekna, 2004; Pekny and Nilsson, 2005).

1.3.3 Astrogliosis and GFAP

Throughout the adult lifespan of mice, rat and human, GFAP gradually increases with age (Eng and Lee, 1998; Nichols et al., 1993). Nevertheless, in the CNS of higher vertebrates, following injury as a result of mechanical trauma, brain ischemia, chemical insult, tumors, or neurodegenerative diseases, astrocytes become activated and respond in a manner called " astrogilosis" or "reactive gliosis", which causes hypertrophy of existing astrocytes and the proliferation of new astrocytes (Eng and Ghirnikar, 1994; Aschner, 1998). This is a prominent feature for astrocytes adjacent to the site of lesion, as they can proliferate and migrate to injury. The upregulation of GFAP, together with vimentin, is a crucial step for astrocyte activation in response to a wide range of insults to the brain (Steward, et al., 1991; Hansen et al., 1990; Khurgel et al., 1992). Unexpectedly, nestin is also re-expressed (Umeoka et al., 2001), though it is usually only expressed in immature astrocytes (Eddleston and Muche, 1993; Eng and Ghirnikar, 1994; Frisen et al., 1995; Ridet et al., 1997; Eng et al., 2000). The conserved nature of the astrocyte response to injury suggest that it might have a protective effect (Eddleston and Mucke, 1993), although other studies implicate reactive astrocyte as major inhibitors of axonal regeneration (Privat, 2003).

Reactive gliosis has been observed in a broad range of neurodegenerative disease, such as multiple screlosis (Hallpike et al., 1983), adrenoleukodystrophy (Schaumburg et al., 1975), amyotrophic lateral sclerosis, Alzheimer's disease, Parkinson's disease, Huntington's disease, Wilson's disease, Pick's disease, Gerstmann-Straussler syndrome, and Down's disease

(Calne, 1994). Moreover, astrogliosis also occurs in the brains of amygdala-kindled subjects (Khurgel et al., 1992; Racine et al., 1989), epilepsy (Hawrylak et al., 1993; Vessal et al., 2004), stroke, trauma, and tumor (Pekny and Nilsson, 2005).

1.3.4 Functions of GFAP by gene knockout studies

Since GFAP accumulation is a prominent feature of reactive astrocytes, several groups have focused on studying the function of astrocytes and GFAP by inhibiting GFAP synthesis through either anti-sense technology (Lefrançois et al., 1997; Chen and Liem, 1994; Weinstein et al., 1991) or gene knockout approach. Mice carrying a null mutation in GFAP have been generated by several groups (Pekny et al., 1995; Gomi et al., 1995; Liedtke et al., 1996; McCall et al., 1996; Shibuki et al., 1996). Surprisingly, GFAP deficient (GFAP–/–) mice show normal development, reproduction, gross CNS morphology and behaviour, and are indistinguishable from their wild-type littermates (Pekny et al., 1995; Gomi et al., 1995; McCall et al., 1996). This absence of apparent phenotypes is not caused by compensatory upregulation of vimentin and nestin, as expression levels of both proteins are unaltered in GFAP null mice (Gomi et al., 1995; Liedtke et al., 1996; McCall et al., 1996; Pekny et al., 1998). Interestingly, astrocytes devoid of GFAP are still able to elaborate processes (stellation) when cocultured with neurons and exhibit increased cell saturation density (Pekny et al., 1998). Consistent with these results are observations made in tumor cells that GFAP-negative cells show higher proliferation rate and longer cell processes (Rutka and Smith, 1993; Toda et al., 1994) compared to GFAP-positive cells (Hara et al., 1991; Kajiwara et al., 1992).

1.3.5 Modulation of neuron functions by GFAP

Neuron and glia are densely packed and make up most of the volume of the brain. Glia contains two major cell types, microglia and macroglia, which are primarily composed of oligodendrocytes and astrocytes in the CNS. Whilst microglia act as phagocytic cells, the immune cells of the CNS, to remove debris after nerve injury, oligodendrocytes form insulating myelin sheath around axons of neurons that conduct electrical signals, similar to the functions of Schwann cells in the PNS. Astrocytes control access of blood vessels to the extracellular fluid surrounding nerve cells, thereby help to form the blood-brain barrier to prevent large molecules/particles in the blood from entering the brain (Janzer and Raff, 1987). The dynamic interaction between neurons and astrocytes due to close apposition of their membranes contributes to additional functions for astrocytes, as summarised in Table 1.4.

Table 1.4 Astrocyte functions in the central nervous system

Functions of astrocytes	Reference
Control of extracellular homeostasis of water and electrolytes, e.i. K^+ ions	Hertz, 1965; Orkand et al., 1966; Walz, 1989
Induction and maintenance of the blood-brain barrier in endothelial cells	Janzer and Raff, 1987
Production of neurotrophic factors	Rudge et al., 1992; Müller et al., 1995
Uptake and metabolism of neurotransmitters released by neurons during synaptic transmission	Smith, 1992
Protecting neurons from oxidative stress in stroke	Kraig et al., 1995
Modulation of neuronal proliferation, as the guidance migrating neurons during development	Yoshimura et al., 1998; Gomes et al., 1999
Providing neurotrophic support to neurons	Voutsinos-Porch et al., 2003; Zonta et al., 2003
Regulation of synaptogenesis and synaptic plasticity	Allen and Barres, 2005
Functioning as neural stem cells	He and Sun, 2006
Engaging in inflammatory processes that defend the CNS from pathogens and preservation of the CNS integrity after stress and injury	Skaper, 2007

The exact function and role of the astrocytic IF in these processes are not well understood. However, after suppressing GFAP expression by the approach of antisense oligonucleotides, it has been shown that GFAP is essential for the formation of astrocytic processes and growth regulation in cultured astrocytes (Weinstein et al., 1991; Rutka and Smith, 1993; Toda et al., 1994). Moreover, they are also important in the guidance of migrating neurons during development, in the repair of the nervous system, in the removal of debris and in the regulation of metabolites and transmitters.

Mice ablated of GFAP provide direct evidence that a primary defect in astrocytes influences modulation of neuronal functions. In fact, GFAP knockout mice demonstrate signs of altered neuronal functions, including changes in motor control (Shibuki et al., 1996; McCall et al., 1996), disorganisation of white matter architecture, late-onset impaired blood-brain barrier integrity and leading to late-onset demyelination of oligodendrocytes in the CNS (Liedtke et al., 1996). Furthermore, GFAP-null mice also exhibit deficient cerebellar long-term depression, impaired eyeblink conditioning, but normal motor coordination (Shibuki et al., 1996) along with enhanced long-term potentiation in hippocampal neurons (McCall et al., 1996). These observations indicate that GFAP is vital for astrocyte-neuron interactions and astroctye processes are essential to modulating synaptic efficacy in the CNS. In addition, it has been demonstrated that loss of GFAP impairs Schwann cell proliferation and delays nerve regeneration after damage (Triolo et al., 2006).

GFAP is the principal component of the glial scar. It is proposed that glial scar may play a role as a physical barrier to neurite outgrowth (Houle and Reier, 1989; Hatten et al., 1991; Eng et al., 1992), since they are largely formed by astrocytic IFs networks that are compact at the scarring area. Supporting data from GFAP/vimentin double knockout studies (Pekny et al., 1999) show that GFAP and vimentin are required for glial scar formation after spinal cord or brain injury. Interestingly, mice devoid of either one of the IF proteins exhibit normal scar

formation after the CNS injury (Pekny et al., 1995; Galou et al., 1996), suggesting that some degree of functional overlap exists between these IF proteins. A parallel study showed that whilst astrocytes from either GFAP or vimentin null-mice can still maintain their volume in response to change in osmotic pressure, astrocytes from GFAP/vimentin deficient mice had compromised volume regulation. The complete loss of IF structure in GFAP/vimentin-null astrocytes strongly suggests that IF cytoskeleton is involved in astrocyte volume regulation. In addition, the loss of IFs in astrocytes also results in a less prominent thickening of astrocytic processes, the immediately increased synaptic loss at the initial stage after neurotrauma, and later on association with increased axonal sprouting of supraspinal systems and synaptic regeneration in the hippocampus (Menet et al., 2003; Wilhelmsson et al., 2004). Furthermore, in the absence of GFAP and/or vimentin, cell migration is compromised (Eckes et al., 1998; Lepekhin et al., 2001). These findings highlight the pivotal role of GFAP in maintaining cell shape and in particular astrocyte hypertrophy.

In the retina, GFAP and vimentin ablated in astroglial cells leads to improved integration of retinal transplants, and provides a permissive environment for grafted neurons to migrate and extend neurites (Kinouchi et al., 2003; Emsley et al., 2004; Quinlan and Nilsson, 2004; Pekny et al., 2004). Besides, under mechanical stress, the absence of IFs from Müller cells leads to decreased ability of newly formed blood vessels to traverse the inner limiting membrane within the retina (Lundkvist et al., 2004). In this scenario, the loss of vimentin can partially be compensated by GFAP (Galou et al., 1996; Eliasson et al., 1999; Pekny, 2001). These studies greatly strengthen the postulation that a primary defect in astrocytes can influence neuronal physiology.

1.4. Alexander disease

Alexander disease (AxD) is a rare, but often fatal degenerative disorder of the CNS, first described by W. S. Alexander in 1949 in a 15-month infant with progressive hydrocephalus, mental retardation and physical developmental delays (Alexander, 1949). Before death, the infant suffered from Jacksonian seizures, vomiting, diarrhea and fever, and died of a pulmonary embolus and thrombosis of the lateral sinus after an 8-month illness. At autopsy, the most striking finding is large numbers of fibrinoid fuchsinophil bodies disseminated throughout the brain, especially distributed in the subpial, subependymal and perivascular zones, where the astrocytes presented hypertrophied fibrillary morphology and degeneration. These bodies were rod-shaped with tapered, rounded or blunt ends, up to about 30 μm in length, which are now known as Rosenthal fibres (RFs) (Rosenthal, 1898).

1.4.1 Clinical manifestations

In 1964, AxD was proposed as an eponym by Friede in his case report (Friede, 1964). Fifty years on, around 111 AxD cases have been reported worldwide, age range from birth to adult (Barkovich and Messing, 2006), unlike most of the other neurodegenerative diseases, which are usually late-onset. Russo et al. (1976) reviewed the cases and reappraised AxD was divided into three subtypes based on the age of onset: infantile, juvenile, and adult forms (Li et al., 2005).

Apart from some rare familial cases (Wohlwill et al., 1959; Seil et al., 1968; Barbieri et al., 1980; Duckett et al., 1992; Howard et al., 1993; Honnorat et al., 1993; Schwankhaus et al., 1995; Thyagarajan et al., 2004; Shiihara et al., 2004), most of the AxD cases are sporadic. With onset from birth to two years of age, the infantile form is the most common and fatal; especially if the onset is at birth (Townsend et al., 1985) or during the neonatal period (Springer et al., 2000). Typically, the infantile form is characterized by megalencephaly,

42

hydrocephalus, seizures, psychomotor retardation, spastic quadriparesis, and increased intracranial pressure can present (Garcia et al., 1992). The patients usually die early within the first decade, but some survive into their early teens.

The juvenile form occurs from 2 years of age to the middle or late teens with frequent bulbar or pseudobulbar signs (e.i., dysphagia and speech difficulties), accompanied by ataxia and spasticity, particularly affecting the lower limbs (Borrett and Becker, 1985; Goebel et al., 1981; Pridmore et al., 1993; Sawaishi et al., 2002; Probst et al., 2003). Some cases show kyphoscoliosis (Deprez et al., 1999; Nonomura et al., 2002). The psychic and intellectual functions are essentially normal. The patients run a more slowly progressive course than the infantile form, and generally die within 10 years of onset.

The clinical features of the adult-onset form are variable. Some cases are asymptomatic (Riggs et. al., 1988) or present cerebellar ataxia, palatal myoclonus, tetraparesis, and other brainstem signs (Howard et al., 1993; Schwankhaus et al., 1995; Namekawa et al., 2002; Okamoto et al., 2002; Mastri and Sung, 1973; Honnorat et al., 1993; Martidis et al., 1999). Others demonstrate the symptoms resembling the juvenile form, with a more protracted course, or mimic multiple sclerosis (Seil et al., 1968; Spalke and Mennel, 1982; Walls et al., 1984; Herndon et al., 1970; Klein, 1970).

1.4.2 Pathology

The pathological hallmark of AxD is widespread accumulation of RFs throughout the CNS (Alexander, 1949; Rosso et al., 1976; Borrett and Becker, 1985; Pridmore et al., 1993; Herndon et al., 1970; Kepes and Ziegler, 1972; Mastri and Sung, 1973; Soffer and Horoupian, 1979; Riggs et al., 1988; Wilson et al., 1996). These round or rod-shaped deposits are insoluble hyaline and eosinophilic inclusion bodies in the cytoplasm of astrocytes, reside in the perikarya, processes or end-feet. In the CNS, RFs may form either as a focal or as a

diffuse process, which is a relatively non-specific change in astrocytes and usually reflects chronicity of disease.

In addition to AxD, RFs are observed in a variety of conditions as a focal phenomenon, including syringomyelia and intramedullary ependymoma (Rosenthal, 1898), slowly growing astrocytic gliomas, especially pilocytic astrocytomas, cerebellar astrocytomas, and optic nerve gliomas (Gullotta and Fliedner, 1972), long-standing reactive gliosis around craniopharyngiomas, hemangioblastomas, pineal cysts, and syringomyelic cavities (Grcevic and Yates, 1957; Gluszez, 1964; Tihen, 1972; Smith et al., 1975; Albright et al., 1986; Herndon, 1970; Kuroiwa et al., 1999; Cillekens et al., 2000), multiple sclerosis (Herndon et al., 1970; Ogasawara, 1965), progressive parkinsonism and dementia (Friedman and Ambler, 1992), debilitating systemic disease like acquired immune disease syndrome (AIDS) (Jacob et al., 2003), and rat brains with nickel implanted (Kress et al., 1981; Horoupian et al., 1982). However, the abundance and widespread distribution of RFs in AxD are unique. They are characteristically located in the subpial and subependymal regions with a diffuse and perivascular pattern.

Ultrastructurally, RFs reveal as granular, osmiophilic, and electron-dense masses enmeshed in extensive collections of glial IFs (Schochet et al., 1968; Herndon et al., 1970; Borrett and Becker, 1985; Seil et al., 1968), mainly GFAP (Johnson and Bettica, 1986; Johnson and Bettica, 1989; Bettica and Johnson, 1990; Tomokane et al., 1991). Two small heat shock proteins, αB-crystallin and HSP27 are also found to be the components of RFs, as well as ubiquitin (Tomokane et al., 1991; Iwaki et al., 1989; Iwaki et al., 1993; Head et al., 1994). Some of the αB-crystallin is ubiquitinated (Goldman and Corbin, 1991) and phosphorylated (Mann et al., 1991; Kato et al., 2001). Elevation of αB-crystllin and HSP27 in the cerebrospinal fluid has been reported (Ochi et al., 1991; Takanashi et al., 1998; Imamura et al., 2002), whereas study of the gene for αB-crystallin fails to reveal mutations (Iwaki et

al., 1992). Furthermore, post-translational modification including advanced glycation modification (Castellani et al., 1997) and lipid peroxide modification (Castellani et al., 1998) are found in RFs of AxD brains. According to the previous findings, although knowing the components in RFs and whose post-translational modification, however, the precise pathogenicity of RFs to AxD is currently not understood.

1.4.3 Radiological features

Brain images of AxD cases from ultrasound, computed tomography (CT) or magnetic resonance imaging (MRI) showed extensive white-matter changes throughout the neuraxis and relative axonal sparing. Due to the pronounced destruction of the white matter and the involvement of demyelination or dysmyelination, AxD is therefore classified as a leukodystrophy. By MRI, pathologically leukodystrophy can be divided into three categories: dysmyelination — abnormal formation of white matter; demyelination — spongiform or cystic degeneration of myelin; and hypomyelination — delayed or decreased production of myelin (Noetzel, 2004). In AxD white matter abnormalities progressively spread from the frontal to the posterior lobes and from the periventricular to subcortical regions with time. The severity of myelin abnormalities in white matter generally decreases in a rostrocaudal gradient of the telencephalon (Wohlwill et al. 1959; Crome, 1953; Friede, 1964; Escourolle et al., 1979). In younger patients, the myelin loss is predominant in the frontal lobes (Arend et al., 1991; Knaap et al., 2001), while it is obvious in the cerebrum (Schwankhaus et al., 1995), brain stem, cerebellum or upper cervical cord (Probst et al., 2003; Namekawa et al., 2002; Okamoto et al., 2002) in older patients.

In 2001, MRI criteria for diagnosing infantile and juvenile AxD have been defined by van der Knaap et al. (van der Knaap et al., 2001) (Fig. 1.6): (1) extensive cerebral white matter abnormalities with frontal predominance, presented by the extent of the white matter

abnormalities, the degree of swelling, the degree of signal change, or the degree of tissue loss (i.e., white matter atrophy or cystic degeneration); (2) presence of a periventricular rim dominated by decreased signal intensity on T2-weighted images, and elevated signal intensity on T1-weighted images; (3) abnormalities in the basal ganglia and thalami; (4) brain stem abnormalities, particularly involving the midbrain and medulla; (5) contrast enhancement involving ventricular lining, periventricular rim of tissue, frontal white matter, optic chiasma, fornix, basal ganglia, thalamus, dentate nucleus, or brain stem, which show the highest density of RFs. An MRI-based diagnosis for AxD requires fulfilment of four of these five criteria. Consistent with the results of Farrell et al. (1984), the contrast enhancement is caused by the insufficiency of the blood-brain barrier due to astrocytic dysfunction.

Aside from one case exhibiting unusual ocular motility abnormalities (Gingold et al., 1999), the majority of the infantile (Hess et al., 1990; Bobele et al., 1990; Schuster et al., 1991; Garcia et al., 1992; Staba et al., 1997; Madsen et al., 1999) and juvenile AxD (Reichard et al., 1996; Deprez et al., 1999) are confirmed by histopathologic diagnosis and MRI findings presented mainly white matter abnormalities. Nevertheless, since four patients of AxD have been observed without apparent leukodystrophy, but possessing ventricular garlands with prominent abnormalities in the medulla and spinal cord (van der Knaap et al., 2006), AxD is not simply a leukodystrophy (Barkovich and Messing, 2006).

In concern of the role of GFAP in AxD, Brenner and cooperators disclose that genetic defects in GFAP gene are a primary cause of AxD (Brenner et al., 2001). Most recently, GFAP accumulation is found to synergistically damage proteasome activity and activate JNK signalling pathway (Tang et al., 2006), and in turn, JNK activation leads to increased GFAP accumulation and inhibited proteasome function.
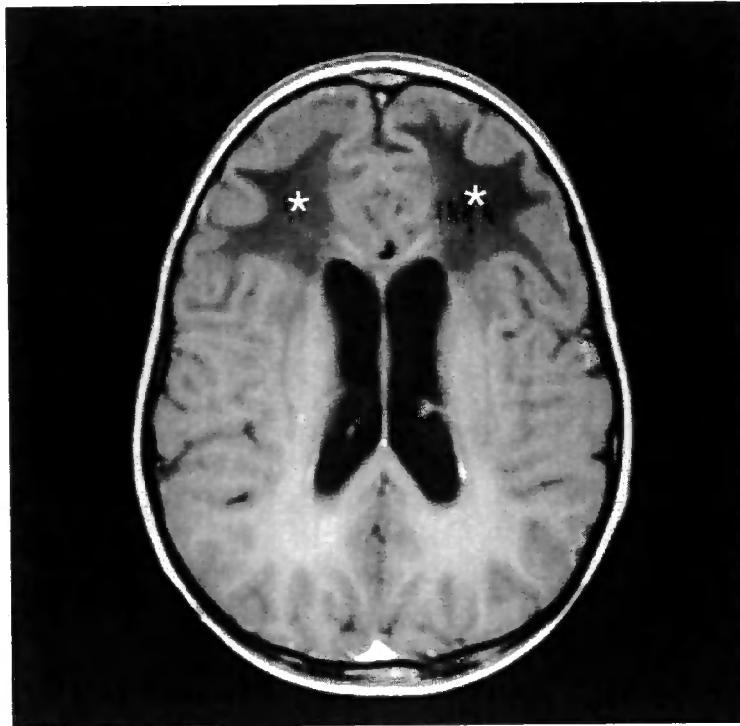
Figure 1.6. Magnetic resonance image of Alexander disease. A ten year old boy with Alexander disease was shown extensive abnormalities (asterisks) of the cerebral white matter with frontal predominance by magnetic resonance imaging. This figure is reprinted from (Messing and Goldman, Alexander disease, Elsevier, Amsterdam, 2004) with permission.

1.4.4 Genetic diagnosis (GFAP mutations)

As GFAP is primarily expressed in astrocytes and a major component of RFs, it is conceivable that GFAP gene might be a candidate for the pathogenesis of AxD. Two lines of evidence have provoked the question "is there any GFAP gene defect in AxD?" First, the transgenic mice engineered to constitutively express human GFAP developed a fatal encephalopathy with protein aggregates in perinuclear regions and processes of dystrophic astrocytes that are immunohistochemically and morphologically indistinguishable from RFs (Messing et al., 1998). Second, primary astrocytes cultured from transgenic mice carrying human GFAP gene induce RF formation (Eng et al., 1998). These discoveries provide strong evidence that a primary alteration in the expression of GFAP could lead to the hallmark feature of AxD.

Based upon these findings, GFAP coding region was evaluated and non-observative point mutations were found in 11 of 12 infantile cases and in the single older patient examined (Brenner et al., 2001). Following this initial report, a number of other studies have extended these findings. A diagram showing the distribution of all confirmed mutations in relation to the protein subdomains of GFAP and variants of AxD is shown in Fig. 1.7. Websites that continue to update newly identified GFAP mutations can be found at the Human Intermediate Filament Mutation Database (http://www.interfil.org) and University of Wisconsin-Madison (http://www.waisman.wisc.edu/alexander).

To date, at least 53 mutations have been found within the GFAP coding region in the clinically or pathologically proven cases of AxD, affecting 45 sites in the protein (see Appendix 4). Nearly all of the disease-causing mutations in GFAP occur as heterozygous single base-pair changes within the coding region, mostly in the conserved central α-helical rod domain but with a few occurring in the amino- and carboxy-terminal tail domains. Exceptions include a 6-bp insertion (Li et al., 2005), a 6-bp duplication and a 6-bp deletion-
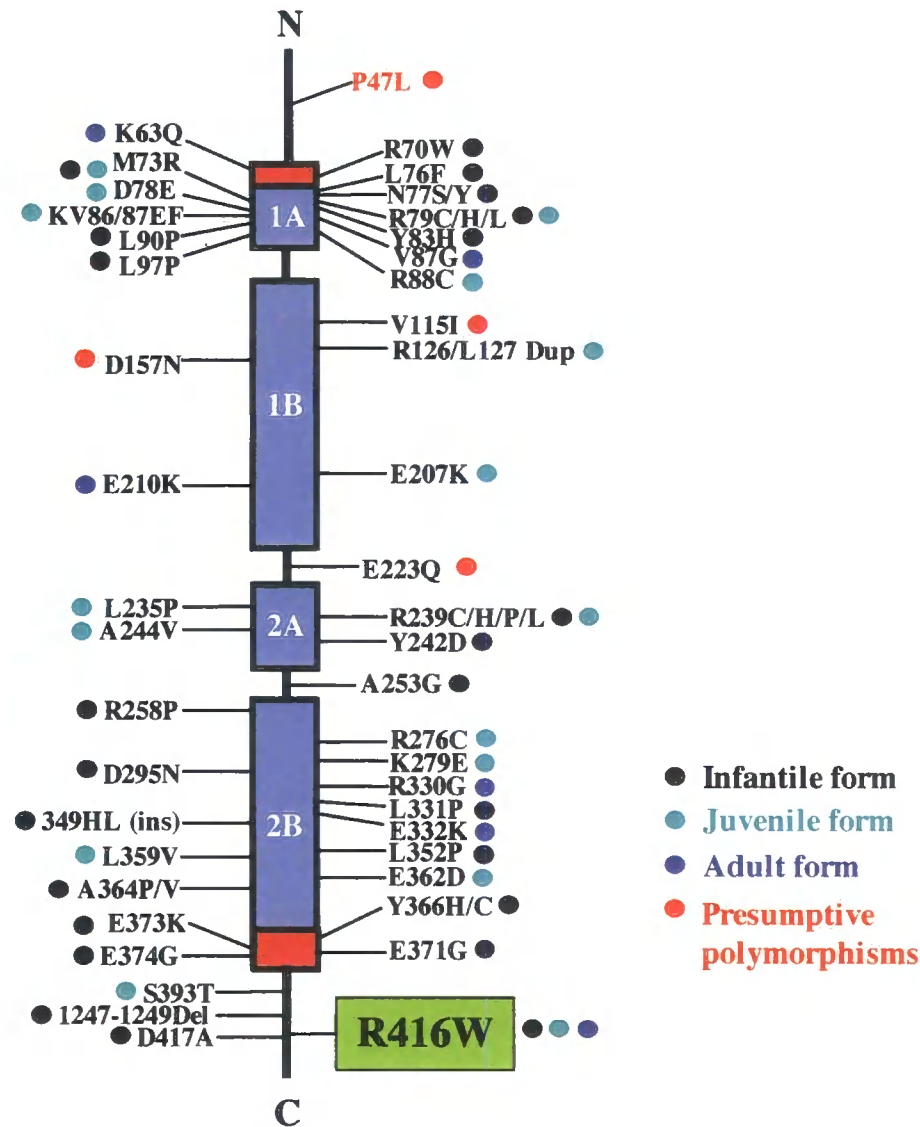
Figure 1.7. Location of Alexander disease-causing mutations in GFAP in relation to the domain structure of IFs.
Like other IF proteins, GFAP consists of a central α-helical rod domain, flanked by non-helical amino-terminal head (N) and carboxy-terminal tail (C) domains. The blue boxes indicate the four α-helical subdomains within the central α-helical rod domain, separated by non-helical linkers. The red boxes at the ends of the rod domain reflect the location of the highly conserved LNDR and TYRKLLEGE motifs. Symbols are coloured coded for clinical category based on the age of onset. The R416W mutation (as indicated by the green box) in the tail domain is associated with three forms of Alexander disease. This diagram is adapted and updated from Figure 1 of Li et al., Int. J. Devel. Neurosci. 2002.

insertion (van der Knaap et al., 2006). Two mutation hotspots are apparent at R79 and R239, accounting for almost half of all reported cases. The arginine residue has been recognised as being particularly prone to mutation due to methylation of CpG dinucleotide (Cooper and Youssoufian, 1988).

The heterozygous nature of GFAP mutations suggests that they are dominant. For most of the reported cases where parents were available for testing, the parents were genotypically and phenotypically normal, confirming these mutations often occurred *de novo*. There is one example of inherited GFAP mutation occurring in a family of adult-onset cases where mother and two children were affected and carried the same V87G mutation (Okamoto, Y, 2002).

The finding that GFAP mutations were found in nearly all forms of AxD implicates that the same basic mechanism may underlie all forms of the disease. The genotype-phenotype correlations, however, are not clear (Rodriguez et al., 2001). For instance, whilst R239H is usually associated with the infantile form and presents the most severe clinical case of AxD (Li et al., 2005), R79C, R79H, R239C and R416W mutations occur in at least two forms of AxD. R416W, in particular, has been found in three forms of AxD cases.

1.4.5 GFAP mutations

Most of the GFAP mutations of AxD are clustered in the central α-helical rod domain (see Fig. 1.7) and several GFAP mutations occur within an amino acid sequence that is highly conserved among IF proteins (Quinlan et al., 1995). For instance, M73, L76, N77, R79 and E373 are located within the highly conserved ends of the rod domain, and each mutation has a homologous counterpart among disease-causing keratin mutations (Li et al., 2002). Particularly, R79 is frequently mutated in AxD and this position is also the hot spot for keratin mutations. In addition, R88 and R239 GFAP mutations are homologous to those in lamin A/C mutations (Bonne et al., 2000; Brown et al., 2001). Like R79, R239 is frequently

50

mutated, but R239 appears to produce more severe phenotype than mutations at the highly conserved rod ends. Previous studies have demonstrated that whilst R239C mutation does not appear to affect filament formation *per se*, the mutation alters the normal solubility and organisation of GFAP networks (Hsiao et al., 2005).

One of the common mutations outside the central rod domain of GFAP that causes all forms of AxD (Brenner et al., 2001; Gorospe et al., 2002; Kinoshita et al., 2003; Thyagarajan, 2004; Li et al., 2005) is R416W. This mutation lies in the tail domain within the KTVEMRDGE motif that is highly conserved among nearly all GFAP from multiple species, as well as the related type III IF proteins vimentin and desmin. Recent studies have demonstrated that R416W GFAP mutation dramatically alters IF assembly *in vitro* and network formation in transfected cells, and does so in a dominant manner (Perng et al., 2006, see appendix 5). A mutation exactly homologous to the R416W in GFAP has been found in the muscle-specific IF protein desmin, which is the primary underlying cause of desmin-related cardiomyopathies (Bär et al., 2007). Although homologous sites are affected, most of the IF mutations lead to loss of function, because the similarity of phenotypes between the human patients and mouse knockouts of the relevant genes (Fuchs and Cleveland, 1998). In contrast, the dominant effect of GFAP mutations appears to be caused by a gain of function rather than loss of function, because GFAP-null mice do not show AxD phenotypes and human GFAP-null mutations have not been found (Li et al., 2002). One study, however, reports late onset dysmyelination in GFAP knockout mice (Liedtke et al., 1996), suggesting the loss of GFAP function may also involved in certain aspects of AxD pathology.

In addition to GFAP mutations associated with AxD, GFAP gene sequencing has revealed the presence of nucleotide changes in both unaffected parents and AxD patients. These GFAP variants, including P47L, V115I, D157N, E223Q, were tentatively classified as polymorphisms. For instance, P47L was found in conjunction with disease-causing mutations

R239C and R416W, which alone appear to be sufficient to cause disease (Brenner et al., 2001). This mutation may act as genetic modifier, as its presence is likely to ameliorate the consequences of these other mutations rather than increasing the severity of the disease. In several instances, it is not clear if a coding change is a rare polymorphism or disease-related. For instance, although V115I, D157N, E223Q mutations are tentatively classified as uncommon polymorphisms by their presence in normal parents, they could be disease-related mutations with incomplete penetrance. Finally, it is important to note that GFAP mutations have not been found in all cases of AxD, indicating that there could be other genetic, epigenetic or environmental causes for this diseases (Omary et al., 2004).

The effort to screen GFAP gene had greatly expanded the number of AxD patients found to have GFAP coding mutations (Li et al., 2005), particularly for the late onset patients. The immediate benefit derived from the close association of GFAP mutations with AxD is that screening of GFAP mutations appears to be a reliable diagnostic tool for AxD. The dominant GFAP missense mutations underlying most cases of AxD provide a unique window for illuminating the mechanism of the disease.

1.4.6 Possible disease mechanisms

Whilst the genetic basis for AxD is firmly established, little is known regarding the mechanism by which GFAP mutations lead to AxD. To study the pathomechanism of this primary astrocyte disorder, mice engineered with the most common GFAP mutations R76H and R236H (corresponding to human R79H and R239H) develop RFs at sites where astrocytes appear reactive and total GFAP expression is increased. Although mutant mice demonstrated increased GFAP expression by themselves, further elevation of GFAP by crossing with wild-type human GFAP overexpressed mice leads to a decreased GFAP solubility, an increased stress response and premature death. These studies provide a formal

proof linking GFAP mutations with RF formation and oxidative stress, and demonstrate a clear correlation between total GFAP levels and phenotype severity.

In AxD patients, RF accumulation is usually found in patients at sites where GFAP is highly expressed. The observation that elevated GFAP level is a consistent component of AxD pathology leads to the hypothesis that GFAP mutations might cause the disease by raising the levels of GFAP, perhaps by increasing its stability or by decreasing its turnover. Indeed, it has been suggested that IF network may play an important role in organising degradative complexes that remove aberrant proteins (Garcia-Mata et al., 1999). The accumulation of GFAP in the form of RFs may compromise astrocytic protein degradation machinery, which could be a primary event that affects the stability and turnover of GFAP. In addition, the presence of accumulated aggregate may reflect the inability of astrocyte to handle excessive GFAP properly and is a potential stress that could compromise normal astrocyte function.

In support of this hypothesis is the finding that transgenic mice engineered to constitutively overexpress wild-type GFAP develop RFs, which was lethal for highest expression lines (Messing et al., 1998). Recently the effects of wild-type GFAP overexpression were studied in these same mice by microarray analysis (Hagemann et al., 2005). The expression profiles of GFAP transgenic mice reveal initial stress response in astrocytes, which results in the activation of microglia and compromised neuronal functions during the advanced stages of pathology. These studies strongly imply that astrocyte dysfunction has deleterious consequences on the functions of other cell types in AxD. In this respect, it is worth mentioning that a primary clinical feature of AxD is hypomyelination or demyelination, rather than astrocyte degeneration. Myelin defects involved in AxD highlights the importance of astrocyte-oligodendrocyte interactions in the formation and maintenance of myelin, and raises the possibility that this interaction is impaired in AxD. Whilst the mechanism(s) underlying

53

these impaired interactions remain unclear, alterations in astrocyte gene expression can initiate a cascade of changes affecting multiple cell types throughout the CNS.

1.5. Outline of this study

The discovery of the GFAP mutations has paved the way to develop several cell-based models to investigate the initiating events that accompany the expression of GFAP mutants. Transient transfection of mutant GFAP into primary astrocytes or established cell lines have revealed that the presence of mutant GFAP causes a wide range of effects that include altered filament stability/solubility (Hsiao et al., 2005), elevated GFAP levels (Tang et al., 2006), activation of stress kinase pathways (Tang et al., 2006), increased association with plectin (Tian et al., 2006) and sequestration of HSP27 and αB-crystallin into GFAP aggregates (Perng et al., 2006). These events may all contribute to the disease mechanism.

Whilst transient transfection provides a quick and convenient way to analyse expressed GFAPs in cells, this does not allow the critical steps immediately preceding aggregate formation to be studied. Clinical materials provide single snapshots of endpoint pathology, but it is difficult to obtain a series of brain biopsies over a time-course from symptom-appearing AxD patients to follow the progression of pathology. Therefore, inducible cell lines provide an excellent experimental system to identify crucial steps in the disease process and study the sequence of events leading to pathology.

In this study, a common GFAP mutation R416W that is associated with all forms of AxD was investigated in detail to reveal its biological effects on astrocytes and obtain insights into the disease progression. I selected mouse astrocytoma DBT cells to established inducible cell lines in which human wild-type and R416W GFAP expression are regulated by a Tet-On gene expression system. In addition, I have also generated an inducible cell line using a human astrocytoma U343 MG-A cells with Tet-Off gene expression system. This cell line would be

expected to better mimic the scenario of R416W GFAP being expressed in a human astrocyte cell background and removes potential species conflicts. These inducible cell lines with regulated GFAP expression, aided in part with use of antibodies specific to R416W mutant GFAP or human GFAP, allow me to answer the following questions: 1) What are the downstream consequences of GFAP mutant expression? 2) Whether cells expressing mutant GFAP are more sensitive to stresses? 3) Whether GFAP aggregate formation affects GFAP stability and turnover? 4) What is the critical ratio of mutant GFAP to wild-type GFAP that leads to aggregate formation and astrocyte dysfunction? I have also designed a range of stress assays to investigate the effects of the mutant GFAP upon astrocyte function. In the following chapters, I will detail how these inducible cell lines were generated and used stress assays to help define the cell biological basis of AxD.

Chapter 2

Materials and Methods

2.1 Chemicals

All chemicals and reagents were purchased from Sigma (UK) or VWR (UK) unless otherwise stated.

2.2 Plasmid construction and site-directed mutagenesis

Total RNA extraction from human astrocytoma U373 MG-A cells was performed by the RNeasy kit (Qiagen, West Sussex, UK). The complete human GFAP cDNA was produced by RT-PCR in the use of SuperScript™ RT-PCR system (Invitrogen, Paisley, UK) with oligonucleotides 5'-CATATG GAGAGGAGACGCAT-3' and 5'-TCACATCACATCCTTGTGCT-3' as the forward and reverse primers, respectively. The amplified PCR product was cloned into the pGEM®-T Easy vector (Promega, Southampton, UK) to generate pGEM®-T Easy-WTGFAP, and the entire sequence was confirmed against the GeneBank® data base entry (accession no. J04569). By QuickChange site-directed mutagenesis (Stratagene, La Jolla, CA), the R416W mutation was introduced using pGEM®-T Easy-WTGFAP vector as the template. The desired C→T mutation at nucleotide position 1246 as underlined: 5'-GAAGACCGTGGAGATGTGGGATGGAGAGGTCAT-3' and 5'-ATGACCTCTCCATCCCACATCTCCACGGTCTTC-3' were synthesised within the mutagenic oligonucleotides. The amplified PCR products consisting of R416W mutation was further cloned into the pGEM®-T Easy vector and the mutation sequence was confirmed by full DNA sequencing.

For expression in cultured mammalian cells, both the wild-type and R416W GFAP in pGEM-T easy® vector were subcloned into pcDNA3.1(-) vector (Invitrogen, Paisley, UK) through the *Xba*I and *Eco*RI restriction sites. For expression in bacteria, wild-type GFAP

56

plasmids were created by subcloning the cDNA of a *Nde*I-*Eco*RI fragment into pET23b vector (Novagen, Nottingham, UK) as well as R416W GFAP.

2.3 Purification of recombinant human wild-type and R416W GFAP

pET23b vector containing human wild-type or R416W GFAP cDNA was transformed into *E. coli* strain BL21(DE3) pLys (Novagen, Nottingham, UK) under the control of T7 RNA polymerase. The transformed cultures were inoculated with 1:100 dilution into LB (Luria Bertain) medium supplemented with 100 mg/ml ampicillin and 34 μg/ml chloroamphenicol and grown at 37°C overnight with vigorous shaking at 225 rpm. Once the OD_{600} of the cultures reached 0.5-0.6, protein expression was induced by adding 0.5 mM isopropyl-1-thio-β-D-galactopyranoside (IPTG) for 3 hours. After induction, the cultures were harvested by centrifugation at 5,000 rpm for 30 minutes at 4°C using a JA-10 rotor (Beckman, UK). The bacteria pellet was resuspended in 50 ml TEN buffer (50 mM Tris-HCl pH 8.0, 1 mM EDTA (ethylene diamine tetra-acidic acid), 300 mM NaCl) with additional 0.1% (v/v) protease inhibitor cocktail and 0.2 mM PMSF (phenylmethylsulfonyl fluoride), and lysed by several cycles of freeze and thaw before homogenised in a 50 ml Dounce homogeniser. The whole extract was clarified by centrifugation at 18,000 rpm by a JA-20 rotor (Beckman, UK) for 30 minutes at 4°C. Expressed GFAP formed inclusion bodies, which were prepared as described (Quinlan et al., 1989). Isolated inclusion bodies were extracted with 1.5 M KCl, 5 mM EDTA, 0.5 % (v/v) Triton X-100, 10 mM Tris-HCl pH 8.0, at room temperature. After washing in 150 mM NaCl, 5 mM EDTA, 10 mM Tris-HCl pH 8.0, at room temperature, inclusion bodies were dissolved in extraction buffer (8 M urea, 20 mM Tris-HCl pH 7.4, 5 mM EDTA, 1 mM EGTA (ethylene glycol tetra-acetic acid), 1 mM DTT (dithiothreitol), and 1 mM PMSF) at room temperature for 3 hours. The insoluble material was removed by centrifugation at 100,000 *g* for 30 minutes at room temperature in a

benchtop Optima MAX Ultracentrifuge using an MLA-80 rotor (Beckman Coulter). The expressed proteins were further purified by ion-exchange chromatography using a Merck-Hitachi Biochromatography system equipped with a Fractogel-EMD TMAE-650S column (Merck) that was pre-equilibrated with column buffer (6 M urea, 20 mM sodium formate pH 4.0, 5 mM EDTA, 1 mM EGTA, 1 mM DTT, and 1 mM PMSF). GFAP was eluted from the column using a linear gradient of 0-500 mM NaCl in the same buffer over 1 hour at a flow rate of 1 ml/minute. The GFAP-enriched fractions were pooled, concentrated, and applied to a Fractogel EMD COO-650S column (Merck) pre-equilibrated with column buffer (6 M urea, 20 mM sodium formate pH 4.0, 5 mM EDTA, 1 mM EGTA, 1 mM DTT, and 1 mM PMSF). After washing in column buffer, GFAP was eluted with a linear gradient of 0-500 mM NaCl in the same buffer. GFAP-containing fractions were selected by SDS-PAGE, and stored at −80°C. Protein concentrations were determined by bicinchonic acid assay (BCA reagent; BCA reagent, PerBio Science, UK) using bovine serum albumin (BSA) as standard.

2.4 Cell culture

Human astrocytoma cell lines, U343 MG-A and U373 MG-A, were cultured in α-minimum essential medium (α-MEM; GIBCO, UK) and Dulbecco's modified eagle's medium (DMEM; Sigma, UK) respectively, supplemented with 10% (v/v) fetal calf serum (FCS; Sigma, UK), 2 mM L-glutamine, 100 U/ml penicillin and 100 μg/ml streptomycin (Sigma, UK). Except U373 cells, primary mouse astrocytes (generously provided by Dr. Milos Pekny, Institute for Neuroscience and Physiology, Sahlgrenska Academy, Göteborg University, Sweden), mouse astrocytoma DBT (delayed brain tumor) cells (a kind gift from Dr. Kumanishi, T., Department of Neurosurgery, Toyama Medical and Pharmaceutic University, Toyama, Japan) and human breast cancer epithelial MCF-7 cells obtained from European Collection of Cell Cultures (Sigma, Poole, UK), were also grown in DMEM

containing 10% (v/v) FCS, 2 mM L-glutamine, 100 U/ml penicillin and 100 μg/ml streptomycin. These cells were maintained at 37°C in a humidified incubator of 95% (v/v) air and 5% (v/v) CO_2.

2.5 Transient transfection

The constructs used for transient transfection were human wild-type and R416W GFAP in pcDNA3.1(-) vector (Invitrogen, UK), which were prepared by MaxiPrep kits (Qiagen, West Sussex, UK). Transfection was performed by GeneJuice™ transfection reagent (Novagen, UK) according to the manufacturer's instructions. Briefly, twenty-four hours after seeded on 10 cm Petri dish plates (Greiner Bio-One Ltd, Gloucestershire, UK), 6 well plates or 96 well plates, cells were transfected with 4 μg/plate, 1 μg/well or 0.05 μg/well of plasmid DNA, respectively, at the density of 40-60% depending upon the cell line in question. Forty-eight hours post-transfection, cells were processed for immunoblotting, double label immunofluorescence microscopy or cell viability assay described as below.

2.6 Inhibition of cellular events

For inhibition of proteasome activity, cells were exposed to carbobenzoxy-L-leucyl-L-leucyl-L-leucinal (MG-132; CalBiochem, UK) for 24 hours before harvesting for immunoblot analysis and immunoprecipitation, or cell viability assay at different time intervals. To inactivate MAPK phosphorylation, cells were pretreated with SB203580 (Biomol Research Laboratories, Plymouth Meeting, PA) for inhibition of p38 kinase, SP600125 (Biomol Research Laboratories, Plymouth Meeting, PA) for inhibition of JNK (c-Jun N-terminal kinase), and U0126 (Cell Signaling, UK) for inhibition of MEK1/2 (MAP kinase kinase 1/2), upstream kinase of ERK (extracellular-signal-regulated protein kinase), 1 hour before induction of human GFAP. Suppression of caspase activity was performed by a

59

pan-caspase inhibitor, benzyloxycarbonyl-Val-Ala-Asp-Fluoromethyloketone (Z-VAD-FMK; Biomol Reserch Laboratories, Plymouth Meeting, PA) before or incubated with induction of GFAP.

2.7 Preparation of the soluble and insoluble fractions

Confluent cells grown on 10-cm Petri dishes were harvested with three washes in cold phosphate buffered saline (PBS; Sigma, UK), and lysed in 500 μl RIPA (radioimmunoprecitation assay) buffer (50 mM Tris-HCl, pH 8.0, 150 mM NaCl, 0.5% (w/v) deoxycholate, 1% (w/v) Nonidet P-40 (NP-40)) containing 1 mM PMSF (Merck, UK) and Complete™ proteinase inhibitor cocktail (Roche Diagnostic, Mannheim, Germany) on ice for 15 minutes (Fig. 2.1). In some experiments, phosphatase inhibitors including 1 mM sodium pyrophosphate, 10 mM sodium orthovanadate, 100 units/ml aprotinin and 100 mM NaF are added in the lysis buffer to detect protein phosphorylation. After cells scraped off from the plates by a rubber policeman, the extracts were homogenised by 1 ml Dounce homogeniser (Wheaton, Millville, NJ) or 20 strokes in a 25-gauge needle, and then centrifuged at 13,000 rpm at 4°C for 15 minutes in a pre-cooled benchtop centrifuge (Eppendorf, Hamburg, Germany). Protein concentrations in whole lysates were determined using BCA reagent (PerBio Science, UK). The supernatant was diluted in Laemmli's sample buffer (62.5 mM Tris-HCl, pH 6.8, 25% (v/v) glycerol, 2% (w/v) SDS, 0.01% (w/v) bromophenol blue; Laemmli, 1970). The pellet was resuspended in pelleting buffer (20 mM Tris-HCl, pH 8.0, 10 mM $MgCl_2$ and 1 mM PMSF) containing 250 U/ml benzonase nuclease (Novagen, Nottingham, UK), and incubated at room temperature for 30 minutes. After homogenisation and centrifugation at 13,000 rpm at 4°C for 15 minutes, the final pellets were washed in PBS containing 1 mM PMSF, and resuspended in Laemmli's sample buffer, in a volume that was proportional to the original sample size. Equal volumes of each supernatant

Cells

↓

Washed with cold PBS

↓

Extracted in **RIPA** buffer

| 15 minutes
↓

Homogenisation

↓

Centrifugation for 15 minutes

↙   ↘

Supernatant   **Pellet**

↓   ↓

Diluted in sample buffer   Resuspended in pelleting buffer

↓ | 30 minutes
↓

Boiled for 5 minutes   Homogenisation

↓

Centrifugation

| 15 minutes
↓

Washed in PBS

↓

Resuspended in sample buffer

↓

Boiled for 5 minutes
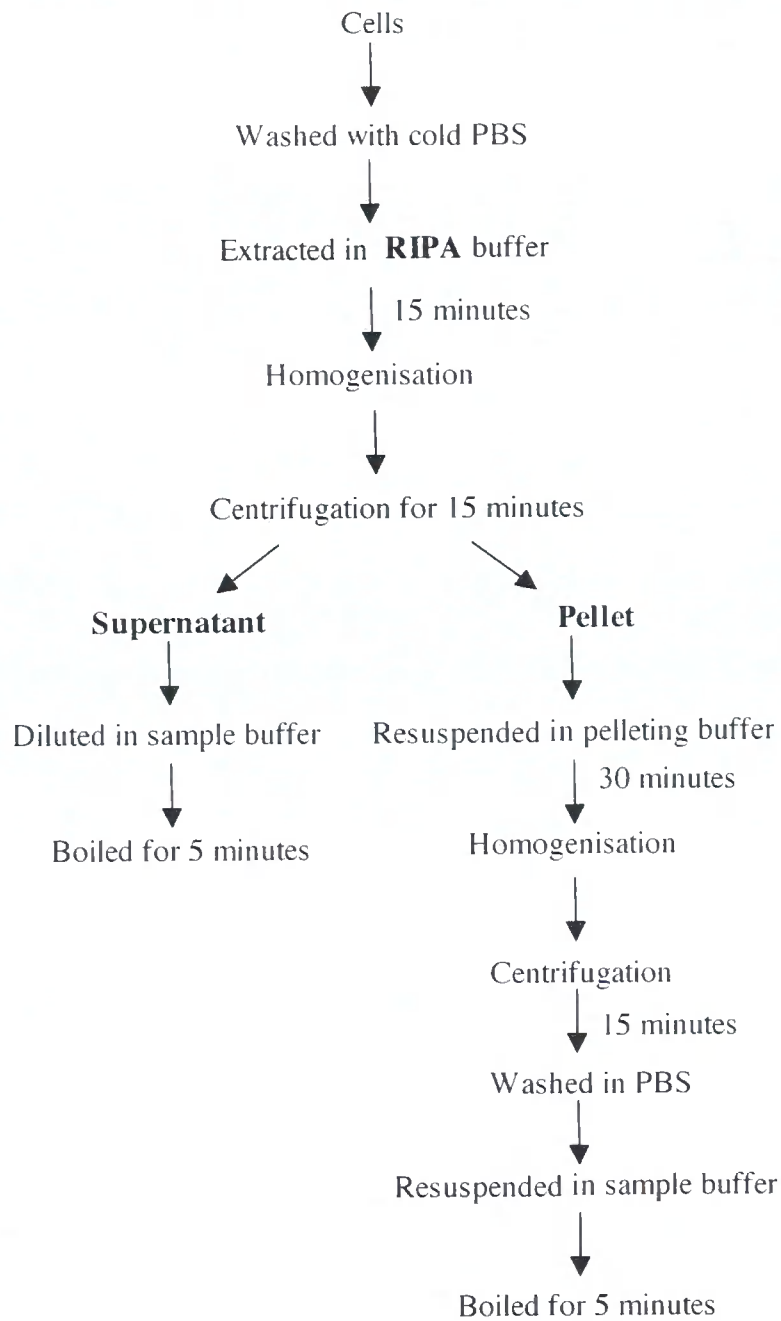
Figure 2.1. Preparation of the soluble and insoluble fractions.

and pellet fractions were boiled for 5 minutes in Laemmli's sample buffer and resolved on 10% or 12% (w/v) sodium dodecyl sulphate-polyacrylamide gel electrophoresis (SDS-PAGE) or subjected to immunoblotting analysis. For SDS-PAGE, the gels were stained with 0.5% (w/v) Coomassie® Brilliant Blue (CBB) R-250 (Merck-BDH, UK) in 50% (v/v) methanol and 10% (v/v) acetic acid for 10 minutes at room temperature. After destained in 10% (v/v) methanol and 5% (v/v) acetic acid for several times, the gels were visualized by Luminescent image analyser (LAS-1000 plus, Fuji Film, Japan) with Image Gauge Software (Version 4.0, Fuji Film, Japan).

2.8 Preparation of the cytoskeletal fractions

Confluent cells cultured on 10-cm Petri dish plates were washed with cold PBS several times, and treated with cold Buffer I (10 mM Tris-HCl, pH 7.4, 140 mM NaCl, 1% (w/v) Triton X-100) for 3-5 minutes on bench (Fig. 2.2). After removal of the buffer, cells were incubated with cold high salt Buffer II (10 mM Tris-HCl, pH 7.4, 1.5 M KCl, 140 mM NaCl, 0.5% (w/v) Triton X-100) for 30 minutes on bench or until the visible peeling of the cells on the dishes. Cells were scraped off with a rubber policeman and transferred into a 15-cm homogenizer (Wheaton, Millville, NJ), followed by centrifuged at 4,300 rpm at $4^{o}C$ for 20 minutes. The pellet was washed by resuspension in PBS and centrifuged at 4,300 rpm at $4^{o}C$ for 20 minutes. Afterwards, the pellet was resuspended again in Buffer III (10 mM Tris-HCl, pH 7.4, 140 mM NaCl, 5mM EDTA) into a 1.5 ml Eppendorf tube and re-pelleted at 10,000 rpm at $4^{o}C$ for 10 minutes in a pre-cooled benchtop centrifuge (Eppendorf, Hamburg, Germany). The resulting pellet was resuspended in PBS using the spatula to remove the salt, and further pelleted at 10,000 rpm at $4^{o}C$ for 10 minutes to generate the final pellet, the cytoskeleton proteins. These proteins were eluted in Buffer IV (10 mM Tris-HCl, pH 8.0, 5 mM EDTA, 2% (w/v) SDS, 1 mM PMSF), and mixed with the equal volume of Laemmli's

Cells

↓

Washed with cold PBS

↓

Incubated with 1% Triton

↓ 3-5 minutes

Extracted in 1.5 M KCl

↓ 30 minutes

Homogenisation

↓

Centrifugationn for 20 minutes

↙   ↘

Supernatant   **Pellet**

↓

Resuspended in washing buffer

↓ Centrifugation for 10 minutes

Resuspended in PBS

↓ Centrifugation for 10 minutes

Cytoskeleton fractions

↓

Dissolved in 2% SDS

↓ Mixed with sample buffer

Boiled for 5 minutes

Figure 2.2. Preparation of the cytoskeletalfractions.

sample buffer before 5 minutes of boiling and processed for SDS-PAGE or analysed by immunoblotting.

2.9 Immunoprecipitation

Confluent cells grown on 10 mm Petri dish plates were harvested in 500 μl of immunoprecipitation buffer (50 mM Tris-HCl, pH 8.0, 150 mM NaCl, 1% (w/v) NP-40) containing 1 mM PMSF and complete proteinase inhibitor cocktail (Roche Diagnostic, UK) (Fig. 2.3). After centrifugation at 13,000 rpm at 4°C for 15 minutes, cell lysates were divided into supernatant and pellet fractions. For immunoprecipitation of human GFAP, the supernatants were incubated with 2 μl SMI-21 antibody for 2 hours on ice, followed by adding of 30 μl protein G-Sepharose beads (Sigma, UK) to incubate on wheeler at 4°C overnight. For immunoprecipitating overexpressed human GFAP in pellet, the pellets were first resuspended with 50 μl of resuspension buffer (10 mM Tris-HCl, pH 7.4, 5 mM EDTA, 2% (w/v) SDS, 10 % (v/v) glycerol containing complete proteinase inhibitor cocktail (Roche Diagnostic, UK)), and then diluted into 950 μl of 20 mM Tris-HCl, pH 7.4, 150 mM NaCl, 1% (w/v) NP-40, 5 mM EDTA and proteinase inhibitor mixtures (Sigma, UK). The diluted lysate was incubated with 2 μl SMI-21 antibody for 2 hours on ice, and incubated with 30 μl protein G-Sepharose beads by gentle rotation at 4°C overnight. Afterwards, the cell lysates were washed five times in immunoprecipitation buffer before the bound immunocomplexes were eluted by boiling in 50 μl Lammeli's sample buffer and then subjected to immunoblotting analysis.

2.10 Immunoblotting

Immunoblotting was carried out using the semi-dry electrotransfer according to the manufacturer's recommendations (Bio-Rad Laboratories, UK). The SDS-PAGE gel was

Cells

↓

Washed with cold PBS

↓

Extracted in immunoprecipitation buffer

↓

Homogenisation

↓

Centrifugation for 15 minutes

↙   ↘

Supernatant   **Pellet**

Supernatant	Pellet
↓	↓
Incubated with SMI-21	Resuspended in resuspension buffer
↓ 2 hours	↓
Adding protein G	Diluted in dilution buffer
↓ O/N	↓
Washed in immunoprecipitation buffer	Incubated with SMI-21
↓	↓ 2 hours
Boiled in sample buffer	Adding protein G
	↓ O/N
	Washed in immunoprecipitation buffer
	↓
	Boiled in sample buffer

Figure 2.3. Procedures of immunoprecipitation.

transferred to nitrocellulose membranes (0.45 μm; Merck-BDH, UK) for two hour at 0.8

mA/cm^2. Blots were rehydrated with deionised water and stained with 0.2% (w/v) Ponceau S

in 3% (v/v) glacial acetic acid for 5 minutes to assess protein transfer efficiency. After the

blot had been destained with Tris-buffered saline (TBS; 20 mM Tris-HCl, pH 7.4 and 150

mM NaCl), the membranes were blocked in blocking buffer consisting of 5% (w/v) BSA in

TTBS (TBS containing 0.2% (v/v) Tween 20) at room temperature for 1 hour. Thereafter, the

membrane was probed with primary antibodies diluted into 5% (w/v) BSA in TTBS for 1

hours at room temperature or overnight at 4°C. The membrane was washed with TTBS three

times, and incubated with horseradish peroxidase (HRP)-conjugated secondary antibodies,

anti-mouse IgG (1:1000) or anti-rabbit IgG (1:1000; DakoCytomation Ltd., Cambridgeshire,

UK), at room temperature for 1 hour. After several washes in TTBS, the blots were

visualized by enhanced chemiluminescence reagent (ECL plus; Amersham Biosciences, UK)

using Luminescent image analyser (LAS-1000 plus, Fuji Film, Japan) with Image Gauge

Software (Version 4.0, Fuji Film, Japan). Quantification of the blots was performed by the

same Software. In some experiments, the membrane was deprobed with Restore^{TM} western

blot stripping buffer (Pierce, UK), and reblotted with individual primary antibodies. Further

procedures are proceeding as above.

Immunoblotting of brain samples was carried out using anonymous, frozen tissues

generously provided by Dr. Jim Goldman and Goumei Tang (New York). The tissues were

homogenised by Dounce homogeniser on ice in 10 mM Tris-HCl pH 7.4, 2 mM β-

mercaptoethanol, 100 mM NaCl, 5 mM EDTA, and 1 X protease inhibitor cocktail (Sigma)

at a 10:1 (v/w) buffer:tissue ratio. The homogenate was centrifuged at 80,000 g for 1 hour at

4°C, and the resulting pellet was dissolved in 15 volumes of the above buffer containing 2%

(w/v) SDS. Protein concentrations were determined by BCA reagent (Pierce). 500 ng of

aliquots of each extract were resolved on 10% (w/v) SDS-PAGE and transferred to Hybond

ECL membranes (Amersham Pharmacia Biotech). The signals of blots were detected by ECL (Amersham Pharmacia Biotech) and visualised using a ChemImager 4400 (Alpha Innotech).

2.11 Antibodies

The primary antibodies used for immunoblotting were described as Tabel 2.1. R416WGFAP specific antibodies were generously provided by Dr. Michael Brenner, University of Alabama. Antibodies against phosphorylated αB-crystallin at Ser-19, Ser-45 and Ser-59 were a kind gift from Dr. Kanefusa Kato, Institute for Developmental Research, Aichi Human Service Centre. Anti-Nrf2 and anti-Keap1 were obtained from Dr. Michael McMahon, Biomedical Research Centre, University of Dundee.

2.12 Immunofluorescence Microscopy

Cells cultured on 13-mm glass coverslips were washed three times with PBS, and fixed either in ice-cold methanol/acetone (1:1, v/v) for 20 minutes at –20°C, or in 4% (w/v) paraformaldehyde prepared from 16 % (w/v) paraformaldehyde (Agar Scientific, Stansted, UK) for 15 minutes followed by permeabilized with 0.2% (w/v) NP-40 at room temperature for 5 minutes. The coverslips were then washed three times with washing buffer (PBS containing 0.02% (w/v) BSA and 0.002% (w/v) sodium azide), and blocked with blocking buffer (10% (v/v) normal goat serum in washing buffer) for 30 minutes at room temperature. After three washes in washing buffer, coverslips were incubated with primary antibodies diluted into blocking buffer for 1 hour at room temperature, followed by washed three times with washing buffer. For secondary antibody staining, coverslips were incubated with 4,6-diamidino-2-phenylindole (DAPI; 1 µg/ml; Molecular Probe Inc., Eugene, OR) for nuclear staining, and Alexa®488 (1:600)- and Alexa®594 (1:600)-conjugated secondary antibodies (Molecular Probe Inc., Eugene, OR) diluted into blocking buffer for 45 minutes at room

Table 2.1 Antibodies used for immunoblotting analysis

Antigen	Source	Clone	Epitope	Isotype	Dilution (IB[*])	Supplier/Reference
GFAP	[*]mMouse	GA-5	Pig GFAP	IgG1	1:5000	Sigma
GFAP	mMouse	52	*a.a.418-432	IgG1	1:1000	BD Biosciences, Palo Alto, CA
GFAP	*pRabbit	3270	GFAP		1:5000	Perng et al., 1999
GFAP	mMouse	SMI-21		IgG1	1:5000	Sternberger Monoclonals, Baltimore, MD
R416W GFAP	mMouse	1A3	C-terminal	IgG	1:1000	Perng et al., 2006
R416WGFAP	mMouse	19.2	C-terminal	IgG	1:1000	Perng et al., 2006
αB-crystallin	mMouse	2D2B6	αB-crystallin		1:50	Sawada et al., 1993
αB-crystallin	pRabbit		a.a.1-10		1:100	CHEMICON International, USA
p-αB-crystallin Ser-19	pRabbit		a.a. 17-27		1:500	Ito et al., 1997
p-αB-crystallin Ser-45	pRabbit		a.a. 44-54		1:1000	Ito et al., 1997
p-αB-crystallin Ser-59	pRabbit		a.a. 57-67		1:1000	Ito et al., 1997
HSP27	mMouse	ER-D5			1:2000	King et al., 1987
p-HSP27	mMouse	1.2	Ser82		1:100	
HSP25	pRabbit		Recombinant mouse HSP25		1:1000	Stressgen, Victoria BC, Canada #SPA-801
Actin	mMouse	AC-40	C-terminal	IgG2a	1:1500	Sigma, UK #A-4700
HSP70	mMouse	MB-H1		IgG2a	1:1000	Hopwood et al., 1997
Ubiquitin	mMouse	P4D1	1-76 a.a.	IgG1	1:1000	New England BioLabs, UK #3936
Cyclin D1	mMouse	DCS6	151-170 a.a.	IgG2a	1:1000	New England BioLabs, UK #2926
Nrf2	pRabbit				1:1000	McMahon et al., 2006
Keap1	pRabbit				1:1000	McMahon et al., 2006
p-JNK Thr183/Tyr185	pRabbit		Thr183/ Tyr185	IgG	1:1000	New England BioLabs, UK, #9251
JNK	mRabbit	56G8	JNK2/MBP	IgG	1:1000	New England BioLabs, UK, #9258
p-p38 Thr180/Tyr182	pRabbit		Thr180/ Tyr182	IgG	1:1000	New England BioLabs, UK, #9211
p38		A-12	213-360 a.a.	IgG1	1:200	Santa Cruz Biotechnology, USA, #sc-7972
p-ERK Thr202/Tyr204	pRabbit		Thr202/ Tyr204	IgG	1:1000	New England BioLabs, UK, #9101
p-c-Jun Ser63	mRabbit	54B3		IgG	1:1000	New England BioLabs, UK, #2361

* IB, immunoblotting; m, monoclonal; p, polyclonal; a.a., amino acid.

The dilution of antibodies used for immunofluorescence microscopy is 1:10 less than for IB.

68

temperature. After rinsing three times in washing buffer, the glass coverslips were mounted onto microscope slides using fluorescent protecting agent Citifluor® (Citifluor Labs, UK). The fluorescent labelling was observed with a Zeiss LSM 510 confocal laser scanning microscope (Carl Zeiss Inc., Jena, Germany), equipped with a 40 X, 1.4NA (numerical aperture) oil immersion objective. Optical sections were set to ~1.0 μm. Images were processed and prepared for figures using Adobe® Photoshop 7.0 (Adobe System, San Jose, CA, USA). Quantification of GFAP filament phenotypes was obtained by visual assessment of the cells, and scoring as cells with or without GFAP containing aggregates. Approximately 100-150 transfected cells were counted and each experiment repeated at least 3 times.

2.13 RNA extraction

HeLa, human cervical carcinoma cell line, was maintained in minimum essential medium (Invitrogen) supplemented with 8% FCS, 100 U/ml penicillin, 100 mg/ml streptomycin and 2 mM glutamax (Lemin et al., 2007). DBT stably expressing wild-type or R416W GFAP cells were cultured in the absence or presence of 1 μg/ml Dox in for 4 days. For transient transfection experiments, DBT cells were mock transfected or transfected with wild-type and R416W GFAP plasmid DNA for 72 hours. Cells were then treated with 1% (v/v) sterile water (mock) or with 10 mM DTT for 6 hours (HeLa) or 3 hours (DBT stable cell lines and transient transfected DBT cells), followed by extraction in TRIzol (Invitrogen, Carlsbad, CA). Total cell RNA was extracted according to the manufacturer's instruction and resuspended in 30 μl DEPC (diethyl pyrocarbonate) water after precipitation. RNA was quantitated by UV spectrophotometry.

2.14 RT-PCR

After dilution to 50 ng/ml, 50 ng total RNA was subjected to reverse transcriptase polymerase chain reaction (RT-PCR) using the AccessQuick RT-PCR kit (Promega). Two primers for RT-PCR were used, XBP1 (X-box binding protein 1; GAAACTGAAAAACAGAGTAGCAGC and GCTTCCAGCTTGGCTGATG) and β-actin (CCACACCTTCTACAATGAGC and ACTCCTGCTTGCTGATCCAC), to detect the relative expression of these mRNAs. The thermal cycling profile consisted of the following: stage 1, 1 cycle at 45°C for 1 hr; stage 2, 1 cycle at 94°C for 2 min; stage 3, 30 cycles at 94°C for 30 sec, 60°C for 1 min, and 72°C for 1 min; stage 4, 1 cycle at 72°C for 5 min. XBP1 cDNA was then subjected to *Pst*I digestion (see below). All cDNA was either analysed by 1% agarose gel (XBP1 before *Pst*I digestion) or analysed by 2% agarose gel (after all *Pst*I digests) at 100 mV for ~50 min before visualised by UV light.

2.15 XBP1 RT-PCR splicing analysis

For *Pst*I digestion, amplified XBP1 cDNA was subjected to *Pst*I (MBI/Fermentas) digestion to detect the presence of spliced mRNA. Total RT-PCR product (or total PCR product minus 5 µl if XBP1 RT-PCR product was loaded beforehand) was digested by 1 µl *Pst*I in a total volume of 15 µl digests at 37°C for 2 hours. DNA was extracted from the *Pst*I digestion using the PCR purification kit (Qiagen) following the manufacturer's instructions. The digested DNA was then run on 2% agarose gel to visualise the activated spliced (XBP1$_S$) and unspliced (XBP1$_U$) products. Actin was used as a control.

2.16 Cell viability assay

For stress assay, cells were seeded into 96 microwell cell culture plates at the density of 5,000-10,000 cells/well depended on the type of experiment. After 48-72 hours of

incubation, while the cells reached ~70-80% confluence, stress including osmotic shock, oxidative stress and proteasome inhibition was applied. Cells were recovered in normal growth medium for various time intervals. Cell viability was examined by the 3-(4,5-dimethyl-thiazol-2yl)-5-(3-carboxymethoxyphenyp)-2-(4-sulfophenyl)-2H-tetrazolium (MTS) using CellTiter 96® Aqueous one solution cell proliferation assay (Promega, UK) and the procedures were described by the manufacturer. Briefly, 20 μl of MTS labelling reagent was added to 100 μl growth medium per well, and incubated for a further 1.5, 1.5 and 3.5 hours for U343 MG-A, U373 MG-A and DBT cells respectively, to dissolve the formazan crystals. The optical density (OD) was measured at a wavelength of 490 nm on a microplate luminometer (Anthos Lucy 1; Salzburg, Austria). Each time point was carried out in triplicates wells and each experiment was repeated at least three times. Results represent the OD value at indicated time points as the mean and standard deviation (SD).

2.17 Statistical analysis

One factor analysis of variance (ANOVA) was used to distribute cells into statistically balanced groups for equality of growth before and after treatment. Two tailed paired t test was applied to compare pre- and post-treatment growth within groups over time. Two tailed unpaired t test was employed to compare growth between untreated and treated cells at single time points. All values were expressed as mean ± SD, and represented as an average of three independent experiments. In all analysis, $P < 0.05$ was considered statistically significant.

Chapter 3

Generation of tetracycline-regulated cell lines

3.1 Introduction

The tetracycline (Tet)-regulated gene expression system has served as a valuable genetic tool that permits the expression of any gene construct introduced into either cultured cells or transgenic animals including mice, rats, insects and fly, to be precisely controlled (Gossen et al., 1993; Sprengel and Hasan, 2007). This expression system comprises two components, a regulatory vector based on the prokaryotic repressor of Tet and a response vector that expresses the gene of interest under the control of an element responding to Tet and its analogues, e.g. doxycycline (Dox). In particular, this system is applicable to the study of genes where their expressions are toxic to cells and provides fundamental insight into how these gene expressions regulate cell morphology, cell structure/function, growth, differentiation, and disease progression.

3.1.1 Principles of tetracycline-regulated expression system

3.1.1.1 Elements of tetracycline-regulated system

Tet-regulated expression system was originally developed by Gossen and Bujard (1992) and primarily derived from the Tet-resistance operon encoded in transposon Tn*10* of *E. coli*. The cytoplasmic membrane embedded *tet*A resistance protein, a proton-[Tet.Mg]$^+$ antiporter, enables *E. coli* to resist Tet (Yamaguchi et al., 1990). Under regular conditions, *tet*A is not expressed due to Tet repressor (*tet*R) blocking its expression. *tet*R contains 207 amino acids with 10 α-helices as interaction surfaces for *tet*R dimerization and binding sites for Tet operator (*tet*O) sequences and Tet (Orth et al., 2000). The *tet*O sequence O2 of Tn*10* is a 19-bp inverted repeat to which *tet*R binds as a 46-kDa homodimer (Hillen and Berens, 1994). In the absence of Tet, *tet*R dimers can bind to the *tet*O and *tet*A promoter regions and hinder

their transcriptional initiation, thereby down-regulating expression of these genes. This process is reversed by increasing intracellular concentrations of Tet to encourage binding to *tet*Rs resulting in a conformational change in the Tet-*tet*R complex, and rendering it incapable to bind *tet*Os (Hillen and Berens, 1994). Accordingly, in order to achieve reversible control gene expression in eukaryotes, changing *tet*R affinity for *tet*O in *E. coli* by Tet is the prerequisite consideration.

3.1.1.2 Tetracycline-controlled gene expression system

The Tet-regulated expression systems, Tet-On and Tet-Off, are binary transgenic systems composing a regulator vector and a response plasmid. In both systems, the expression of a target transgene is dependent on the activity of an inducible transcriptional activator, which can be modulated reversibly and quantitatively by exposing the expression construct to varying concentrations of Tet or its derivatives. In the Tet-Off system, the transgene is expressed in the absence of Tet. In the Tet-On system, the transcription of the transgene is activated in the presence of Tet.

3.1.1.2.1 Tet-Off system

The Tet-Off system was successfully modified by Gossen and Bujard from the well-defined elements of the Tn10 Tet operon in prokaryotes as a genetic switch to control gene expression in eukaryotes (Gossen and Bujard, 1992). The scheme is to incorporate two separate genetic modifications into HeLa cells. First, they converted *tet*R into a Tet-controlled transcriptional activator by fusing the herpes simplex virus (HSV) transcription activator virion protein (VP16) to the C-terminus of *tet*R, and this fusion protein is referred to as tTA (tetracycline-controlled transactivator) (Fig. 3.1A). *tet*R domain binds to heptamerized *tet*O

(A)

(B)
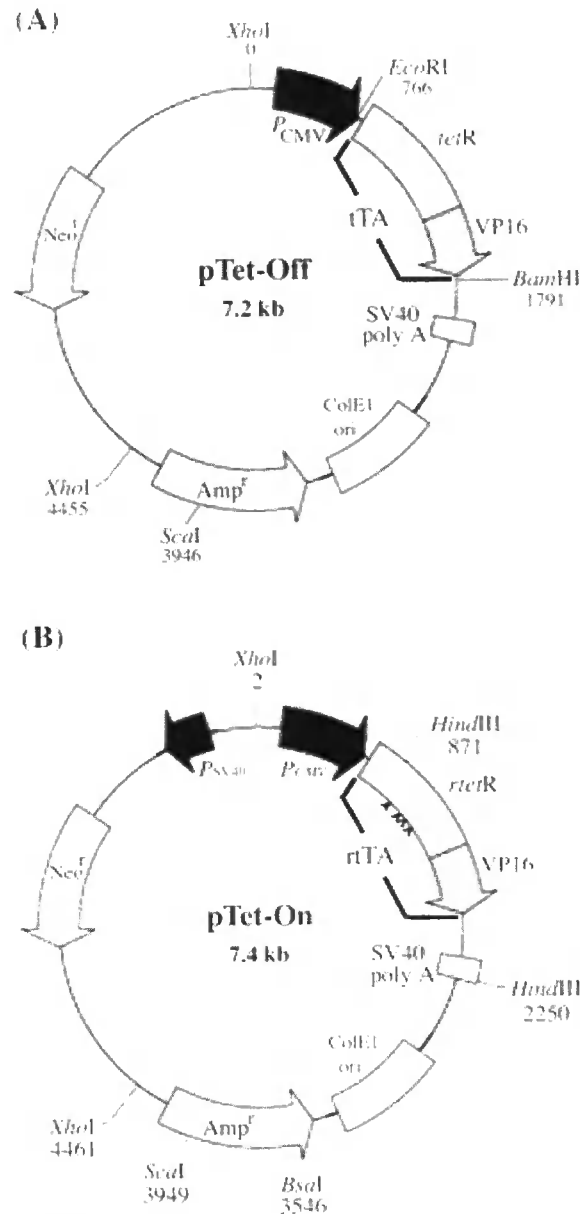
Figure 3.1. pTet-Off and pTet-On vector maps. (A) pTet-Off. pTet-Off (pUHD15-1neo) expresses the tTA (tetracycline transactivator) regulator protein from the immediate early promoter of cytomegalovirus (P_{CMV}) that permits high-level expression of the tetR (tetracycline repressor) gene. Downstream of the 3' end of VP16 (herpes simpex virus transcription activator virion protein 16). SV40 poly A (SV40 early polyadenylation signal) allows efficient transcription termination and polyadenylation of mRNA. ColE1 ori (Colicin E1 origin) permits high-copy number replication and growth in *E. coli*. Two antibiotic resistance genes, Amp^r (ampicillin resistance gene) and Neo^r (neomycin resistance gene) are designed for selection of stable transfectants in *E. coli* and mammalian cells, respectively. (B) pTet-On. pTet-On expresses the rtTA (reverse tetracycline transactivator) regulator protein from the P_{CMV}. rtTA contains four amino-acid mutations (as marked on the map) in the rtetR (reverse tetraycycline repressor) gene. In addition to possessing several silent mutations different from pTet-Off, pTet-On is identical to pTet-Off in all other respects. These diagrams are adapted from Vector Information (BD Biosciences Clontech) at www.bdbiosciences.com/clontech.

sequences, whilst the C-terminal VP16 domain takes part in the recruitment of the RNA polymerase II (Pol II) transcriptional initiation complex for initiating transcription. Second, by linking seven *tet*O sequences to a minimal version of the human cytomegalovirus immediate early gene IE1 promoter (*P*minCMV) containing the Pol II transcriptional start site, they generated a tTA-dependent promoter called the Tet response element (TRE) (Fig. 3.2A). tTA initiates transcription within the CMV-promoter fragment by binding to the TRE. With the addition of Tet, tTA binds the antibiotic and subsequently disassociates from the promoter region. This is the Tet-Off system because without tTA bound to *tet*Os, the promoter is inactive. Hence, tTA allows gene expression to be switched on and off in response to Tet (Fig. 3.3A).

3.1.1.2.2 Tet-On system

Tet-On system was achieved by exchanging the *tet*R of tTA to *rtet*R (reverse tetracycline repressor) of rtTA (reverse tTA) generated from four point mutations in *tet*R (Fig. 3.1B). These mutations, E71K, D95N, L101S and G102D, in the *tet*R DNA binding moiety alter the binding characteristics of rtTA (Hecht et al., 1993) so that it only recognises the *tet*O sequences in the TRE of the target transgene when bound by Dox, a Tet derivative. Interestingly, Tet itself is unable to activate rtTA (Gossen et al., 1995). Thus, transcription of the TRE–regulated target gene is activated by rtTA when Dox is present (Fig. 3.3B).

3.1.1.2.3 Comparison of Tet-Off and Tet-On systems

Tet-inducible transgenic systems allow reversible, temporal regulation of transgene expression (Gossen and Bujard, 1992; Gossen et al., 1995). The Tet-On system requires
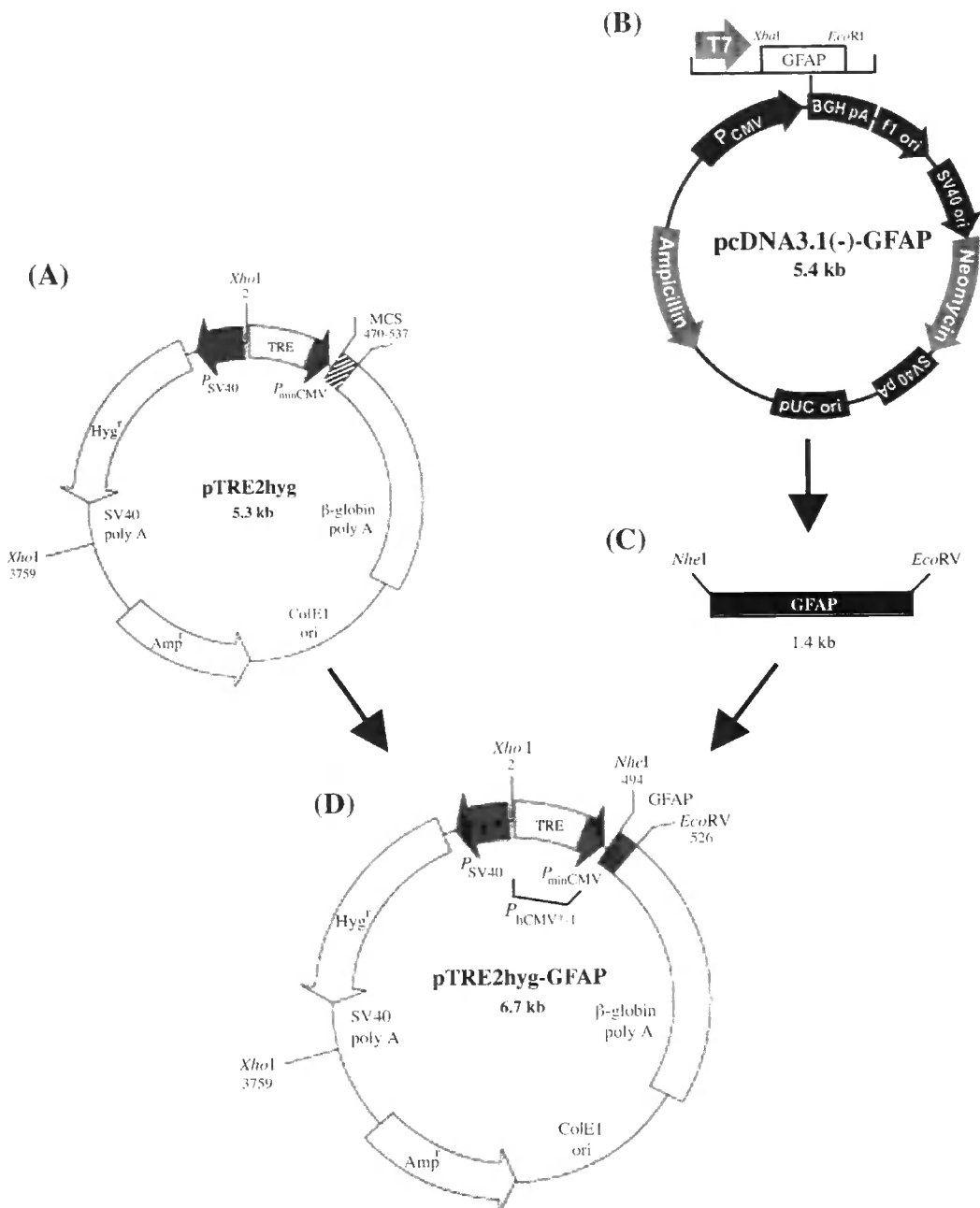
Figure 3.2. Construction of pTRE2hyg-GFAP. GFAP gene (C) excised from pcDNA3.1(-)-GFAP (B) using *Nhe*I and *Eco*RV restriction sites is inserted into the multiple cloning sites (MCS) within the response pTRE2hyg vector (A). The insertion is immediately downstream of the Tet-resposive $P_{hCMV*-1}$ promoter (D). $P_{hCMV*-1}$ consists of two components, the tetracycline response element (TRE) and the minimal cytomegalovirus promoter (P_{minCMV}). The TRE comprises seven copies of a 19-bp tetracycline operator (*tet*O). P_{minCMV} lacks the enhancer that is part of the complete CMV promoter in the regulatory plasmids. $P_{hCMV*-1}$ is silent in the absence of bound *tet*R (tetracycline repressor) or *rtet*R (reverse tetracycline repressor) to the *tet*O sequences. Two polyadenylation signals (poly A), β-globin poly A and SV40 poly A, ensure transcription termination and polyadenylation of mRNA. ColE1 ori (colicin E1 origin) allows high-copy number replication. Amp^r (ampicillin resistance gene) and Hyg^r (hygromycin resistance gene) are designed for transformant selection in *E. coli* and mammalian cells respectively. These vector maps are adapted from Vector Information (BD Biosciences Clontech) at www.bdbiosciences.com/clontech.
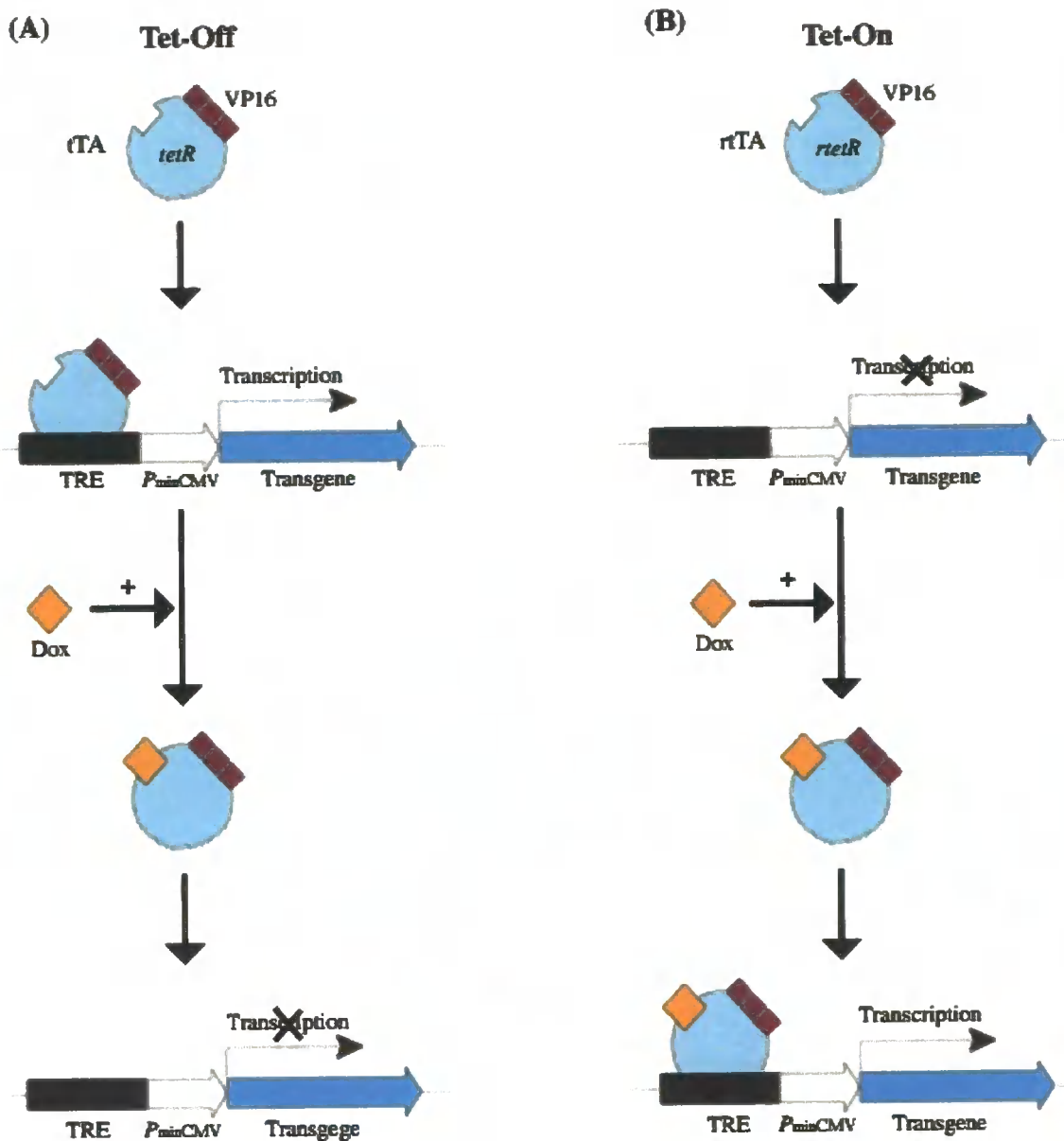
Figure 3.3. Schematic gene regulation in the tetracycline modulatable system.
(A) Tet-Off. tTA (tetracycline-controlled transactivator) containing *tet*R (tetracycline
repressor) and VP16 transcription activator binds to the TRE (tetracycline response
element) that is located upstream of the minimal immediate early promoter of
cytomegalovirus (P_{minCMV}), and initiates transcription of transgene. In the presence
of Dox, tTA is unable to bind to the TRE, and thereby transgene transcription under
the control of the TRE is turned-off. (B) Tet-On. The TRE is silent in the absence of
Dox for activation of rtTA (reverse tetraycycline-controlled transactivator), which
contains *rtet*R (reverse tetracycline repressor) and VP16. Addition of Dox allows
rtTA to bind to the TRE and stimulate transgene transcription. This diagram was
adapted from The BD™ Tet-Off and Tet-On systems at www.bdbiosciences.com.

administration of Dox for the induction of transgene expression (Lee et al., 1998), whereas the transgene expression in the Tet-Off system is only activated after removal of Dox. Since the removal of Dox in the Tet-Off system tends to be slower, the Tet-On system is superior to the Tet-Off system in this regard. The Tet-Off system, however, is less leaky than the Tet-On system because the basal transcriptional activity and requirement of lower concentrations of Dox to regulate gene expression (Mizuguchi and Hayakawa, 2002). This perspective is supported by comparing regulation factors of tTA and rtTA, which are evaluated by the ratio of gene expression level in the induced condition to the uninduced condition in Hela cells. The 10^5 value of regulation factor of tTA in the Tet-Off system shows better efficiency than 10^3 of rtTA in the Tet-On system (Kistner et al., 1996). Thus, the sensitivity of rtTA is approximately 100 times less than tTA. Indeed, previous findings have revealed that while 1 μg/ml of Dox was required to activate rtTA-dependent reporter gene transcription, 10 ng/ml of Dox was sufficient for full inactivation in the tTA system (Gossen et al., 1995).

Compared with the Tet-On system, the Tet-Off system is less suitable for gene therapy applications. First, induction of the Tet-Off system is slower as it depends on the pharmacological elimination of Dox (Gossen et al., 1995; Kistner et al., 1996; Mohammadi et al., 1997). Second, the Tet-Off system requires persistent administration of Dox to suppress gene expression, which may not be ideal while using a lentiviral vector that provides life long gene expression. In addition to rapid induction of gene expression (Belteki et al., 2005), recent improvements in the rtTA protein, including reduced basal activity and increased Dox sensitivity (Urlinger et al., 2000; Das et al., 2004), make the Tet-On system a better choice for transcriptional regulation in most gene therapy applications.

3.1.1.2.4 Efficacy of tTA and rtTA

The efficiency of Tet-controlled gene expression is influenced by the cell line tested and is far more complex in transgenic mice where residual activity is dependent on the tissue even in the absence of the transactivator (Furth et al., 1994; Kistner et al., 1996). Residual activity might be produced by binding of transcription factors to the CMV core promoter (Furth et al., 1994).

Overexpression of the VP16 domain as a fusion protein in either the Tet-On or Tet-Off system can be toxic, as it causes transcriptional squelching (Kühnel et al., 2004) as a consequence of titrating key components of the transcriptional machinery from their intracellular pools. In particular, stable expression of tTA in some cells, such as mouse epithelial cells, results in morphological changes, alterations in cell cycle distribution and growth rate attenuation (Gallia and Khalili, 1998).

Tissue specificity can be achieved by driving tTA or rtTA promoter expression (Kistner et al., 1996), which may be also affected by the chromosomal insertion site of a TRE-regulated transgene. Indeed, randomly integrated transgenes tend to express unstably in the durability and uniformity owing to the positional effect that is contingent on the local chromatin structure (Masui et al., 2005).

3.1.2 Tetracycline and its derivatives

Tet is a broad-spectrum antibiotic that kills gram-negative, gram-positive bacteria and atypical organisms including Chlamydiae, Mycoplasmas, Richettsiae and protozoan parasites by blocking protein synthesis (Epe and Woolley, 1984; Chopra and Roberts, 2001). Given their high membrane permeability and affinity to tTA and rtTA, Tet and its derivatives (Fig. 3.4) are suitable for gene regulation in mammalian cells. Affinity for tetR and antibiotic potency are mediated by different chemical moieties in Tet-derived antibiotics. For instance,
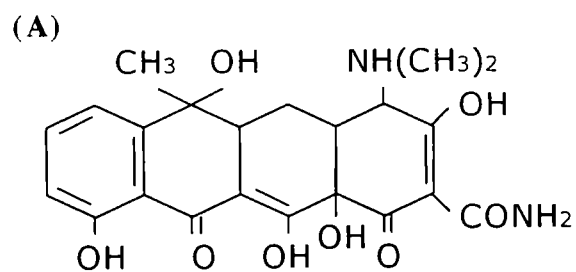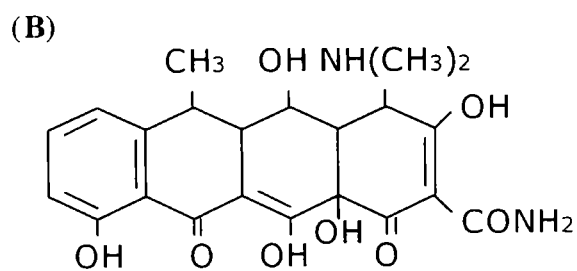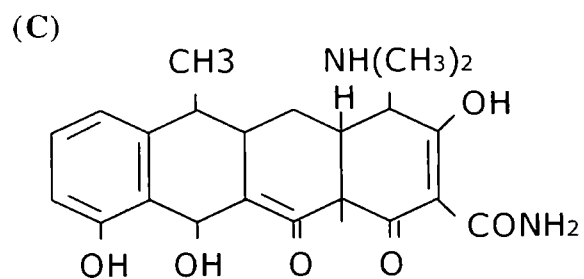
Figure 3.4. Structures of tetracycline and its derivatives. Tetracycline (A),
Doxycycline (B) and Anhydrotetracycline (C) have similar chemical structures.
This diagram was adapted from Figure 1. Of Liu et al., Curr. Med. Chem. 2001.

the affinity of inducers for *tet*R including Tet (Ka = ~10^9 M^{-1}), Dox (Ka = ~10^{10} M^{-1}) and

anhydrotetracycline (ATc, Ka = ~10^{11} M^{-1}) is three to five fold higher than the affinity of

these inducers to prokaryotic ribosomes (Takahashi et al., 1986; Lederer et al., 1996). Two

molecules of Tet binding to a *tet*R dimer are sufficient to reduce the affinity of *tet*R for *tet*O

by nine folds (Lederer et al., 1996). Among these inducers, ATc is much more effective than

Tet and Dox in inactivating tTA (Degenkolb et al., 1991) and has a lower antibiotic activity

towards *E. coli* (Oliva et al., 1992; Gossen et al., 1993; Gossen and Bujard, 1993).

3.1.2.1 Administration of Doxycycline

Dox has a longer half-life (18-24 hours) than Tet (12 hours) (Whelton et al., 1974;

Ramamurthy et al., 2001). Thus, Tet is cleared from mice quicker than Dox (Robertson et al.,

2002). Nevertheless, the concentration of Dox required to regulate gene expression is lower

than the concentration that causes toxic side effects (Bocker et al., 1981). It has been

estimated that 200 μg/ml of Dox yields less than 500 ng/ml of Dox-blood levels which is far

below the levels used clinically (Chen et al., 1998). In addition, Dox can be easily delivered to

animals in drinking water, food pellets and intraperitoneal injection. For these reasons, Dox is

considered to be a better drug for regulating gene transcription in the Tet-On and Tet-Off

systems. In fact, the Tet-On system is only responsive to Dox, but not to Tet (Gossen &

Bujard, 1995).

3.1.2.2 Clinical use of Doxycycline

Dox is a second generation, lipophillic Tet derivative that inhibits collagenase activity *in*

vitro (Golub et al., 1995) and *in vivo* (Golub et al., 1990; Golub et al., 1997). In addition, Dox

has anti-inflammatory effects independent of its antimicrobial action (Tikka et al., 2001;

Yrjanheikki et al., 1998). Dox inhibits prokaryotic protein synthesis by reversibly binding to

81

bacterial 30S ribosome subunit and renders its aminoacryl tRNA incapable of binding to mRNA (Igarashi and Kaji, 1970; Chopra, et al., 1992; Schnappinger and Hillen, 1996). By crossing the blood-brain, blood-cerebral spinal fluid and placental barriers, Dox has excellent brain and tissue penetration. Previous reports have revealed that Dox protects hippocampal neurons from global and focal ischemia in both animal and cell models (Yrjanheikki et al., 1998; Yrjanheikki et al., 1999; Tikka et al., 2001) and delays cell death associated with Huntington's disease (Chen et al., 2000). Furthermore, Dox inhibits caspase-3 cleavage, which blocks apoptotic signalling propagation and promotes neuronal cell survival in neonates with hypoxia-ischemia injury (Jantzie et al., 2005). Hence, Dox has been clinically administrated to protect the brain against pathological apoptotic neuronal cell death and neuroinflammation secondary to brain injury owing to its superior ability to penetrate in the brain and the least toxic side effects of the Tet.

3.1.3 Application of Tet-regulated gene expression system to the study of IF functions

Tet regulated expression of transgenes encoding IF proteins or IFs associated proteins in cells or mice has been employed to examine the effects of these proteins on their dynamic properties, transport, stability, and the organization of the cytoskeleton. For instance, Tet regulated expression of vimentin in a certain population of fibroblasts showed no effect on cell growth, cytoplasmic organization, the shape of the nucleus, or the survival to chemical and mechanical traumas (Holwell et al., 1997). Induced expression of GFAP in human GFAP-negative glioma cells resulted in an inhibition of cell motility and proliferation, and a change in cell morphology with extended cell processes (Elobeid et al., 2000).

Expression of Keratin 16 regulated by Dox in the suprabasal epidermis in transgenic mice affected epidermal barrier function (Presland et al., 2004). Inducible expression of filaggrin, a keratin associated protein, increased keratinocyte susceptibility to apoptotic cell death

(Kuechle et al., 2000), resulted in cytoskeletal disruption, loss of cell-cell adhesion, cell cycle arrest (Presland et al., 2001) and altered keratinocyte structure/function, growth, and differentiation (Presland and Fleckman, 2005). Regulated expression of desmoplakin mutant DPNTP led to dissociation of keratin filaments from the junctional plaque, the disassembly of actin filaments from adherens junctions, and further reduced intercellular adhesive strength in keratinocytes (Huen et al., 2002).

Overexpression of NFH-GFP (neurofilament heavy chain-green fluorescence protein) induced by Dox in neuron cells disrupted filament organization and cell function, whereas normal cell structure and function retained when NFH-GFP expressed at low to intermediate levels (Szebenyi et al., 2002). Most recently, inducible expression of NF-L transgene in mice provides *in vivo* evidence that the stationary NF network in axons is pivotal to determine half-life and transport rate of NF proteins (Millecamps et al., 2007).

3.2 Generation of tetracycline regulatable cell lines with GFAP transgene

AxD is associated with heterozygous GFAP mutations, which encode proteins that are genetically dominant and presumably act in a gain-of-function mechanism (Brenner et al., 2001; Li et al., 2002). To date, the exact ratio of mutant to wild-type GFAP in AxD brains is unknown. Whilst it has been demonstrated that GFAP mutants alter filament solubility and stability (Hsiao et al., 2005; Perng et al., 2006), the critical ratio of mutant to wild-type protein leading to the disease remains unknown. Although transient transfection provides a quick and convenient way to analyse expressed GFAP mutant in cells, this does not allow critical steps before or after GFAP mutant expression to be studied. Therefore, I have selected physiologically relevant astrocytoma cells to generate cell lines in which GFAP expression can be regulated by Dox.

3.2.1 Generation of tetracycline-regulated U343 cell lines

3.2.1.1 Experimental strategy

U343 MG-A cell line stably transfected with Tet-Off gene expression system was kindly provided by Dr. J. T. Rutka (Division of Neurosurgery, University of Toronto, Canada). The pUHD15-1*neo* vector (Resnitzky et al., 1994) derived from pUHD15-1 (Gossen and Bujard, 1992) encodes the *E. coli* tTA (Fig. 3.1A), in which transcription of resistance-mediating genes is negatively regulated by the *tet*R. Regulation of Tet-Off system is achieved through tTA, a fusion protein consisting of *tet*R and VP16 activation domain. This hybrid protein binds specifically to the TRE and promotes transcription from the adjacent CMV promoter. Dox binds to tTA and thereby prevent its binding to the TRE. Thus, when dox is present in the cell culture medium, transcription of target gene is inhibited, whereas in its absence target gene expression is induced (Fig. 3.3A).

U343 MG-A cells were initially selected in growth medium containing α-MEM (Invitrogen, Paisley, UK) supplemented with 10% (v/v) FCS, 100 U/ml penicillin, 100 µg/ml streptomycin, 2 µM L-glutamine and 900 µg/ml geneticin (G418; Life Technologies, Inc.) (Tsugu et al., 2000). After selection, cells were maintained in growth medium containing 500 µg/ml of G418 (Melford Laboratories Ltd., Suffolk, UK).

To construct a Tet-regulated GFAP expression plasmid, wild type and R416W GFAP (Fig. 3.2C) were excised from pcDNA3.1(-) (Fig. 3.2B) and inserted into the *Nhe*I and *Eco*RV sites of pTRE2hyg vector (Fig. 3.2A), the Tet response vector (BD Biosciences, Palo Alto, CA), consisting of a multiple cloning site (MCS) immediately downstream of the TRE and *P*minCMV (Fig. 3.2A). The resulting plasmids, pTRE2hyg-WTGFAP and pTRE2hyg-R416WGFAP (Fig. 3.2D), encode a full-length GFAP cDNA under the control of the tTA dependent promoter. U343 MG-A Tet-Off cells grown in 10-cm^2 Petri dishes to 50-60%

confluency were transfected with either pTRE2hyg-WTGFAP or pTRE2hyg-R416WGFAP using the GeneJuice transfection reagent (Novagen) according to manufacturer's instructions.

Selection of stable cell lines was initiated two days post-transfection by 200 µg/ml hygromycin B (Duchefa Biochemie, Haarlem, The Netherlands). This concentration was selected based upon the sensitivy of U343 MG-A Tet-Off cells to hygromycin (Fig. 3.5). The culture medium was replaced at 12 hours intervals. Two to three weeks after selection, but before colony contacts had occurred, individual colonies were isolated using cloning cylinders (Sigma, Poole, UK), and harvested in 12-well plates. When cells reach ~90% confluency, colonies were transferred to 6-well plates, each cell clone was then split into three wells in a new 6-well plate. After retaining one well for propagation and characterisation, the other two were maintained in medium in the presence or absence of 2 µg/ml Dox (BD Biosciences, Palo Alto, CA). To induce GFAP expression, the cells were washed thoroughly with PBS before transferred to fresh growth medium lacking Dox. On the following day, the growth medium was changed to remove Dox completely. The selection medium containing Dox is changed every day to inhibit expression of GFAP. Selected clonal lines were cultivated in growth medium supplemented with 2 µg/ml Dox.

3.2.1.2 Generation and characterisation of R416W-specific antibodies

To screen for inducible expression of R416W GFAP, the insoluble pellets of each clonal lines, either uninduced or induced, were prepared for immunoblotting analysis using anti-R416W GFAP antibodies. Two monoclonal antibodies, clone 19.2 and 1A3, generated by the UAB Epitope Recognition Core using the mutation site centred on the immunogen, KTVEMWDGEVIK (Perng et al., 2006) were used for initial screening.

To validate 1A3 and 19.2 antibodies as the specific probes for R416W GFAP in selected clonal lines, purified recombinant human wild-type and R416W GFAP were first analysed by

(A)

(B)

(C)
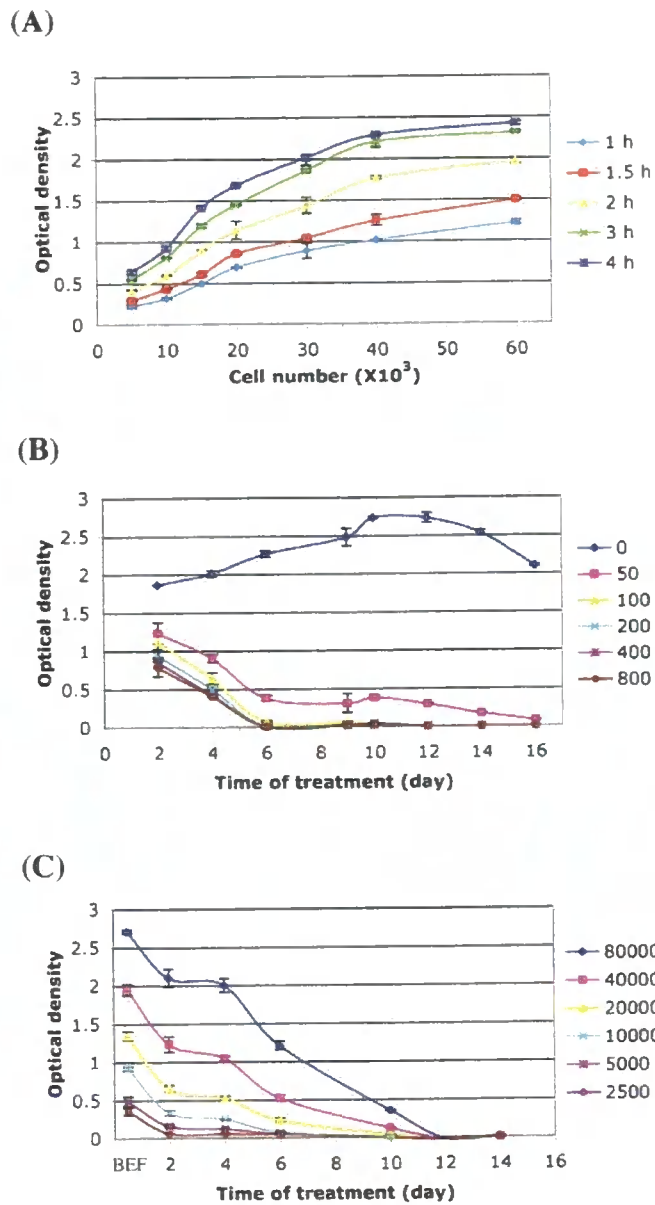
Figure 3.5. Hygromycin killing curves for U343 MG-A cells. (A) Standard curves for cell numbers. Various numbers (5,000, 10,000, 15,000, 20,000, 30,000, 40,000, 60,000) of U343 MG-A cells were grown in 96-well plates for 4 hours. At 100% confluency, cell number is ~20,000 per well in 96-well plate. Cell viability was analysed by MTS assay kit and measured at the indicated times. (B) Dose-response curves for hygromycin. 10,000 U343 MG-A cells were cultured in growth medium untreated or treated with different concentrations (50, 100, 200, 400, 800 µg/ml) of hygromycin for the indicated times. (C) Plating density-dependent curves for hygromycin. U343 MG-A cells were seeded at different numbers (80,000, 40,000, 20,000, 10,000, 5,000, 2,500) and untreated or treated with 200 µg/ml hygromycin for the indicated times. BEF, before treatment. Cell viability was determined by incubating cells in MTS reagent for 3 hours and represented as the measurement of mean ± SD at 490 nm. N = 3.

immunoblotting using anti-human GFAP antibody SMI-21 and anti-R416W GFAP antibodies

1A3 and clone 19.2 (Fig. 3.6A). The SMI-21 antibody recognised both wild-type and mutant

GFAP, whereas the 1A3 and 19.2 antibodies reacted with purified R416W GFAP. This

specificity is pivotal for distinguishing R416W GFAP in induced and uninduced R416W

GFAP-expressing cells for subsequent experiments.

To analyse the expression level and solubility of R416W GFAP in U343 MG-A cells, two

different extraction buffers were used. In the mild extraction protocol, cells were lysed on ice

for 15 minutes in the mild extraction buffer (MEB, 20 mM Tris-HCl, pH 7.4, 140 mM NaCl,

5 mM EDTA, 1 mM EGTA, 0.5% (v/v) NP-40 supplemented with Complete protease

inhibitor cocktail). In the more stringent extraction protocol, which was designed to test the

resistance of GFAP filaments and aggregates to buffer extraction, cells were lysed in 1 ml of

harsher extraction buffer (HEB, 20 mM Tris-HCl, pH 7.4, 140 mM NaCl, 5 mM EDTA, 1

mM EGTA, 1% (v/v) NP-40, 0.5% (w/v) sodium deoxycholate, supplemented with Complete

protease inhibitor cocktail. U343 MG-A cells (Fig. 3.6B) and the human breast cancer

epithelial MCF-7 cells (Fig. 3.6C) grown in 10-cm^2 Petri dishes were either left untransfected

(Fig. 3.6B and C, lanes 1 and 2) or transfected with wild-type (Fig. 3.6B and C, lanes 3 and 4)

or R416W GFAP (Fig. 3.6B and C, lanes 5 and 6). After extraction with MEB, cell lysates

were centrifuged and the resulting supernatant and pellet fractions were analysed by

immunoblotting. Whilst a small fraction of wild-type GFAP remained in the supernatant,

R416W GFAP was found exclusively in the pellet fraction. Analysis of both supernatant and

pellet fractions in MCF-7 cells revealed no endogenous GFAP expressed in untransfected

MCF-7 cells. Under the same extraction protocols, R416W GFAP was found again in the

pellet fraction of U343 MG-A cells transiently transfected with R416W GFAP. Similar results

were observed when HEB was used (Perng et al., 2006, see Fig. 9 in Appendix 5). As R416W

GFAP invariably remained in the pellet fractions after extraction, the pellet fraction prepared

(A)

Purified

WT R416W

←19.2

←1A3

←SMI-21

1   2

(B)

U343MG

-    WT   R416W

S P S P S P

←Total GFAP

←R416W GFAP

←Actin

1 2 3 4 5 6

(C)

MCF7

-    WT   R416W

S P S P S P

←GFAP

←Actin

1 2 3 4 5 6
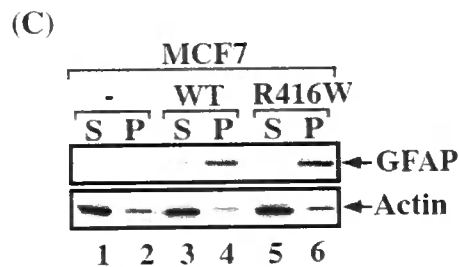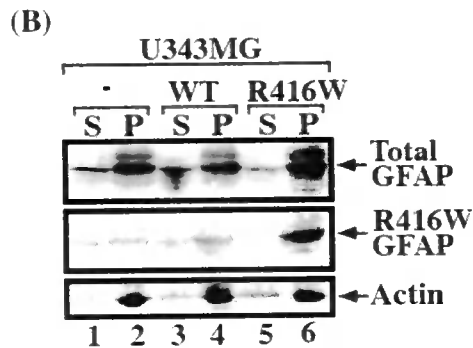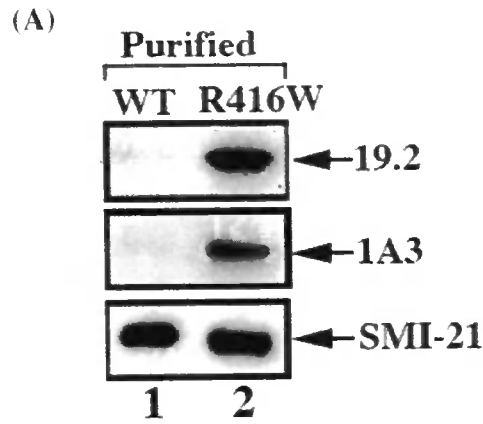
Figure 3.6 Characterisation of R416W-specific antibodies. Immunoblots of the purified recombinant human wild-type (WT) and R416W GFAP were probed with two monoclonal anti-R416W GFAP antibodies, 1A3 and 19.2 and a standard anti-GFAP antibody SMI-21. The anti-R416W GFAP antibodies produce signals from purified R416W GFAP only (A, lane 2), whereas the SMI-21 antibody reacts with both wild-type and R416W GFAP (A, lanes 1 and 2). Wild-type (B, lanes 3 and 4) and R416W GFAP (B, lanes 5 and 6) were transiently transfected into human astrocytoma U343 MG-A cells and lysed in MEB buffer (see section 3.2.1.2). The supernatant (S) and pellet (P) fractions prepared from these cultures were compared with untransfected cells (B, lanes 1 and 2). Immunoblots of cell fractions were probed with antibodies to human GFAP (SMI-21) and R416W GFAP (19.2 and 1A3). Notice that when transfected into this cell line, R416W GFAP was found exclusively in the pellet fraction (B, lane 6). MCF-7 cells were transfected with either wild-type (C, lanes 3 and 4) or R416W GFAP (C, lanes 5 and 6). Untransfected cells were used as a control (C, lanes 1 and 2). At 48 hours after transfection, the supernatant (S) and pellet (P) fractions were prepared and analysed by immunoblotting using anti-GFAP antibody. Most of the wild-type GFAP was detected in the pellet fraction (C, lane 4) with a small proportion remained in the supernatant fraction (C, lane 3), whereas R416W GFAP was found exclusively in the pellet fraction (C, lane 6). Equal loading of each supernatant and pellet fraction was confirmed by probing with anti-actin antibody.

from inducible cell lines will be analysed by immunoblotting in the subsequent studies.

3.2.1.3 Screening of U343 cell lines expressing R416W GFAP

Thirty-one clones were selected for screening of wild-type GFAP expression in U343 MG-A cell lines. Some clones had no detectable GFAP signals, whereas other clonal lines revealed similar GFAP levels between uninduced and induced cells (Fig. 3.7A). In addition, there are currently no antibodies available to distinguish the induced wild-type GFAP from the endogenous human GFAP in U343 MG-A cells. Therefore, a stable cell line with inducible expression of wild-type GFAP is not available for my studies.

Thirty-five clones were selected for screening of R416W-expressing cell lines. One clone was selected by its high R416W GFAP expression under induced conditions and low background in the uninduced conditions. This clonal line, 11/18cl1 that is designated here as U343-GFAP^{R416W}, displays well-regulated expression as shown by the increased level of R416W GFAP in the absence of Dox and suppression of expression in the presence of Dox (Fig. 3.7B, lower panel). Another twenty-four clones selected for screening did not show any R416W GFAP positive signals on blots in the presence or absence of Dox.

The use of the mutant-specific antibody also allowed me to determine the ratio of R416W GFAP to the endogenous level of GFAP in stable U343 MG-A cell lines. To distinguish R416W GFAP from the endogenous GFAP in U343 MG-A cells, cells were extracted with the cytoskeletal extaction buffer (20 mM Tris-HCl, pH 7.4, 140 mM NaCl, 5 mM EDTA, 1 mM EGTA, 1% (v/v) Triton X-100, 1.5 M KCl). After centrifugation, IF-enriched cytoskeletal fractions prepared from uninduced and induced U343-GFAP^{R416W} cells were separated by SDS-PAGE and either visualised by Coomassie Blue staining (Fig. 3.8A) or by immunoblotting with antibody specific to R416W GFAP (Fig. 3.8D). A prominent band
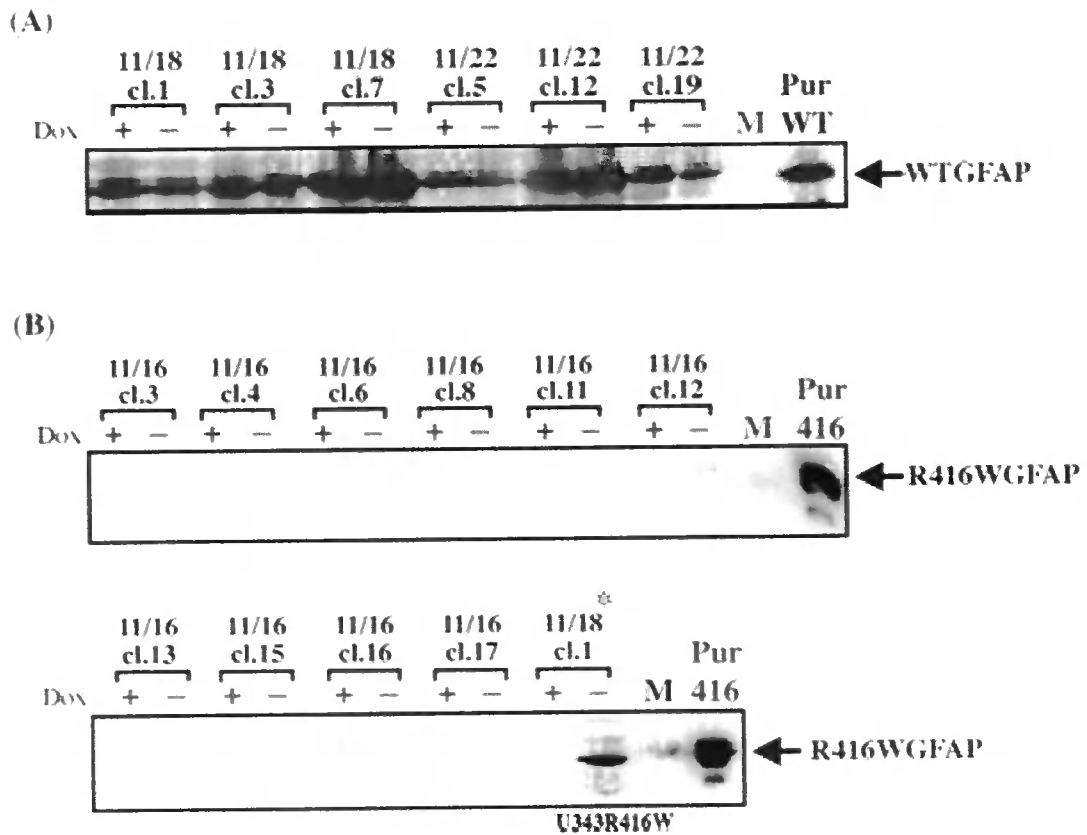
Figure 3.7. Screening of Dox-regulated stable transfectants for GFAP in Tet-Off human astrocytoma cells. U343 harboring wild-type (WT, A) and R416W (B) GFAP plasmid DNA cells were cultured in the absence or presence of 2 μg/ml Dox and harvested at confluency. After extraction in RIPA lysis buffer, the fractioned insoluble pellets were separated by SDS-PAGE and then analysed by immunoblotting using 3270 against wild-type GFAP and R416W GFAP specific antibody clone 19.2 to assess the expression level of R416W GFAP. M, marker. Pur WT, purified recombinant wild-type GFAP. Pur 416, purified recombinant R416W GFAP. Clones were marked as date-clone number. *, indicates the clone of U343-GFAPR416W cells was processed for further experiments. +Dox, uninduced GFAP expression. -Dox, induced GFAP expression.

(A)

Purified GFAP

1   0.5   0.25   0.125   (µg)   U343 (10%)

                       -    +   Dox

← Vim
← GFAP

1   2   3   4   5   6

├──── CBB ────┤

(D)

R416W GFAP

200   100   20   10   (ng)   U343

                  -    +   Dox

← R416W GFAP

1   2   3   4   5   6

├──── WB ────┤
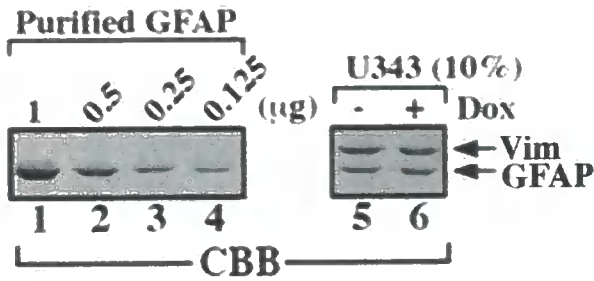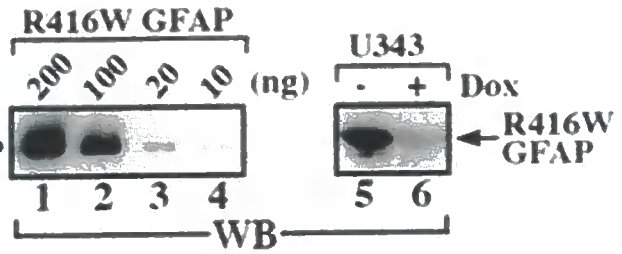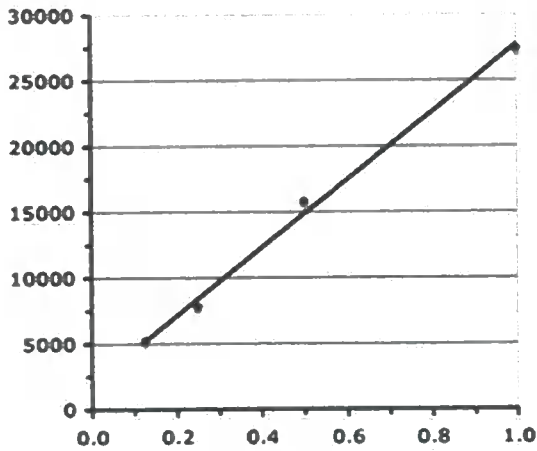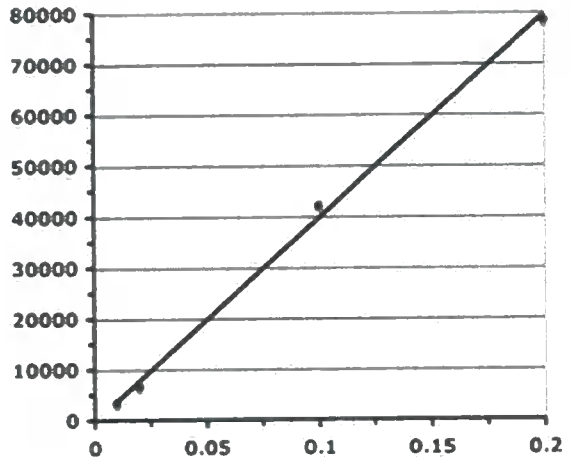
(C)

Optical Density	Total GFAP
27427	1.0 µg
15819	0.5 µg
7814	0.25 µg
5178	0.125 µg
8179 (10%)	0.24 µg
Total GFAP	2.4 µg

(F)

Optical Density	R416W GFAP
78549	200 ng
42119	100 ng
6625	20 ng
3425	10 ng
48550 (50%)	0.13 µg
R416W GFAP	0.26 µg
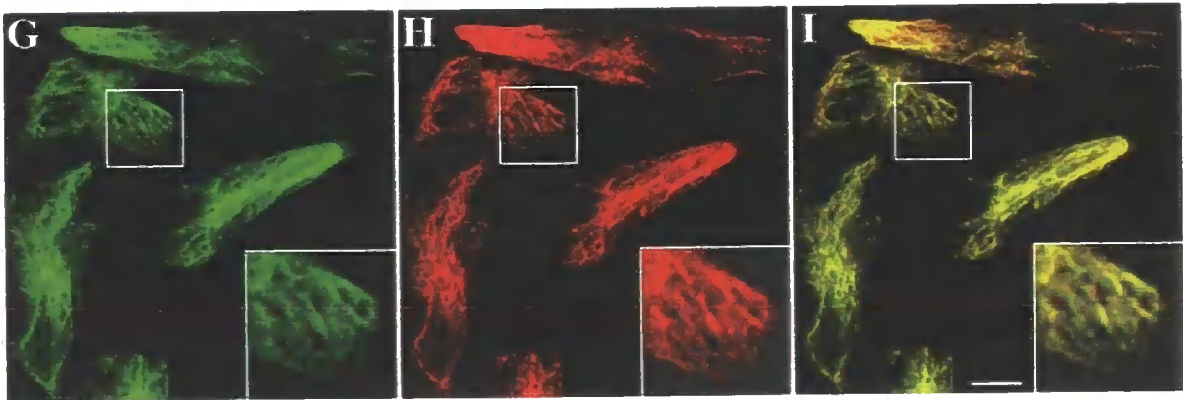
Figure 3.8. Expression of R416W GFAP in U343-GFAPR416W cells resulted in its incorporation into the endogenous GFAP networks. Expression of R416W GFAP in U343-GFAPR416W cells was induced by removal of Dox for 2 days. The cytoskeletal fractions prepared from induced (A and B, lane 5) and uninduced (A and B, lane 6) cells were separated by SDS-PAGE followed by Coomassie Brilliant Blue (CBB) staining (A) or immunoblotting (IB; D). Representative gel shows that vimentin and GFAP are major IF proteins in the cytoskeletal fractions (A, lanes 5 and 6). By immunoblotting, a prominent band corresponding to R416W GFAP was detected by 1A3 antibody in induced cells (D, lane 5), whereas it was barely detectable in uninduced cells (D, lane 6). The amounts of the total GFAP in the cytoskeletal fraction were determined by quantification of Coomassie Blue-stained gel using purified recombinant human GFAP as standards (A, lanes 1-4). The level of R416W GFAP in induced cells was determined by quantification of immunoblot using purified recombinant human R416W GFAP as standards (D, lanes 1-4). Quantification results were shown in (C) and (F). The distribution of R416W GFAP in relation to the endogenous GFAP networks was visualised by double label immunofluorescence microscopy using anti-R416W GFAP (1A3) and standard anti-GFAP (3270). When expressed in U343-GFAPR416W cells, R416W GFAP (G) integrated into the endogenous GFAP networks (H). Merged image showed the region of colocalisation between R416W GFAP and the endogenous GFAP appearing yellow (I), and the colocalisation of filament networks was magnified in inset. Bars = 10 μm.

corresponding to the R416W GFAP was detected in induced cells as revealed by the 1A3 antibody (Fig. 3.8D, lane 5), whereas this band was barely detectable in uninduced cells (Fig. 3.8D, lane 6). Quantification using purified GFAP as standards (Fig. 3.8B and E) revealed that although the induced U343-GFAP^{R416W} cells expressed 10 times more R416W GFAP than uninduced cells, this expression level is still only ~10% of the endogenous GFAP (Fig. 3.8C and F), indicating that the expression level of R416W GFAP is relatively low compared to the endogenous GFAP in U343-GFAP^{R416W} cells. The distribution of R416W GFAP in relation to the endogenous GFAP in GFAP^{R416W} cells was examined by double label immunofluorescence microscopy using antibodies to the R416W GFAP and the total GFAP. Whilst no R416W GFAP signal was detected in uninduced cells (data not shown), the expression of R416W GFAP (Fig. 3.8G) resulted in its incorporation into the endogenous GFAP networks (Fig. 3.8H) in induced U343-GFAP^{R416W} cells. Colocalisation of immunofluorescence signals between R416W GFAP and the endogenous GFAP network were shown in the merged image (Fig. 3.8I). These data suggest that R416W GFAP is capable of integrating into the endogenous GFAP networks when expressed at a low level.

3.2.1.4 Dose-dependent expression of R416W GFAP in U343-GFAP^{R416W} cells

To evaluate the Dox-dependent regulation of the R416W GFAP expression in U343-GFAP^{R416W} cells, insoluble fractions prepared from uninduced and induced cells were separated on SDS-PAGE followed by immunoblotting using the R416W GFAP-specific monoclonal antibody 1A3. The expression level of R416W GFAP decreased gradually as the Dox concentration increased (Fig. 3.9A). In particular, the level of R416W GFAP expressing in U343-GFAP^{R416W} cells in the presence of 1 μg/ml Dox (Fig. 3.9A, lane 3) was nearly half of that in untreated cells (Fig. 3.9A, lane 1) and its signal was undetectable in the presence of 2 μg/ml (Fig. 3.9A, lane 5) and 4 μg/ml Dox (Fig. 3.9A, lane 6). Therefore, U343-GFAP^{R416W}
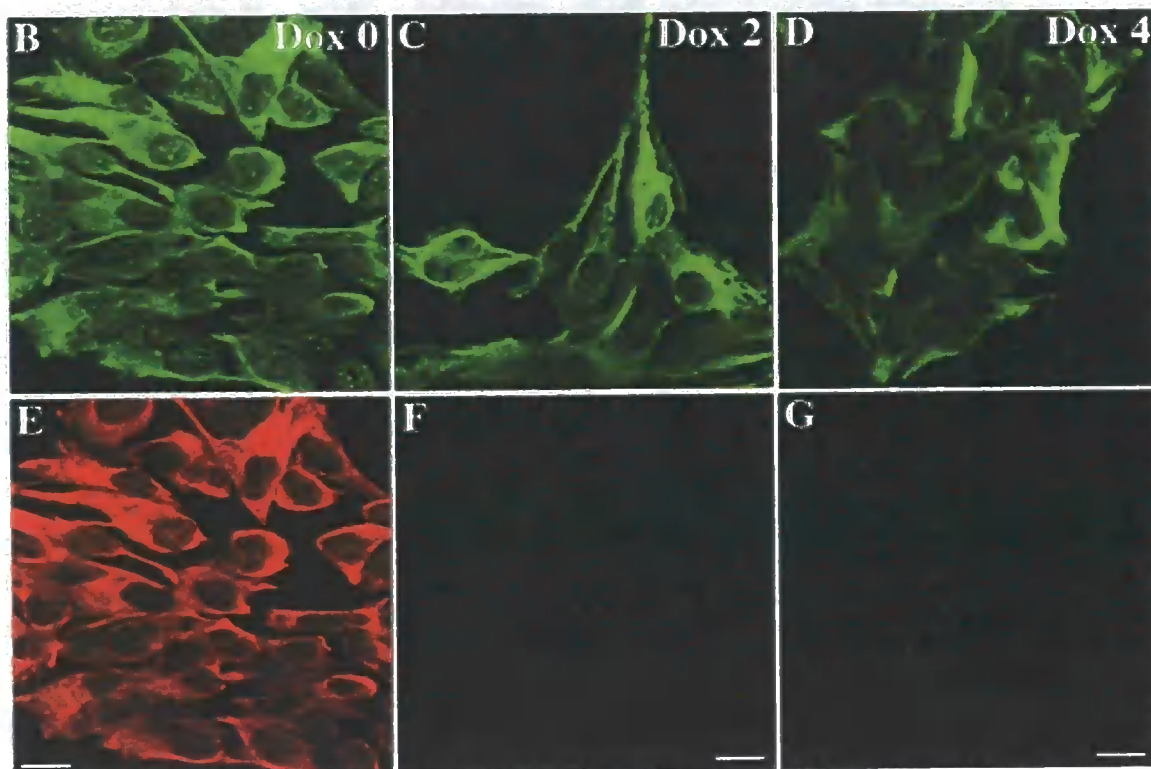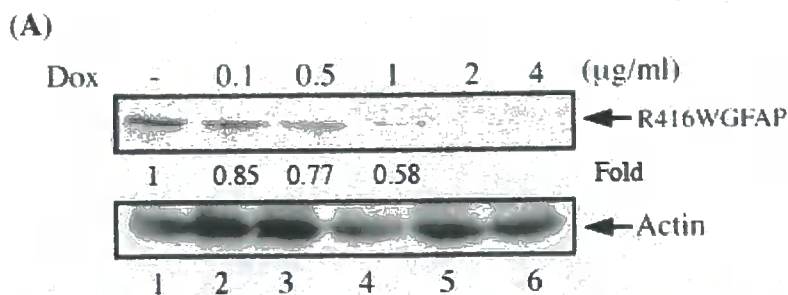
Figure 3.9. Regulation of R416W GFAP expression by Dox in U343-GFAPR416W cells. U343 stably expressing R416W GFAP cells were grown on 10-cm Petri dishes at the indicated Dox concentrations for 4 days. Cells were extracted with RIPA buffer, and the insoluble pellet fractions were subjected to SDS-PAGE followed by immunoblotting with anti-R416W GFAP antibody 1A3 (A). Notice the level of R416W GFAP decreased when Dox concentration increased. At 2 μg/ml Dox, R416W GFAP expression was completely inhibited (A, lane 5). The distribution of R416W GFAP in relation to the endogenous GFAP was visualised by double label immunofluorescence microscopy with use of antibodies to total GFAP (3270, green channel; B-D) and R416W GFAP (1A3, red channel; E-G). In induced U343-GFAPR416W cells (B and E), R416W GFAP expression (E) resulted in its incorporation into the endogenous GFAP networks (B), whereas no R416W GFAP signal was detected in uninduced cells cultured at 2 μg/ml Dox (F) or 4 μg/ml Dox (G). Bars = 10 μm.

cells were maintained in the 2 μg/ml Dox to completely inhibit R416W GFAP expression in the subsequent studies.

The expression and distribution of R416W GFAP in relation to the endogenous GFAP of U343-GFAP^{R416W} cells were examined by immunofluorescence confocal laser microscopy. U343-GFAP^{R416W} cells grown in the absence or presence of 2 and 4 μg/ml of Dox were dual labelled with antibodies to the R416W GFAP and total GFAP. The expression of R416W GFAP (Fig. 3.9E) in induced U343-GFAP^{R416W} cells resulted in its integration into the endogenous GFAP (Fig. 3.9B), whereas no R416W GFAP signal was detected in uninduced cells (Fig. 3.9F and G).

3.2.1.5 IF network organisation in transient and stable expression of R416W GFAP

The effect of R416W GFAP mutation upon GFAP network formation was investigated by transient transfection studies using U343 MG-A cells that express the endogenous GFAP and vimentin. When transfected into U343 MG-A cells, R416W GFAP showed multiple phenotypes including filamentous networks (Fig. 3.10A, arrow), filament bundles (Fig. 3.10A, arrowheads), or mixtures of cytoplasmic aggregates with or without small aggregates at the cell periphery (Fig. 3.10A, asterisks). In contrast, R416W GFAP mainly formed filamentous networks or filament bundles but not aggregates in induced U343-GFAP^{R416W} cells (Fig. 3.10D).

3.2.2 Generation of tetracycline-regulated U373 cell lines

3.2.2.1 Experimental strategy

The human astrocytoma U373 MG-A cells that express the endogenous GFAP were selected to generate stable cell lines with Tet-On gene expression system to mimic the scenario of R416W GFAP being expressed in a human astrocyte background. Regulation of
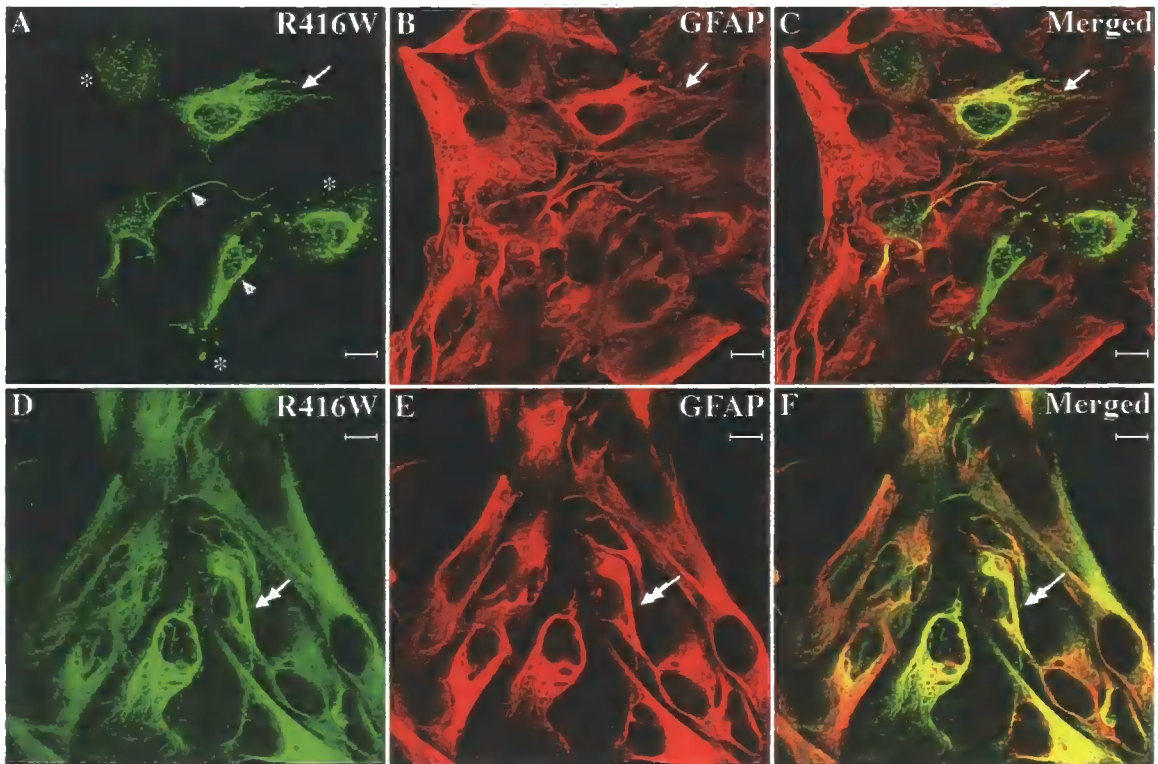
Figure 3.10. Transient and stable expressions of R416W GFAP in U343 MG-A cells. U343 MG-A cells were transiently transfected with R416W GFAP (A-C). At 48 hours after transfection, cells were processed for double label immunofluorescence microscopy with use of antibodies to R416W GFAP (1A3, A and D) and total GFAP (3270, B and E). Transient expression of R416W GFAP leads to several distinct IF structures. Most of the transfected cells formed perinuclear inclusions (A, arrowheads) with small aggregates distributed throughout the cytoplasm (A, asterisks). In some transfected cells, however, R416W GFAP (A, arrow) incorporated into the endogenous GFAP networks (B, arrow). Colocalisation of R416W GFAP and the endogenous GFAP signals appeared yellow (C, arrow). U343-GFAPR416W cells were induced by removal of Dox for 48 hours and then processed for immunofluorescence microscopy as described above. Expression of R416W GFAP in induced U343-GFAP R416W cells mainly formed extended filaments or filament bundles (D, double arrows) that colocalised with the endogenous GFAP (E and F, double arrows). Bars = 10 μm.

the system is achieved through rtTA, which binds the TRE and activates transcription in the presence of Dox (Fig. 3.3B). At 60-70% confluency, U373 MG-A cells were co-transfected with pTet-On and pTRE2hyg vector containing either wild-type or R416W GFAP cDNA. Two days post-transfection, stable cell lines were dual selected for 3~4 weeks with 1 mg/ml G418 and 400 μg/ml hygromycin B. The concentrations of G418 and hygromycin B employed for selection were determined from the killing curves with respect to the antibiotic concentration (Fig. 3.11A) and cell density (Fig. 3.11B). Antibiotic resistant colonies were selected with use of cloning cylinders and seeded on 12-well plates. At 90-100% confluency, each clone was transferred to 6-well plate followed by expansion in three wells in new 6-well plates. One plate of cells was for cell propagation and storage, and the other two plates of cells were used for screening of GFAP expression by immunoblotting. Cells were cultured in the absence or presence of 1 μg/ml Dox in the growth medium. At ~90% confluency, insoluble fractions were prepared from clonal lines by extraction with RIPA buffer followed by immunoblotting with use of antibodies to R416W GFAP or normal GFAP.

3.2.2.2 Screening of U373 cell lines expressing GFAP

Forty-two clones were selected for further analysis of inducible expression of wild-type GFAP in U373 MG-A cell lines. Insoluble pellet fractions (see section 2.7) prepared from these cell lines were analysed by immunoblotting using standard human GFAP antibody SMI-21 (Fig. 3.12A). Evaluation of the GFAP-positive signal from the blots revealed no significant difference in the expression levels between uninduced and induced cells, suggesting that induced U373 MG-A cells express wild-type GFAP at relative low level compared to the endogenous GFAP.

Thirty-eight clones were selected for screening of R416W GFAP expression and four clonal lines express detectable levels of R416W in the presence of Dox and low background
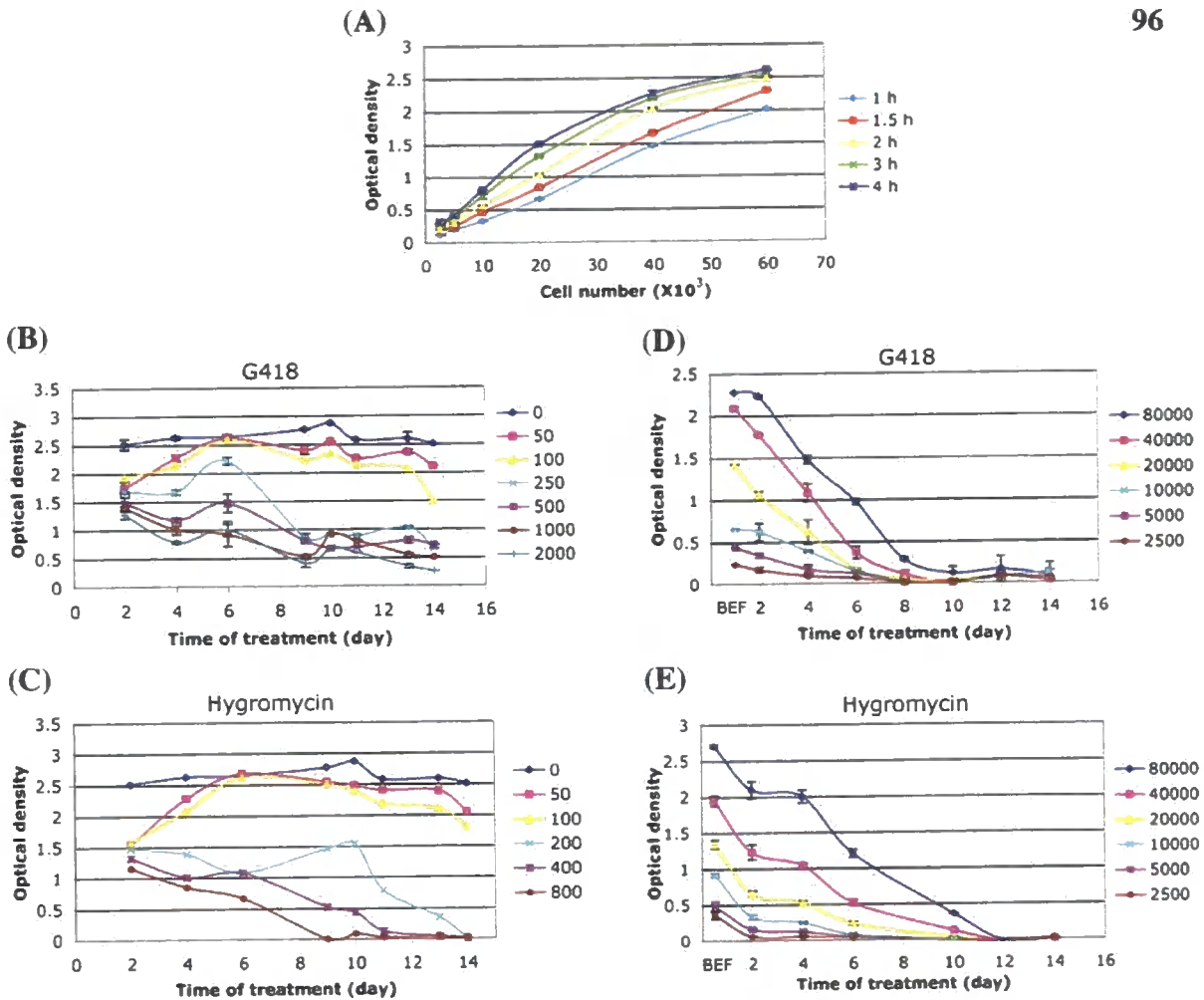
Figure 3.11. G418 and hygromycin killing curves for U373 MG-A cells. (A) Standard curve for cell cumbers. Varied numbers (2,500, 5,000, 10,000, 20,000, 40,000, and 60,000) of U373 MG-A cells were plated onto 96-well plates and incubated at 37°C for 4 hours. Cell number of ~40,000 reaches 100% confluency per well in 96-well plate. Cell viability was analysed by MTS for different incubation times as indicated. (B, C) Dose-response curves for G418 and hygromycin. 20,000 U373 MG-A cells were cultured in growth medium containing various concentrations (0, 50, 100, 250, 500, 1000, 2000 µg/ml) of G418 (B) or (0, 50, 100, 200, 400, 800 µg/ml) of hygromycin (C) for the indicated times. (D, E) The cell density-dependence for killing curves for G418 and hygromycin. U373 MG-A cells were seeded at different cell numbers (80,000, 40,000, 20,000, 10,000, 50,000 and 2,500) and untreated or treated with 1000 µg/ml G418 (D) or 800 µg/ml hygromycin (E) for the indicated times. BEF, before treatment. Cell viability was determined by MTS reagent after 4-hour incubation and expressed as mean ± SD at OD490. N = 3.

in its absence (Fig. 3.12B, asterisks). Among these clones, the 11/16-cl19 line (designated here as U373-GFAP^{R416W}) exhibited well-regulated expression of R416W GFAP in response to Dox and were selected for further characterisation.

3.2.2.3 Characterisation of U373 cell lines expressing R416W GFAP

U373-GFAP^{R416W} cells grown in the absence or presence of Dox were extracted with either RIPA buffer (Fig. 3.13A) or cytoskeletal extraction buffer (Fig. 3.13B). The insoluble pellet fraction (see section 2.7) and cytoskeletal fraction (see section 2.8) were separated by SDS-PAGE and visualised by Coomassie Blue staining. Analysis of the IF compositions revealed that whilst vimentin is the major IF protein in the cytoskeletal fractions, the endogenous GFAP expresses at a low level in selected U373-GFAP^{R416W} cell line. The cytoskeletal fractions were further analysed by immunoblotting with antibodies to R416W GFAP and human GFAP. Whilst the R416W GFAP level increased in induced cells (Fig. 3.13C, lanes 2 and 4), uninduced cells express low level of R416W GFAP as revealed by 1A3 antibody (Fig. 3.13C, lane 3).

The expression and distribution of R416W GFAP in relation to the endogenous GFAP of U373-GFAP^{R416W} cells were visualised by double label immunofluorescence microscopy with use of antibodies to R416W GFAP and human GFAP. The expression of R416W GFAP (Fig. 3.13D) in induced U373-GFAP^{R416W} cells resulted in its integration into the endogenous GFAP (Fig. 3.13E), whereas no R416W GFAP signal was detected in uninduced cells (Fig. 3.13G).

Although the expression level of R416W GFAP in the U373-GFAP^{R416W} cells can be monitored by the R416W GFAP-specific antibody, U373-GFAP^{WT} cell line is not available as a control for the U373-GFAP^{R416W} cells because no antibodies are currently available to specifically detect the induced wild-type GFAP. Therefore, I decided to develop stable cell

98
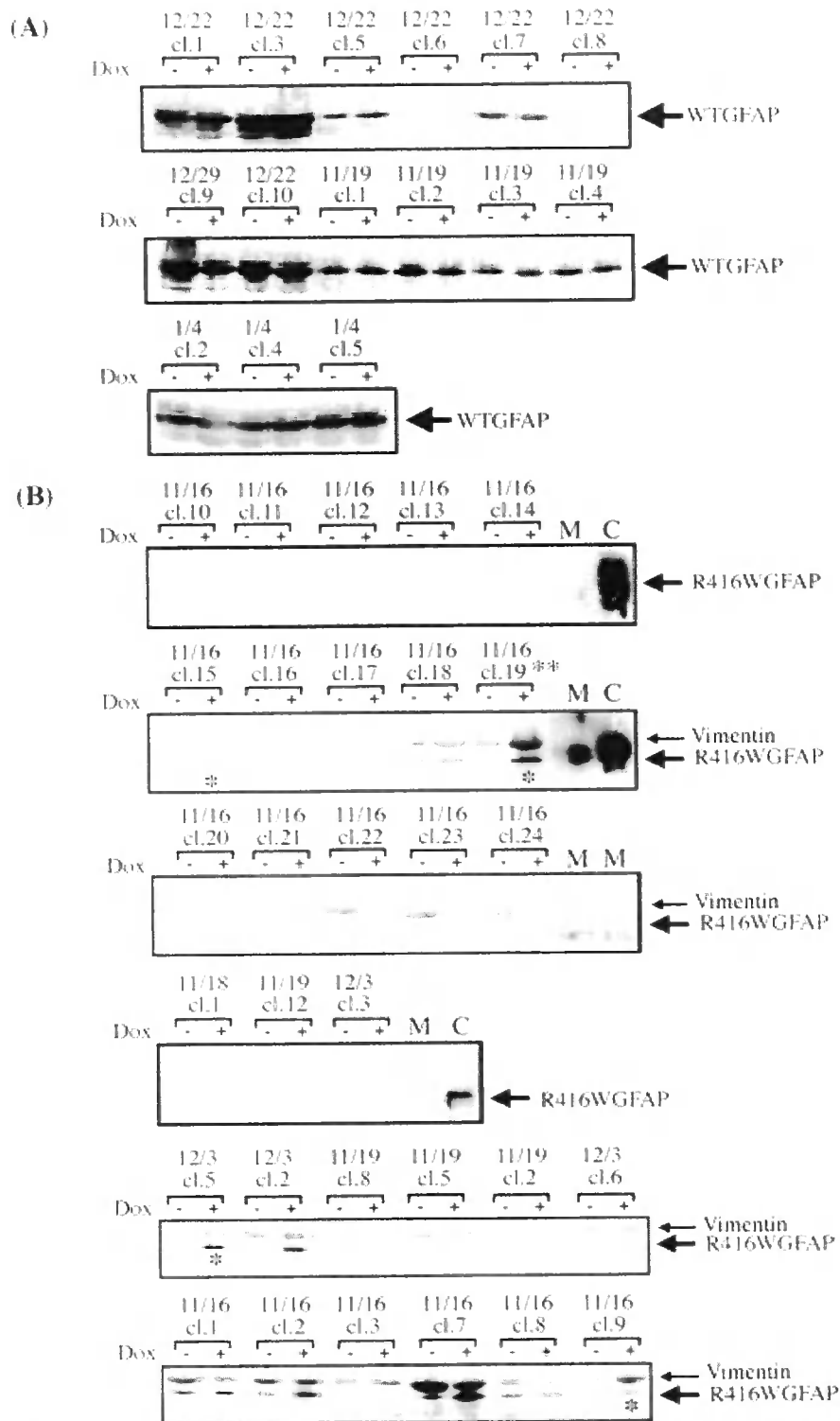
Figure 3.12. Screening of Dox-regulated stable transfectant for GFAP in Tet-On human astrocytoma cells. U373 MG-A containing wild-type and R416W GFAP DNA cells were cultured in the absence or presence of 1 µg/ml Dox, and harvested at confluency. Cells were lysed in RIPA buffer and the insoluble pellets were analysed by SDS-PAGE and immunoblotting using SMI-21 antibody (A) and anti-R416WGFAP clone 19.2 to detect wild-type and R416W GFAP (B) respectively. M, marker. C, purified recombinant R416W GFAP. Clones were marked as date-clone number. *, indicates the clones that show regulatable GFAP expression in the pesence and absence of Dox. **, indicates the clone of U373-GFAP R416W cells was processed for further experiments. -Dox, uninduced GFAP expression. +Dox, induced GFAP expression.

(A)

11/16
cl.19

Dox   -   +   M

Vim
GFAP
Actin

— 90
— 70
— 57
— 42

— 27
— 20

CBB

(B)

11/16
cl.19

Dox   -   +

Vim
GFAP
Actin

CBB

(C)

11/16cl.19

Dox   -   +   -   +

←— GFAP

1   2   3   4

IB   SMI-21   1A3

D   R416W

E   GFAP

F   Merged

G   R416W

H   GFAP
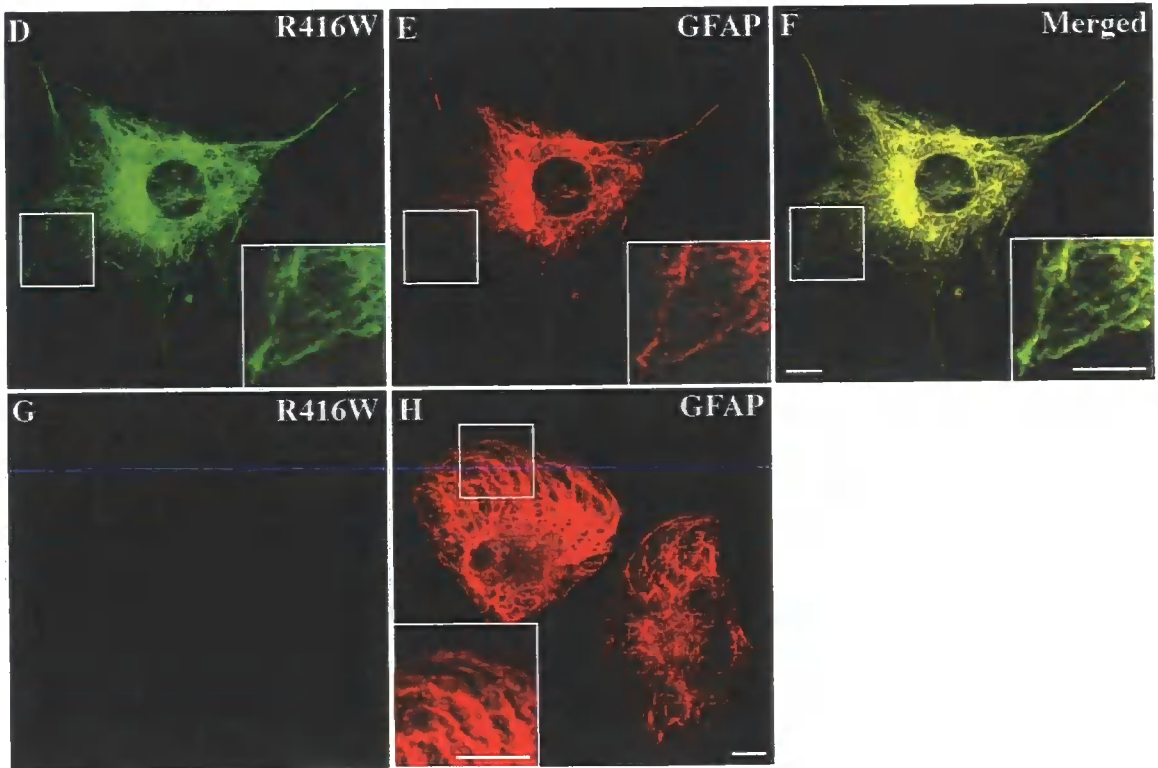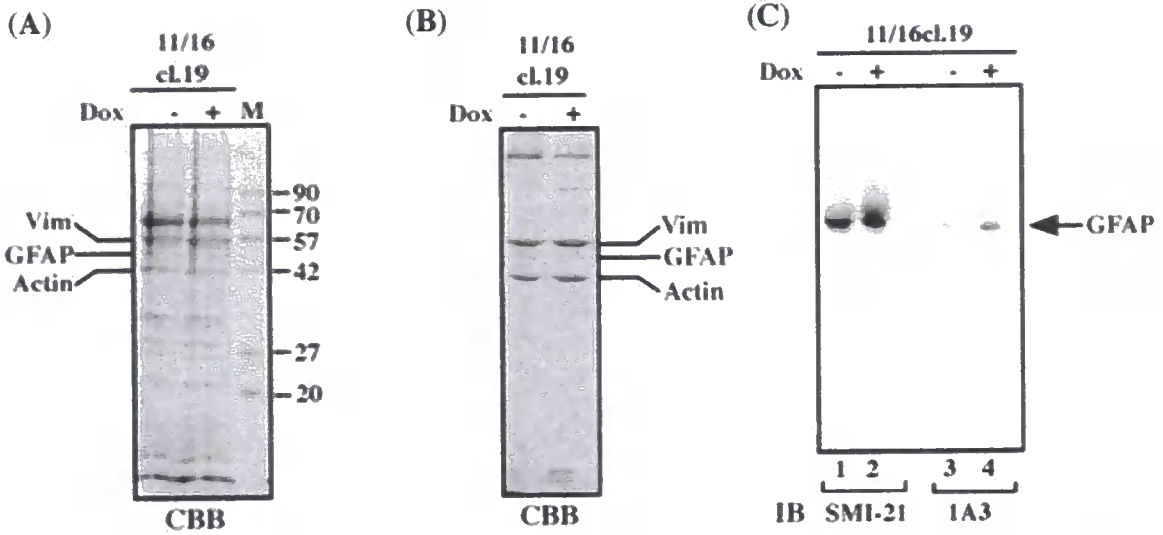
Figure. 3.13. Characterisation of Dox-regulated R416W GFAP-expressing U373 cell line. U373-GFAPR416W cells grown in the absence (-) or presence (+) of Dox were lysed in either RIPA buffer (A) or cytoskeletal extraction buffer (B). The insoluble pellet fraction and cytoskeletal fraction were analysed by SDS-PAGE and the gels stained with Coomassie Blue. The molecular weight of the marker proteins and the main cytoskeletal proteins are indicated. Vimentin is the major IF protein in U373 MG-A cells, whereas the GFAP level is relatively low. The cytoskeletal fractions were further analysed by immunoblotting with anti-human GFAP SMI-21 (C, lanes 1 and 2) and anti-R416W GFAP 1A3 antibodies (C, lanes 3 and 4). Whilst the levels of total GFAP in uninduced and induced cells are similar, R416W GFAP signal increased significantly in induced cells as revealed by 1A3 antibody. To follow the distribution of R416W GFAP, U373-GFAPR416W cells induced at 1 μg/ml Dox for 2 days were processed for double label immunofluorescence microscopy using antibodies to R416W GFAP (D and G) and normal human GFAP (E and H). After induction, R416W GFAP formed extended filaments (D) that colocalised with the endogenous GFAP networks (E and F). In contrast, no R416W GFAP staining was observed in uninduced cells (G). The detailed filamentous networks are magnified in insets (D, E, F and H). Bars= 10 μm.

lines expressing inducible levels of wild-type or R416W GFAP that could be monitored by available antibodies.

3.2.3 Generation of tetracycline-regulated DBT cell lines

3.2.3.1 Experimental strategy

The monoclonal anti-GFAP antibody SMI-21 developed by Sternberger Monoclonals specifically recognises human but not mouse GFAP, which provides an ideal tool to monitor the expression of human wild-type and mutant GFAP in a mouse background. For this reason, I selected mouse astrocytoma DBT cells to generate stable cell lines that express inducible levels of human wild-type and R416W GFAP.

To generate stable cell lines, DBT cells grown in 10-cm^2 Petri dishes to ~40-50% confluency were cotransfected with pTet-On (Fig. 3.1B) and pTRE2hyg vector containing cDNA encoding either wild-type or R416W GFAP (Fig. 3.2D). Regulation of the Tet-On gene expression system is achieved through rtTA, which binds to the TRE and activates transcription in the presence of Dox (Fig. 3.3B).

DBT cells were cotransfected with pTet-On and either pTRE2hyg-WTGFAP or pTRE2hyg-R416WGFAP. Two days after transfection, cells were dual selected with 1 mg/ml G418 and 800 μg/ml hygromycin B for one to two weeks. The concentrations of G418 and hygromycin B used for selection were determined by generating killing curves for each of the two antibiotics with respect to concentration (Fig. 3.14A) and cell density (Fig. 3.14B). After selection, antibiotic-resistant cell colonies were isolated using cloning cylinders and cultured in 6-well plates. Once the cells reach ~80-90% confluency, each cell clone was split into three separated wells in 6-well plates, one for cell propagation and the other two for growing in the absence or presence of Dox. Medium containing Dox was changed every two days to maximise the effect of the inducer.

101

(A)

(B)

(C)

(D)

(E)
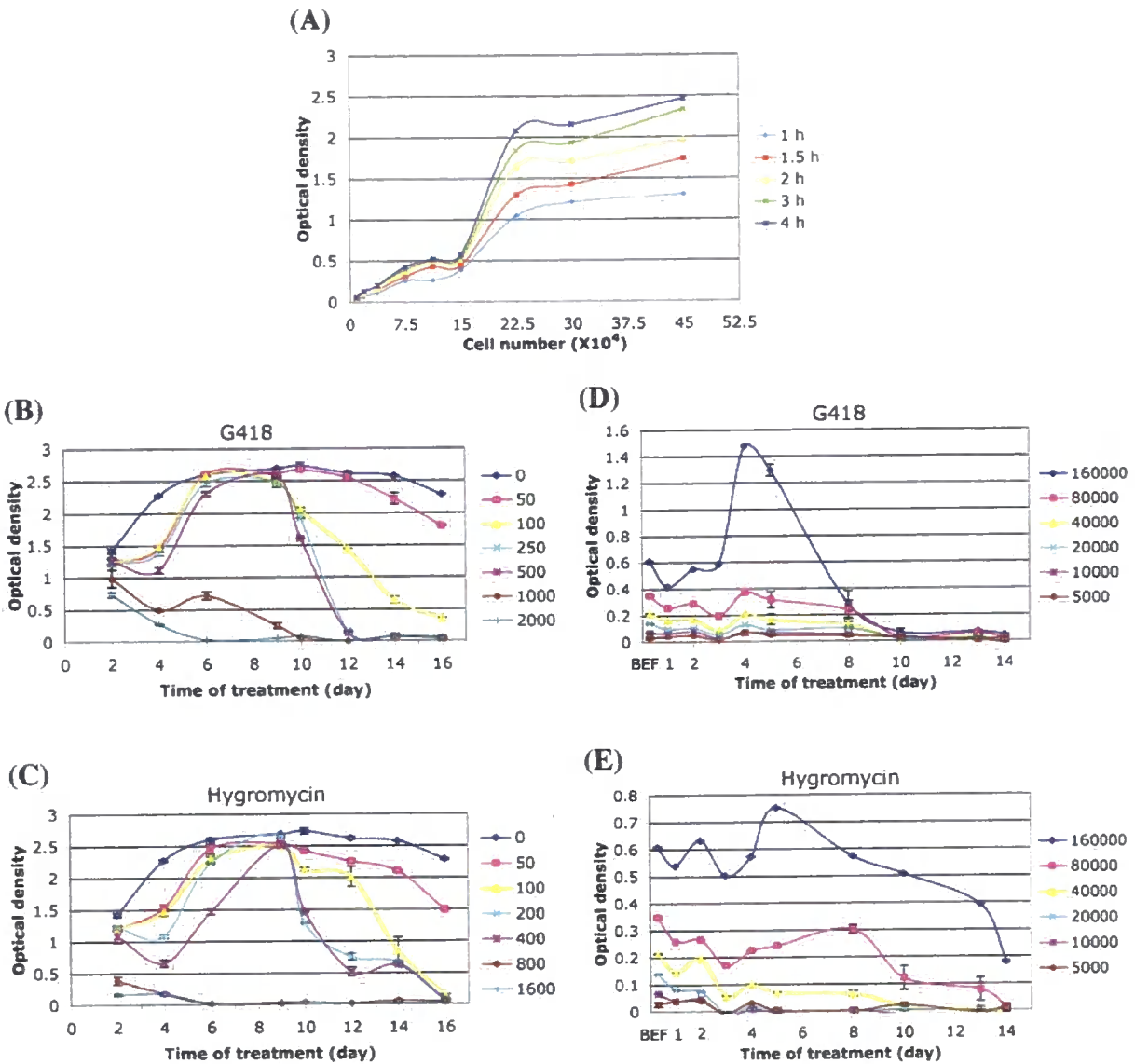
Figure 3.14. G418 and hygromycin killing curves for DBT cells. (A) Standard curve for cell numbers. Different numbers (9,400, 18,800, 37,500, 75,000, 112,500, 150,000, 300,000, and 450,000) of DBT cells were seeded onto 96-well plates for 4 hours. Cell number at ~150,000 show 100% confluency in a well of 96-well plate. Cell viability was determined by MTS and analysed at the indicated times for incubation. (B, C) Dose-response curves for G418 and hygromycin. 20,000 cells were cultured in growth medium containing various concentrations (0, 50, 100, 250, 500, 1000, 2000 µg/ml) of G418 (B) or (0, 50, 100, 200, 400, 800, 1600 µg/ml) of hygromycin (C) for the indicated times. (D, E) Plating density-dependent curves. Cells were seeded at different numbers (160,000, 80,000, 40,000, 20,000, 10,000, and 5,000) and untreated or treated with 1000 µg/ml G418 (D) or 800 µg/ml hygromycin (E) for the indicated times. BEF, before treatment. Cell viability was assessed after four hours of incubation in MTS reagent and represented as mean ± SD by OD_{490}. N = 3.

3.2.3.2 Screening of DBT cell lines inducibly expressing wild-type and R416W GFAP

Before screening DBT cell lines, transient transfection was performed to analyse the expression level and solubility of human GFAP in a mouse background. DBT cells transfected with human wild-type or R416W were solubilised in RIPA extraction buffer and the resulting supernatant (S) and pellet (P) fractions were analysed by immunoblotting using anti-human GFAP antibody SMI-21. When expressed in DBT cells, both wild-type and R416W GFAP were found exclusively in the pellet fraction (Fig. 3.15A). The presence of R416W GFAP in the pellet fraction was confirmed by blotting with anti-R416W GFAP antibody 1A3 (Fig. 3.15B). As human wild-type and mutant GFAP were invariably found in the pellet fraction of DBT cells after extraction, the pellet fraction will be analysed in the subsequent studies (section 3.2.3.3 and 3.2.3.4).

The expression and distribution of both wild-type and R416W GFAP in transiently transfected DBT cells were examined by double label immunofluorescence microscopy. The monoclonal antibody that specifically recognises human GFAP was used to distinguish transfected human GFAP and endogenous mouse GFAP. When expressed in these cells, wild-type GFAP formed filament bundles (Fig. 3.15D), which were largely colocalised with the endogenous GFAP networks (Fig. 3.15C). In contrast, R416W GFAP mainly formed filamentous bundles (Fig. 3.15G, arrowhead) and aggregates (Fig. 3.15G, asterisk), which often collapsed the endogenous IF networks (Fig. 3.15F).

Forty-four wild-type GFAP clones and fifty-two R416W GFAP clones were selected for screening. Among these clones, three wild-type GFAP DBT cell lines and six R416W GFAP cell lines exhibiting high inducible GFAP expression and low background levels when uninduced were selected (Fig. 3.16, asterisks).
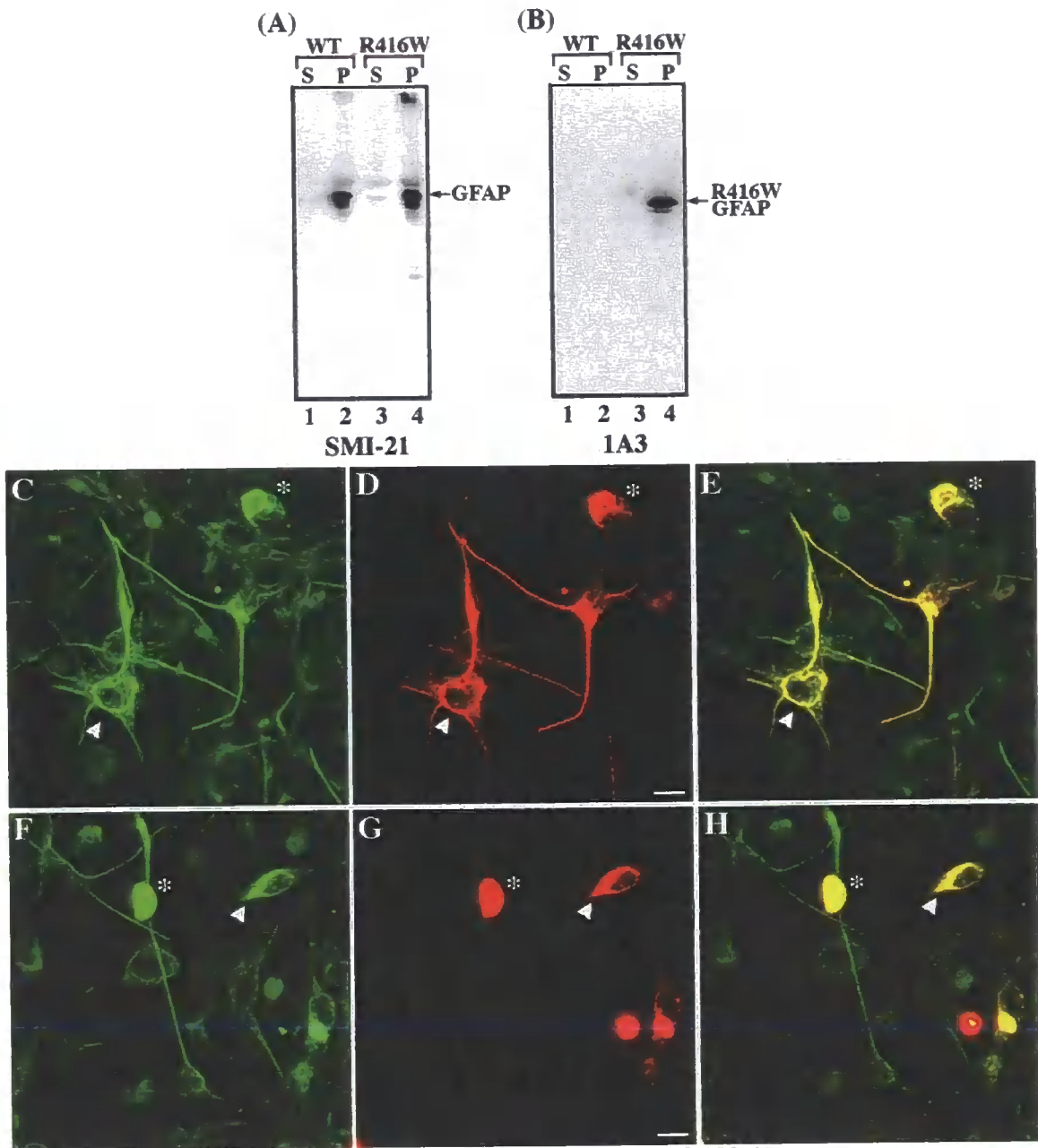
Figure 3.15. Analysis of wild-type and R416W GFAP expression in transiently transfected DBT cells. DBT cells were transiently transfected with either wild-type or R416W GFAP. At 48 hours after transfection, cells were extracted with RIPA buffer and the resulting supernatant (S) and pellet (P) fractions were subjected to immunoblotting analysis with SMI-21 antibody to human GFAP (A) and 1A3 antibody against R416W GFAP (B). Nearly all of the wild-type and R416W GFAP were found in the pellet fractions (P). The presence of R416W GFAP in the pellet fraction was confirmed by probing with anti-R416W GFAP antibody (B). To examine effect of human GFAP expression upon filament networks in mouse cells, DBT cells transiently transfected with wild-type (C-E) or R416W (F-H) GFAP were processed for double label immunofluorescence microscopy using anti-human GFAP antibody (SMI-21) and standard anti-GFAP antibody (3270). When transfected into these cells, wild-type GFAP (D) formed filament bundles that colocalised with the endogenous GFAP (C) networks, whereas R416W GFAP (G) formed cytoplasmic aggregates that often collapsed the endogenous GFAP networks (F). Merged images show the regions of colocalisation between human and mouse GFAP appearing yellow (E and H). Bars = 10 μm. Arrowhead, filamentous bundle. Asterisk, aggregate.
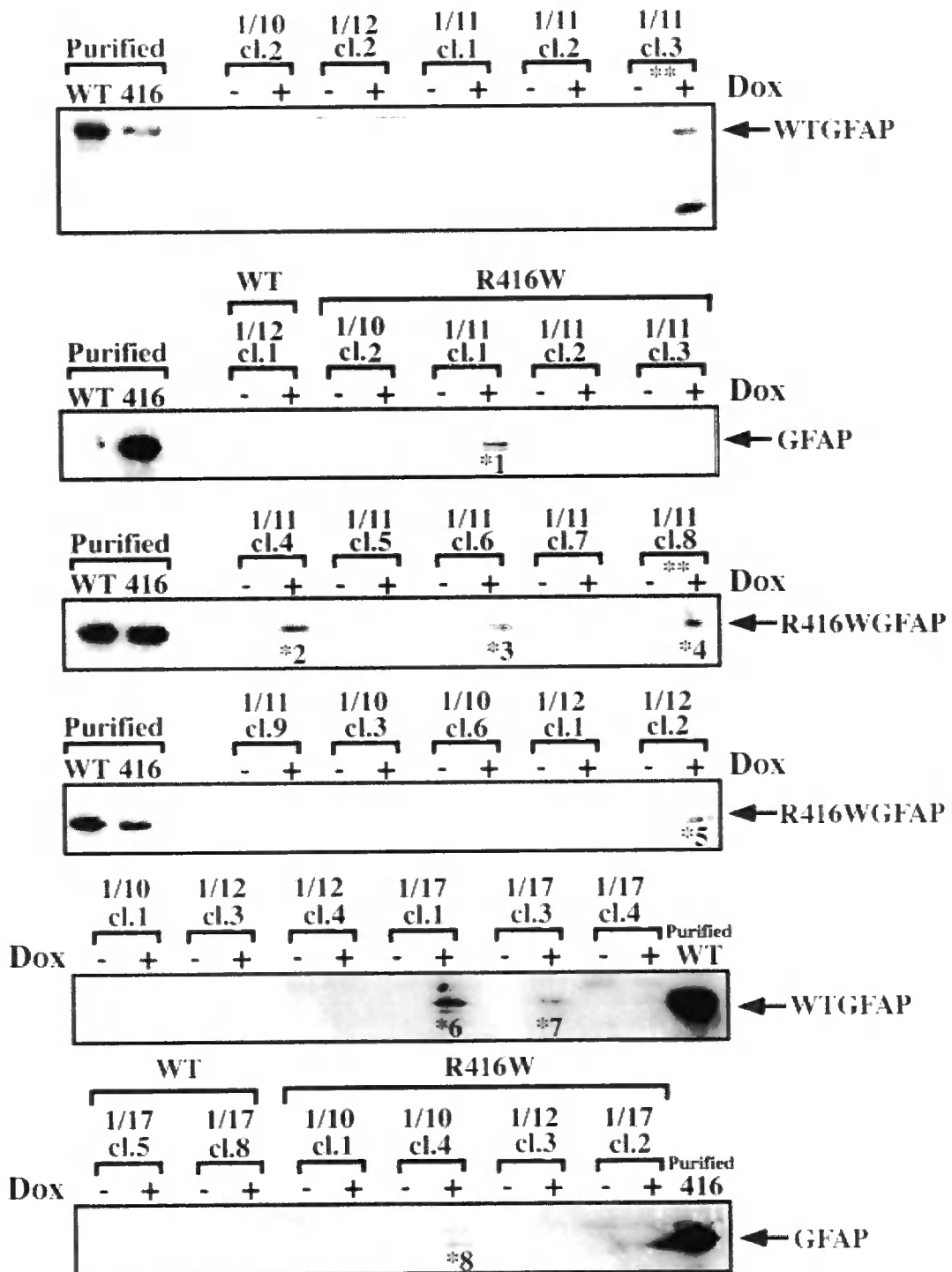
Figure 3.16. Screening of Dox regulated stable transfectants of human GFAP in Tet-On mouse astrocytoma cells. DBT generated wild-type (WT) and R416W GFAP expressing cells were grown in the absence or presence of 1 µg/ml Dox to reach confluency. Cell were harvested and lysed in RIPA buffer. The insoluble pellets were separated by SDS-PAGE and analysed by immunoblotting using SMI-21 antibody against human GFAP. Clones were marked as date-clone number, for example, 1/11cl.3 and 1/11cl.8. *, indicates clones that show regulated GFAP expression in the presence or absence of Dox. **, indicates clones designated as DBTWT and DBTR416W cells in further experimental procedures. -Dox, uninduced GFAP expression. +Dox, induced GFAP expression. Purified WT, purified recombinant WT GFAP. Purified 416, purified recombinant R416W GFAP.

3.2.3.3 Characterisation of DBT cell lines expressing wild-type or R416W GFAP

Two clonal lines of DBT cells expressing wild-type GFAP and R416W GFAP were selected for further characterisation. DBT wild-type and R416W GFAP cell lines were grown in the absence or presence of Dox for four days. Cells were then extracted with RIPA buffer (Fig. 3.17A) or cytoskeletal extraction buffer (Fig. 3.17B), and the insoluble fractions (see section 2.7) and the cytoskeletal fractions (see section 2.8) were separated on SDS-PAGE followed by Coomassie Blue staining. In these DBT cell lines, vimentin is the major IF protein in the pellet fractions, whereas the GFAP level is relatively low and barely detectable by Coomassie Blue staining. The cytoskeletal fractions of the DBT wild-type or R416W GFAP cell lines were further analysed by immunoblotting using antibodies to R416W GFAP and human GFAP (Fig. 3.17C and D). Whilst DBTWTcl.1 (Fig. 3.17C, lanes 1 and 2) and DBTR416Wcl.1 (Fig. 3.17D, lanes 1 and 2) exhibit either low GFAP expression in the induced states (Fig. 3.17C, lane 2, asterisk) or high background in the uninduced states (Fig. 3.17D, lane 1, asterisk), DBTWTcl.3 (Fig. 3.17C, lane 4, GFAP) and DBTR416Wcl.8 (Fig. 3.17D, lanes 4, GFAP) are well-regulated in response to Dox with a nearly undetectable background level in the uninduced condition (Fig. 3.17C and D, lane 3, asterisks). The DBTWTcl.3 designated as DBT-GFAP^{WT} cells and the DBTR416Wcl.8 designated as DBT-GFAP^{R416W} cells are used for my subsequent experiments.

3.2.3.4 Dose-dependent expression of GFAP in DBT-GFAP^{WT} and DBT-GFAP^{R416W} cells

DBT-GFAP^{WT} and DBT-GFAP^{R416W} cells were cultivated for 2 days in the absence or presence of Dox at concentrations as indicated. After cell fractionation, the insoluble fractions from DBT-GFAP^{WT} and DBT-GFAP^{R416W} cells were analysed by immunoblotting using GFAP antibody SMI-21 that specifically recognises human GFAP. After induction of DBT-GFAP^{WT} and DBT-GFAP^{R416W} cells, both wild-type (Fig. 3.18A) and R416W GFAP (Fig.
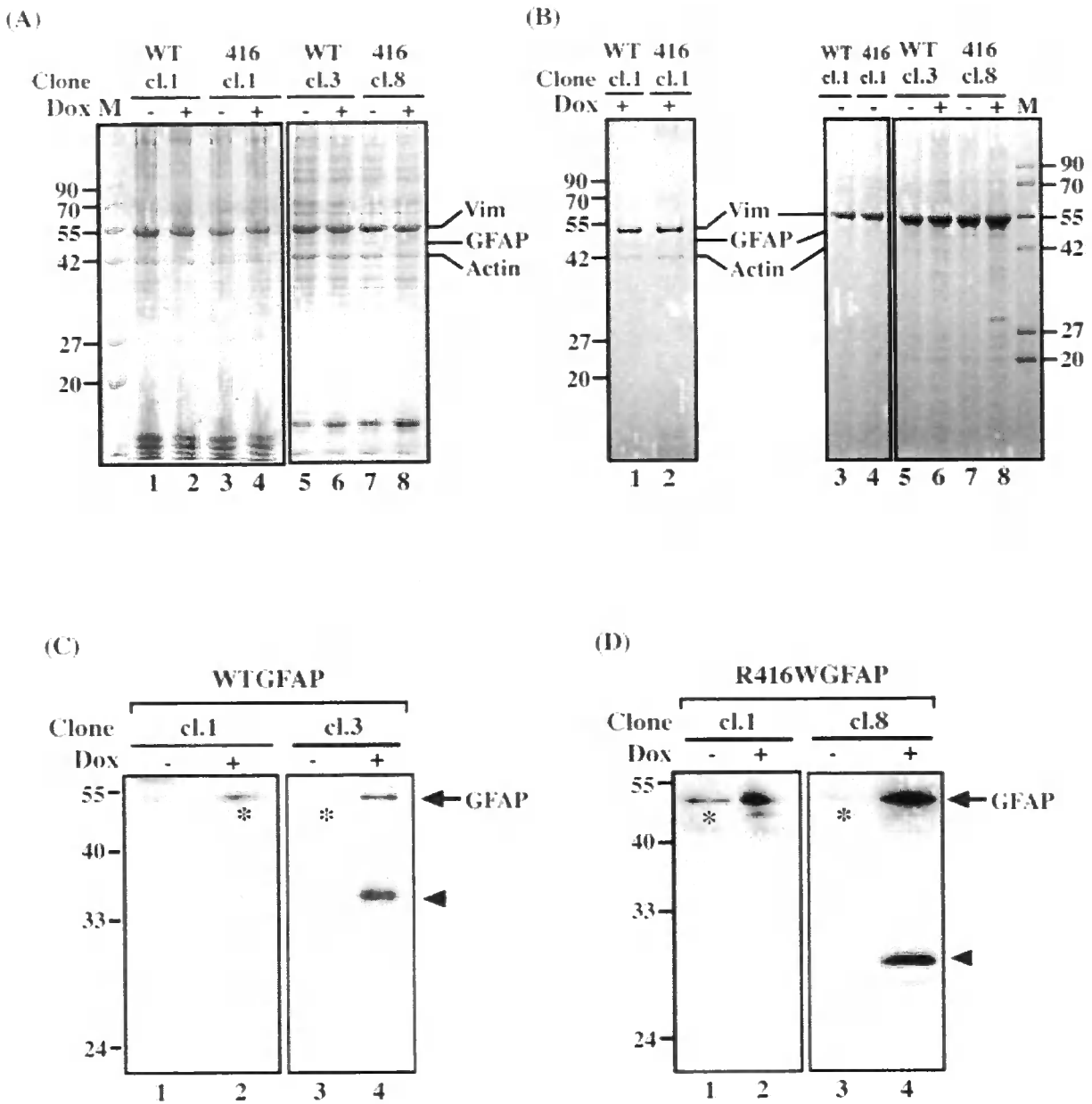
Figure 3.17. Characterisation of GFAP expression in Dox regulatable DBT cells. DBT stably expressing wild-type (WT) and R416W GFAP cells were cultured in the absence or presence of 1 μg/ml Dox for 4 days. (A) Cells were lysed in RIPA buffer. The insoluble pellets were analysed by SDS-PAGE and detected by Coomossie Brilliant Blue. (B) Cells were lysed in cytoskeletal extraction buffer. The cytoskeletal fractions were resolved on SDS-PAGE and stained with Commossie Brilliant Blue. The induction of human wild-type (C) and R416W (D) GFAP in the cytoskeleton fractions was further assessed by immunoblotting analysis using SMI-21, human specific antibody. The clones chracterised here represent the clones selected from screening in Fig. 3.14. WT cl.1, 1/17cl.1; WT cl.3, 1/11cl.3; R416W cl.1, 1/11cl1; R416W cl.8, 1/11cl.8. WT cl.3 and R416W cl.8 are utilised to process further experiments, as the induced expression of GFAP in these clones appear regulated by adding Dox.

3.19A) expression increased in a dose-dependent manner. Analysis of full-length wild-type

GFAP expression demonstrated a 2.6, 4.3, 6.6 and 8.8 fold increase in DBT-GFAP^{WT} cells

induced at 0.1, 0.5, 1 and 2 µg/ml of Dox, respectively (Fig. 3.18B). A similar increase in the

expression of full length R416W GFAP was observed in DBT-GFAP^{R416W} cells (Fig. 3.19B).

When induced at higher Dox concentrations, both DBT-GFAP^{WT} and DBT-GFAP^{R416W} cells

produced proteolytic GFAP fragments. To visualise the total IF proteins and distinguish

endogenous from exogenous GFAP, cytoskeletal fractions isolated from uninduced or induced

DBT stable cell lines were separated by a 6-15% gradient SDS-PAGE followed by Coomassie

Blue staining (Fig. 3.20). Quantification of the Coomassie blue-stained gel shows the relative

expression levels of human wild-type and R416W GFAP are 97% and 84%, respectively, to

the endogenous mouse GFAP. The induction of human GFAP and mouse GFAP were also

confirmed by immunoreactivity with both SMI-21 antibody and 3270 GFAP antibody (Fig.

3.20). Although the expression levels of human GFAP in induced DBT cells were similar to

the endogenous levels of mouse GFAP, this was equivalent to ~10% of the endogenous

levels of vimentin. Therefore, the expression levels of both human wild-type and R416W

GFAP are relatively low compared to the total IF proteins in DBT-GFAP^{WT} and DBT-

GFAP^{R416W} cells.

The expression and distribution of wild-type and mutant GFAP expression in stable DBT

cell lines were visualised by immunofluorescence microscopy with SMI-21 antibody specific

to the human GFAP. After induction, wild-type GFAP formed filaments as well as aggregates

in DBT-GFAP^{WT} cells, and the proportion of cells in which aggregates were formed in the

cytoplasm increases in a does-dependent manner (Fig. 3.18H). In DBT-GFAP^{R416W} cells

induced at 0.1 (Fig. 3.19D) and 0.5 µg/ml (Fig. 3.19E) of Dox, ~60% and ~90% of them

contained GFAP-positive aggregates (Fig. 3.19H). Further increases in Dox concentrations

did not increase the proportion of aggregates formed in DBT-GFAP^{R416W} cells. Therefore, the
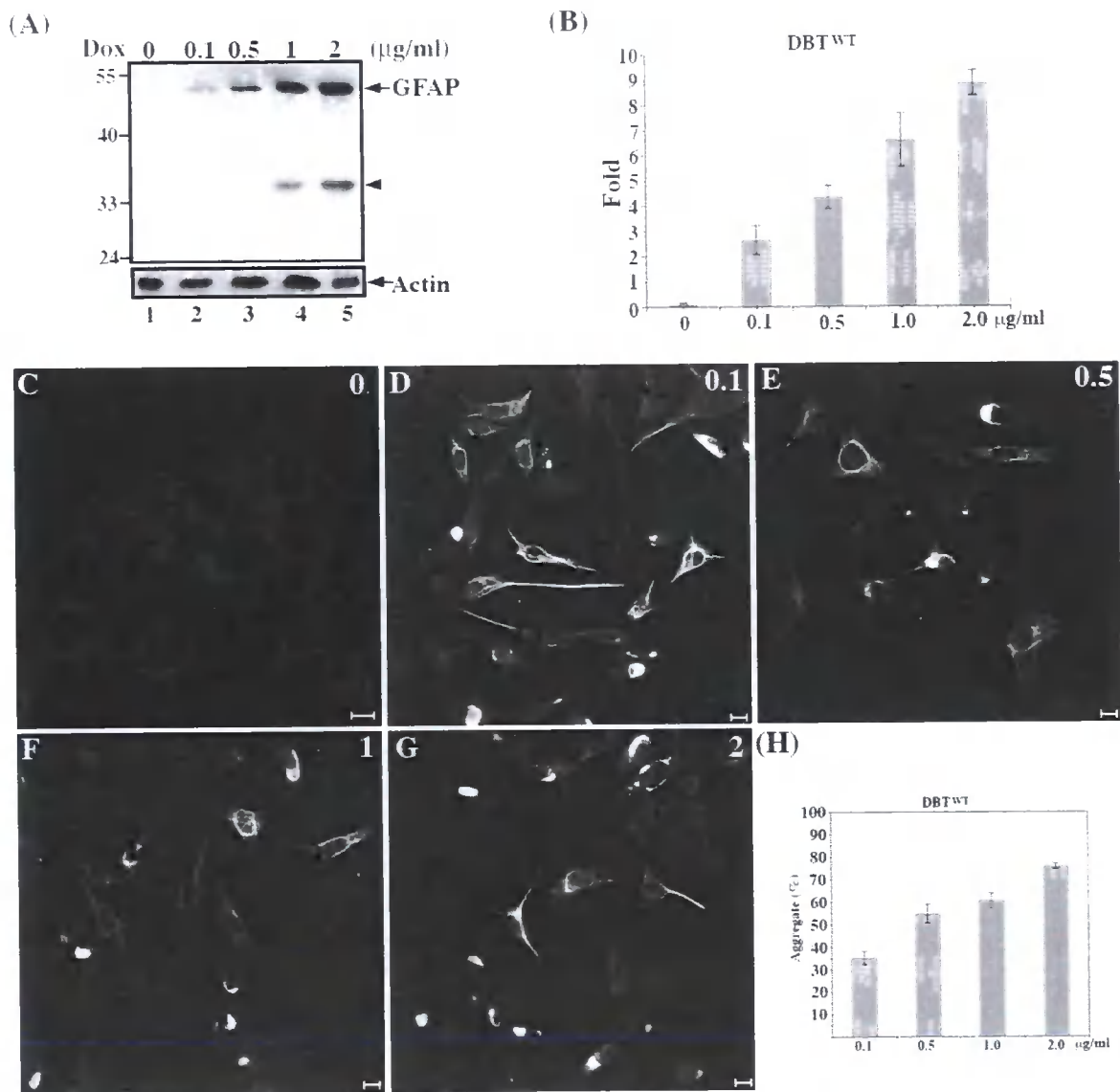
Figure 3.18. Characterisation of DBT-GFAPWT cells. DBT stably expressing wild-type GFAP cells were induced at the indicated Dox concentrations. Four days after induction, the insoluble pellet fractions were analysed by immunoblotting using anti-human GFAP SMI-21 antibody. Representative blots show that the levels of wild-type GFAP (A) are regulated by Dox in a dose-dependent fashion. Equal loading of each protein sample was confirmed by immunoblotting with the anti-actin antibody. The positions of GFAP and actin are indicated. Arrowhead indicated likely GFAP proteolytic fragments. The expression levels of wild-type GFAP were quantified as described in section 2.10. Quantification of the full length wild-type GFAP from three independent experiments are shown as mean ± SD and represented as bar charts (B). Fold changes are expressed in arbitrary units relative to non-induced controls. For immunofluorescence microscopy, DBT-GFAPWT cells were induced at indicated Dox concentrations for 4 days and the distribution of wild-type GFAP was examined by using SMI-21 antibody for human GFAP. Representative images show the distribution of wild-type GFAP induced at the indicated Dox concentrations (C-G). Bars = 10 µm. Cells immunopositive for GFAP were scored for the presence of GFAP-positive aggregates. The average mean ± SD of three independent experiments are shown as bar charts (H).
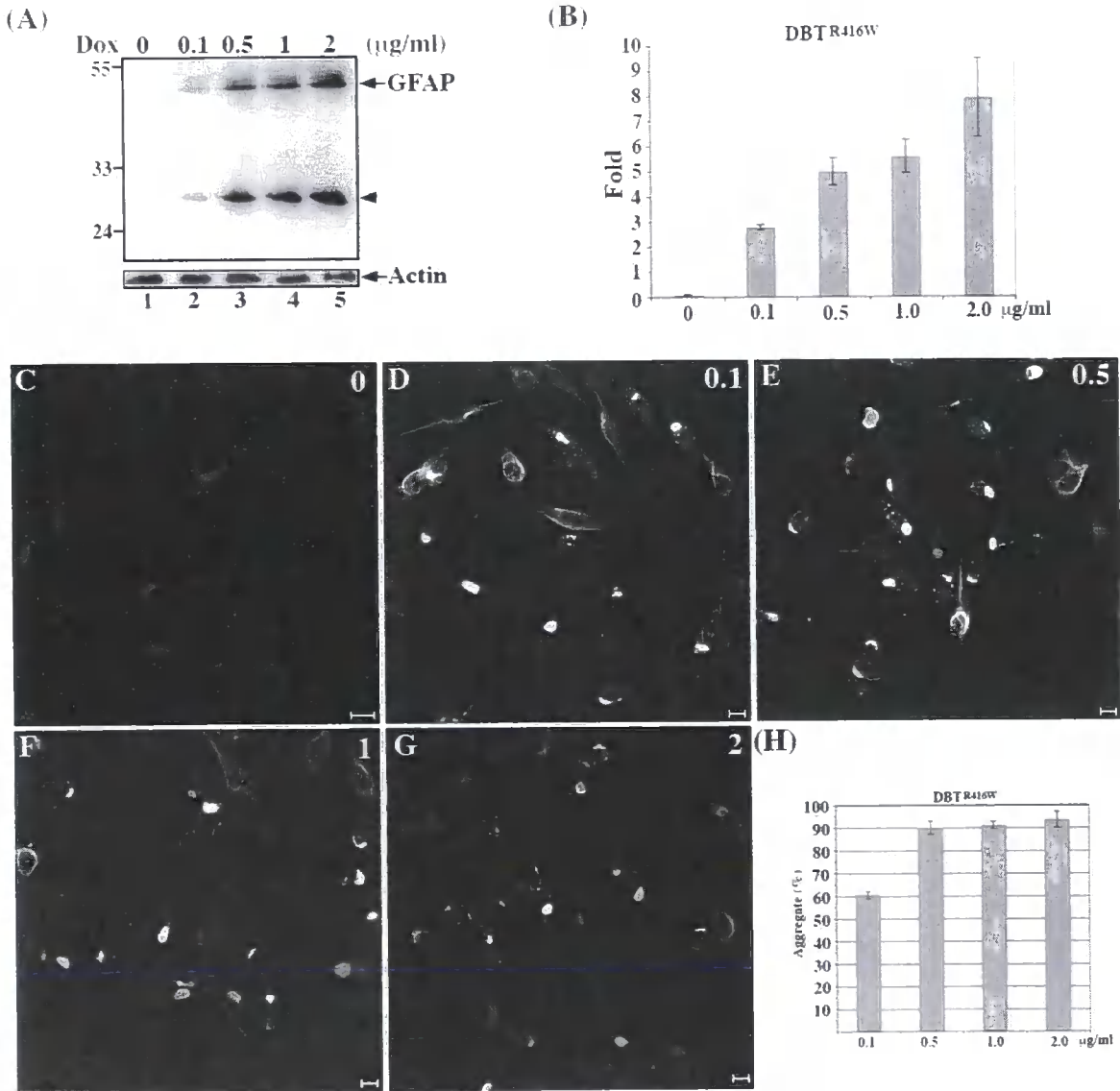
Figure 3.19. Characterisation of DBT-GFAPR416W cells. Does-dependent expression of R416W GFAP in DBT R416W GFAP-expressing cells was shown in (A). The insoluble pellet fractions prepared from DBT-GFAPR416W cells induced at the indicated Dox concentrations were analysed by immunblotting with antibodies to human GFAP and actin, which was used as a loading control. Quantification of the full length R416W GFAP are expressed as bar charts and represent three independent experiments (B). R416W GFAP distribution in cells induced at different concentrations of Dox was examined by immunofluorescence microscopy using anti-human GFAP SMI-21 antibody (C-G). Bars = 10 μm. Cells immunopositive for GFAP were scored for the presence of GFAP-positive aggregates. The indicated mean ± SD for each measurement represents the average of three independent experiments (H).
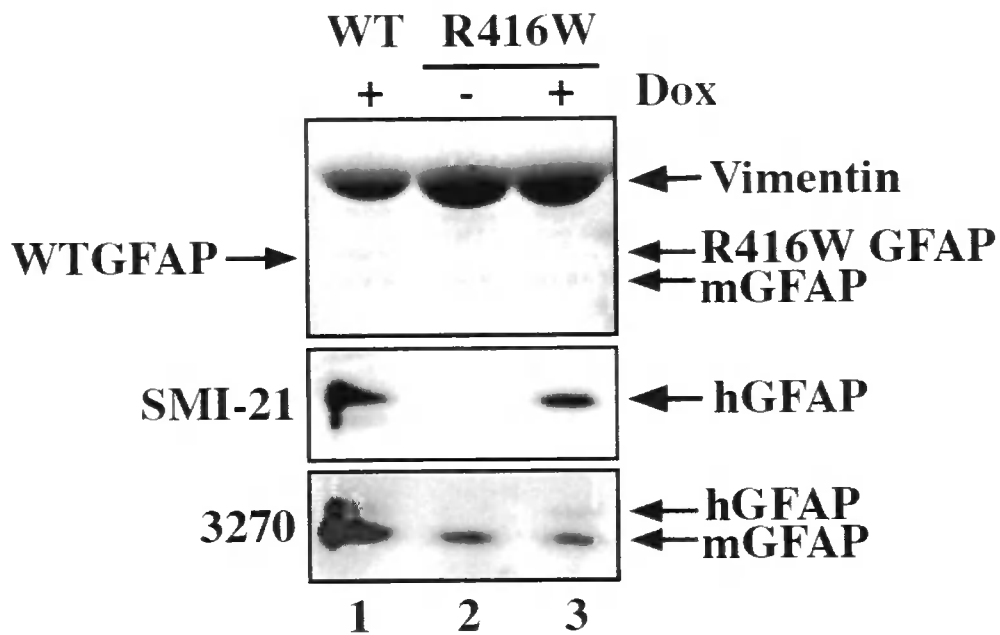
Figure 3.20. Relative expression level of inducible GFAP to endogenous intermediate filament proteins in DBT inducible cell ines. DBT-GFAPWT (lane 1) and DBT-GFAP R416W (lanes 2 and 3) cells, either uninduced (-) or induced (+) with Dox, were extracted with cytoskeletal extraction buffer. The cytoskeletal fractions were separated on 6-15% gradient SDS-PAGE and the major IF proteins were visualised by Coomassie Blue staining. Based on the quantification of Coomassie Blue stained gel, the induced human wild-type and R416W GFAP are 97% and 84%, respectively, to the endogenous mouse GFAP. Vimentin is the major intermediate filament protein in DBT cells, which is about 10 fold more abundant than the endogenous mouse GFAP. Although the expression levels of wild-type and mutant GFAP in Dox-regulated DBT cell lines are similar to the endogenous mouse GFAP, these expression levels are relatively low when compared to the total IF proteins. To further confirm the expression of induced human GFAP and mouse GFAP, the Coomassie Blue stained gel was transferred onto nitrocellulose membrane and blotted with SMI-21 antibody. After stripping, the membrane was reprobed with 3270 anti-GFAP antibody.

R416W GFAP is apparently more prone to aggregation compared to wild-type GFAP when induced to express in DBT cell lines. In fact, when induced at 0.5 µg/ml of Dox where both DBT-GFAP^{WT} and DBT-GFAP^{R416W} cells appear to express comparable levels of GFAP, aggregates formed in DBT-GFAP^{R416W} cells (Fig. 3.19E) is significantly higher than those in DBT-GFAP^{WT} cells (Fig. 3.18E). Representative images show the distribution of GFAP in DBT-GFAP^{WT} (Fig. 3.18C-G) and DBT-GFAP^{R416W} cells (Fig. 3.19C-G) induced at indicated Dox concentrations.

3.3. Discussion

3.3.1 Summary of the established cell lines

In this study, I used three different astrocytoma cell lines, human U343 MG-A, U373 MG-A and mouse DBT to generate stable and inducible cell lines. The average time of the whole selection procedure is variable among these cell lines. The main features of the established cell lines are summarised in Table 3.1.

Table 3.1 Summary of the established stable and inducible cell lines

Cell line	Regulation system	Available clonal lines		Inducible GFAP level	Network organisation	Average time to establish clones
U343 MG-A	Tet-off	R416W		Low	Filaments	2 months
U373 MG-A	Tet-on	R416W		Low	Filaments	3 months
DBT	Tet-on	WT	and	Medium	Aggregates	1 month
		R416W				

U373 MG-A cells proved to be the most difficult one to make the Dox-regulated cell lines. First, they grow much slower than U343 MG-A and DBT cells during the selection process. The decrease in growth rate may be due to induced expression of GFAP that affects cell motility and proliferation (Elobeid et al., 2000). This is probably the reason that stably

112

transfected clones expressing high levels of GFAP cannot be selected (obtained). For instance, U373 MG-A cells. Second, these cells are resistant to G418 even at high concentrations (1.5-2 µg/ml), which induce aberrant cell morphology and eventually cell death. Hence, to increase the efficiency of selection, a combination of hygromycin and G418 were used to select stable U373 MG-A cell lines. This one step procedure, however, still takes a long time to pick up candidate U373 MG-A clonal lines to evaluate GFAP expression by immunoblotting. The average time to establish a Tet-regulated U373 MG-A cell line is about 3 month from the date of transfection to immunoblotting analysis to confirm GFAP expression in selected cultures. The successful rate for generating positive clones with well-regulated expression of GFAP is about 10%.

The establishment of inducible DBT cell lines is the most efficient, with 7% and 11% successful rate for generating wild-type and R416W GFAP expressing clonal lines. It takes about one month to select GFAP-expressing clones after cotransfection of pTet-On and pTREhyg2-GFAP vectors. This efficiency is due partly to the faster growth rate of DBT cells and their sensitivity to synergistic selection of G418 and hygromycin. In addition, the monoclonal antibody SMI-21 that specifically recognises human GFAP allows me to confirm the selection of the extremely well-regulated clones by Dox in a short time.

Unlike DBT and U373 MG-A cell lines, U343 MG-A is a Tet-inducible cell line that contains tTA. This cell line was transfected with Tet responsive vector pTRE2hyg-GFAP followed by selection with hygromycin and G418. In the present study, the successful rate to generate Tet-regulated inducible cell lines in U343 MG-A cells is less than 3%.

For all the selected cell lines, the high GFAP expression in the induced states and low background in the uninduced states were confirmed by immunoblotting with anti-GFAP antibodies. The clonal lines with well-regulated expression in response to Dox are used for further experiments.

3.3.2 Transient expression of R416W GFAP produces heterogeneous phenotypes

Transient transfection provides a quick and convenient way to study GFAP mutants in cells. Initial studies of the effect of R416W mutation on GFAP network formation in cells lacking endogenous IFs revealed that R416W GFAP invariably formed cytoplasmic aggregates and diffused background staining (Perng et al., 2006). When R416W GFAP was transiently expressed in cells expressing the endogenous GFAP, heterogeneous phenotypes were observed. For instance, when transfected into astrocytoma human U343 MG-A cells and mouse DBT cells, R416W GFAP formed cytoplasmic aggregates in most of the transfected cells (Fig. 3.10A and Fig. 3.15G; asterisks). In some transfected cells, however, R416W integrated into the endogenous GFAP networks (Perng et al., 2006). This variation in phenotypes might be attributed to the relative expression levels of the transfected GFAP compared to the endogenous level of GFAP already being expressed in these cells. In fact, unregulated expression of even the wild-type GFAP seriously perturbs filament assembly and promotes filament aggregation in transfected astrocytes (Koyoma and Goldman, 1999; Fig. 3.15D; asterisk), suggesting that the overall level of an IF protein is important to cell homeostasis. This is supported by transgenic mouse studies where the overexpression of GFAP also produces pathologies similar to AxD (Eng et al., 1998; Messing et al., 1998).

Therefore, when comparing the behaviour of wild-type and mutant GFAP by transient transfection, transfection efficiency and expression levels need to be considered. Transfection efficiency varies depending upon the cell lines, so as the expression levels of transfected proteins. These two factors are interdependent and determine the fate of GFAP in transfected cells. In addition, the ability of GFAP, particularly the mutant form, to compromise the function of IF networks also depends on the number and abundance of the endogenous IF proteins in the host cell.

3.3.3 Regulated expression of GFAP in stable cell lines

Whilst transient transfection of R416W GFAP may produce a wide range of phenotypes in transfected cells due to variations of expression level at a given cell, generation of stable cell lines allows R416W GFAP expressed at a controlled level. In the stable U343-GFAP^{R416W} cells, inducible expression of R416W GFAP resulted in its integration into pre-existing GFAP networks without precipitating aggregate formation. However, although R416W GFAP integrated into the endogenous GFAP and formed normal appearing IF networks in induced U343 MG-A cells, it remains to be seen whether they behave differently to wild-type GFAP. Given that the proportion of R416W GFAP expressing in the stable U343-GFAP^{R416W} cells is estimated to be about 10% of the endogenous GFAP (Fig. 3.8B, C, E and F), it is possible that the effects of R416W GFAP expression on filament formation in this cell line could be masked by its greater expression level of the endogenous GFAP. In addition, vimentin is also highly expressed in U343 MG-A cells, which could facilitate correct spacing and organisation of GFAP (Eliasson et al., 1999). In other words, the R416W GFAP may be only dominant over wild-type protein once a critical threshold had been crossed. In fact, recent *in vitro* studies had demonstrated that 25% of R416W GFAP is sufficient to disrupt normal assembly of wild-type GFAP (Perng et al., 2006). Whilst the exact ratio of mutant to wild-type GFAP leading to disease pathologies is not fully understood, initial studies suggested that elevated level of GFAP in addition to GFAP mutation contribute to the pathogenesis of AxD (Hagemann et al., 2006). Mutations in GFAP *per se* may increase its level, as demonstrated by R239C GFAP where its transient expression increases filament stability (Hsiao et al., 2005) and impairs the capacity of the UPS (Tang et al., 2006).

3.3.4 Inducible expression of wild-type and R416W GFAP in stable DBT cell lines

DBT cells express high levels of vimentin that are about 10 times more than those for the endogenous GFAP. The high vimentin/GFAP ratio in DBT cells provides a unique cell background, which is different from U343 MG-A cells, to study R416W GFAP. In induced DBT-GFAP^{R416W} cells, the expression level of R416W GFAP is similar to that of the endogenous mouse GFAP. It was estimated that the R416W GFAP level is 84% of the endogenous mouse GFAP. This expression level may mimic what is seen in AxD patients with heterozygous R416W GFAP expression. The proportion of cells in which aggregates were formed in the DBT-GFAP^{R416W} cells increases to 90% when R416W GFAP level increased approximately five folds (0.5 µg/ml Dox) (Fig. 3.19). When wild-type GFAP induced to express at a similar level (0.5 µg/ml Dox), about 50% of DBT-GFAP^{WT} cells contained GFAP-positive aggregates (Fig. 3.18). These results suggest that R416W GFAP is more prone to aggregation compared to wild-type GFAP when induced to express in DBT cell lines, which is consistent with previous observations (Perng et al., 2006).

Inducible expression of human wild-type GFAP in DBT-GFAP^{WT} cells produced two distinct IF structures, filaments and aggregates. Although the expression level of human wild-type GFAP is similar to the endogenous mouse GFAP, this level is less than 10% to the total IF pool in the DBT cells. Even at this relatively low expression level, wild-type GFAP still formed aggregates in some induced DBT-GFAP^{WT} cells. Expression of human wild-type GFAP in a mouse background raises an interesting question of species conflict. Although the GFAP protein sequence is highly conserved between human and mouse, with 91% identity and 95% similarity (Brenner, 1994), it is possible that minor sequence differences between mouse and human GFAP may contribute to some unexpected observations, such as aggregate formation. However, several lines of evidence argue against this possibility. For instance, the humanised GFAP mice generated by Takemura et al. (2002) with the first 154 codons of the

endogenous mouse GFAP gene being substituted by the corresponding human sequence appeared normal without overt phenotypes. In addition, transient expression of human GFAP in primary mouse astrocytes also resulted in aggregate formation (Koyama and Goldman, 1999). Aggregates still formed when mouse GFAP was transfected into primary mouse astrocytes, indicating aggregate formation did not depend upon differences in species. In induced DBT-GFAP^{WT} cells, the proportion of cells that form aggregate increases with the elevated wild-type GFAP level, suggesting that aggregate formation is induced by excessive accumulation of GFAP that cannot be maintained in a filamentous form. Alternatively, aggregate formation may result from a defective interaction between human GFAP and the endogenous mouse GFAP, but additional studies should be performed before a clear conclusion can be drawn.

Since R416W GFAP mutation results in different phenotypes in cell models and variable age onset in AxD patients, it is of importance to consider the genetic background and epigenetic variation while investigating the pathogenesis of AxD.

Chapter 4

Results

4.1 Introduction

Stress refers to an environmental alteration or potentially detrimental force acting upon something to cause physiological or behavioral changes. Pathology results when tissue cells are unable to cope with stress and research on mechanisms of stress resistance in one form or another constitutes a large part of my study.

Cells have evolved many mechanisms to deal with and survive periods of stress. The best-known interpretation of stress is probably mechanical stress, and yet that is one of the least understood forms of stress in terms of cell sensing and response.

A link between IF deficiency and loss of resistance to mechanical stress is particularly obvious in the diseases caused by keratin mutations, which typically show fragility of the subpopulation of tissue cells in which the mutated keratin is a major structural protein. The best understood and most studied of these disorders is EBS, caused by dominant mutations in K5 or K14 keratin. It was the observations on the phenotype of EBS patients with dominant mutations on keratins that led to the clear understanding that a major function of keratin filaments in the epidermis is to provide essential physical resilience to the epidermal keratinocytes (Kim and Coulombe, 2007).

Mutations in other IF genes that have analogous pathological consequences are also mostly dominant and the majority also show a phenotype suggesting that cell resilience is dependent on the IFs. Biophysical analyses of IFs *in vitro* also indicate that this cytoskeletal element has properties of strain hardening and resilience that make the filaments especially suitable for resisting mechanical stress in tissue cells (Janmey et al., 1998).

The CNS would seem to be one part of the body where mechanical stress is least likely to act except in extreme situations, but in fact this tissue is very susceptible to different types of

stress or injuries. For instance, astrocytes are the most abundant cells in the CNS, and can support neuronal structure, trophy, metabolism and regeneration after brain injury (Pekny and Nilsson, 2005). These functions are dependent on the ability of astrocytes to survive brain insults and reacting actively to the injuries. Therefore, astrocytes play a protective role to defend the CNS against neurotrauma, ischemia and neurodegenerative diseases (Pekny and Lane, 2007), and they show characteristic changes in IF expression in essentially every pathological condition that influences the brain, spinal cord or the retina. The term "reactive gliosis" is commonly used to describe astrocyte activation in stress and pathology that affects the CNS. The upregulation of the IF proteins GFAP and vimentin and reexpression of nestin are hallmarks of reactive gliosis (Li et al., 2007).

In response to chronic gliosis, reactive astrocytes normally increase the expression of GFAP. In both GFAP transgenic mice and humans with AxD, the elevated GFAP expression leads to RFs formation. Although the precise mechanism inciting the formation of these astrocytic inclusions is unknown, RFs may represent an increased CNS stress response to the elevation of GFAP levels (Wippold et al., 2006). Indeed, AxD astrocytes display characteristics of physiological stress response, as demonstrated by the upregulation of sHSPs αB-crystallin and HSP27. Additional evidence for stress, and a suggestion that it may involve oxidative stress, is the association of advanced lipid peroxidation and glycation end-products with RFs (Castellani et al., 1998; Castellani et al., 1997).

As GFAP is mainly expressed in astrocytes, it raises the possibility that aberrant effect of GFAP may be to promote the dysfunction of astrocytes to precipitate AxD. Although the role of protein aggregation in neurodegenerative disorders remains controversial, it is generally agreed that aggregates or the interacting proteins might give rise to pathogenesis, as shown by mutations in NF genes NF-L and NF-M leading to respective Charcot-Marie-Tooth disease 2E and Parkinson's disease (Lariviere and Julien, 2004).

R416W GFAP is the only AxD-causing mutation that associates with all ages of onset of AxD. The phenotypic variation implicates environmental and epigenetic factors could influence the onset of disease progression. Previous studies had demonstrated that the R416W mutation in GFAP has the potential to be very disruptive to filament assembly *in vitro* (Perng et al., 2006). Transient transfection studies suggested, however, that the level of the GFAP expression and the availability of a co-assembly-competent endogenous filament network could ameliorate this potential, to the extent that R416W GFAP could fully integrate into an endogenous GFAP/vimentin network without overt effects upon its distribution (Perng et al., 2006). When induced to express at low levels, R416W GFAP was found to incorporate into normal appearing filaments in stable U343 MG-A cell lines. The potential functional impact of incorporating low levels of the disease-causing GFAP mutant into the pre-existing GFAP networks was further investigated here.

4.2 The presence of R416W GFAP compromised the ability of human astrocytes to recover from stress

4.2.1 Determination of stress conditions for human astrocytoma cells

To test whether the GFAP IF network could be compromised by the R416WGFAP mutation and render cells less able to cope with and recover from stress, I assessed the cell viability of inducible U343-GFAP^{R416W} cell lines after stress-induced insults. Hyperosmotic shock and oxidative stress are common physiological stresses with which astrocytes have to cope and they lead to transient cell shrinkage. The extreme cell-shape changes induced by these stresses lead me to investigate the possibility that the status of functional GFAP network is important for cell survival. First, the effect of Dox, urea and H_2O_2 on the U343 MG-A cell viability was assessed by cell proliferation assay (Fig. 4.1A-C). This assay is based upon the conversion of the MTS tetrazolium compound into coloured formazan products by

mitochondrial dehydrogenase enzymes in metabolically active cells (Shearman, 1999), which reflects cell viability and proliferation as well as the integrity of the mitochondria. As shown in Fig. 4.1, cells grown in the presence of 2 µg/ml Dox for up to 6 days did not produce any noticeable effects upon cell viability (Fig. 4.1A). In contrast, cells treated with urea (Fig. 4.1B) or H_2O_2 (Fig. 4.1C) dramatically lost the viability in a time- and dose-dependent manner. Comparison of cell survival one day after stress treatment revealed that 600 mM urea (Fig. 4.1B, asterisk) and 400 µM H_2O_2 (Fig. 4.1C, asterisk) for one-hour treatment are the best concentrations for stress assays. This is because both stresses did not cause massive cell death but decreased cell's metabolic activity that can recover to pretreated levels over time. Immunofluorescence microscopy revealed that the profound cell-shape changes triggered by urea and H_2O_2 treatments also induced the collapse of IF networks (Fig. 4.2B and C, insets).

4.2.2 R416W GFAP expression compromises cell recovery from stresses

The effect of R416W GFAP on cell recovery from hyperosmotic shock or oxidative stress was examined. U343-GFAP[R416W] cells under uninduced or induced conditions were treated with either 400 µM H_2O_2 (Fig. 4.3A) or 600 mM urea (Fig. 4.3B) for one hour. Following these treatments, cells were cultivated in normal growth medium for a further 5 days and cell viability was measured by cell proliferation assay. Whilst uninduced U343-GFAP[R416W] cells had recovered well with ~84% and ~73% recovery after urea and H_2O_2 treatments, induced cells had only ~55% recovery from these treatments. Similar results were observed when U343-GFAP[R416W] cells were challenged with 900 mM urea (Fig. 4.3C). These harsher conditions caused a ~90% drop in cell viability so that the long-term recovery is required. After 9 days recovery, ~80% of uninduced cells had recovered, whereas induced cells had only ~43% recovery from this treatment.

121
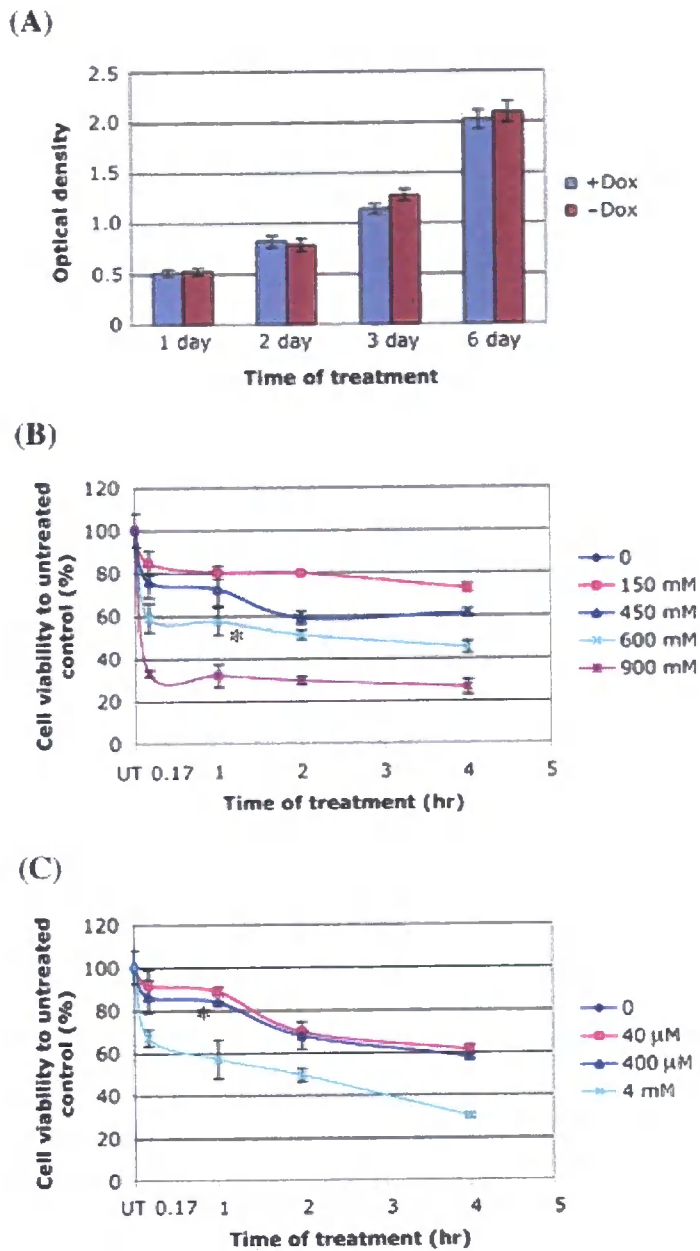
Figure 4.1. Effect of Dox and various stresses upon cell viability in U343 cells. U343 cells were cultivated in the absence or presence of 2 μg/ml Dox. Cell viability was measured at the indicated times. Results from three independent experiments are shown as mean ± SD and present as bar charts (A). To test the effect of osmotic shock and oxidative stress upon cell survival, cells cultured for three days were either left untreated or treated with the indicated concentrations of urea (B) or H_2O_2 (C). Following treatments, cells were allowed to recover in normal growth medium for one day and cell viability was examined by MTS cell proliferation assay. UT, untreated. The viability of treated cells relative to untreated cells was expressed as percentages in panels (B) and (C). Data were represented as mean ± SD and analysed by unpaired t test. N = 3. *, $P < 0.05$, compared with untreated control cells.
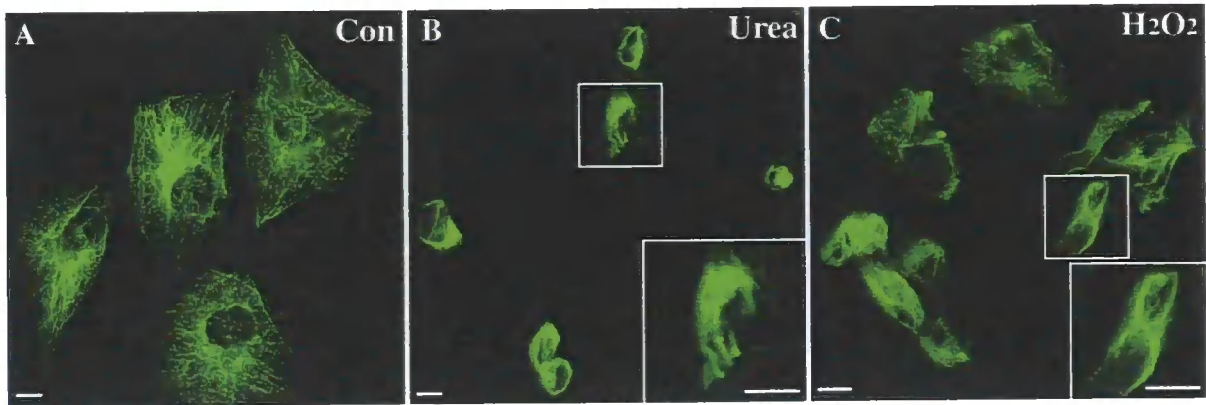
Figure 4.2. Effect of hyperosmotic shock and oxidative stress upon GFAP network formation in U343 cells. After plating in glass coverslips for 3 days, U343 clls were untreated (Control; A) or treated with 600 mM urea (B) or 400 μM H2O2 (C) for 1 hour. Change in the GFAP networks following stress treatments were visualised by immunofluorescence microscopy. Cells were fixed and stained with anti-GFAP antibody. Notice that GFAP networks collapse and filament bundling were observed in U343 cells after stress treatments (B and C). The higher magnification views of filament collapse and bundling in the boxed areas of panels B and C were shown in the respective inset. Bars = 10 μm.
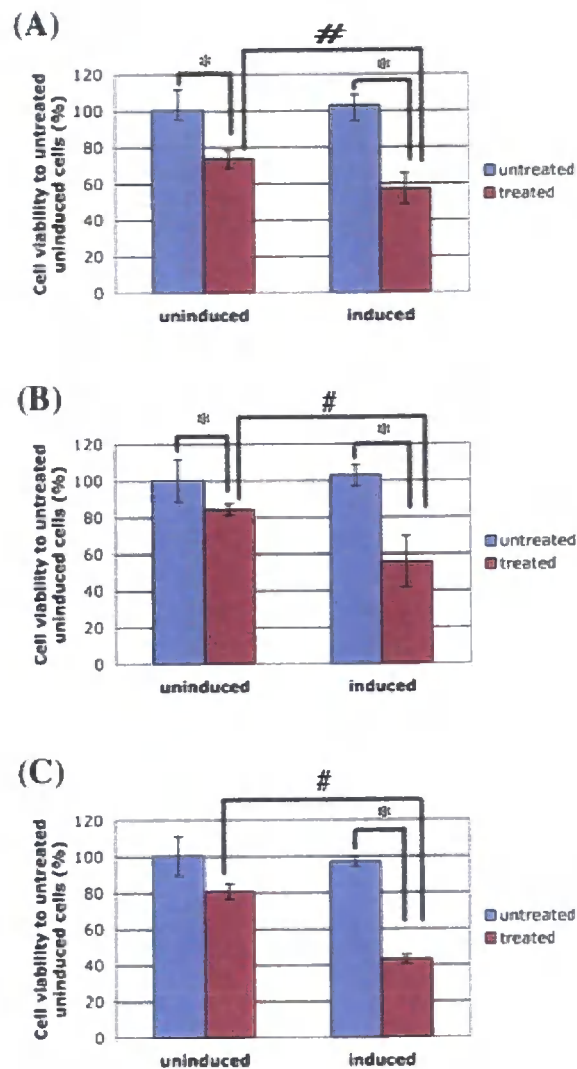
Figure 4.3. Effect of R416W expression upon cell viability after hyperosmotic shock and oxidative stress. U343 stably expressing R416W cells grown in the presence (uninduced) or absence (induced) of 2 μg/ml Dox. After two days of incubation, cells were untreated or treated with either 400 μM H_2O_2 (A) or 600 mM urea (B). Following these treatments, cells were allowed to recover in normal growth medium for 5 days and cell survival was determined by MTS-based cell viability assay. Whilst uninduced cells had recovered well, induced cells had only 50% recovery after stress treatments. Similar results were observed on cells treated with 900 mM urea (C). Nine days following this treatment uninduced cells had ~70% recovery, whereas induced cells had only 50% recovery from this treatment. Results from three independent experiments are shown as mean ± SD, and expressed as bar charts. Statistical significance was determined by unpaired t test and asterisks (*) highlight P value < 0.05 when comparing the viability between treated and untreated cells in uninduced or induced condition. #, indicates $P < 0.05$ between treated induced cells and treated uninduced cells.

By double label immunofluorescence microscopy, it was observed that untreated cells expressing R416W GFAP had extended filaments throughout the cytoplasm (Fig. 4.4A-C). In contrast, urea (Fig. 4.4D-F) and H_2O_2 (Fig. 4.4G-I) treatments caused the collapse of GFAP IF networks and their accumulation in the perinuclear region of U343-GFAP[R416W] cells. These cells recovered much slower when compared to unstressed cells.

4.2.3 R416W GFAP mutation sensitizes cells in response to proteasome inhibition

Proteosome inhibition has been widely reported to cause cell death and has been implicated in AxD (Tang et al., 2006). To assess the effect of R416W GFAP upon cell recovery from proteolytic stress, cells were treated with the proteosome inhibitor MG-132 and cell viability was measured 2 days after recovery (Fig. 4.5A). To determine the best concentration for cell viability assay, a broad range of MG-132 concentrations were tested. U343 MG-A cells treated with 10 μM MG-132 for 24 hours had noticeable effect upon cell viability and a ~15% drop in metabolic activity was detected (Fig. 4.5A). These conditions were used to stress U343-GFAP[R416W] cells and cell viability was measured at 48 hours after MG-132 treatment. Whilst uninduced cells had recovered well (~91% of pre-treated level), induced cells attained only ~66% recovery (Fig. 4.5B). Taken together, these data suggest that the presence of R416W GFAP compromised the ability of astrocytes to recover from osmotic, oxidative and proteolytic stresses.

4.2.4 Evaluation of stress kinases and stress proteins in U343-GFAP[R416W] cells

Induction of cellular stress response is accompanied by the activation of one or more SAPK pathways, most notably JNK and p38 (Gabai and Sherman, 2002). To investigate whether the expression of R416W GFAP in U343-GFAP[R416W] cells induced a cellular stress response, whole cell lysates prepared from parental U343 MG-A cells and U343-GFAP[R416W]
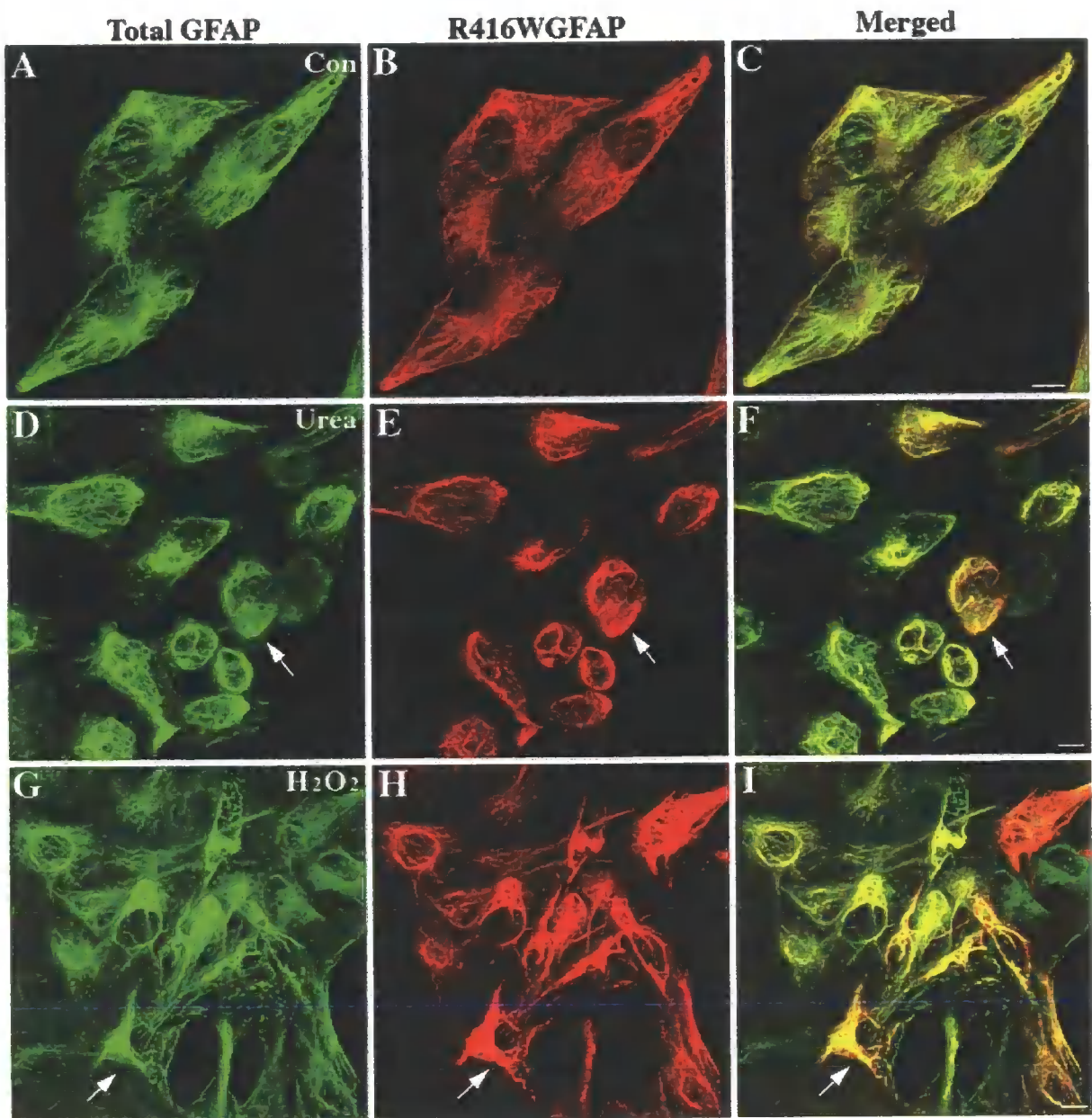
Figure 4.4. Distribution of R416W GFAP in relation to the endogenous GFAP networks in recovered U343-GFAPR416W cells following stress treatments as revealed by double label immunofluorescence microscopy. Induced U343-GFAPR416W cells expressing R416W GFAP were either untreated (A-C) or treated with 600 mM urea (D-F) or 400 μM H_2O_2 (G-I). Following these treatments, cells were allowed to recover to 5 days prior to processing for double label immunofluorescence microscopy with antibodies to total GFAP (A, D, and G) and R416W GFAP (B, E, and H). Merged images show the superimposition of the green and red signals with areas of overlap in yellow (C, F, and I). Note that R416W GFAP (B) incorporated into the endogenous GFAP (A) and formed extended filament networks in untreated cells, whereas cells treated with urea or H_2O_2 had morphological changes accompanied by extensive filament collapse and bundling (D-I; arrow). These cells recovered much slower when compared to those under uninduced conditions. Images were acquired by a confocal laser scanning microscope. Bars = 10 μm.

(A)

(B)
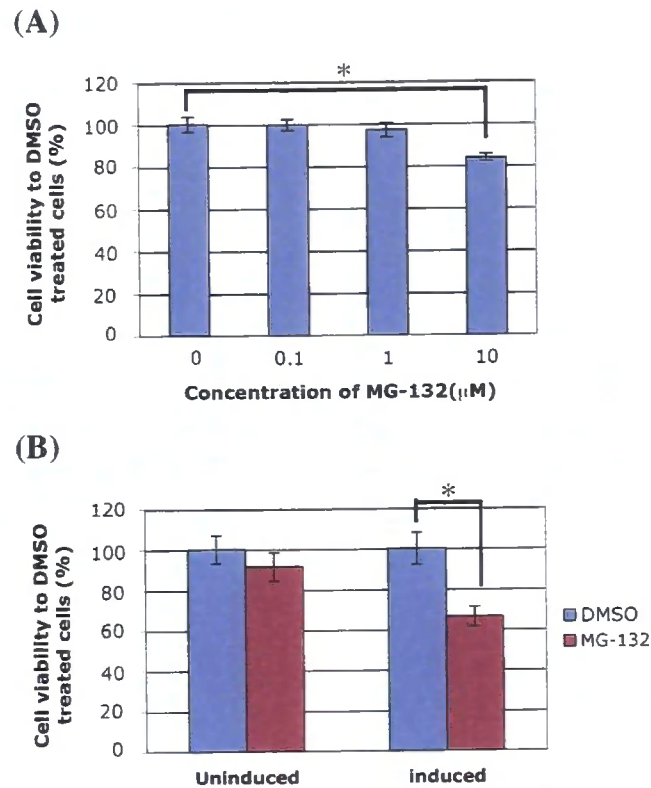
Figure 4.5. Proteosome inhibition resulted in delayed recovery of cells expressing R416W GFAP. (A) U343 cells were cultured in the growth medium for 3 days, followed by treated with 0.1% (v/v) DMSO (labelled 0) and various concentrations of MG-132 as indicated. Cell viability was measured 24 hours after treatment. Cells treated with 0.1% DMSO was used as a control. At all concentrations tested, cells showed the greatest sensitivity to 10 μM MG-132 treatment and a significant decrease in cell viability was observed. (B) To test the effect of R416W expression upon cell viability following proteosome inhibition, U343 stably expressing R416W cells were grown in the presence (uninduced) or absence (induced) of 2 μg/ml Dox. After two days of culture, cells were treated with 0.1% DMSO or 10 μM MG-132. At 24 hours post-treatment, cells were recovered in normal growth medium for 2 days and cell survival was measured by cell viability assay. The OD_{490} readings were normalised to those of untreated cells. Values are mean ± SD of three independent experiments and presented as bar charts. Statistic significance was analysed by t test and asterisks (*) highlight P value < 0.05 when compared with DMSO-treated cells.

cells were subjected to immunoblotting analysis with antibodies to phospho-JNK and phospho-p38 (Fig. 4.6A). Whilst no significant difference was observed on the levels of phospho-JNK and phospho-p38 between uninduced and induced U343-GFAP^{R416W} cells, the levels of phospho-JNK and phospho-p38 were higher in stable U343-GFAP^{R416W} cells than those in parental U343 MG-A cells. These results suggest that generation of the U343-GFAP^{R416W} cell line already elicits a cellular stress response. In fact, when U343-GFAP^{R416W} cells were subjected to urea or H_2O_2 treatments, the level of phospho-JNK/p38 was only marginally increased (Fig. 4.6B), indicating that this cell line exhibited a sustained activation of the SAPK pathway. Whilst no marked difference was detected in the levels of HSPs between induced and uninduced cells (Fig. 4.6B, lanes 1 and 4, HSP70, HSP27 and αB-cry), the amounts of these proteins slightly increased in the cells treated with H_2O_2. Compared to untreated cells (lane 1), ~1.2 fold of increase was observed on HSP27 and αB-cry blots in H_2O_2 treated induced cells (Fig. 4.6B, lanes 3, HSP27 and αB-cry).

4.2.5 Transient expression of R416W GFAP in astrocytes leads to various IF structures

Whilst regulated expression of R416W GFAP resulted in its integration into the endogenous GFAP networks in the U343-GFAP^{R416W} cell line, transient transfection was used to investigate the effect of R416W mutation on IF network formation in primary astrocytes or U343 MG-A cells. This cell system would be expected to better mimic the scenario of R416W GFAP being expressed in a physiological relevant cell background.

The distribution of transfected GFAP in relation to the endogenous GFAP was visualized by double label immunofluorescence microscopy using monoclonal antibody SMI-21 (Fig. 4.7A and C) that specifically detects human GFAP, and polyclonal anti-pan-GFAP antibody, which recognises both the endogenous mouse GFAP and the transfected human GFAP (Fig. 4.7B and D). Mouse primary astrocytes transiently transfected with wild-type GFAP mainly formed

(A)

U343   U343^{R416W}

Dox   –   +   –   +

GFAP

R416W GFAP

p-JNK

JNK

p-p38

p38

HSP70

HSP27

αB-cry

Actin

1   2   3   4

(B)

	induced			uninduced		
H₂O₂	–	–	+	–	–	+
Urea	–	+	–	–	+	–
Dox	–	–	–	+	+	+

R416W GFAP

p-JNK

JNK

p-p38

p38

p-ERK

HSP70

HSP27

| Fold | 1.14 | 1.18 | 1.34 | 1 | 1.02 | 1.04 |

αB-cry

| Fold | 1.12 | 1.07 | 1.36 | 1 | 1 | 1.2 |

Actin

1   2   3   4   5   6
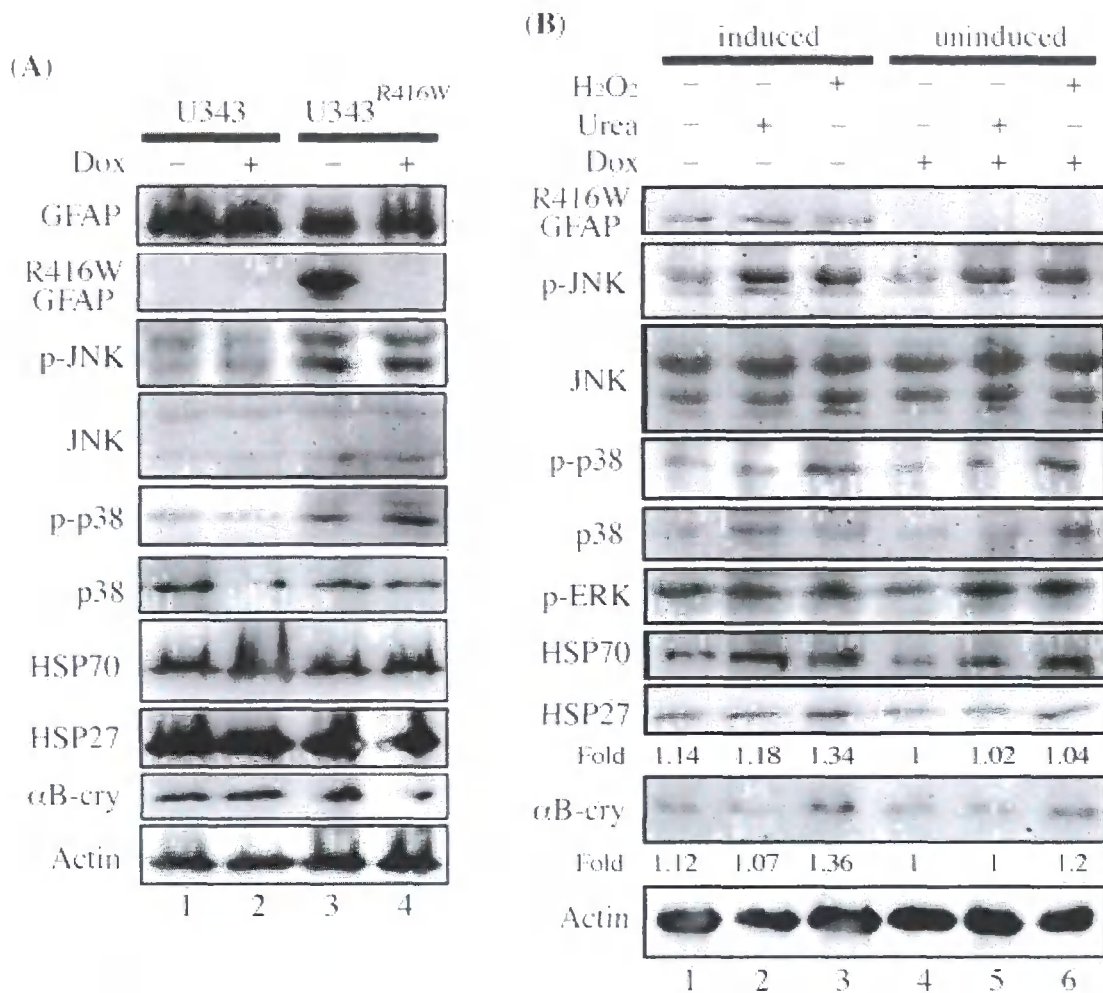
Figure 4.6. Effect of R416W GFAP expression on activation of SAPKs and induction of stress protein. Parental U343 MG-A cells and stable U343-GFAPR416W cell line were grown in uninduced (+Dox) or induced (-Dox) condition for 4 days. Total cell lystaes were prepared from these cultures followed by immunoblotting analysis with antibodies to the indicated epitopes (A). The expression of R416W GFAP was confirmed by blotting with anti-R416W GFAP antibody (A, lane 3). To test the effect of R416W GFAP on SAPK activation following stress treatments, induced and uninduced cells were treated with either 600 mM urea or 400 μM H₂O₂ for 1 hour. Following these treatments, whole cell lysates were prepared and analysed by immunoblotting with antibodies to the indicated epitopes (B). Notice that cells subjected to urea and H₂O₂ treatments marginally increased phospho-JNK (B, lanes 2 and 5) and phospho-p38 (B, lanes 3 and 6) signals when compared to untreated cells (B, lanes 1 and 4). The increase of αB-crystallin level was particularly obvious in cells treated with H₂O₂ (B, lane 3). Equal loading of each sample was confirmed by monitoring actin levels by immunoblotting with anti-actin antibody.
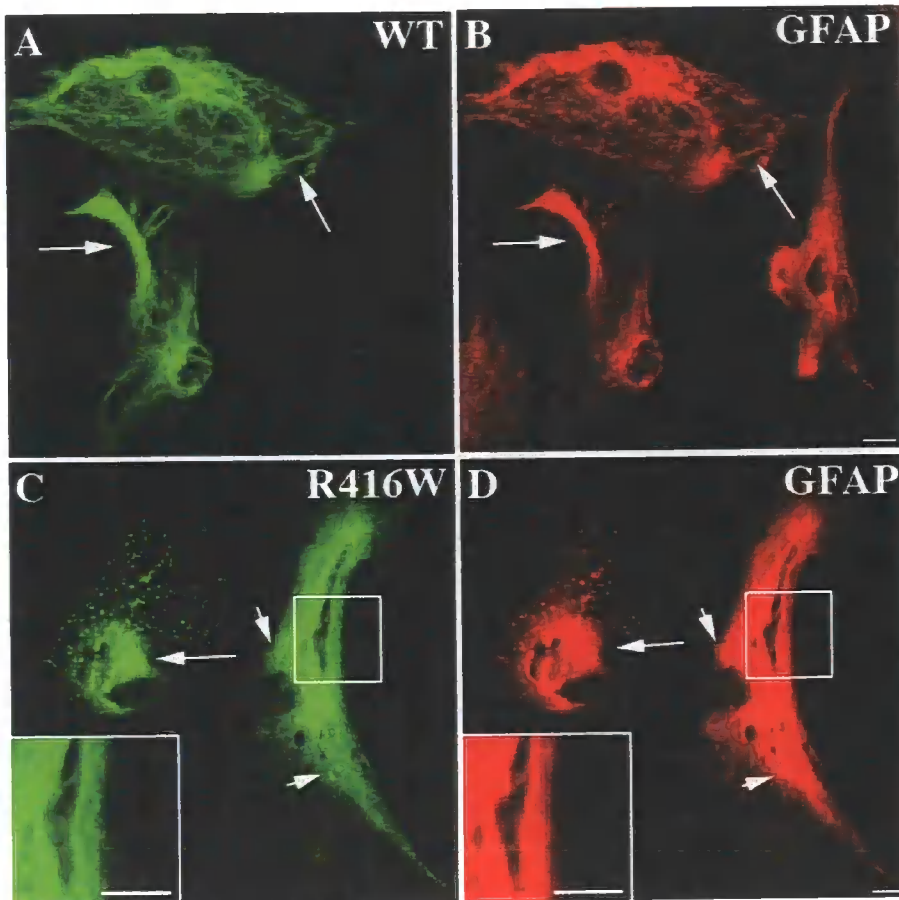
Figure 4.7. Transient expression of wild-type or R416W GFAP in primary mouse astrocytes. Primary astrocytes transfected with either wild-type (A and B) or R416W (C and D) GFAP were processed 48 hours after transfection for double label immunofluorescence microscopy using antibodies to human GFAP (A and C) and total GFAP (B and D). When transiently expressed into these cells, wild-type GFAP formed extended filaments and filament bundles (A, arrows) that largely colocalised with the endogenous mouse GFAP (B, arrows). In contrast, transfected cells expressing R416W GFAP exhibited aggregate (C, arrows) as well as filamentous staining pattern (C, arrowheads), which also costained with the endogenous GFAP (D, arrows and arrowheads respectively). Magnification view of small aggregates intermingled with the GFAP filaments were shown in insets in panels C and D. Bars = 10 μm.

filaments (Fig. 4.7A) that colocalised with the endogenous GFAP network (Fig. 4.7B). In contrast, most of the cells transfected with R416W GFAP contained cytoplasmic aggregates with smaller particles at the cell periphery (Fig. 4.7C, arrows), which colocalised with collapsed endogenous GFAP networks (Fig. 4.7D, arrows). In some transfected cells, however, expressed R416W GFAP was incorporated into the endogenous GFAP networks without any apparent changes in filament organisations (Fig. 4.7C and D; cell on the right). Careful examination revealed that there were small aggregates intermingled with the filaments (Fig. 4.7D, arrowheads and inset), which were immunopositive for the human R416W GFAP, indicative of perhaps an early change in the organisation of the GFAP filaments preceding the eventual collapse of the network.

Similar results were observed when R416W GFAP was transiently expressed in human astrocytoma U343 MG-A cells. The use of this cell line eliminated the potential variability of expressing human GFAP in a mouse background. To distinguish transfected wild-type GFAP from the endogenous GFAP, the anti-GFAP antibody was titrated down to the point where the endogenous GFAP appeared as background staining on untransfected cells (Fig. 4.8). When GFAP levels were elevated by transient transfection, the signal becomes obvious above background. When transfected into U343 MG-A cells, wild-type GFAP formed extended filaments (Fig. 4.9A, asterisks) that colocalised with the endogenous GFAP networks (Fig. 4.9B, asterisks). The R416W GFAP-specific monoclonal antibody was used to follow the fate of R416W GFAP in the presence of the endogenous human GFAP. When transfected into this cell line, R416W GFAP produced two distinct IF structures, aggregates (Fig. 4.9D, arrows) and bundled filaments (Fig. 4.9D, arrowheads), which are largely colocalised with the endogenous GFAP (Fig. 4.9E, arrows and arrowheads, respectively). These data show that R416W GFAP is capable of disrupting the endogenous networks of wild-type GFAP
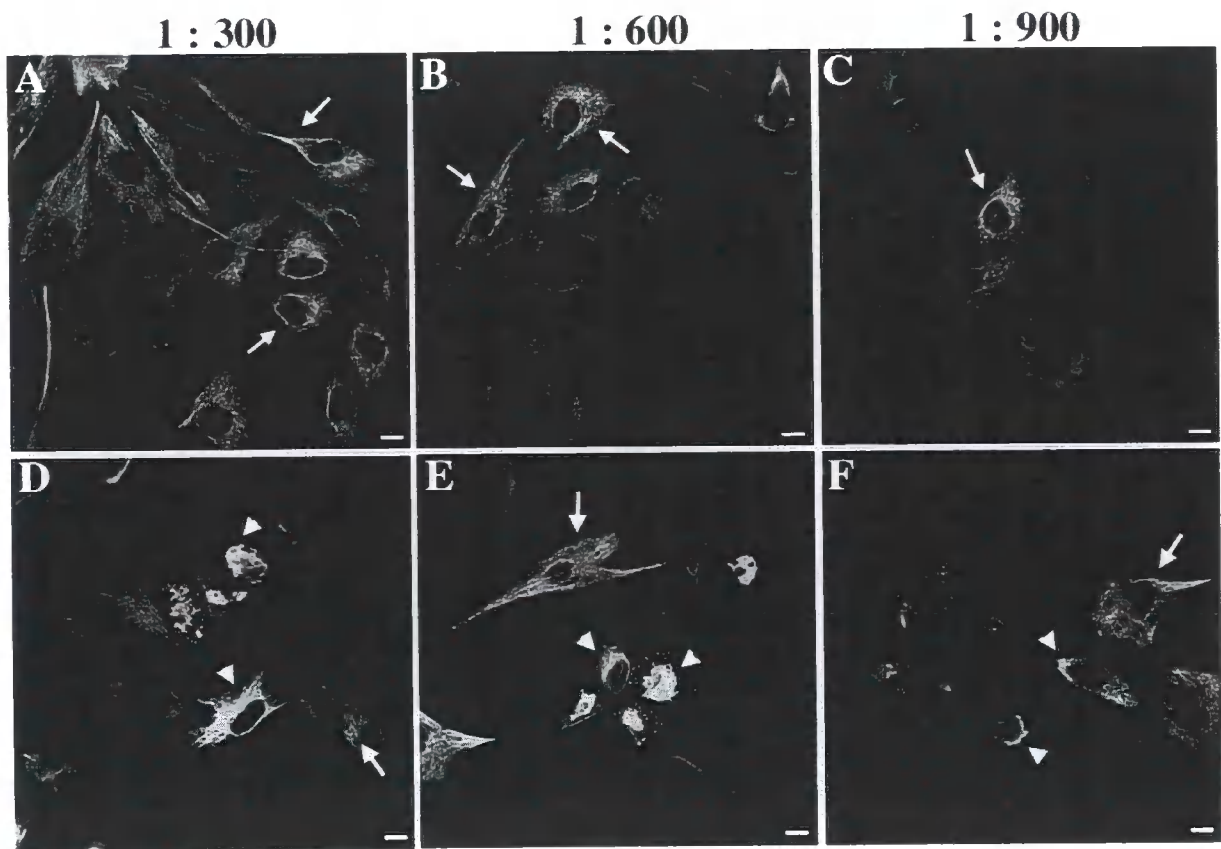
Figure 4.8. Titration of human GFAP antibody in human astrocytoma cells. U343 MG-A
cells were either untransfected (A-C) or transfected with R416W GFAP (D-E) for 48 hours.
Upon processed for immunofluorescence microscopy, human GFAP antibody SMI-21 was
added at various dilutions to 10% goat serum in BSA/PBS as indicated to detect both
endogenous GFAP and overexpressed R416W GFAP in cells. At 1 : 300 dilution (A, D), the
endougenous GFAP demonstrated observed signals (A, arrows) that were not dramatically
different from overexpressed R416W GFAP (D, arrowheads). At 1 : 600 dilution (B, E), the
immunoreactivity of R416W GFAP (E, arrowheads) was brightened up, whereas the
endogenous GFAP (B and E, arrows) showed faint background staining. At 1 : 900 dilution
(C, F), the R416W GFAP staining (F, arrowheads) was not increased significantly compared
to the endogenous GFAP staining (C and F, arrows). Hence, the dilution of 1 : 600 was
chosed for SMI-21 antibody used in immunofluorescence microscopy procedures.
Bars = 10 µm.
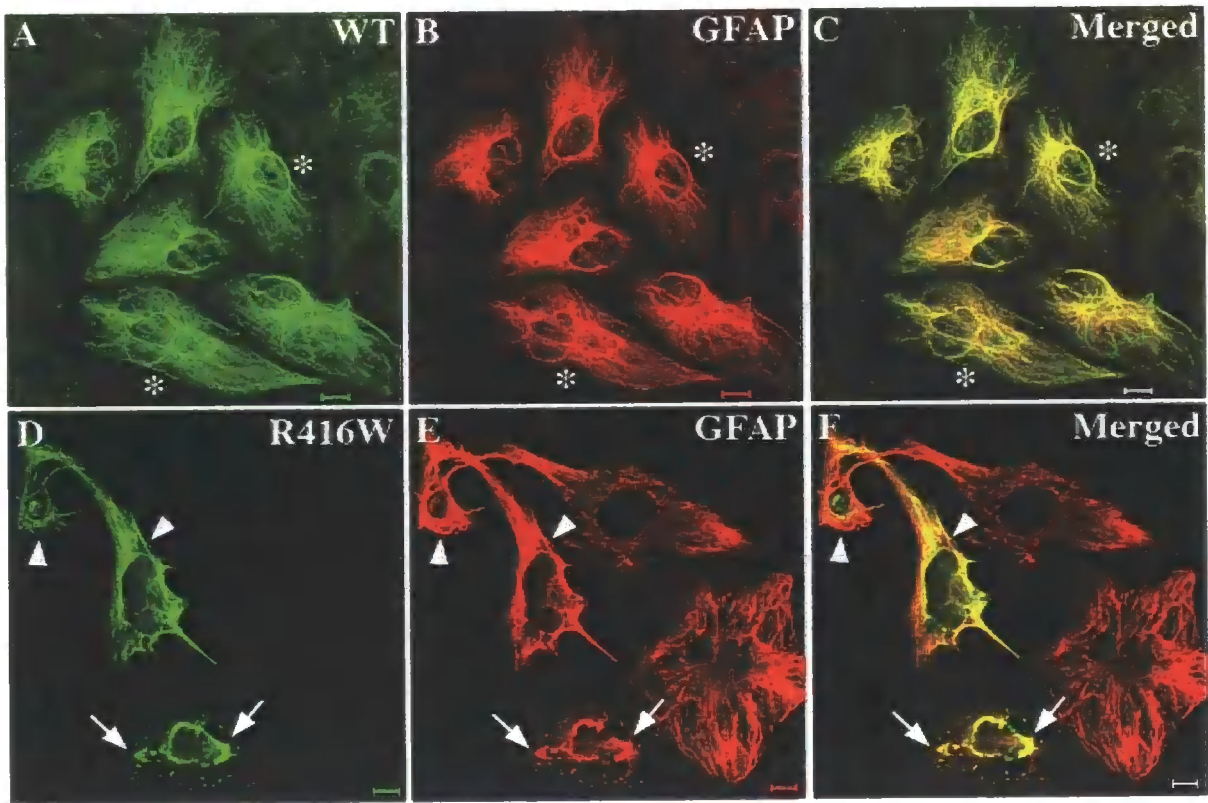
Figure 4.9. Expression of R416W mutant into human astrocytoma U343 MG-A cells resulted in the formation of filamentous and aggregated IF structures. U343 MG-A cells were transfected with either wild-type (A-C) or R416W GFAP (D-F). At 48 hours after transfection, cells were processed for double label immunofluorescence microscopy with use of anti-human GFAP (A) and anti-R416W (D) GFAP antibodies and counter stained with anti-pan GFAP antibody (B and E). To distinguish transfected GFAP from the endogenous GFAP, it was first necessary to titrate the anti-GFAP antibodies to the point where the endogenous GFAP appeared as background staining on untransfected cells. When GFAP levels were elevated by transient transfection, the signal becomes obvious above background. When expressed in this cell line, wild-type GFAP formed filaments (A; asterisks) that colocalised with the endogenous GFAP (B). The expression of R416W GFAP resulted in both filamentous (D; arrowheads) and aggregate staining patterns (D; arrows), which also costained with the endogenous human GFAP networks (E; arrowheads and arrows, respectively). The merged images show superimposition of GFAP signals with areas of overlap appearing yellow (C and F). Bars = 10 μm.

filaments within the context of a human astrocytoma cell line and demonstrate the dominant negative potential of the R416W GFAP on the endogenous IFs.

4.2.6 Association of R416W GFAP with stress proteins and stress kinases

In previous studies of AxD pathology, several other proteins were also found to associate with GFAP aggregates, including αB-crystallin and HSP27 (Iwaki et al., 1993). Therefore, I examined whether these proteins would associate with the aggregates formed by R416W GFAP. Double label immunofluorescence microscopy revealed that R416W GFAP induce the formation of GFAP-rich aggregates (Fig. 4.10B, arrows), which also collapsed the endogenous GFAP (Fig. 4.10A, arrows). Both αB-crystallin (Fig. 4.10E, arrows) and HSP27 (Fig. 4.10H, arrows) colocalised with the GFAP-containing aggregates in these cells (Fig. 4.10D and G, respectively; arrows). These data show that aggregates formed by R416W GFAP have many features similar to RFs.

Recent studies showing that the accumulation of the GFAP mutant R239C induces SAPK activation and alters phospho-JNK distribution (Tang et al., 2006) lead me to further investigate whether phospho-JNK is associated with the aggregates formed by R416W GFAP. Double label immunofluorescence microscopy with antibodies to phospho-JNK and R416W GFAP demonstrated that a proportion of phospho-JNK (Fig. 4.10K, inset) are associated with GFAP-rich aggregates in R416W GFAP-transfected cells (Fig. 4.10J, inset). The association of phospho-p38 with GFAP aggregates was also tested, but the results were equivocal because of the lack of cross reactivity of the antibody with human proteins.

To obtain biochemical evidence of the association of these proteins with aggregates formed by R416W GFAP, the supernatant and pellet fractions prepared from transfected cells were analysed by immunoblotting. The solubility of GFAP and the associated proteins were also monitored by cell fractionation followed by immunoblotting. With the use of an
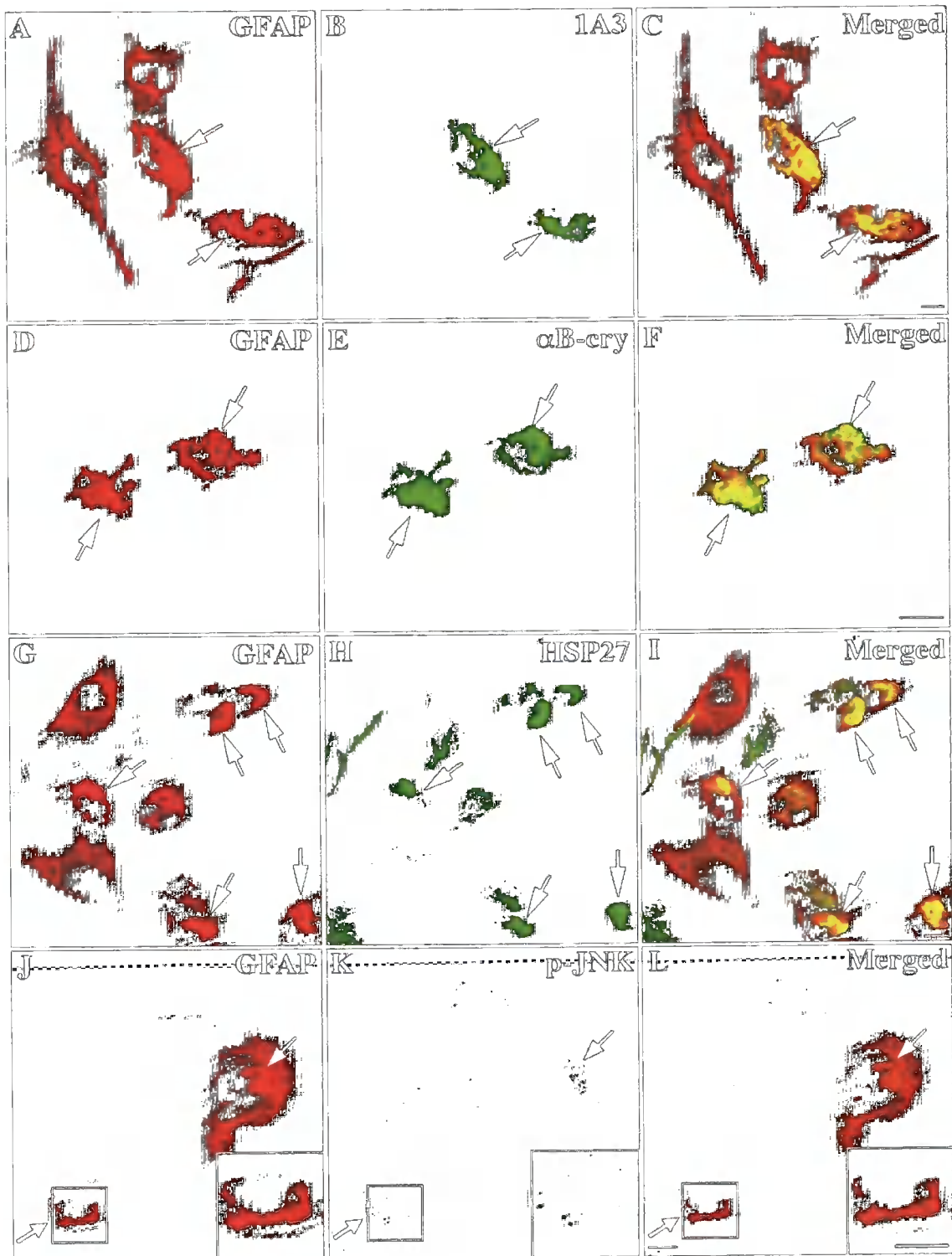
Figure 4.10. Aggregates formed by R416W GFAP recruited small heat shock proteins and phosph-JNK. U343 MG-A cells were transiently transfected with R416W GFAP and stained with polyclonal anti-GFAP antibody and then were double stained with mouse monoclonal antibodies specific to R416W GFAP, αB-crystallin or HSP27. Notice that GFAP-containing aggregates are also positive for αB-crystallin and HSP27. To demonstrate the presence of phospho-JNK in the GFAP aggregates, R416W GFAP-transfected cells were double stained with phospho-JNK and R416W GFAP. Merged images show the regions of colocalisation between red and green signals appearing yellow. Note that a proportion of phospho-JNK (K, arrows) is colocalised with R416W GFAP-containing aggregate (J, arrows). The colocalisation of phospho-JNK and R416W GFAP was magnified in insets of panels J, K and I. Bars = 10 μm.

extraction buffer containing the detergent deoxycholate, wild-type GFAP was almost completely extracted from the pelleted untransfected (Fig. 4.11A; Mock) and wild-type GFAP-transfected cells (Fig. 4.11A; WT), conditions that also extracted stress proteins and phospho-JNK/p38. In contrast, R416W GFAP remained almost entirely in the pellet fraction of the extracted cells that had been transfected with R416W GFAP (Fig. 4.11A; R416W). When the blots were also probed with antibodies to αB-crystallin, HSP27 and HSP70, a significant proportion of both αB-crystallin and HSP27, but not HSP70, remained in the pellet fractions of R416W GFAP-transfected cells (Fig. 4.11A). These data confirm that a proportion of sHSPs associated with the insoluble R416W GFAP. Since HSP70 was completely extracted from the R416W GFAP-transfected cell pellets, the association of the sHSPs with R416W GFAP is specific and not a general event for all protein chaperones. It is also interesting to note that some of the phospho-JNK associated with the pellets of GFAP aggregates in cells transfected with R416W mutant (Fig. 4.11A).

Immunoblotting analysis of brain tissues of AxD patients with R416W mutation using antibodies to GFAP and phospho-p38 revealed that the levels of GFAP and phospho-p38 increased in both Triton-soluble and insoluble fractions. A significant proportion of phospho-p38 cofractionated with R416W GFAP into the Triton-insoluble fraction suggests phospho-p38 is associated with insoluble R416W GFAP (Fig. 4.11B).

4.3 Stress response of mouse astrocytoma cells expressing wild-type or R416W GFAP

Whilst the mutant-specific antibody provides an ideal tool to monitor R416W GFAP expression in U343-GFAP^{R416W} cells, the control U343-GFAP^{WT} cell line is not available because there is no way to distinguish the induced wild-type GFAP from the endogenous human GFAP. Therefore, I decided to generate a stable cell line using mouse astrocytoma

(A)

	Mock		WT		R416W	
	S	P	S	P	S	P

←GFAP
←p-JNK
←p-p38
←αB-cry
←HSP27
←HSP70
←Actin

1 2 3 4 5 6

(B)

	Soluble		Insoluble	
	Con	AxD	Con	AxD

←p-p38
←GFAP
←GAPDH

1 2 3 4
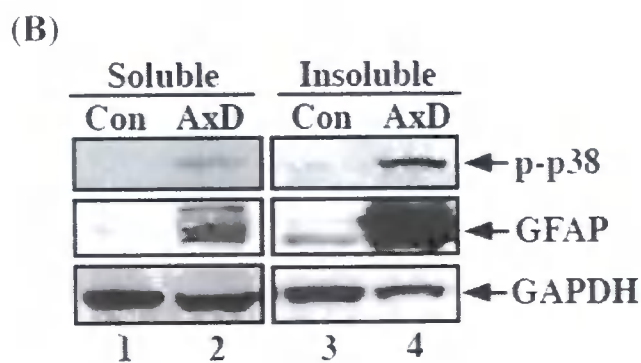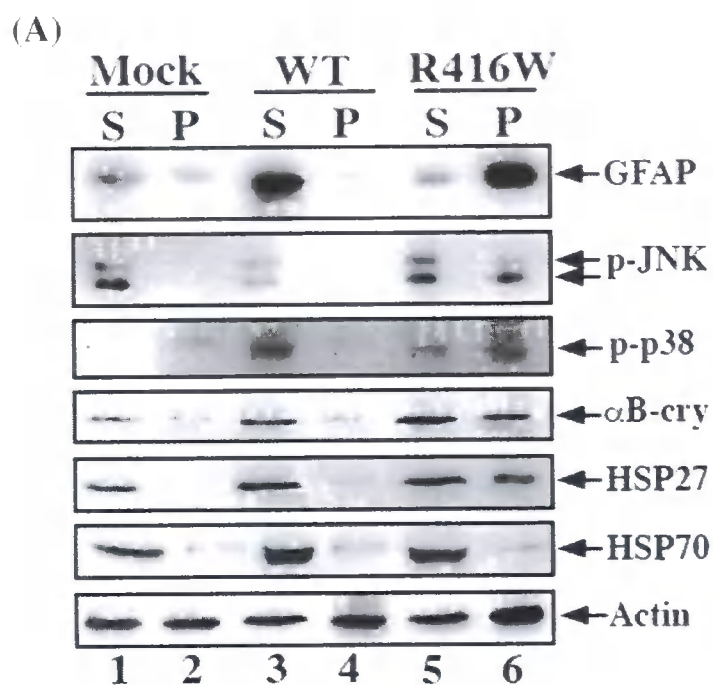
Figure 4.11. Immunoblotting confirmed the associations of small heat shock proteins and phospho-JNK/p38 with R416W GFAP. Wild-type and R416W GFAP were transiently transfected into U343 MG-A cells. At 48 hours after transfection, supernatant (S) and pellet (P) fractions were prepared from these cell cultures and compared to mock transfected cells. Immunoblots of supernatant and pellet fraction from each cell culture were probed with antibodies to GFAP, phospho-JNK, phospho-p38, αB-crystallin, HSP27, HSP70 and finally actin. The latter was used as a loading control. Cell fractionation used harsh extraction buffer almost completely solubilised wild-type GFAP, whereas most of the R416W GFAP remained in the pellet fraction. Notice that when cells were transfected with R416W GFAP, a significant proportion of phospho-JNK,phospho-p38, αB-crystallin and HSP27 but not HSP70, cofractionated with R416W GFAP into the pellet fractions. The phosphorylation states of p38 was also assessed in brain tissue samples from an Alexander disease patient with R416W GFAP (AxD) and compared with those from age-matched control (Con). Immunoblotting with antibodies to GFAP and phospho-p38 revealed that the levels of GFAP and phospho-p38 were increased in both Triton-soluble and insoluble fractions of R416W brain tissue (B). A significant proportion of phospho-p38 cofractionated with GFAP into insoluble fraction suggests the association of phospho-p38 with insoluble GFAP. Immunoblotting with antibody to glyceraldehyde 3-phosphate dehydrogenase (GAPDH) was used as a loading control.

DBT cells because the anti-human GFAP antibody SMI-21 can be used to follow the expression of human GFAP in a mouse cell background.

4.3.1 Determination of stress conditions for mouse astrocytoma cells

To identify the best conditions for my proposed stress assays, different stressful stimuli were applied to DBT cells. First, the effects of different concentrations of Dox, urea and H_2O_2 upon the cell survival of DBT cells were evaluated by cell viability assay. A wide range of Dox concentrations were examined and cell viability was determined at 1 and 2 days after treatment (Fig. 4.12A). Dox, even at a concentration as high as 4 µg/ml, did not produce any obvious effects upon cell viability. On the other hand, urea (Fig. 4.12B) and H_2O_2 (Fig. 4.12C) treatments dramatically decrease cell viability in a does-dependent manner. Comparison of the effect of different concentrations of urea and H_2O_2 on cell viability revealed that DBT cells show great sensitivity, but no more than ~40% of cell loss, to 450 mM urea (Fig. 4.12B, asterisk) and 400 µM H_2O_2 (Fig. 4.12C, asterisk) treatments and these conditions were used for subsequent experiments.

4.3.2 R416W GFAP mutant sensitises cells in response to stresses

To assess whether the presence of either wild-type or R416W GFAP makes cells more susceptible to stresses, DBT Dox-regulated cell lines induced for 2 days were treated with either 450 mM urea or 400 µM H_2O_2 for 1 hour. Following these treatments, cells were allowed to recover for three days and the cell survival was determined by cell viability assay. DBT cells induced to express wild-type GFAP had recovered well from stress treatments (Fig. 4.13A), whereas R416W GFAP-expressing cells induced by 1 µg/ml Dox had only ~55% recovery from urea treatment and ~40% recovery from H_2O_2 treatment (Fig. 4.13B).
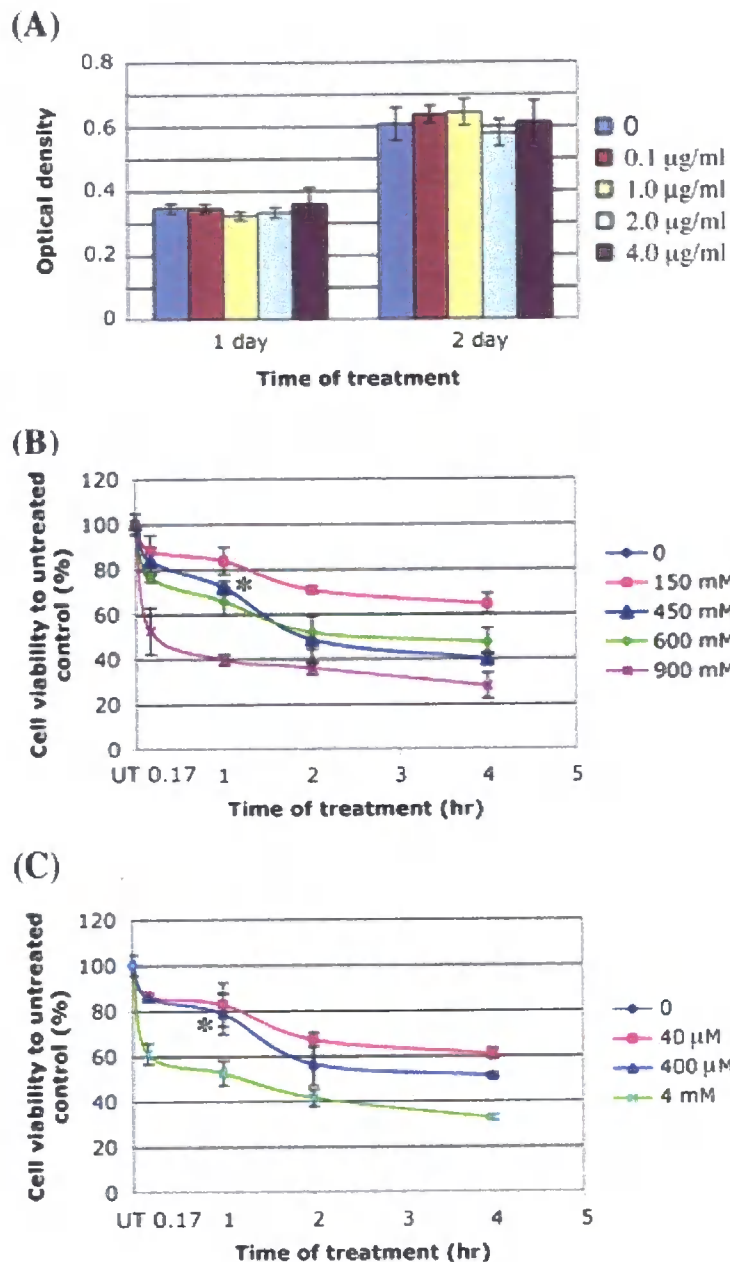
Figure 4.12. Effect of various concentrations of Dox, urea and H_2O_2 on DBT cells. DBT cells were grown in the absence or presence of indicated concentrations of Dox and cell viability was determined at 1 and 2 days (A). Dox, even at a concentration of 4 µg/ml, did not produce a noticeable effect upon cell survival. To test the sensitivity of cells to osmotic shock and oxidative stress, cells were incubated with a wide range of concentrations of urea and H_2O_2 for the indicated times. Following these treatments, cells were recovered in normal growth medium for 1 day and cell viability was measured as decribed above. The readings were normalised to untreated cells and the percentage of cell viability was shown. Data from three independent experiments are presented as mean ± SD. Statistical significance was determined by t test and asterisks (*) highlight P value < 0.05 when comparing untreated and treated cells. UT, untreated.
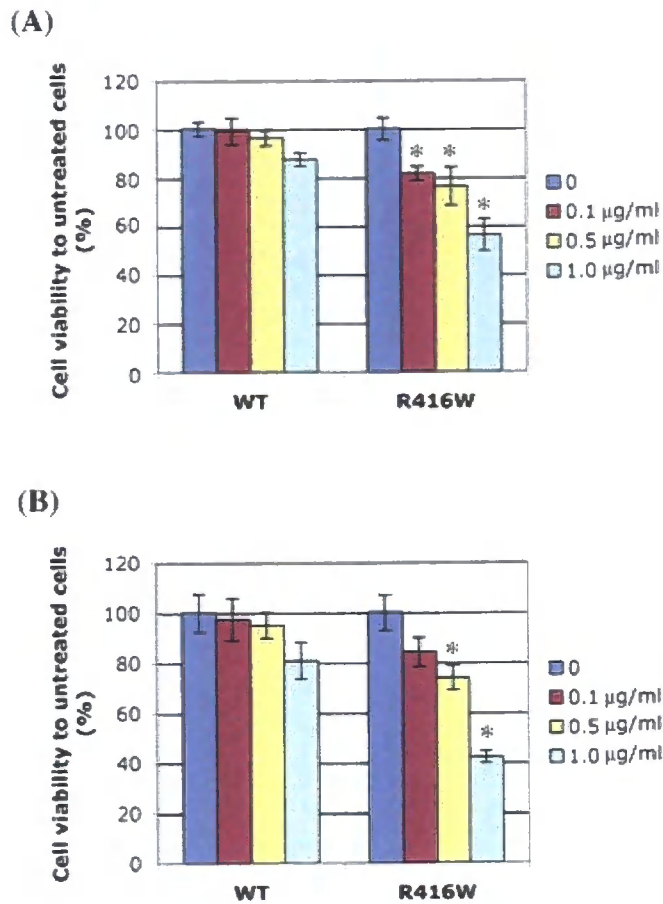
Figure 4.13. GFAP expression level-dependent effect on cell viability after stress.
DBT stably expressing wild-type or R416W GFAP cells were grown in the absence
(labelled 0) or presence of various concentrations of Dox. Two days post-culture,
cells were treated with 450 mM urea (A) or 400 µM H2O2 (B) for 1 hour, and
incubated in fresh growth medium for another 2 days. Cell viability was determined
by MTS reagent and represented as the percentage comparing Dox-treated cells to
untreated cells. Data were expressed as mean ± SD and analysed by t test. N = 3.
*, P < 0.05 relative to Dox-untreated cells.

4.3.3 Expression of R416W reduces cell viability after proteasome inhibition and serum deprivation

The ability of DBT-GFAP^{WT} and DBT-GFAP^{R416} cell lines to respond to different stressful insults was also examined. First, the effect of proteosome inhibition upon cell survival was tested on parental DBT cells. Cells treated with 1 μM MG-132 had noticeable effect upon cell viability and at 10 μM of MG-132, ~35% loss in cell viability was observed (Fig. 4.14A). When DBT cell lines expressing either wild-type or R416W GFAP were treated with MG-132, cell viability significantly decreased (Fig. 4.14B), suggesting a synergistic effect of GFAP expression and proteosome inhibition upon cell survival. DBT cell expressing R416W GFAP exhibited the highest sensitivity to proteosome inhibition, with a ~70% loss in cell viability by 10 μM MG-132 treatment being detected (Fig. 4.14B).

Similar results were observed when cell lines were challenged by serum starvation (Fig. 4.14C), another type of metabolic stress. When cultured in low serum conditions (1% and 0.1% serum), DBT cells expressing R416W GFAP showed a significant decrease in cell viability. In contrast, cells expressing wild-type GFAP in similar low serum conditions were comparable to those grown under normal growth conditions (10% serum). Taken together, these results show that cells expressing the R416W GFAP appeared to be more vulnerable to the serum-deprivation stress treatment as compared with cells expressing wild-type GFAP.

4.3.4 Activation of JNK and p38 correlated with GFAP expression

The increased cellular vulnerability leads me to further investigate whether the presence of GFAP evokes cellular stress response. As mentioned earlier, induction of the cellular stress response can be easily monitored by detection of SAPK activation and upregulation of the sHSPs, such as αB-crystallin and HSP25 (a homologue of human HSP27). The activation of
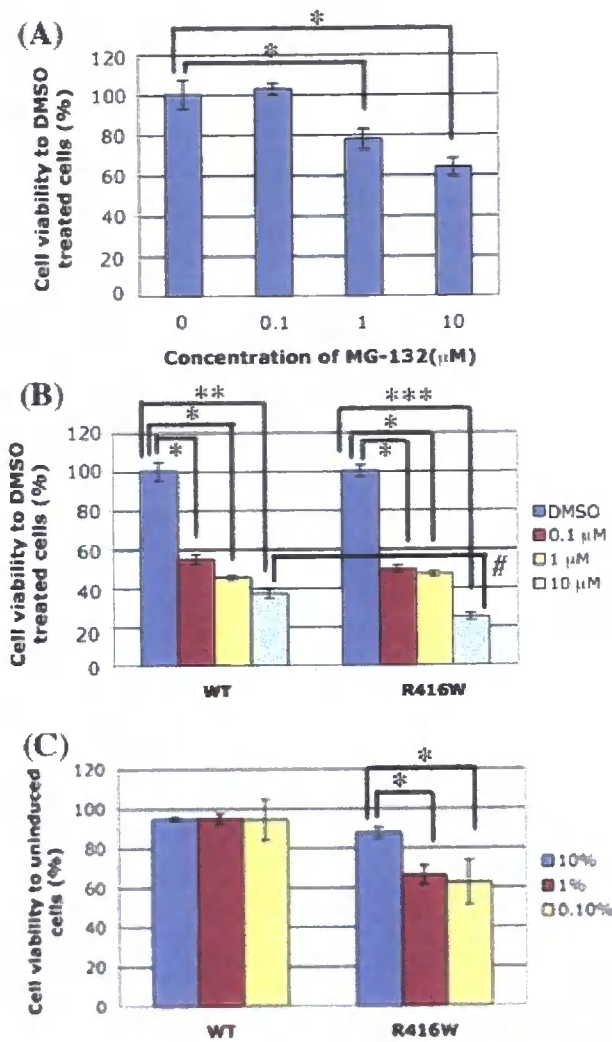
Figure 4.14. Effect of R416W expression upon cell viability following proteosome inhibition and serum starvation. (A) To test the effect of proteosome inhibition upon cell survival, parental DBT cells were treated with increasing concentrations of MG-132. Cells treated with 0.1% (v/v) DMSO was used as a control (labelled as 0). At 24 hours after treatment, cell viability was determined by cell proliferation assay kit. The effect of MG-132 on cell survival was noticeable at 1 μM. At 10 μM, a ~35% drop in cell viability was detected. (B) To assess the effect of GFAP expression and proteosome inhibition upon cell survival, DBT cells induced to express either wild-type or R416W GFAP for 3 days were treated with MG-132 for 24 hours. Following this treatment, cell survival was determined by cell viability assay. Results from three independent experiments are shown as mean $\pm$ SD. Statistical significance was analysed by t test. *, $P < 0.05$; **, $P < 0.01$; ***, $P < 0.001$ MG-132-treated cells relative to 0.1% DMSO-treated control cells (A, B). # , $P < 0.05$ between MG-132 treated R416W GFAP cells and wild-type GFAP cells (B). (C) The effect of serum starvation upon cell viability was also evaluated. DBT cells uninduced or induced to express either wild-type or R416W GFAP were cultured in growth medium containing 10%, 1% or 0.1% serum for 6 days and cell survival was measured by cell viability assay. The readings were normalised to uninduced cells grown in medium containing 10%, 1% or 0.1% serum, respectively. Data were represented as the percentage relative to uninduced control cells and expressed as mean $\pm$ SD of three independent experiments. *, $P < 0.05$ between serum-deprived cells and cells grown in 10% serum by t test.

SAPK pathway in response to the expression of GFAP was investigated by monitoring the phosphorylation of JNK and p38.

DBT cells induced at different concentrations of Dox were lysed in extraction buffer and the resulting supernatant and pellet fractions were analysed by immunoblotting. After induction, both wild-type (Fig. 4.15A) and mutant GFAP (Fig. 4.15B) expression levels increased in a does-dependent manner and they were found exclusively in the pellet fractions (Fig. 4.15A and B, labelled P). Immunoblotting analysis revealed that whilst phospho-JNK (p-JNK) and phospho-p38 (p-p38) were not detected in uninduced DBT cell lines (Fig. 4.15A and B, lanes 1 and 2), significant increases in p-JNK and p-p38 were observed in cells expressing wild-type (Fig. 4.15A) and R416W GFAP (Fig. 4.15B). These results indicate that expression of GFAP in the DBT cells activate SAPK pathways. The increased levels of p-JNK and p-p38 were greater in cells expressing R416W GFAP than in cells expressing wild-type GFAP and a proportion of p-p38 signal was found in the pellet fractions (Fig. 4.15A and B, lanes 6, 8 and 10), suggesting the possible association of p-p38 with insoluble GFAP. It is also interesting to note that whilst p-JNK was almost entirely soluble in cells expressing wild-type GFAP (Fig. 4.15A, lanes 7 and 9, labelled S), most of the p-JNK signals were found in the pellet fraction of cells expressing R416W GFAP (Fig. 4.15B, lanes 2, 4, 6, 8 and 10, labelled P).

Upregulation of sHSPs is a hallmark of astrocytes in response to stress. Therefore, the levels of αB-crystallin and HSP25 were examined in DBT cells expressing either wild-type or R416W GFAP. Immunoblotting analysis revealed the level of αB-crystallin increased in both the supernatant and pellet fractions of cells expressing R416W GFAP (Fig. 4.15B, αB-crystallin) when compared to cells expressing wild-type GFAP (Fig. 4.15A, αB-crystallin). In contrast, HSP25 greatly soluble in the supernatant fraction and its level was similar between cells expressing wild-type (Fig. 4.15A) and R416W GFAP (Fig. 4.15B). Increased association
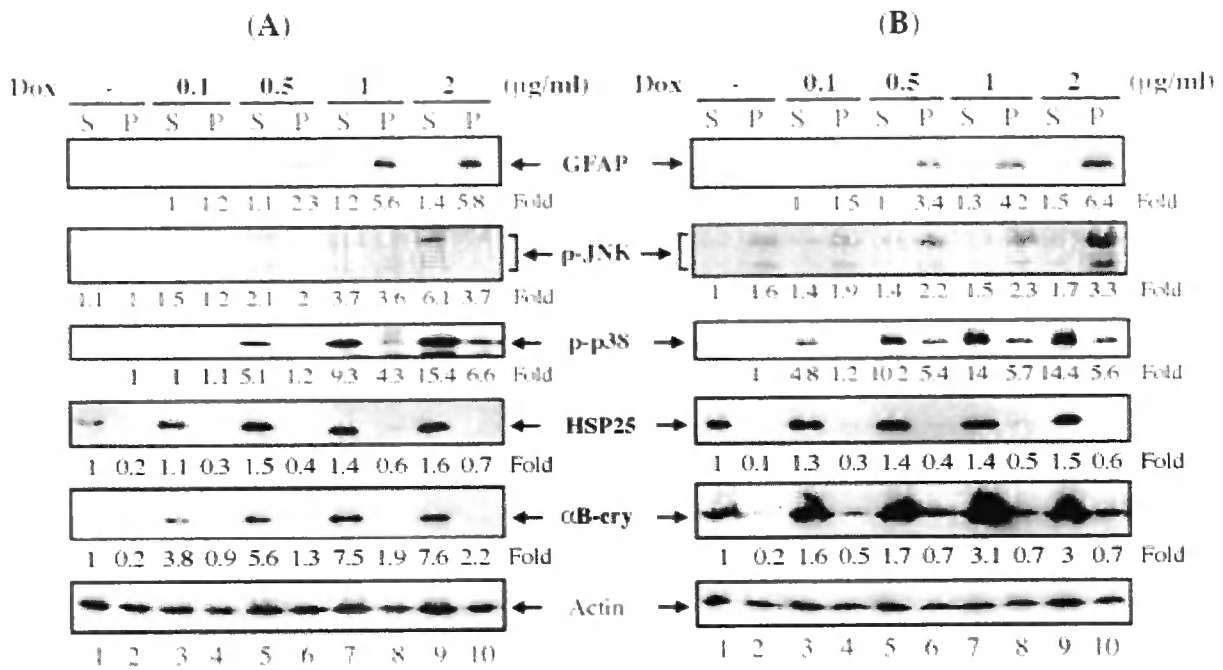
Figure 4.15. DBT cells expressing human GFAP induce SAPK activation as reflected by the increased phosphorylation of JNK and p38. DBT cells expressing wild-type (A) and R416W (B) GFAP were grown in the absence (lanes 1 and 2) or presenece of increasing concentrations of Dox (lanes 3-10) for 4 days. Cells were then lysed in RIPA extraction buffer and the resulting supernatant (S) and pellet (P) fractions were subjected to SDS-PAGE, followed by immunoblotting with antibodies to human GFAP, p-JNK, p-p38, HSP25 and αB-crystallin and finally actin, which serves as a loading control. Both wild-type (A) and R416W (B) GFAP levels increased in induced DBT cell lines in a does-dependent manner (GFAP). The increased expression of GFAP also induced elevated levels of p-p38 that cofractionated with GFAP into the pellet fractions (A, lanes 8 and 10; B, lanes 6, 8 and 10). The increased levels of p-JNK were also observed, particularly in cells expressing high levels of GFAP. Whilst most of the p-JNK was almost entirely soluble in cells expressing wild-type GFAP (A, lanes 7 and 9), p-JNK appeared to remain insoluble in cells expressing R416W GFAP (B, lanes 2, 4, 6, 8 and 10). Notice that elevated expression of R416W GFAP also increased αB-crystallin levels in both the supernatant and pellet fractions (B). The fold of increased in signal strength was shown at the bottom of each panel. The levels of HSP25 in DBT cells expressing wild-type GFAP (A) were similar to those expressing R416W GFAP (B).

of HSP25 with insoluble R416W GFAP, however, was detected upon higher expression levels of R416W GFAP (Fig. 4.15B, lanes 8 and 10, HSP25). These data show that cells expressing R416W GFAP induce activation of SAPK and increased expression of αB-crystallin and HSP25, indicative that these cells are undergoing a cellular stress response.

4.3.5 Colocalisation of Dox-induced GFAP expression and p-JNK or p-p38

To explore the association of p-JNK or p-p38 and GFAP, cells expressing either wild-type or R416W GFAP were processed for double label immunofluorescence microscopy with antibodies to GFAP and p-JNK or p-p38. Whilst some p-JNK (Fig. 4.16A) and p-p38 (Fig. 4.16G) were colocalised with aggregates formed by wild-type GFAP (Fig. 4.16B and H), they were also detected by diffuse staining in other parts of the cells. In contrast, both p-JNK (Fig. 4.16D) and p-p38 (Fig. 4.16J) colocalised with GFAP-containing aggregates (Fig. 4.16E and K) in cells expressing R416W GFAP. These results confirm that the associations of p-JNK and p-p38 with aggregates formed by either wild-type or mutant GFAP.

4.3.6 Assessment of levels of activated JNK and p38 after stress

The activation of JNK and p38 related to GFAP expression after stress was examined by immunoblotting using the insoluble lysates prepared from DBT-GFAP^{WT} and DBT-GFAP^{R416W} cells treated with urea and H_2O_2. Whilst the expression level of human GFAP in wild-type cells was compatible with R416W cells (Fig. 4.17, lanes 4-6, 10-12), no dramatic difference was detected in terms of p-JNK and p-p38 levels between the induced cells (Fig. 4.17, lanes 4-6, 10-12) and the uninduced cells (Fig. 4.17, lanes 1-3, 7-9). In addition, the amount of p-JNK and p-p38 in treated wild-type (Fig. 4.17, lanes 11 and 12) GFAP-expressing cells exhibited similarity to untreated cells (Fig. 4.17, lanes 4 and 10), albeit p-JNK levels elevated slightly under GFAP induction with urea treatment condition (Fig. 4.17, lanes 5 and 11).
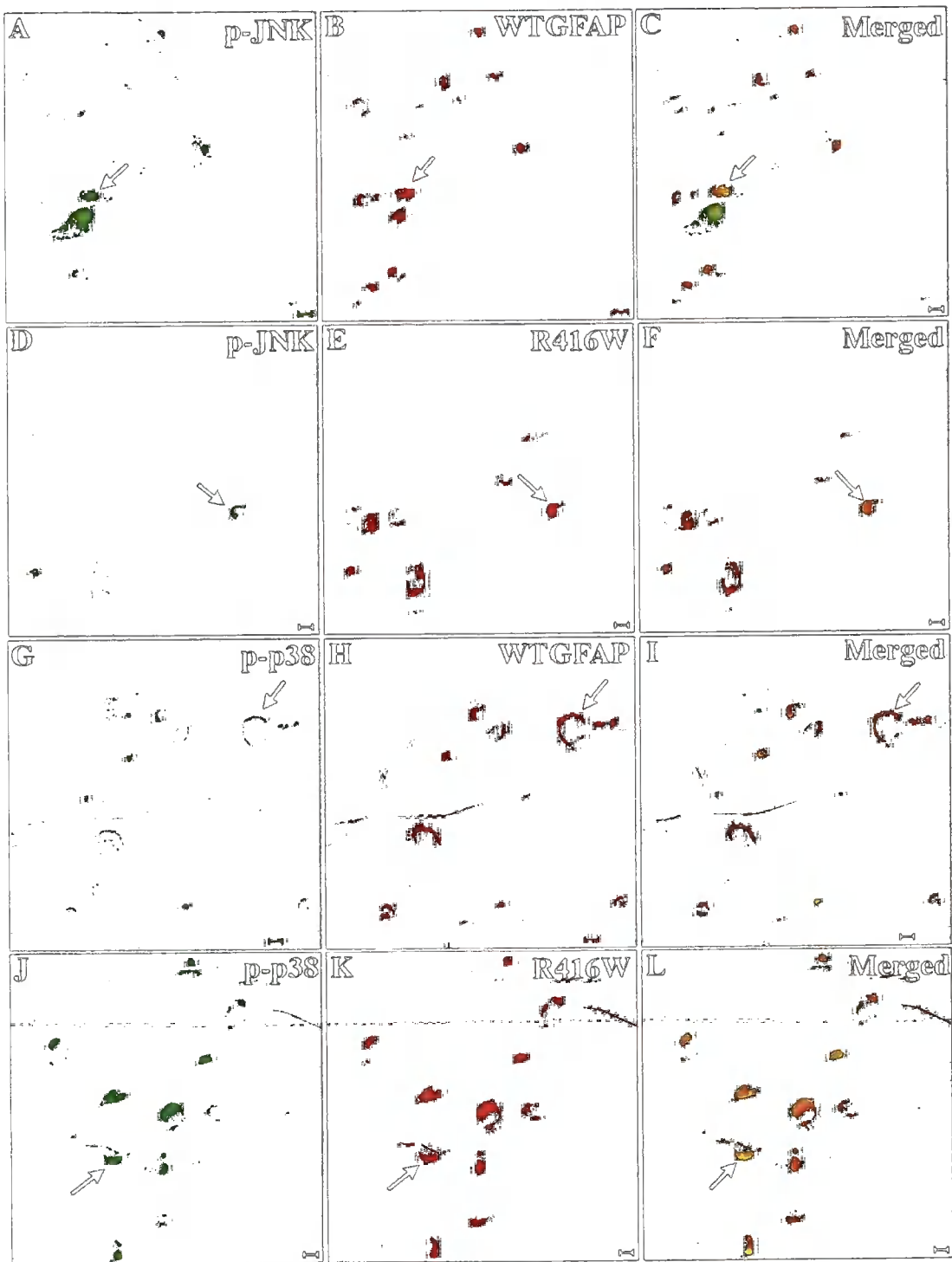
Figure 4.16. Colocalisation of GFAP with p-JNK and p-p38 in DBT cells. DBT-GFAPWT (A-C and G-I) and DBT-GFAPR416W (D-F and J-L) cells grown in the presence of 1 µg/ml Dox for 4 days were stained with anti-human GFAP antibody (B, E, H and K) and then were double stained with antibodies to phospho-JNK (A and D) and phospho-p38 (G and J). The distributions of p-JNK and p-p38 in relation to GFAP were visualised by confocal laser scanning microscopy. Merged images show regions of colocalisation between GFAP and p-JNK or p-p38 signals appearing yellow (C, F, I and L). Notice that whilst some p-JNK (A) and p-p38 (G) were colocalised with aggregates formed by wild-type GFAP (B and H), they were also detected by diffuse staining in other parts of the cells. The staining of p-JNK (D) and p-p38 (J) staining were largely colocalised with staining of GFAP aggregates formed by R416W mutant (E and K). Bars = 10 µm. Arrow, aggregates colocalised with p-JNK or p-p38.

	WT						R416W					
	uninduced			induced			uninduced			induced		
H₂O₂	−	−	+	−	−	+	−	−	+	−	−	+
Urea	−	+	−	−	+	−	−	+	−	−	+	−
Dox	−	−	−	+	+	+	−	−	−	+	+	+
hGFAP												
p-JNK												
JNK												
p-p38												
p38												
Actin												
	1	2	3	4	5	6	7	8	9	10	11	12
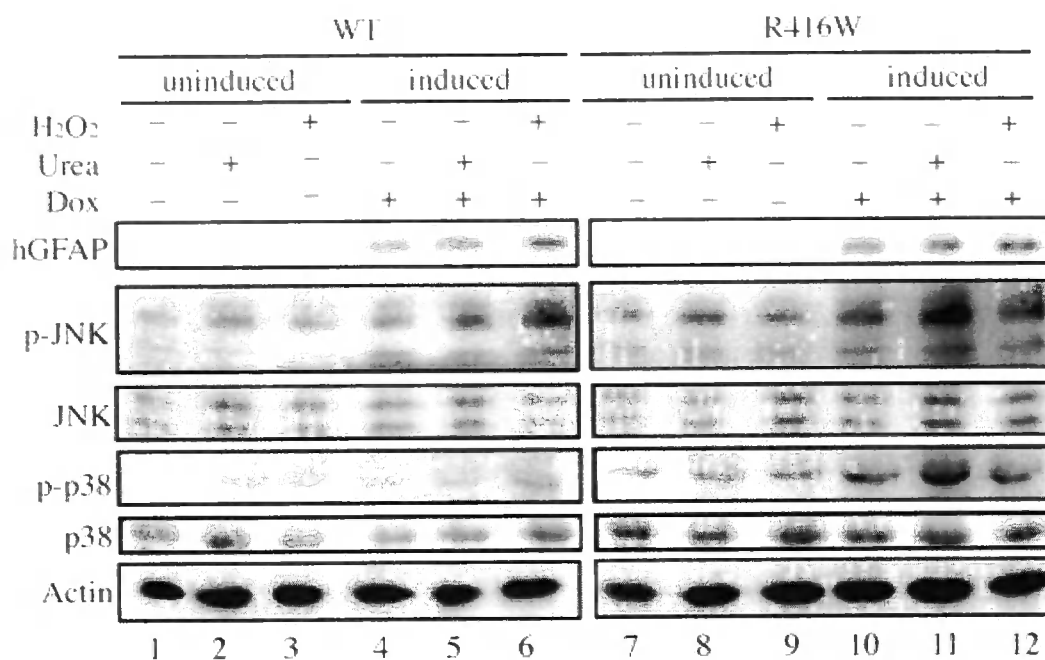
Figure 4.17. Effect of GFAP expression on SAPK activation after stress. DBT stably expressing wild-type and R416W GFAP cells were cultured in the absence (lanes 1-3, 7-9) or presence (lanes 4-6, 10-12) of 1 µg/ml Dox. After 4 days of culture, cells were either left untreated (lanes 1, 4, 7, 10) or treated with 450 mM urea (lanes 2, 5, 8, 11) or 400 µM H₂O₂ (lanes 3, 6, 9, 12) for 1 hour. Cells were then lysed in RIPA buffer and the pellet fractions prepared from the whole cell lysates were analysed by immunoblotting using SMI-21 antibody against human GFAP. The rest of antibodies used included phospho-JNK (p-JNK), JNK, phospho-p38 (p-p38), and p38 antibodies. Anti-actin was used to detect actin as a loading control. No significant difference was observed in activated p-JNK and p-p38 between the induced cells (lanes 4-6, 10-12) and the uninduced cells (lanes 1-3, 7-9). The amount of these proteins in treated wild-type (lanes 5 and 6) or R416W (lanes 11 and 12) GFAP-expressing cells displayed similarly to untreated cells (lanes 4 and 10), although p-JNK increased slightly as GFAP expression was induced synergistically with urea treatment (lanes 5, 11).

In respect to the levels of p-JNK and p-p38 in GFAP-expressing cells, the activation of these two SAPKs did not increase predominantly after stress treatment. These findings are consistent with previous data showing that regardless of the extrinsic stress, stable GFAP expression especially the R416W GFAP mutation, is able alnoe to activate JNK and p38. Therefore, it raises the possibility that the levels of p-JNK and p-p38 can not further increase dramatically under stress treatment conditions, as they are already highly activated by GFAP expression.

4.3.7 Rescue of cell survival by inhibition of JNK and p38 after hyperosmotic shock

Given the fact that the presence of R416W GFAP induces SAPK activation and makes cells more stress-sensitive, it is reasonable to assume that inhibition of SAPK activation could increase cell viability after stress-induced recovery. According to the previous results that showed urea treatment leading to an increase in p-JNK levels (Fig. 4.17), GFAP-expressing cells DBT-GFAP^{WT} (Fig. 4.18A) and DBT-GFAP^{R416W} cells (Fig. 4.18B) were exposed to 900 mM urea following pretreated with a wide range of cellular signalling inhibitors, including JNK inhibitor SP600125, p38MAPK inhibitor SB203580, ERK inhibitor U0126, and general caspase inhibitor Z-VAD-FMK. Cells were then allowed to recover for four days and cell survival was determined by cell viability assay. Suppression of p38 activation by SB203580 led to increases in cell viability of both DBT-GFAP^{WT} and DBT-GFAP^{R416W} cells. In contrast, inhibition of JNK activation by SP600125 significantly increased cell viability of the DBT-GFAP^{R416W} cells after stress-induced recovery. Immunoblotting confirmed that treatment of DBT-GFAP^{R416W} cells with 50 µM JNK inhibitor SP600125 (Fig. 4.18C, lane 3) and 30 µM p38 inhibitor SB203580 (Fig. 4.18D, lane 3) before hyperosmotic shock decreased JNK and p38 phosphorylation by ~70% and ~75% respectively. These results strongly suggest the presence of R416W GFAP compromised the ability of astrocyte to recover from physiological stress and this is specifically correlated with
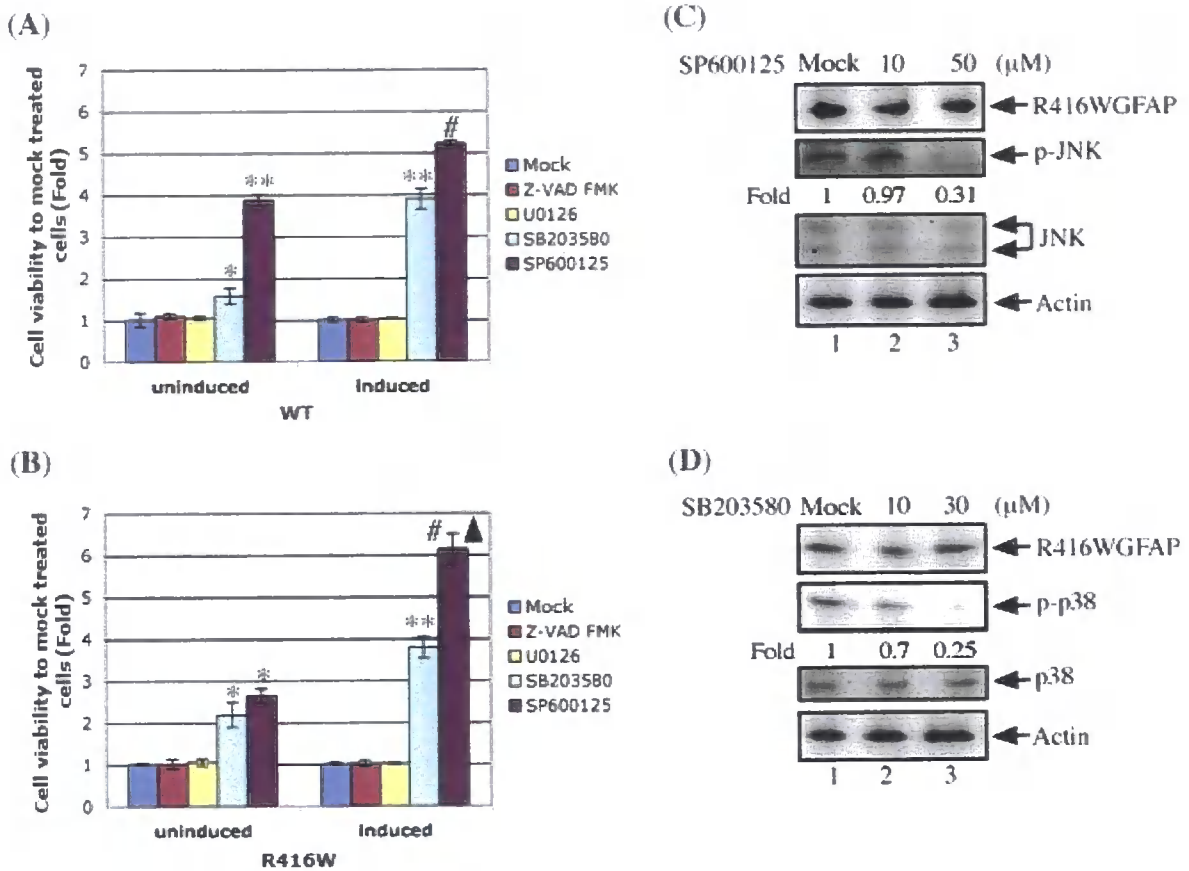
Figure 4.18. Inhibition of JNK and p38 phosphorylation increases cell viability after stress-induced recovery. DBT-GFAPWT (A) and DBT-GFAPR416W (B) cells were mock treated with 0.1% (v/v) DMSO or pre-treated for one hour with 20 µM Z-VAD-FMK, 20 µM U0126, 30 µM SB203580 or 50 µM SP600125. After pre-treatments, cells were grown in either uninduced or induced conditions for 2 days, followed by treatment again with the above inhibitors for 1 hour. Cells were then subjected to hyperosmotic shock by exposure to 900 mM urea for 1 hour. Following this treatment, cells were allowed to recover in normal growth medium for 4 days and cell survival was determined by cell viability assay. Data from three independent experiments are shown as mean $\pm$ SD and present as bar charts. Statistical significance was determined by t test and asterisks (*) highlight P value < 0.05 when compared to mock-treated cells. **, $P < 0.01$. #, $P < 0.001$ (A, B). ▲, $P < 0.05$ compared to SP600125 treated wild-type GFAP-expressing cells (B). Immunoblotting confirmed that cells treat with 50 µM SP600125 (C, lane 3) and 30 µM SB203580 (D, lane 3) significantly decrease the phosphorylation of JNK and p38, respectively. Notice that the levels of total JNK and p38 in untreated cells (C and D, lane 1) were similar to those in inhibitor-treated cells (C and D, lanes 3 and 4). The same blots probed with anti-actin antibody were used as loading controls.

the activation of SAPK pathways, as inhibition of these pathways increased the stress resistance of the R416W GFAP-expressing cells.

4.4. Possible disease mechanisms related to R416W GFAP compromising cell recovery from stresses

4.4.1 R416W GFAP is more stable than wild-type GFAP when induced to express

Whilst the genetic basis for AxD is now firmly established, little is known regarding the mechanisms by which GFAP mutations lead to disease. One possible mechanism by which GFAP mutations are responsible for the disease is by raising levels of the protein; for instance, by increasing its stability, as shown in R239C GFAP-transfected cells (Hsiao et al., 2005).

To assess the stability of wild-type and R416W GFAP, DBT-GFAP^{WT} and DBT-GFAP^{R416W} cells were induced by Dox for 3 days. After induction, cells were cultured for further 4 days either in the presence of Dox for continuous induction or in the absence of Dox to switch off GFAP expression. The insoluble fractions were prepared from these cultures and analysed by immunoblotting with an anti-human GFAP antibody. After induction, the levels of both wild-type (Fig. 4.19A, lanes 2-7) and mutant GFAP (Fig. 4.19B, lanes 2-7) increase over time. Whilst R416W GFAP expression can be detected one day after induction (Fig. 4.19B, lane 2), wild-type GFAP was not expressed until the third day of induction (Fig. 4.19A, lane 3). To shut down GFAP expression, cells were first induced for three days and then returned to normal growth conditions for various times as indicated. Removal of Dox from growth medium rapidly turned off wild-type GFAP expression (Fig. 4.19A, lanes 8-11), whereas this occurs slowly for R416W GFAP (Fig. 4.19B, lanes 8-11). These results suggest R416W mutation in GFAP may alter the normal turnover of GFAP and possibly increase GFAP filament stability that remains to be investigated. In line with that R239C mutant was reported to alter the extraction solubility and
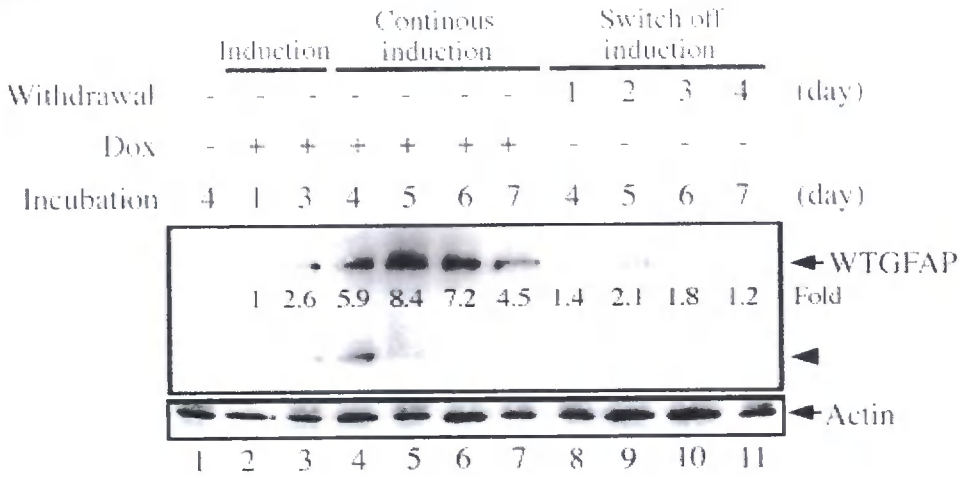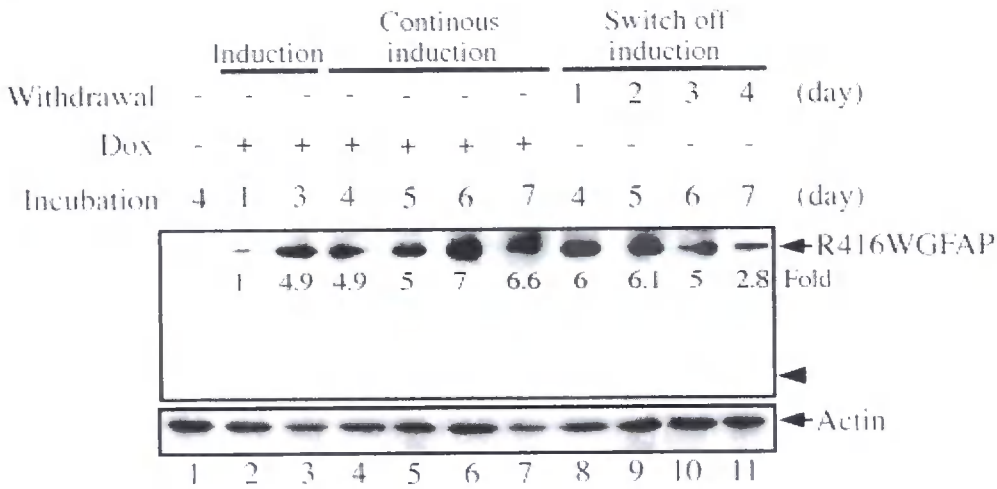
Figure 4.19. Expression of R416W mutant alters the normal turnover of GFAP in DBT cells. DBT-GFAPWT (A) and DBT-GFAPR416W (B) cells were first induced for 1 and 3 days (lanes 2 and 3) at 1 ug/ml of Dox. After induction, cells were cultured either in the presence of Dox for continued induction of GFAP expression (lanes 4-7) or in the absence of Dox to switch off GFAP expression (lanes 8-11) for the indicated time intervals (shown as withdrawal time in days). DBT cell lines grown in the absence of Dox for 4 days were used as a negative control (lane 1). Insoluble fractions prepared from these cultures were analysed by immunoblotting with antibodies to human GFAP and actin, which was used as a loading control. The levels of wild-type and R416W GFAP expression in induced cells increase in a time-dependent manner. Whilst R416W GFAP expression can be detected as early as one day after induction (B, lane 2), wild-type GFAP was not expressed until the third day of induction (A, lane 3). Notice that removal of Dox switched off wild-type GFAP expression rapidly (A, lanes 8-11), whereas this occurred slowly for R416W GFAP (B, lanes 8-11). Arrowhead, proteolytic product from GFAP.

influence the stability of GFAP (Hsiao et al., 2005), here the findings in R416W GFAP after withdrawal of Dox further confirmed the stable status of mutant GFAP.

4.4.2 The UPS-mediated proteolysis of GFAP

RFs are astrocytic inclusions that accumulate in the brains of AxD patients. Previous biochemical analysis of RF-enriched fractions showed that GFAP, ubiquitin and the small stress proteins αB-crystallin and HSP27 are the major components (Tomokane et al., 1991), and ubiquitylated conjugates of αB-crystallin were found in RFs (Goldman and Corbin, 1991). In addition to RFs, ubiquitin has also been found in association with a variety of abnormal IF accumulations seen in pathological conditions (Lowe et al., 1992; Johnston et al., 1998). These include NFs in the neurofibrillary tangles of Alzheimer's disease and Lewy bodies of Parkinson's disease, nestin in desmin-related myopathies (Goebel and Warlo, 2000), Pick bodies of Pick's disease and keratin in Mallory bodies in alcoholic cirrhosis. The presence of ubiquitin in these inclusions indicates that cells have identified the pernicious potential of aggregates and seeks their destruction, albeit without success.

More direct evidence of ubiquitin involved in IFs protein turnover emerged for K8 and K18. The turnover of K8 and K18 was interfered with when they are ubiquitylated. Hence, inactivation of proteasome can stabilise their turnover (Ku and Omary, 2000). Most recently, R239C, the severest GFAP mutation causing AxD, was found to possess feedback interactions with proteasome activity, as the cytoplasmic inclusions induced by R239C human GFAP impaired proteasome function, and in turn, resulted in GFAP accumulation (Tang et al., 2006). These reports provided an insight to study the involvement of ubiquitylation on the turnover of GFAP.

4.4.2.1 The presence of R416W GFAP partially compromises the UPS function

The increased GFAP stability resulted from R416W mutation may lead to aberrant protein aggregation that impairs UPS function and increases protein ubiquitination. To test whether

152

expression of R416W GFAP increases ubiquitin conjugates, insoluble fractions prepared from uninduced and induced cultures were subjected to immunoblotting analysis with antibodies to GFAP and ubiquitin. After induction, the levels of both wild-type (Fig. 4.20A, lanes 2 and 3) and R416W GFAP (Fig. 4.20B, lanes 2 and 3) increased, whereas ubiquitinated proteins could not be detected (Fig. 4.20A and B, lanes 2 and 3, (Ub)n). These results suggest the basal level of the endogenous ubiquitin conjugates may be low and the extent of detectable ubiquitin signal is minimal.

To increase the ability to detect ubiquitinated proteins, DBT cell lines were treated with proteosome inhibitor MG-132 for 24 hours. Following this treatment, the level of detectable ubiquitinated proteins significantly increased. Both wild-type (Fig. 4.20A, lanes 4-6) and R416W GFAP (Fig. 4.20B, lanes 4-6) and their degradation products (Fig. 4.20A and B, lanes 5 and 6, arrowheads) were also increased. Several ubiquitin conjugates were detected in cells expressing R416W GFAP (Fig. 4.20B, lanes 5 and 6). Interestingly, GFAP expression was detected in DBT cells treated with MG-132 in the uninduced conditions (Fig. 4.20A and B, lane 4). On the one hand, GFAP could be considered as a stress protein, whose expression could be induced under proteolytic stress. On the other hand, Tet-On regulated protein induction in DBT-GFAP cell lines is likely to show leakiness for GFAP expression, since accumulation occurs after proteasome inhibition whereas it is processed by the UPS under normal condition.

Immunoblotting with antibody to αB-crystallin revealed that its level profoundly increased in MG-132-treated DBT cells (Fig. 4.20A and B, lanes 4-6), confirming that cells induce a stress response when proteosome function is inhibited. In conclusion, wild-type and R416W GFAP expression impairs the UPS function and in turn leads to GFAP accumulation. Consequently, accumulated GFAP and overwhelmed UPS promote cell death, as demonstrated in the GFAP-expressing cells treated with MG-132 (Fig. 4.14B).
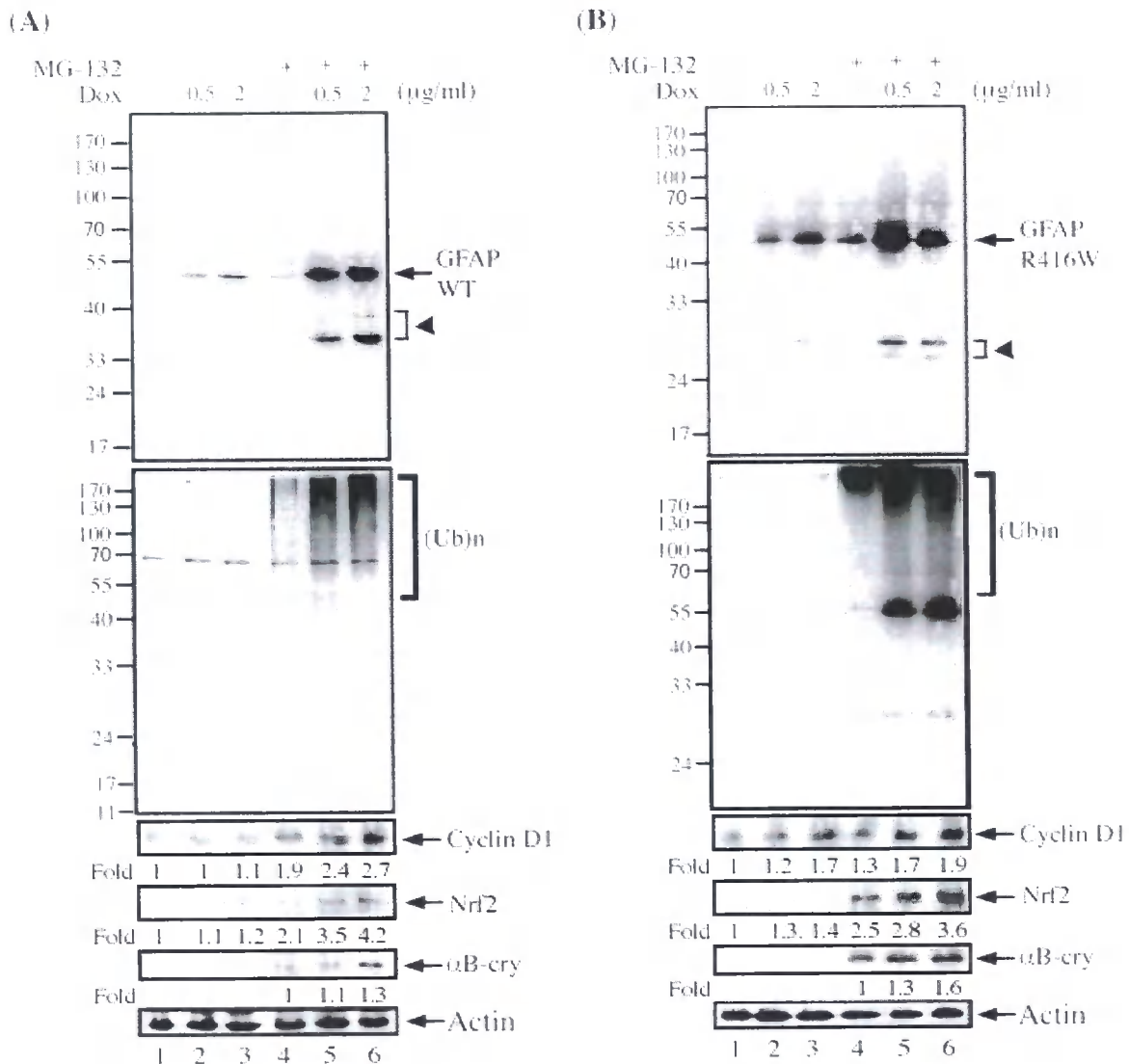
Figure 4.20. Effect of R416W mutation upon GFAP ubiquitination. DBT-GFAPWT (A) and DBT-GFAPR416W (B) cells were uninduced or induced at the indicated concentrations of Dox. Four days after induction, cells were then either untreated (A and B, lanes 1-3) or treated with 2 μM MG-132 for 24 hours (A and B, lanes 4-6). Insoluble fractions prepared from these cultures were analysed by immunoblotting with antibodies to GFAP, ubiqutin, cyclin D1, Nrf-2, αB-crystallin and finally actin, which was used as a loading control. Notice that the levels of both wild-type and R416W GFAP significantly increased in cells treated with MG-132 (A and B, lanes 5 and 6). Proteosome inhibition induced more ubiquitinated conjugates in cells expressing R416W GFAP (B, lanes 5 and 6). That the levels of cyclin D1 and Nrf-2 only marginally increased in DBTR416W GFAP cells following MG-132 treatment (B, lanes 5 and 6) suggests R416W GFAP partially inhibits the UPS function. Proteosome inhibition induces cellular stress response, as demonstrated by the increase in αB-crystallin level in DBT cells treated with MG-132 (A and B, lanes 4-6). The full-length wild-type and R416W GFAP were indicated by arrows and the low molecular weight bands, which likely represent proteolytic fragments, were indicated by arrowheads. (Ub)n, polyubiquitination.

4.4.2.2 GFAP expression affects turnover of cyclin D1 and Nrf-2

To assess whether aggregates formed by R416W GFAP compromise proteosome function, the turnover of defined proteosome substrate, such as cyclin D1 (Diehl et al., 1997), was examined. Immunoblotting analysis revealed that the level of cyclin D1 is low in DBT cells expressing wild-type GFAP (Fig. 4.20A, lanes 2 and 3) and slightly increased in R416W GFAP expressed DBT cells (Fig. 4.20B, lanes 2 and 3). Following treatment with MG-132, cyclin D1 was markedly elevated in wild-type GFAP-expressing cells (Fig. 4.20A, lanes 5 and 6), but only marginally increased in R416W GFAP expressed cells (Fig. 4.20B, lanes 5 and 6).

Similar observations were made on another proteosome substrate Nrf-2. Whilst the basal level of Nrf-2 is very low in both DBT-GFAP^{WT} (Fig. 4.20A, lanes 1-3) and DBT-GFAP^{R416W} cell lines (Fig. 4.20B, lanes 1-3), Nrf-2 level significantly increased after treatment with MG-132 (Fig. 4.20A and B, lanes 4-6) and the highest level was observed in R416W GFAP-expressing cells (Fig. 4.20B, lanes 5 and 6). These results suggest that the presence of R416W GFAP partially compromises the UPS function, as demonstrated by interfering with the turnover of proteosome substrates cyclin D1 and Nrf-2.

4.4.2.3 Immunoprecipitation reveals that R416W GFAP is ubiquitinated

Proteosome inhibition of DBT cells by MG-132 markedly increased GFAP levels (Fig. 4.21A and C; lanes 1 and 3) and generated GFAP ladders in induced DBT-GFAP^{R416W} cells (Fig. 4.21C, lane 3), which likely represent ubiquitin conjugates of R416W GFAP. To test GFAP ubiquitination, insoluble fractions prepared from induced DBT cells were solubilised, immunoprecipitated with GFAP antibody and analysed by immunoblotting with antibody to ubiquitin. The results showed that in the induced DBT-GFAP^{R416W} cells a protein band of ~58 kDa recognised by both GFAP (Fig. 4.21C, lane 4, asterisk) and ubiquitin (Fig. 4.21D, lane 4,

(A)

MG-132   -   -   +   +
         P IP P IP

170
130
100
70
55   ← GFAP
40
                      ◄
33

24

      1   2   3   4

(B)

MG-132   -   -   +   +
         P IP P IP

                      ⎤
170   ⎥ (Ub)n
130   ⎥
100   ⎦
70
55   ◄—HC
40

33

                      ◄—LC
24

      1   2   3   4

(C)

MG-132   -   -   +   +
         P IP P IP

170
130
100
70
55   * ← GFAP
40

33
                      ◄
24

      1   2   3   4

(D)

MG-132   -   -   +   +
         P IP P IP

170   ⎤
130   ⎥ (Ub)n
100   ⎥
70   ⎦
55   *
40

33

                      ←LC
24

      1   2   3   4
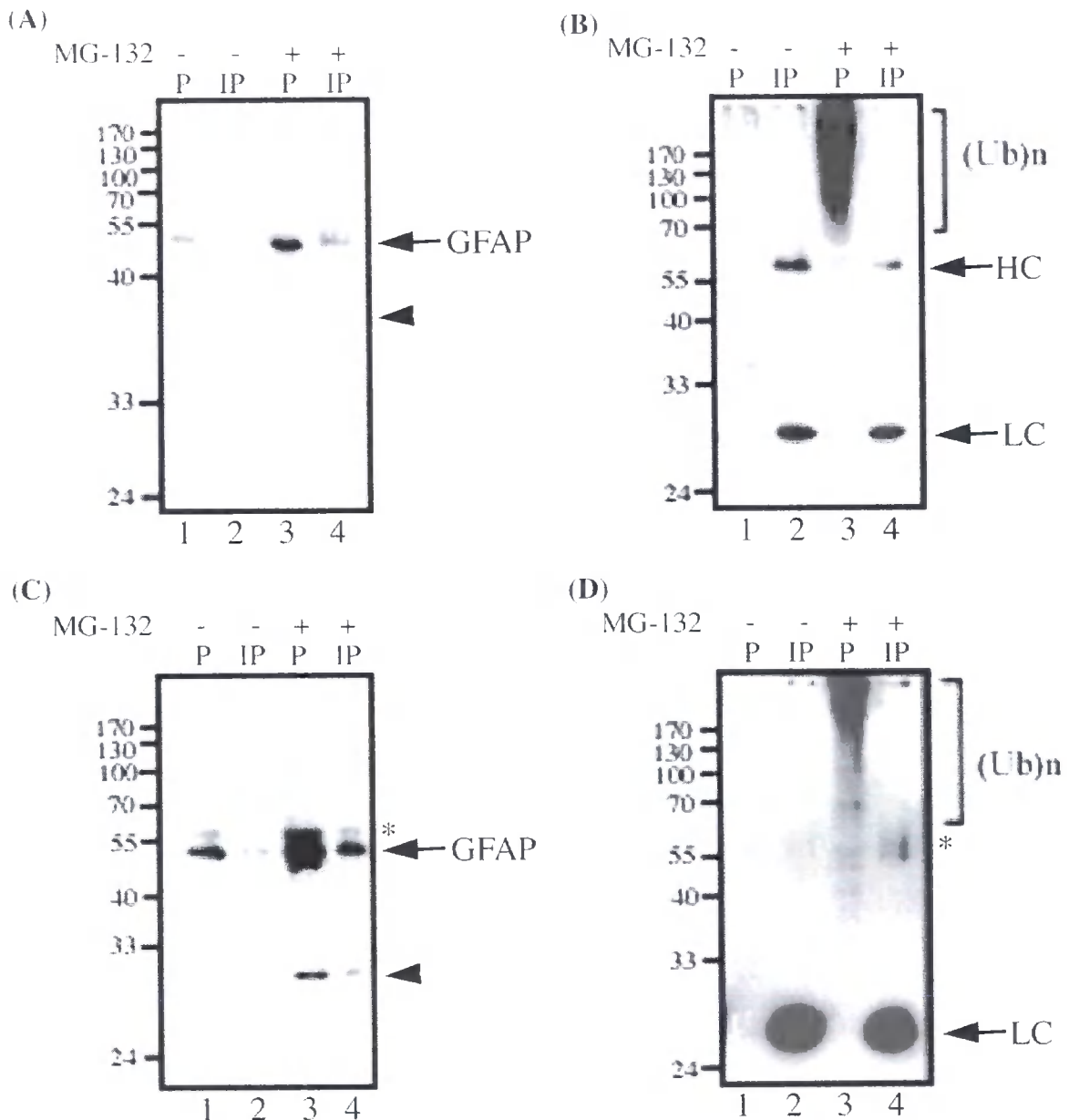
Figure 4.21. Analysis of GFAP ubiquitination by immunoprecipitation.
DBT-GFAPWT (A and B) and DBT-GFAPR416W cells (C and D) induced
for three days at 1 µg/ml of Dox were either left untreated (A-D, lanes 1 and 2)
or treated with 2 µM MG132 for 24 hours (A-D, lanes 3 and 4). The IF-enriched
cytoskeletal pellets (P) prepared from these cultures were solubilised,
immunoprecipitated (IP) with a monoclonal anti-human GFAP antibody and
analysed by immunoblotting with polyclonal anti-GFAP antibody (3270)
(A and C) and monoclonal anti-ubiquitin antibody (P4D1) (B and D). Notice
that monoubiquitinated R416W GFAP that was immunopositive for both GFAP
(C, lane 4, asterisk) and ubiquitin (D, lane 4, asterisk) was detected in MG-132-
treated DBT-GFAPR416W cells. The heavy chain (HC) and light chain (LC) of
immunoprecipitating antibody are indicated. Arrowheads highlight low molecular
weight bands that likely correspond to proteolytic fragments (A and C). Arrowhead,
proteolytic fragment. (Ub)n, polyubiquitination.

asterisk) antibodies likely corresponds to monoubiquitinated R416W GFAP. In contrast, the level of ubiquitinated wild-type GFAP in DBT-GFAP^{WT} cells was undetectable by immunoblotting (Fig. 4.21A and B, lane 4). These data indicate that R416W GFAP is more prone to ubiquitination, particularly with enhanced level of ubiquitinated species upon proteosome inhibition.

4.4.3 The unfolded protein stress is not activated by GFAP expression

Accumulation of misfolded protein in the endoplasmic reticulum (ER) triggers an adaptive stress response, termed the unfolded protein response (UPR), which is mediated by UPR transducers, PKER kinase (PERK), activating transcription factor 6 (ATF6) and inositol-requiring enzyme 1 (IRE1). Among these transducers, IRE1 is particularly important in modulating the excision of a 26-nucleotide intron from X-box binding protein 1 (XBP1), resulting in the generation of a transcriptional activator (Yoshida et al., 2001). Spliced XBP1 migrates to the nucleus and induces the expression of ER chaperones (often termed Grps), many of which are homologous to the cytosolic HSPs (Chapman et al., 1998; Welihinda et al., 1999), for protein folding and genes involved in the degradation of misfolded proteins (Lee et al., 2003). Prior to analysing the relationship between GFAP expression and the UPR, the conditions for induction of the UPR was tested by stimulating the human HeLa cells with 10 mM DTT for 6 hours. Given the fact that activation of XBP1 resulted in removal of an unique *Pst*I site from the mRNA transcript (Calfon et al., 2002), a higher molecular weight band was observed on agarose gels after the XBP1 cDNA was digested with *Pst*I (Fig. 4.22, lane 2). In the absence of DTT, however, XBP1 cDNA was not spliced and *Pst*I-containing cDNA was digested into two fragments (Fig. 4.22, lane 1). To investigate whether accumulation of GFAP induces the UPR, total mRNA prepared from DBT cells expressing wild-type (Fig. 4.22, WT) or R416W GFAP (Fig. 4.22, R416W), either inducibly (Fig. 4.22, lanes 3-10) or transiently
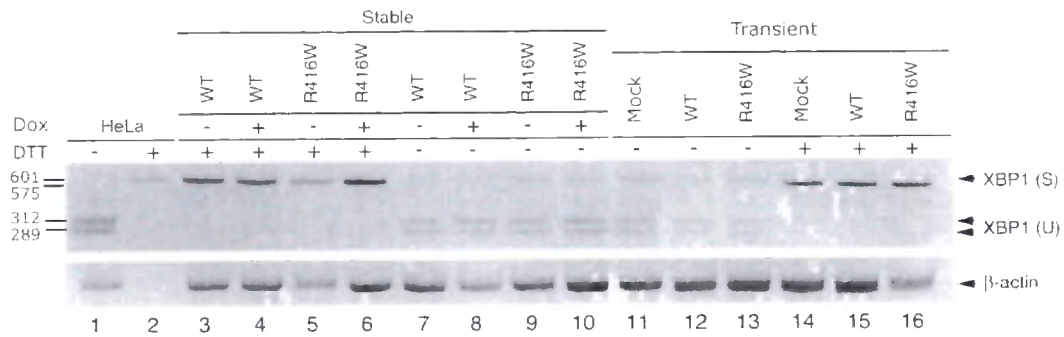
Figure 4.22. XBP1 mRNA is not spliced in GFAP-expressing cells. As pre-condition experiments, HeLa cells were untreated (lane 1) or treated with 10 mM DTT (lane 2) for 6 hours. DBT stably expressing wild-type GFAP (WT) or R416W GFAP (R416W) cells were cultured in the absence or presence of 1 µg/ml Dox for 4 days (lanes 3-10), followed by treated without (lanes 7-10) or with 10 mM DTT (lanes 3-6) for 3 hours. For transient transfection, DBT cells were transfected with pcDNA3.1 (Mock) or WT and R416W GFAP plasmid DNA. After 72 hours transfection, cells were either left untreated or treated with 10 mM DTT for 3 hours. Following DTT treatment, cells were lysed in TRIzol reagent, and the extracted total RNA was subjected to RT-PCR to detect XBP1. The resulted cDNA was digested with *Pst*I, and analysed by 2% agarose gel to visualise the activated spliced (S) and unspliced (U) XBP1. Actin served as a control (lower panel). After DTT treatment, a high molecular weight band (~575 bp) represented the spliced undigested XBP1 was observed in HeLa cells (lane 2), which was used as a positive control. Neither WT nor R416W GFAP expression induced the splicing of XBP1 in the absence of DTT. In contrary, XBP1 remained unspliced and resulted in one high molecular weight band as well as two digested fragments from *Pst*I (lanes 1, 7-13) digestion. No significant difference was shown between stable cell lines (lanes 3-10) and transient transfected cells (lanes 11-16) expressing WT or R416W GFAP.

(Fig. 4.22, lanes 11-16), were subjected to RT-PCR. XBP-1 cDNA were then digested with

PstI and the resulting products were analysed by 1% or 2% agarose gel. Whilst induction of

XBP1 processing by DTT treatment generated a single *PstI*-resistant band (Fig. 4.22, lanes 3-6

and 14-16), untreated cells produced a *PstI*-sensitive product that was digested into two low

molecular weight fragments (Fig. 4.22, lanes 7-13). Cells expressing either wild-type or

R416W GFAP exhibited similar digestion patterns as those in untreated HeLa cells (Fig. 4.22,

lane 1), suggesting that the UPR is not activated in wild-type or R416W GFAP expressed cells.

Given that GFAP expression does not activate the UPR signalling cascades, it is suggested that

osmotic shock and oxidative stress-induced cell loss in GFAP-expressing cells does not result

from the ER stress.

4.4.4 Proteolytic fragments induced by GFAP expression are not generated by caspase cleavage

Several lines of evidence have demonstrated proteolysis of the cytoskeleton proteins is

mediated by caspases, a conserved family of cysteine proteases which specifically degrade

aspartate containing substrates. For instance, proteolysis of actin, the actin-serving protein

gelsolin or Gas2 by caspases cleavage leads to the disassembly of actin microfilament

networks (Brancolini et al., 1995; Kayalar et al., 1996; Kothakota et al., 1997; Mashima et al.,

1999). Also, keratin 14, 18 and keratin 19 (Caulín et al., 1997; Ku et al., 1997) along with the

lamins (A, B, C) (Lazebnik et al., 1995; Orth et al., 1996; Rao et al., 1996; Takahashi et al.,

1996) are cleaved by caspase-6 (and/or other caspases) at their respective L1-L2 linker

domain, resulting in the cytoskeleton reorganization during apoptotic cell death. Similarly,

proteolysis of desmin by caspase-6 at VXMD motif in L1-L2 linker domain also interferes

filament assembly, and the large aggregates that are formed promote apoptosis (Chen et al.,

2003).

As for the IFs in astrocytes, vimentin, a multiple cleavage substrates of caspase-3, -7 (Asp[85]) and -6 (IDVA[259]), can induced apoptosis by either caspase proteolysis to dismantle IFs, or producing a pro-apoptotic cleavage fragment to amplify cell death signal (Byun et al., 2001). Most recently, GFAP cleaved fragments were found generated by caspase-3 in Alzheimer's disease brains (Mouser et al., 2006). In line with this GFAP possesses a possible caspase cleavage site of the motif VELA in L1-L2 linker domain, corresponding to IDVA in vimentin, these findings suggest that the proteolysis of GFAP could be mediated by the caspase apoptotic pathway.

Immunoblotting analysis with anti-GFAP antibody revealed that the insoluble cytoskeletal fraction prepared from induced cultures not only produced prominent bands corresponding to full-length GFAP (Fig. 4.23A, arrow), but also generated proteolysed GFAP fragments with higher electrophoretic motilities (Fig. 4.23A, arrowheads). Whilst expression of wild-type GFAP in DBT-GFAP[WT] cells generated a ~36 kDa fragment (Fig. 4.23A, lane 4), a ~29 kDa fragment was observed in cells expressing R416W GFAP (Fig. 4.23A, lane 6). To investigate whether these low molecular weight bands correspond to proteolytic fragments generated by caspase, cells were treated with broad-spectrum caspase inhibitor Z-VAD-FMK (Fig. 4.23B and C, lanes 2 and 3). Treatment of DBT cells expressing either wild-type (Fig. 4.23B) or R416W GFAP (Fig. 4.23C) with caspase inhibitor (Fig. 4.23B and C, lanes 2 and 3) did not prevent GFAP proteolysis, suggesting that these proteolytic fragments were not generated by caspase cleavage.
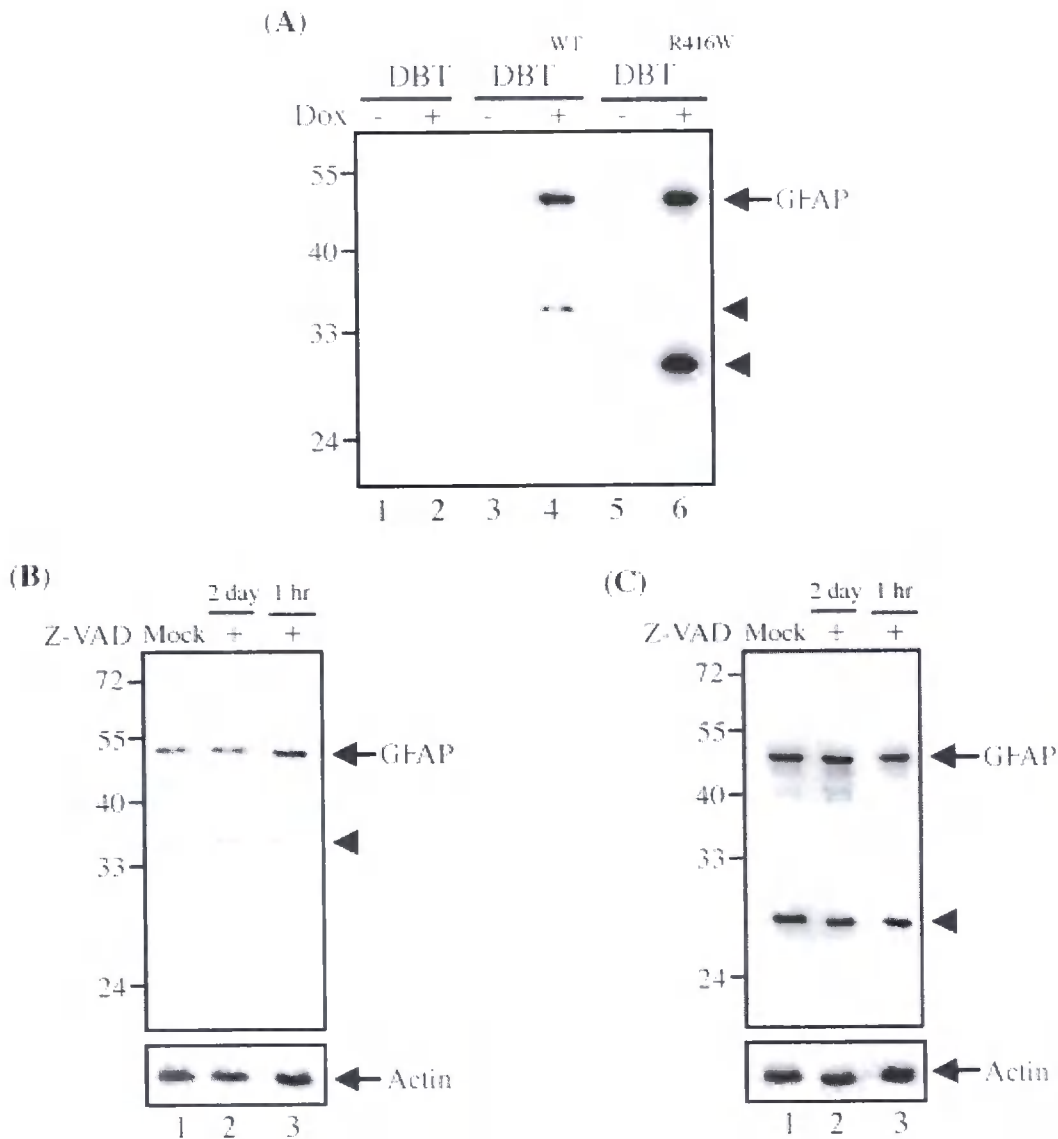
Figure 4.23. Expression of both wild-type and R416W GFAP generates proteolytic fragments. DBT-GFAPWT (A, lanes 3 and 4) and DBT-GFAPR416W (A, lanes 5 and 6) cells were grown in the absence (-) or presence (+) of Dox for 4 days. Parental DBT cells grown in the same conditions were used as a control (A, lanes 1 and 2). The insoluble fractions prepared by cytoskeletal extraction were subjected to immunoblotting analysis with anti-human GFAP antibody. Notice that whilst DBT cells induced to express wild-type GFAP generated a ~36 kDa proteolyitc fragment (A, lane 4, arrowhead), a fragment of ~29 kDa in size was detected in cells expressing R416W GFAP (A, lane 6, arrowhead). To test whether these fragments were generated by caspase cleavage, DBT-GFAPWT and DBT-GFAPR416W cells were pre-treated with 20 µM general caspase inhibitor Z-VAD-FMK for one hour (B and C, lane 3). After this treatment, cells were induced to express either wild-type (B) or R416W (C) GFAP in the presence of 20 µM Z-VAD-FMK for two days (B and C, lane 2). Induced cells treated with 0.1% (v/v) DMSO for the same period of time was used as a control (B and C, lane 1). Representative blots showed the same degradation pattern between control cells and Z-VAD-FMK-treated cells, suggesting that the caspase inhibitor did not prevent GFAP from proteolysis. Equal loading of each sample was confirmed by immunoblotting with anti-actin antibody.

4.5 Discussion

Intracellular or extracellular protein aggregates resulted from unfolded/misfolded or mutant proteins are ubiquitously characterized in a wide variety of neurodegenerative diseases (Forman et al., 2004). For instance, accumulation of NFs is pathologically featured in various neurodegenerative diseases, such as Parkinson's disease (Schmidt et al., 1991), Alzheimer's disease (Pollanen et al., 1994) and amyotrophic lateral sclerosis (Julien, 2001). The pathogenesis of neurodegeneration, however, remains to be resolved by the questions including: (1) the nature of the misfolded or aggregated proteins, how do they lead to neurodegeneration? (2) the toxicity of the aggregates, are they themselves one of the species being toxic to the cells? (3) the selected vulnerability of proteins, what is the underlying mechanism to sensitize the proteins ubiquitously expressed in the brain?

In the present study, I present evidence to suggest that the R416W mutation in GFAP causes AxD by compromising astrocyte sensitivity to stress. The reported cases of patients with R416W mutation displaying a wide range of disease severity as reflected in the age of onset, led me to further investigate whether environmental and epigenetic factors could influence the onset of disease progression. My initial studies had demonstrated that the R416W mutation has the potential to be very disruptive to filament assembly *in vitro* (Perng et al., 2006). Transient transfection studies suggested, however, that the level of GFAP expression and the availability of a co-assembly-competent endogenous filament network could ameliorate this potential, to the extent that R416W GFAP could fully integrate into an endogenous GFAP/vimentin network with no overt effects upon its distribution (Perng et al., 2006). Indeed, when I established stable, Dox-inducible astrocytic cell lines, then R416W GFAP was found to not always disrupt the endogenous IF networks, but to incorporate into GFAP networks when expressed at low levels. The potential functional impact of incorporating low levels of the disease-causing GFAP mutant into the pre-exiting GFAP networks is that this cell line responded poorly to both hyperosmotic and oxidative stresses in the presence of R416W GFAP. These data show for the first time that it

is possible to experimentally separate the dominant effects upon IF assembly of a GFAP mutation from the potential negative consequences on function. The compromised function of R416W mutation in GFAP was revealed only when astrocytes were stressed by either hyperosmotic or oxidative insults and thus offers a potential explanation for the phenotypic variations seen in the age of disease onset for this particular GFAP mutation.

4.5.1 Dominant-negative mutant can incorporate into the endogenous GFAP

The most abundant cells in the CNS are astrocytes, which can support neuronal structure, trophy, metabolism and regeneration after brain injury (Pekny and Nilsson, 2005). These functions are dependent on the ability of astrocytes to survive brain insults and react actively to the injuries. As GFAP is the major IF in astrocytes, it raises the possibility that aberration of GFAP may promote the dysfunction of astrocytes to precipitate AxD. In support this human wild-type GFAP expression in transgenic mice showed lethal effects mimicing AxD (Messing et al., 1998; Hagemann et al., 2005), most recently the knock-in mice with human homologous GFAP mutations generated RFs that correlated GFAP levels to the severity of AxD (Hagemann et al., 2006). Gain-of-function mechanisms occurred in IFs cause cell malfunction and subsequent cell death.

U343 MG-A cells express high endogenous levels of GFAP and its assembly partner vimentin. Transient expression of R416W GFAP in this cell line can either form aggregates or integrate into filamentous networks. These results suggest that the mutation was only dominant over wild-type protein once a certain threshold had been crossed and the relative levels between R416W GFAP and the endogenous GFAP could determine the final IF network organisation. To test this hypothesis, I established a stable cell line using U343 MG-A cells. The expression of R416W GFAP in this cell line was followed by a monoclonal antibody that specifically recognised the mutant but not the wild-type GFAP (Perng et al., 2006). Quantification of relative levels of R416W and total GFAP revealed that although the induced U343-GFAP[R416W] cells expressed 10

times more R416W GFAP than the uninduced cells, this expression level is still only ≤ 10% of the endogenous GFAP, indicating that the expression level of R416W GFAP is relatively low compared to the endogenous GFAP in U343-GFAP^{R416W} cells. Double label immunofluorescence microscopy revealed that at this expression level R416W GFAP integrates into the endogenous GFAP, suggesting that GFAP filaments can tolerate the incorporation of a GFAP mutant that is by itself assembly incompetent. Lacking a functional assay for IF in cells, however, it can only be maintained that a GFAP network including R416W GFAP appears normal by immunofluorescence microscopy.

4.5.2 Stress – a key factor in Alexanders disease

IFs are extremely sensitive to stress and the collapse of IF is part of the stress response (Kopito and Sitia, 2000; Welch et al., 1985). These observations suggest to me that the mutational effects may not be revealed unless cells are stressed. Because relatively few studies have been undertaken on stressing IFs to date (Pekny and Lane, 2007), there is no clear consensus yet on the best methods to use. I have tried various stressful conditions to test the relationships between IF mutation and astrocyte dysfunction. The first based on assays to test the reaction of astrocytic IF cytoskeleton to volume regulation (Pasantes-Morales et al., 1990), which provide a functional cell assay in which the impact of stress on IFs can be induced and analysed (Lane and Pekny, 2004). The response of mutant IFs in astrocytes to osmotic and oxidative conditions is enigmatic. Only astrocytes ablated of GFAP or vimentin respond less efficiently to osmotic stress, as measured by taurine efflux (Ding et al., 1998).

Cells exposed to hyperosmotic stress are initially shrunk and then regain their osmotic balance by a compensatory mechanisms called regulatory cell volume increase (RVI) that is achieved by the activation of ion pumps and carriers (Haussinger, 1996; Okada et al., 1994). The reverse, hypoosmotic stress causes cell swelling and returned to their normal volume by the regulatory volume decrease (RVD) by loss of cellular water. Most mammalian cells have developed these

two opposite mechanisms to respond to osmotic stress. Nonetheless, unable to cope with the extreme non-physiological conditions, many types of cells are disrupted by osmotic stress as the fate of death, or survival to reconstruct from the disturbed cell architecture and functions (Schwartz and Osborne, 1993; Kultz and Burg, 1998).

In the initial studies, I tested a range of hypo-osmotic conditions to stress established cell lines, but no significant effect was observed. It was only when the cells were challenged with hyperosmotic shock that the deleterious effect of the R416W mutation became apparent. DBT-GFAP^{R416W} cells expressing R416W GFAP had delayed recovery after hyperosmotic shock campared to uninduced cells or the control cells expressing wild-type GFAP. These results implicate the integrity of the GFAP network as playing a critical role in protecting astrocytes against osmotic shock. The GFAP cytoskeleton network compromised by the dominant-negative mutation could also render cells less able to cope with, and recover from osmotic stress. These effects are not due to the expression of human GFAP in the mouse cell background, because similar results were observed when a human astrocytoma clonal cell line, U343-GFAP^{R416W}, was established. Once again, no effect was seen upon the endogenous GFAP networks, but once R416W GFAP was present then these cells recovered poorly from osmotic stress.

I expected that these effects would not be limited to just osmotic stress and therefore I used an oxidative stress, exposing the various cell lines to hydrogen peroxide and monitoring their recovery, with the idea that oxidative stress has been implicated in a mouse knock-in R236Hh mutant GFAP (Hagemann et al., 2006). Cells in the CNS are extremely susceptible to oxidative insult, as they consume high amount of oxygen and possess enriched polyunsaturated fatty acids in their membranes. Oxidative stress implicated in aging (Bachman et al., 1993) or brain injuries- and neurodegenerative diseases-associated pathologic processes is mainly induced by excess production of reactive oxygen species (ROS) (Coyle and Puttfarcken, 1993). This can damage neurons as well as alter astrocyte functions (Robb and Connor, 1998) such as protecting neurons from oxidative injury (Desagher et al., 1996). The demonstration of ROS involved in the

pathological features of Alzheimer's disease like neurofibrillary tangles, senile plaques, mitochondrial dysfunction, and microglia activation (Smith et al., 1996; Blass et al., 1990; Colton and Gilbert, 1987), indicate that oxidative stress plays a role in the pathogenesis of Alzheimer's disease. Nevertheless, oxidative stress events such as including protein oxidation, lipid peroxidation, and peroxynitrite formation (Behl, 1999; Benzi and Moretti, 1995; Butterfield et al., 1994; Markesbery and Carney, 1999; Smith et al., 1998), might not be the primary causative event in Alzheimer's disease.

Analysis of the consequences of oxidative stress in Tet-regulated cell lines, showed that those cells expressing R416W GFAP were significantly inhibited in their recovery. The change in filament distributions after the stress and during recovery was also investigated. Immunofluorescence microscopy revealed that R416W mutation induces filaments to bundle more extensively, but this is only apparent when the cells have been stressed. These observations provide an interesting parallel with the *in vitro* studies (Perng et al., 2006), which suggested that the mutation encouraged filament- filament associations. These data provide convincing evidence to support the conclusion that the R416W mutation is indeed a dominant mutation, rather than simply one that predisposes to disease as has been seen for some liver diseases caused by keratin mutations (Cavestro et al., 2003; Ku et al., 2005). These data also show for the first time that some GFAP with disease-causing mutations can integrate into an existing GFAP network without causing aggregate formation. The compromised function of GFAP only develops when the cells are stressed, implying that the R416W mutation requires additional factors to precipitate AxD.

These results further highlight how important stress is to reveal the impact of the R416W GFAP upon astrocytes. It is noticeable that amongst the known mutations causing AxD, the R416W has so far been found to induce all three forms of the disease – infantile-, juvenile- and adult-onset. This has led some to suggest that the patients' genetic background, environment and epigenetic factors could all contribute to the disease progression (Kinoshita et al., 2003). The present data support this view and suggest that chronic stress could be significant contributory

factors to the phenotypic variation seen for this particular mutation in GFAP.

With mutant GFAP expression, the noticeable cell death as a consequence of stress on astrocytes might be caused by various mechanisms. Swelling of astrocytes has been reported to represent a major component of the oedema (Martinez, 1968; Norenberg, 1997, 2001; Traber et al., 1989), perhaps attributed to the elevation of ammonia level in the brain. This hypothesis is supported by observed swelling of astrocytes after ammonia infusion in primates (Voorhies et al., 1983) or cultured astrocytes (Norenberg et al., 1991; Zwingmann et al., 2000). Oxidative stress implicated in the pathogenesis of ammonia neurotoxicity (Norenberg, 2003) can consequently activate MAPKs (Kyriakis and Avruch, 1996; Aikawa et al., 1997; Mielke and Herdegen, 2000; Ono and Han, 2000). Indeed, such activation has been shown in astrocytes in response to oxidant signalling (Luo and Roth, 2000; Mizuhashi et al., 2000; Chen S. H. et al., 2001; Lennon et al., 2002; Jayakumar et al., 2006).

Perturbation of cytoskeleton network is one of the early targets of oxidative stress (Dalle-Donne et al., 2001; Zhao and Davis, 1998), it has been suggested as the initial step of oxidant-induced cell damage. Selectively, oxidative injury changes cytoskeletal proteins (Aksenov et al., 2001), as represented in the altered structure and spatial organization of actin filaments (Dalle-Donne et al., 2001). Via direct oxidation of lipids, proteins and DNA, H_2O_2, a major source of ROS and as a signalling molecule, can also mediate cell damage by triggering cellular apoptotic pathways (Butterfield and Lauderback, 2002; Howe et al., 2004; Huang et al., 2004; Lin et al., 2004; Shin et al., 2004; van Rossum et al., 2004).

4.5.3 Activation of stress response in cells expressing an Alexander disease-causing mutation

JNK and p38 are reported to be involved in neurodegenerative mechanisms (Ferrer et al., 2001; Otth et al., 2003), the involvement of both kinases in AxD, however, is not clearly defined. p38 has been hypothesized to cause cytoskeletal reorganisation and protein aggregation in amyotrophic lateral scrclosis (Bendotti et al., 2004). It is known that the association of p38α with

aberrant phopshorylation of NFs consequently leads to accumulation of NFs (Ackerley et al., 2004).

In several models of AxD, expression of either wild-type or mutant GFAP have been shown to induce cellular stress responses (Quinlan et al., 2007). Such a response involves induction of sHSPs, and activation of stress kinases. For instance, some of the downstream consequences of the expression of R239C GFAP, the most common AxD mutation, include the accumulation of αB-crystallin and activation of stress kinases JNK and the upstream MLKs including MLK2, MLK3 and ASK1 (Tang et al., 2006). Our expression of wild-type or R416W GFAP in astrocytoma cell lines also induces similar responses in SAPK activation, as reflected by an increased phosphorylation of both JNK and p38, with R416W GFAP producing a greater effect than the wild-type protein. In addition, it was observed that there was significant colocalisation of p-JNK and p-p38 with the GFAP aggregates that were formed. These associations also held for AxD brain samples with R416W mutation, as demonstrated by elevated level of p-p38 and its cofractionation with the mutant GFAP into the Triton-insoluble fraction when compared to age-matched controls. Interestingly, pharmacologic inhibition of JNK and p38, but not ERK activation significantly increases cell survival after stress-induced recovery particularly in cells expressing R416W GFAP. These results strongly suggest that the presence of R416W GFAP decreases cell viability by rendering astrocytes more stress sensitive and this is correlated with the activation of SAPKs. Consistent with this is the observation in Alzheimer's disease model showing activation of JNK and p38 were associated with amyloid deposition due to aging, as well as tau phosphorylation and loss of synapophysin that can precede disease pathology (Savage et al., 2002), protein accumulation may act as a stress signal to proceed to SAPKs phosphorylation.

Activation of SAPK is part of the apoptotic signalling pathway and it plays an important role in several disorders including liver (Kaplowitz, 2002), cardiac (Baines and Molkentin, 2005) and neuronal diseases (Gallo and Johnson, 2002). Whether the enhanced sensitivity of astrocytes to stress leads to apoptosis remains to be experimentally verified. Recently, Tang et al. (2006)

investigated whether overexpression of wild-type or R239C GFAP induced apoptotic cell death. No significant difference was observed in U251 cells stably expressing either wild-type or R239C GFAP genes. Expression of R239C GFAP, however, leads to increased susceptibility of cells to apoptotic stimuli induced by camptothecin when compared to cells expressing wild-type GFAP. These data suggest that JNK pathway is important in propagating the deleterious effects of GFAP mutations.

Apart from protein deposits, JNK is activated by response to osmotic shock (Niisato et al., 1999; D'Alessandro et al., 2002) and other stress stimuli like UV (Derijard et al., 1994), γ-irradiation (Chen et al., 1994), and mechanical stress (Kippenberger et al., 2000). Osmotic stress-induced cell growth arrest is connected with MAPK intracellular signal transduction pathways that are activated in response to changes in osmolarity (Burg et al., 1996; Han et al., 1994; Matsuda et al., 1995; Galcheva-Gargova et al., 1994). For instance, MAPKs are activated by hypoosmotic swelling in astrocytes (Crépel et al., 1998; Haussinger, 1996; Lang et al., 1998) or by hyperosmotic stress in mouse astrocytes after exposure to sorbitol (Da Silva et al., 1997) and in rat astrocytes responding to mannitol (Arima et al., 2003). Hyperosmotic stress also causes cell growth arrest in association with MAPK activation in murine kidney cells (Kultz et al., 1998), and induces degradation of cyclin D1 that is mediated by proteasome in the lymphoma cell line Granta-519 (Casanovas et al., 2000). In addition, cell growth arrest is observed in hypoosmotic stressed human cells, owing to reduced protein synthesis, and subsequent degradation of cyclins and Cdks by proteasome activation (Tao et al., 2002). In addition to MAPK, both hypo- and hyper-osmotic conditions can also activate a variety of kinases, including Janus tyrosine kinases (Gatsops et al., 1998) and Rho kinase (Koyama et al., 2000).

Activation of JNK and p38 is prerequisite for H_2O_2 and 4-hydroxynonenal mediated cell death that is induced by amyloid β peptide (Aβ), a major pathogenesis of Alzheimer's disease (Tamagno et al., 2003). Moreover, JNK and p38 are also activated by H_2O_2-induced apoptosis in oligodendrocytes (Bhat and Zhang, 1999) and cardiac myoblasts (Hong et al., 2001). Concerning

the mechanism of H2O2-induced phosphorylation of JNK and p38, it is hypothesized that H2O2 might directly activate the upstream regulators of JNK, such as Rac1 (Vojtek and Cooper, 1995), as suggested by the fact that reactive oxygen intermediates (ROI) mediate IL-1 and TNFα-dependent activation of JNK (Lo et al., 1996). H2O2 induces reorganization of actin network and causes activation of p38 kinase which subsequently activates MAPKAPK-2/3 and HSP27 (Huot et al., 1998; Pearl-Yafe et al., 2004).

It has been suggested that JNK-mediated degenerative process is the result of activation of c-Jun transcription factor. Also, as potent effectors of apoptosis, JNKs possibly trigger and stabilize p53 (Fuchs et al., 1998; Mielke and Herdegen, 2000), which suppresses Bcl-2 and enhances Bax induction (Chen et al., 2003). Activation of p53 leading to mitochondrial dysfunction has been involved in the pathophysiology of Huntington's disease (Bae et al., 2005; Steffan et al., 2000). The presented results showed that R416W GFAP significantly diminished cell viability, this was prevented by inhibitors of JNK and p38 which attenuate a decline of viable cells. Blockade of JNK particularly promoted cell survival. SP600125 is an inhibitor of JNKs but does not interfere ERK and p38 activity (Han et al., 2001). SB203580 is known to inhibit p38α and β isoforms and can equally to the activated and non-activated p38 kinase (Gum et al., 1998). Both inhibitors can reduce the production of cytokines including TNF-α that is an initiator in the extrinsic apoptotic pathway.

Mechanisms underlying the differential effect of activated MAPKs upon astrocyte dysfunction are unclear. The distinct upstream regulators might account for the difference between JNK and p38 kinases. Inhibition of JNK or p38 tends to rescue R416W GFAP-expressing cells more than wild-type GFAP expressing-cells. Application of inhibitors to non-R416W cells completely prevented cell death, but only partially rescued R416W GFAP-expressing cells. On contrary, such approach to impede cell loss is not dramatic in wild-type cells, albeit they appear the similar trend of increasing cell viability as mutant cells. This discrimination indicates that the cell death in R416W GFAP-expressing cells is primarily caused by mutant GFAP in concert with JNK and p38

170

activation, whereas in wild-type GFAP-expressing cells death is more due to overexpression, rather than activation of JNK or p38. How does MAPKs activation link to AxD? Possibly, through activating the downstream kinases and transcription factors (Chen Z. et al., 2001) or by antagonising Akt-mediated survival signals (Sunayama et al., 2005), MAPKs may cause the astrocyte abnormalities seen.

4.5.4 The role of small heat shock proteins in Alexander disease

The response of mammalian cells to abrupt changes in their local environment entails a series of coordinated transcription and translation events leading to an increased expression of a group of proteins referred to as heat shock or stress proteins (Welch, 1992). Many of these heat shock proteins (HSPs) are thought to provide the cell with some degree of protection during environmental insults as well as to interact with unfolded and denatured proteins to prevent aggregation by promoting their (re-)folding and correcting their assembly (Stromer et al., 2003). Among these HSPs are small HSPs, comprising a structurally divergent group with molecular mass ranging from 12 to 43 kDa. Of the 10 current known sHSP genes in human (Franck et al., 2004; Taylor and Benjamin, 2005), some are ubiquitously expressed and others are known to be induced by stress (Head et al., 1994; Klemenz et al., 1991). For instance, increased expression of αB-crystallin and HSP27 confer resistance to a variety of physiological stresses, including heat shock and oxidative stress (Lavoie et al., 1993; Mehlen et al., 1995). αB-crystallin and HSP70 have been found to attenuate malfunction of the UPS by preventing aberrant protein aggregation produced by mutant desmin (Liu et al., 2006). In addition, αB-crystallin is associated with tau inclusions in glia (Bruijn et al., 1998; Dabir et al., 2004), while upregulation of HSP27 is found in aggregates of G93A mutant SOD1 in Amyotrophic lateral sclerosis (Steiber et al., 2000). The major histopathological feature of AxD is RFs that contain sHSPs αB-crystallin (Iwaki et al., 1989) and HSP27 (Iwaki et al., 1993). This association of sHSPs with AxD is specific, as the HSP70 class of chaperone is not included in RFs. Other protein aggregates often contain HSP70.

but whenever human diseases cause the accumulation of IF proteins into aggregates, sHSPs are also found (Lowe et al., 1992; Sun and MacRae, 2005). In this scenario, the sHSP association can be interpreted as a failed attempt to prevent or remove the IF aggregates.

My initial studies using transient transfection have demonstrated that αB-crystallin and HSP27 specifically associate with aggregates formed by R416W GFAP in transfected U343 MG-A cells (Perng et al., 2006). In addition, αB-crystallin was also found in the pellet fraction together with the insoluble R416W GFAP in the induced stable DBT cell lines. These sHSPs normally minimize filament-filament associations (Perng et al., 1999) and their overexpression can dissolve accumulations of wild-type GFAP filaments (Koyama and Goldman, 1999) and facilitate IF network formation (Perng et al., 2004). Their presence, however, in both brain astrocytes of patients with AxD and in cultured cells does not prevent filament aggregation or the formation of RFs by R416W GFAP. The association of αB-crystallin and HSP27 with R416W GFAP and its stability is likely due to the altered filament properties induced by this mutation. Although other stresses have been shown to stimulate the association of both HSP27 and αB-crystallin with GFAP filaments (Iwaki et al., 1993; Perng et al., 1999), these studies involved wild-type proteins. The results show clearly that it is specifically the presence of the R416W GFAP, but not wild-type GFAP, that stabilizes GFAP and leads to the sequestration of sHSPs.

Mice engineered to constitutively overexpress human GFAP develop a fatal encephalopathy with astrocyte inclusions similar to RFs (Messing et al., 1998). These mice have elevated levels of αB-crystallin and HSP27 mRNAs but not HSP70 mRNA in their brains. The formation of RF-like inclusions is also observed in astrocytes derived from these mice (Eng et al., 1998), suggesting that an overexpression of GFAP in astrocytes induces a specific sHSP response. The sequestration of αB-crystallin and HSP27 into GFAP aggregates could potentially compromise the astrocyte stress response and therefore contribute to the initiation of AxD. For example, it has already been shown that either the reduction of HSP27 or the loss of αB-crystallin compromises cytoskeletal integrity and function (Mairesse et al., 1996) or induces muscular atrophy (Brady et al., 2001),

respectively. HSP27 is a key protein in protecting neurons against apoptosis (Benn et al., 2002) and preserving mitochondrial function (Paul et al., 2002). In addition, HSP27 has also been implicated in regulating the stress response through the ubiquitin-mediated proteosomal regulation of the key transcription factor, NF-κB (Parcellier et al., 2003). Furthermore, HSP27 protects cells against other protein aggregation–based diseases caused by huntingtin (Wyttenbach et al., 2002) and α-synuclein (Zourlidou et al., 2004). A more specific role of αB-crystallin has been implicated in modulating cellular redox states (Rajasekaran et al., 2007) and in conferring resistance to apoptosis by inhibiting caspase activity (Kamradt et al., 2002; Kamradt et al., 2005). Such studies identify diminution of sHSP levels as a potential Achilles' heel in the cellular response to protein aggregate–based diseases that require either upregulation (Benn et al., 2002) or overexpression (Zourlidou et al., 2004) to ameliorate the disease phenotype. These observations suggest that the early sequestration of sHSPs into GFAP aggregates and RFs is a key event at the onset of AxD.

4.5.5 GFAP accumulation impairs proteosome function

Although the role of protein aggregation in neurodegenerative disorders remains controversial, it is generally agreed that aggregates or the interacting proteins might give rise to pathogenesis. Cytoplasmic aggregates or inclusions are associated with disease-causing IF mutations, including desmin in myopathy (Goebel, 2003), keratin in liver disorders (Fuchs et al., 1998; Irvine and McLean, 1999; Denk et al., 2000), GFAP in AxD (Li et al., 2002), and NF-L and NF-M leading respectively to Charcot-Marie-Tooth disease 2E and Parkinson's disease (Lariviere and Julien, 2004). This suggests these mutant IFs cannot be processed properly by the host cells. Consequently, the accumulating IFs deposits cause cell death and potential stress. The filamentous IFs, however, can also sensitize the cells. For example, expression of mutant keratins 5 and 14 makes cells vulnerable to osmotic stress that can activate stress kinases (D'Alessandro et al., 2002).

Cells are protected against the accumulation of misfolded or aggregated proteins by quality-control mechanisms. For instance, molecular chaperones can promote protein refolding as well as prevent aggregation of non-native protein (Hartle and Hayer-Hartl, 2002). Apart from activities of the phagosome-lysome system, the remaining misfolded proteins are primarily degraded by the UPS, this is true for R239C GFAP (Tang et al., 2006), keratin K8 and K18 (Ku and Omary, 2000). If the cellular quality-control machinery is overwhelmed by misfolded proteins, it can lead to the deposition of protein aggregates, and ultimately cell death in some neurodegenerative diseases. Dysfunction of the UPS has been implicated as the pathogenesis of various neurodegenerative diseases, it might be predicted that AxD is following this etiology.

Depending on their nature and location, GFAP mutations exert a wide range of effects on the formation and organisation of filaments. For instance, the tail mutation, R416W, has deleterious effects on GFAP assembly and network organisation, whereas the rod mutation, R239C, does not appear to affect filament formation and organisation. Instead, the R239C mutation increases the stability of GFAP filament, as judged by its lower extractability at high salt concentrations (Hsiao et al., 2005). Similar results were observed when R416W GFAP was transfected into U343 MG-A cells. With use of a harsh extraction buffer containing deoxycholate, most of the wild-type GFAP was solubilised in cells expressing wild-type GFAP, whereas R416W protein remained entirely in the pellet fraction of the R416W GFAP transfected cells. These results suggest that AxD mutations could confer increased GFAP stability by decreasing the soluble pool. Alternatively, AxD-causing mutations could increase GFAP stability by affecting the UPS function.

Recent studies provide several pieces of evidence that GFAP accumulation impairs proteosome function (Tang et al., 2006). First, at least some of the overexpressed GFAP was degraded through the UPS in an ubiquitin-dependent manner. Second, expressing either wild-type or R239C GFAP led to impaired proteasome function, as demonstrated by accumulation of a reporter protein GFP-U and *in vitro* proteolytic assays. One possible mechanism for this inhibition is that the

accumulated GFAP saturates the capacity of free cytosolic ubiquitin that is required for the UPS function. Another possible mechanism might involve a direct interaction between the proteasome and GFAP filaments that might retain proteasomes in GFAP inclusions. Thus, a competition between the excess GFAP and other cellular proteins for proteasome degradation might occur, leading to slowed protein turnover. The data presented here support this notion by showing that R416W mutation alters normal turnover of GFAP, as demonstrated by the sustained levels of R416W GFAP in cells after its expression is switched off. In addition, expression of R416W GFAP leads to aberrant protein aggregation that partially impairs the UPS function and increases protein ubiquitination. It has been suggested that the IF network may play a role in organising components of the degradation machinery that removes aberrant proteins (Kopito and Sitia, 2000), and if this function were compromised by the mutant GFAP, increasing levels of the mutant GFAP would lead to more aggregate formation.

4.5.6 Some IF proteins behave like stress proteins

The data presented here also show that the levels of GFAP increase in cells following proteosome inhibition, suggesting that GFAP could act as a stress protein. Indeed, some of the keratins and type III IF proteins behave like classical stress proteins, as their expression is induced rapidly in response to cell stress. For instance, keratins 6 and 16 expression are upregulated in many pathological situations from psoriasis to cancer and they are also upregulated in epidermal wound healing (DePianto and Coulombe, 2004; Mansbridge and Knapp, 1987). Nonkeratin IFs can also change their expression in response to stress. For instance, the astrocytic IF proteins GFAP, vimentin and nestin change their expressions in these cells at different developmental stages and in many pathological conditions (Pekny and Pekna, 2004). Through several analyses of knockout mice, it has been established that IFs in astrocytes are functionally linked to the stress response seen after brain and spinal cord trauma (Nawashiro et al., 1998; Pekny et al., 1999) and osmotic stress (Anderova et al., 2001; Ding et al., 1998). Upregulation of GFAP and vimentin and

reexpression of nestin were found in reactive astrocytes in response to trauma, such as ischemia, physical injury and neurodegeneration (Eliasson et al., 1999; Li et al., 2007; Shibuya et al., 2002). Increased expressions of vimentin and nestin were also observed during the early stage of regeneration after muscle injury (Vaittinen et al., 2001).

4.6 Future perspectives

4.6.1 Potential interactions of astrocytes with oligodendrocytes and neurons

AxD is unique among the neurodegenerative diseases associated with abnormal protein aggregates in that the most severe consequences of the disorder are not manifested in the astrocyte bearing the inclusion body, but rather in other cell populations in the brain. For instance, there is a major dysfunction of oligodendrocytes as revealed by the severe hypo-myelination that accompanies the infantile forms of this disease and apparent demyelination in older patients. In the late onset form of AxD, neuronal dysfunctions are suggested by the clinical signs with dramatic changes in white matter and pathology predominantly affecting cerebellum and brainstem. These clinical and pathological manifestations suggest that critical interactions of astrocytes with oligodendrocytes and neurons must play a central role in this disease. What are the mechanisms by which accumulation of mutant GFAP in astrocytes produces deleterious effects on their neighbouring cells? One possibility is that accumulation of mutant GFAP in astrocytes may induce a stress response, and as part of this response, soluble factors are released that are toxic to neighbouring oligodendrocytes and perhaps neurons as well. These factors could include TNF-α, a cytokine that is toxic to oligodendrocytes (Ledeen and Chakraborty, 1998). Interestingly, TNF-α toxicity is exacerbated by iron (Zhang et al., 2005), whose accumulation was reported in mice overexpressing GFAP (Hagemann et al., 2005). In addition, astrocytes express growth factors, such as platelet-derived growth factor (PDGF), basic fibroblast growth factor (BFGF) and insulin-like grow factor 1 (IGF1), which promote proliferation and differentiation of oligodendrocyte progenitors (Dubois-Dalcq and Murray, 2000; Orentas and Miller, 1998). Expression of mutant

GFAP in astrocytes may reduce the secretion of these factors, leading to compromised oligodendrocyte development and consequently a defect of myelination.

The second possibility is that mutant GFAP-mediated astrocyte dysfunction may compromise one or more neuronal support functions, thus damaging vulnerable neurons. Astrocytes are the most abundant cells in the CNS, and outnumber neurons by about ten to one in the adult human brain. Astrocytes are known to respond to various kind of stress and in this respect can be viewed as guardians of the CNS. They provide essential services to the neurons they support, including roles in regulating cerebral blood flow and maintaining synaptic function, and they also transport various nutrients and metabolic precursors to neurons (Maragakis and Rothstein, 2006). The best known example is their essential role in rapid recovery of glutamate, the primary excitatory neurotransmitter in the CNS from synaptic clefts by astrocyte glutamate transporters Glt-1 and Glast (also known as EAAT2 and EAAT1 respectively). The activation of stress response induced by expression of mutant GFAP may cause a significant decrease of Glt-1 in astrocytes. A defect in glutamate uptake leading to increase in synaptic glutamate level and exitotoxicity (Maragakis and Rothstein, 2004) could explain the seizures commonly observed in early-onset infantile patients and kainate–induced seizures in GFAP mutant knock-in mice (Hagemann et al., 2006; Tanaka et al., 2007). Indeed, Glt-1 knockout mice have demonstrated that defective glutamate transport by astrocytes can lead to an increase in seizure activity (Tanaka et al., 1997). In addition, increased glutamate can be toxic to both neurons and oligodendrocytes (Johnston, 2005; Matute et al., 2002). In particular, the hypersensitivity of oligodendrocytes to glutamate could explain the demyelination that often occurrs in infantile cases of AxD.

4.6.2 Splice variant of GFAP and its role in Alexander disease

Whilst exactly how GFAP mutations in astrocytes translate into catastrophe for neurons and oligodendrocytes remains unknown, there is clearly abundant evidence for how astrocytes might regulate the properties of these cells (Lobsiger and Cleveland, 2007). It is worth mentioning that

GFAP is not only expressed in astrocytes, but it is also expressed in a range of other cells, including enteric glia, nonmyelinating Schwann cells, liver stellate cells, breast myoepithelial cells, lymphocytes and respiratory tract chondrocytes (see (Su et al., 2004) and references therein). The GFAP levels are low in these other cells, suggesting that its primary role is not to form filament networks. In addition, GFAP expresses several splice variants at low levels (reviewed recently in (Quinlan et al., 2007), about which much less is known than the most common GFAP isoform, α-GFAP. One of these splice variants, ε-GFAP arises by alternative splicing and produces a protein with a novel C-terminal tail that interacts specifically with presenilin (Nielsen et al., 2002). Transcription infidelity might also lead to the expression of abnormal forms of GFAP (van Leeuwen et al., 1998), some of which are expressed in neurons (Hol et al., 2003). Interestingly, a subpopulation of GFAP-positive astrocytes (Laywell et al., 2000; Roelofs et al., 2005) and radial glial (Campbell and Gotz, 2002; Noctor et al., 2001) have been identified as multipotent neuron stem cells in the adult mammalian brain. If mutant GFAPs were to exert their effects at the level of such stem cells, the defect could then be manifested in a diverse population of cellular progeny.

Chapter 5

Conclusions

In this study, I started with transient transfection to investigate the properties of the mutant GFAPs in a range of cell lines. I focused mainly on the R416W GFAP, a relatively common but unusual mutation that can give all three forms of AxD. Some studies were also performed on the most common AxD mutation R239C as a comparative purpose. When expressed in IF-free cell lines such as SW13 (vim⁻) cells or primary mouse astrocytes derived from GFAP/vimentin double knockouts, both yielded only aggregates or diffuse background staining, and this effect was dominant upon cotransfection with the wild-type GFAP (Perng et al., 2006). Unexpectedly, transient expression of R416W GFAP in primary mouse astrocytes resulted in aggregate formation as well as filament integration. Similar observations were made on the astrocytoma-derived U343 MG-A cell lines. In this case, an R416W-specific monoclonal antibody was used to reveal the integration of the R416W GFAP into the endogenous human GFAP, eliminating the possibility that aggregate formation was due to a species incompatibility. The conclusion from these transfection studies was that R416W GFAP could be integrated into existing GFAP filament networks without precipitating aggregate formation. In other words, the mutation was only dominant over wild-type protein once a certain threshold had been crossed.

The previous history of IFs, their proposed role as mechanical integrators and those diseases of skin and muscle tissues where structure is paramount, has conditioned us to expect that mutations in IF proteins should be disruptive and induce aggregate formation. This study has challenged this assumption and demonstrates for the first time that it is possible to have a disease causing GFAP mutation that does not dramatically alter the filament network, providing the levels and cell environment are close to those in the target cells.

Whilst wild-type GFAP can incorporate into extended IF networks, R416W GFAP formed aggregates in most of the transfected cells. Colocalisation studies showed that GFAP-containing aggregates are also positive for chaperone proteins and signalling molecules, including αB-crystallin and HSP27 and phospho-JNK. GFAP aggregates are also ubiquitinated, as demonstrated by co-tranfection of His$_6$-myc tagged ubiquitin with R416W GFAP (Perng et al., 2006, see Fig. 9 in Appendix 5). Subcellular cofractionation studies provide direct biochemical evidence that these components are all associated with GFAP aggregates. With the use of the mutant-specific antibody, it was also shown for the first time that mutant protein is a component in GFAP-containing aggregates of transfected human astrocytoma cells. These results suggest the aggregates formed by R416W GFAP in cultured cells have many features similar to RFs. The key question is what are the downstream consequences of RFs formation? Are RFs directly involved in the toxic gain-of-function mechanism, part of the protective response, or only an innocent bystander of the secondary effect of astrocyte dysfunction?

To answer these questions, I have established several Dox-inducible stable cell lines to investigate the biological effect of GFAP aggregates on astrocyte function. These cell lines allow me to 1) determine the time course of events leading to GFAP expression and aggregate formation; 2) establish whether abnormal accumulation of GFAP results in astrocyte stress response; 3) determine the critical wild-type to mutant GFAP ratio giving rise to aggregate formation to be determined. The data show that R416W GFAP is capable of integrating into GFAP networks when expressed at a low level. The incorporation of the dominant-negative mutant can potentially change the filament properties by increasing filament stability and altering inter-filament interactions. It was only when these cells were challenged with either osmotic or oxidative stress that the deleterious effects of the R416W mutation apparent.

In the DBT cell lines, initiation of GFAP expression resulted in aggregate formation, with R416W GFAP being observed to form aggregates at a significantly higher frequency than wild-type GFAP. The aggregate formation induces a stress response, as demonstrated by the elevated expression of the sHSP αB-crystallin and activation of stress protein kinases, such as JNK and p38. These proteins are also associated with the GFAP-enriched aggregates formed by R416W GFAP, which may compromise astrocyte function. This is supported by the findings that expression of R416W GFAP leads to increased susceptibility of cells to stressful stimuli when compared to cells expressing wild-type GFAP. Furthermore, the presence of R416W GFAP partially compromises the UPS function and increases GFAP filament stability, as demonstrated by the slowed turnover of, GFAP, Nrf2 and cyclin D1. This in turn may further increases GFAP level and more aggregation. In fact, GFAP itself may act as a stress protein, whose expression is induced in response to stress.

From this study, together with the wealth of information now emerging on the intracellular pathways, I propose a model, in which pathogenic GFAP mutations set in motion events that I believe to be important in the development of AxD (Fig. 5.1). It is worth noting that although AxD is a primary disorder of astrocyte, the clinical consequences are myelination defects and neurodegeneration. This feature highlights the critical importance of interactions of astrocytes with oligodendrocytes and neurons. Whilst how these cells communicate with each other remains elusive, there are many possibilities for astrocytes to become dysfunctional and to impair the function of other cell types in the CNS. I incorporate some of the current hypothesis in this model to highlight the inter-cell interactions that could be mediated by soluble cytoplasmic factors, such as growth factors and cytokines.

Last but not least, several publications provide direct or indirect evidence that mitochondrial defects also play an important role in AxD, although whether this occurs independently or as a consequence of the disease remains unclear. For instance, transgenic

mice overexpressing human GFAP induce an oxidative stress response (Hagemann et al., 2005) and examination of AxD brain samples shows the presence of lipid peroxidation end-products in RFs (Castellani et al., 1998). In addition, an elevated level of lactate and mitochondrial abnormalities have been reported in several cases of AxD patients (Caceres-Marzal et al., 2006; Nobuhara et al., 2004). Furthermore, the clinical symptoms of the mitochondrial disorder Leigh syndrome are remarkably similar to those of infantile AxD. My study also showed that cells expressing R416W GFAP are particularly sensitive to oxidative stress. Taken together, the role of mitochondrial dysfunction in AxD is beginning to emerge. Therefore, I also include mitochondrial defect as a potential contributor to the disease progression of AxD.

Figure 5.1. A proposed model in which GFAP mutations lead to Alexander disease. The presence of the R416W mutation decreases the solubility of the GFAP, probably by increasing GFAP filament stability or altering the filament-filament interactions in a manner that encourages aggregation (1). GFAP aggregation increases sHSP expression (2A, red arrow), induces stress-activated protein kinase (2B, SAPK) activation (red arrow) and impairs ubiquitin-proteosome system (2C, UPS) function (red arrow). This is accompanied by the sequestration of sHSPs (3A, broken line) and phophorylated SAPKs (3B, broken line), which compromise cellular stress response and render cells more susceptible to stressful stimuli (4). GFAP aggregates may undergo a maturing process, with additional posttranslational modifications of integral components, such as the phosphorylation (P) and ubiquitination (Ub) of αB-crystallin to form the Rosenthal fibres (RFs). This model is not exclusive to R416W GFAP, since RFs are a characteristic diagnostic feature of Alexander disease. Other GFAP mutations may differ in the details of the mechanism by which they produce aberrant filament-filament interactions leading to the formation of stabilized aggregates, but, once formed, they then follow a common pathway to RFs formation. Possible disease mechanisms also involve toxic cellular interactions mediated by signalling molecules and receptors. Upregulation of stress pathway by the presence of GFAP aggregates may cause a decreased expression of glutamate transporter in astrocytes (5). Excessive glutamate due to reduced glutamate uptake through astrocyte glutamate transporters causes neuronal toxicity. In addition, astrocytes under stress may release soluble substances, such as cytokines (6A) and growth factors (6B), which are toxic to oligodendrocytes. The effects of GFAP mutation at the level of cell-cell interactions may be relatively far downstream from the immediate effects of aggregate formation. However, they may represent a final common pathway for many aspects of pathogenesis. Finally, mitochondrial abnormalities as a result of astrocyte dysfunction may produce reactive oxygen species (ROS) (7), which are toxic to astrocytes and its neighboring cells.
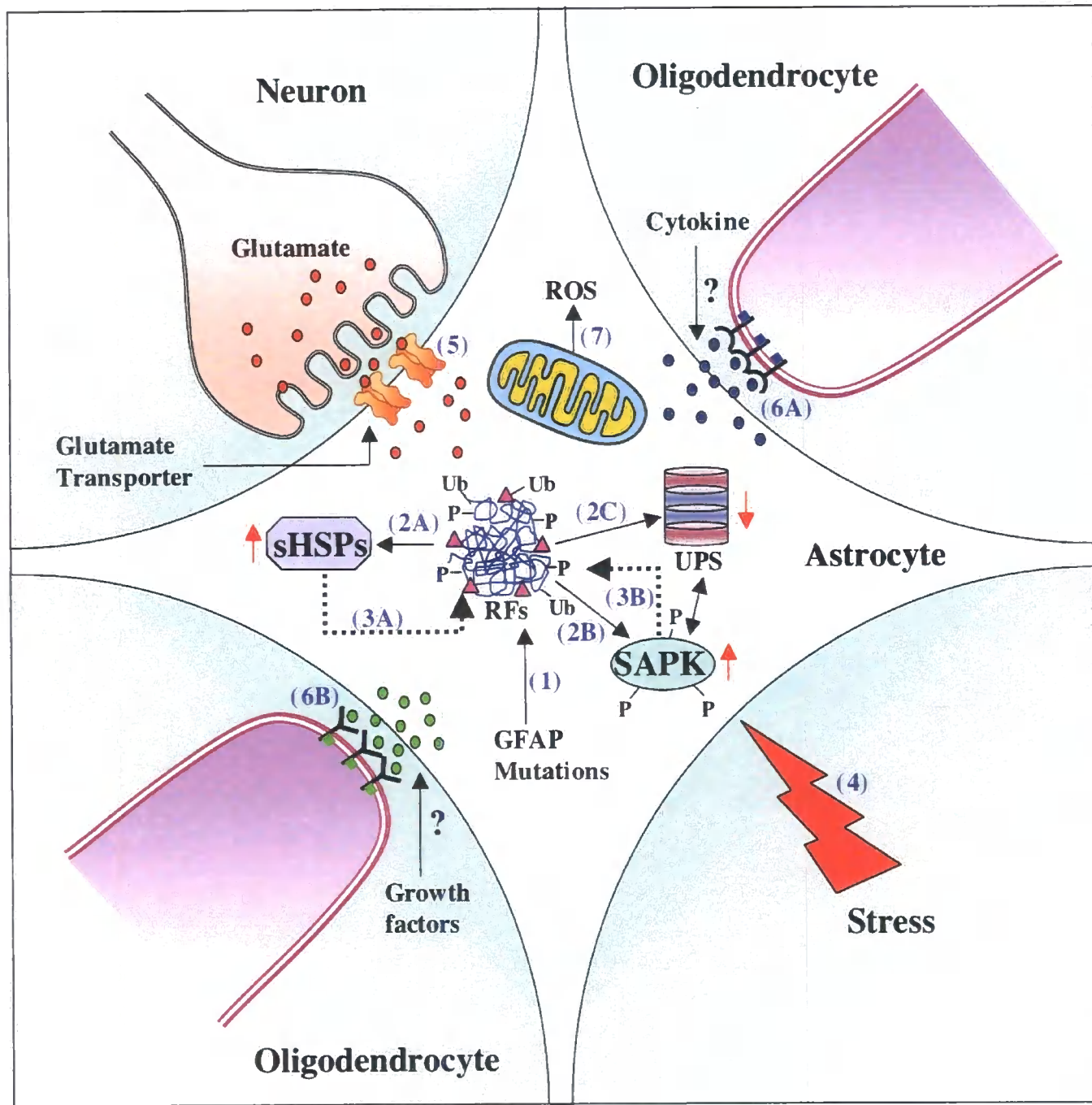
References

Aebi, U., Cohn, J., Buhle, L., and Gerace, L. (1986) The nuclear lamina is a meshwork of intermediate-type filaments. Nature 323: 560-564

Akhmanova, A. and Steinmetz, M. O. (2008) Tracking the ends: a dynamic protein network controls the fate of microtubule tips. Nat. Rev. Mol Cell Biol. 9: 309-322

Aksenov, M. Y., Aksenova, M. V., Butterfield, D. A., Geddes, J. W., and Markesbery, W. R. (2001) Protein oxidation in the brain in Alzheimer's disease. Neuroscience 103(2): 373-383

Al-Chalabi, A., and Miller, C. C. (2003) Neurofilaments and neurological disease. Bioessays 25: 346-355

Allen, N. J., and Barres, B. A. (2005) Signaling between glia and neurons: focus on synaptic plasticity. Curr. Opin. Neurobiol. 15: 542-548

Almazan, G., Ahar, D. E., and Bell, J. C. (1993) Phosphorylation and disruption of intermediate filament proteins in oligodendrocyte precursor cultures treated with calyculin A. J. Neurosci. Res. 36: 163-172

Anderova, M., Kubinova, S., Mazel, T., Chvatal, A., Eliasson, C., Pekny, M., and Sykova, E. (2001) Effect of elevated K(+), hypotonic stress, and cortical spreading depression on astrocyte swelling in GFAP-deficient mice. Glia 35: 189-203

Angelastro, J. M., Ho, C. L., Frappier, T., Liem, R. K., and Greene, L. A. (1998) Peripherin is tyrosine-phosphorylated at its carboxyl-terminal tyrosine. J. Neurochem. 70: 540-549

Aoki, Y., Haginoya, K., Munakata, M., Yokoyama, H., Nishio, T., Togashi, N., Ito, T., Suzuki, Y., Kure, S., Iinuma, K., Brenner, M., and Matsubara, Y. (2001) A novel mutation in glial fibrillary acidic protein gene in a patient with Alexander disease. Neurosci. Lett. 312: 71-74

Arend, A. O., Leary, P. M., and Rutherfoord, G. S. (1991) Alexander's disease: a case report with brain biopsy, ultrasound, CT scan and MRI findings. Clin. Neuropathol. 10: 122-126

Asahina, N., Okamoto, T., Sudo, A., Kanazawa, N., Tsujino, S., and Saitoh, S. (2006) An infantile-juvenile form of Alexander disease caused by a R79H mutation in GFAP. Brain Dev. 28: 131-133

Aschner, M. (1998) Astrocytic functions and physiological reactions to injury: the potential to induce and/or exacerbate neuronal dysfunction—a forum position paper. Neurotoxicology 19: 7-17 (discussion 37-38)

Bachetti, T., Caroli, F., Bocca, P., Prigione, I., Balbi, P., Biancheri, R., Filocamo, M., Mariotti, C., Pareyson, D., Razazzolo, R., and Ceccherini, I. (2008) Mild functional effects of a novel GFAP mutation allele identified in a familial case of adult-onset Alexander disease. Eur. J. Hum. Genet. 16: 462-470

Bae, B. I., Xu, H., Igarashi, S., Fujimuro, M., Agrawal, N., Taya, Y., Hayward, S. D., Moran, T. H., Montell, C., Ross, C. A., Snyder, S. H., and Sawa, A. (2005) p53 mediates cellular dysfunction and behavioral abnormalities in Huntington's disease. Neuron 47(1): 29-41

Baines, C. P., and Molkentin, J. D. (2005) Stress signaling pathways that modulate cardiac myocyte apoptosis. J. Mol. Cell Cardiol. 38: 47-62

Balbi, P., Seri, M., Ceccherini, I., Uggetti, C., Casale, R., Fundarò, C., Caroli, F., and Santoro, L. (2008) Adult-onset Alexander disease: report on a family. J. Neurol. 255: 24-30

Balcarek, J. M., and Cowan, N. J. (1985) Structure of the mouse glial fibrillary acidic protein gene: Implications for the intermediate filament multigene family. Nucleic Acids Res. 13: 5527-5543

Baldin, V., Lukas, J., Marcote, M. J., Pagano, M., and Draetta, G. (1993) Cyclin D1 is a nuclear protein required for cell cycle progression in G1. Genes Dev. 7: 812-821

Bang, M. L., Gregorio, C., and Labeit, S. (2002) Molecular dissection of the interaction of desmin with the C-terminal region of nebulin. J. Struct. Biol. 137: 119-127

Bär, H., Goudeau, B., Wälde, S., Casteras-Simon, M., Mücke, N., Shatunov, A., Goldberg, Y. P., Clarke, C., Holton, J. L., Eymard, B., Katus, H. A., Fardeau, M., Goldfarb, L., Vicart, P., and Herrmann, H. (2007) Conspicuous involvement of desmin tail mutations in divers cardiac and skeletal myopathies. Hum. Mutat. 28: 374-386

Barber, P. C., and Lindsay, R. M. (1982) Schwann cells of the olfactory nerves contain glial fibrillary acidic protein and resemble astrocytes. Neuroscience 7: 3077-3090

Barbieri, F., Filla, A., De Falco, F. A., and Buscaino, G. A. (1980) Alexander's disease: a clinical study with computerized tomographic scans of the first two Italian cases. Acta Neurol. 35: 1-9

Barkovich, A. J., and Messing, A. (2006) Alexander disease: not just a leukodystrophy anymore. Neurology 66: 468-469

Bassuk, A. G., Joshi, A., Burton, B. K., Larsen, M. B., Burrowes, D. M., and Stack, C. (2003) Alexander disease with serial MRS and a new mutation in the glial fibrillary acidic protein gene. Neurology 61: 1014-1015

Behl, C. (1999) Alzheimer's disease and oxidative stress: implications for novel therapeutic approaches. Prog. Neurobiol. 57(3): 301-323

Behrens, A., Sibilia, M., and Wagner, E. F. (1999) Amino-terminal phosphorylation of c-Jun regulates stress-induced apoptosis and cellular proliferation. Nat. Genet. 21: 326-329

Bellin, R. M., Sernett, S. W., Becker, B., Ip, W., Huiatt, T. W., and Robson, R. M. (1999) Molecular characteristics and interactions of the intermediate filament protein synemin. Interactions with alpha-actinin may anchor synemin-containing heterofilaments. J. Biol. Chem. 274: 29493-29499

Belteki, G., Haigh, J., Kabacs, N., Haigh, K., Sison, K., Costantini, F., Whitsett, J., Quaggin, S. E., and Nagy, A. (2005) Conditional and inducible transgene epression in mice through the combinatorial use of Cre-mediated recombination and tetracycline induction. Nucleic Acids Res. 33(8): 2765

Bendotti, C., Atzori, C., Piva, R., Tortarolo, M., Strong, M. J., DeBiasi, S., and Migheli, A. (2004) Activated p38MAPK is a novel component of the intracellular inclusions found in human amyotrophic lateral sclerosis and mutant SOD1 transgenic mice. J. Neuropathol. Exp. Neurol. 63(2): 113-119

Ben-Levy, R., Hooper, S., Wilson, R., Paterson, H. F., and Marshall, C. J. (1998) Nuclear export of the stress-activated protein kinase p38 mediated by its substrate MAPKAP kinase-2. Curr. Biol. 8: 1049-1057

Benn, S. C., Perrelet, D., Kato, A. C., Scholz, J., Decosterd, I., Mannion, R. J., Bakowska, J. C., and Woolf, C. J. (2002) Hsp27 upregulation and phosphorylation is required for injured sensory and motor neuron survival. Neuron 36: 45-56

Bettica, A., and Johnson, A. B. (1990) Ultrastructural immunogold labeling of glial filaments in osmicated and unosmicated epoxy-embedded tissue. J. Histochem. Cytochem. 38: 103-109

Bies, J., and Wolff, L. (1997) Oncogenic activation of c-Myb by carboxyl-terminal truncation leads to decreased proteolysis by the ubiquitin-26S proteasome pathway. Oncogene 14: 203-212

Bilak, S. R., Sernett, S. W., Bilak, M. M., Bellin, R. M., Stromer, M. H., Huiatt, T. W., and Robson, R. M. (1998) Properties of the novel intermediate filament protein synemin and its identification in mammalian muscle. Arch. Biochem. Biophys. 355: 63-76

Bloemendal, H., Benedetti, E. L., Ramaekers, F., and Dunia, I. (1981) The lens cytoskeleton. Intermediate-sized filaments, their biosynthesis and association with plasma membranes. Mol. Biol. Rep. 7: 167-168

Bobele, G. B., Garnica, A., Schaefer, G. B., Leonard, J. C., Wilson, D., Marks, W. A., Leech, R. W., and Brumback, R. A. (1990) Neuroimaging findings in Alexander's disease. J. Child Neurol. 5: 253-258

Bock, E., Moller, M., Nissen, C., and Sensenbrenner, M. (1977) Glial fibrillary acidic protein in primary astroglial cell cultures derived from newborn rat brain. FEBS Lett. 83: 207-211

Bocker, R., Estler, C. J., Maywald, M., and Weber, D. (1981) Comparison of distribution of doxycycline in mice after oral and intravenous application measured by a high-performance liquid chromatographic method. Arzneimittelforschung 31: 2116-2117

Bonne, G., Mercuri, E., Muchir, A., Urtizberea, A., Becano, H. M., Recan, D., Merlini, L., Wehnert, M., Boor, R., Reuner, U., Vorgerd, M., Wicklein, E. M., Eymard, B., Duboc, D., Penisson-Besnier, I., Cuisset, J. M., Ferrer, X., Desguerre, I., Lacombe, O., Bushby, K., Pollitt, C., Toniolo, D., Fardeau, M., Schwartz, K., and Murtoni, F. (2000) Clinical and molecular genetic spectum of autosomal dominant Emery-Dreifuss muscular dystrophy due to mutations of the lamin A/C gene. Ann. Neurol. 48: 170-180

Bonne, S., Gilbert, B., Hatzfeld, M., Chen, X., Green, K. J., and van Roy, F. (2003) Defining desmosomal plakophilin-3 interactions. J. Cell Biol. 161: 403-416

Bornslaeger, E. A., Corcoran, C. M., Stappenbeck, T. S., and Green, K. J. (1996) Breaking the connection: displacement of the desmosomal plaque protein desmoplakin from cell-cell interfaces disrupts anchorage of intermediate filament bundles and alters intercellular junction assembly. J. Cell Biol. 134: 985-1001

Borrett, D, and Becker, L. E. (1985) Alexander's disease. A disease of astrocytes. Brain 108: 367-385

Bovolenta, P., Liem, R. L., and Mason, C. A. (1984) Development of cerebellar astroglia: transition in form and cytoskeletal content. Dev. Biol. 102: 248-259

Boyer, S. N., Wazer, D. E., and Band, V. (1996) E7 protein of human papilloma virus-induces degradation of retinoblastoma protein through the ubiquitin-proteasome pathway. Cancer Res. 56: 4620-4624

Brady, J. P., Garland, D. L., Green, D. E., Tamm, E. R., Giblin, F. J., and Wawrousek, E. F. (2001) AlphaB-crystallin in lens development and muscle integrity: a gene knockout approach. Invest. Ophthalmol. Vis. Sci. 42: 2924-2934

Breitshopf, K., Zeiher, A. M., and Dimmeler, S. (2000) Ubiquitin-mediated degradation of the proapoptotic active form of bid. A functional consequence on apoptosis induction. J. Biol. Chem. 275: 21648-21652

Brenner, M. (1994) Structure and transcriptional regulation of the GFAP gene. Brain Pathol. 4: 245-257

Brenner, M., Johnson, A. B., Boespflung-Tanguy, O., Rodriguez, D., Goldman, J. E., and Messing, A. (2001) Mutations in GFAP, encoding glial fibrillary acidic protein, are associated with Alexander disease. Nat. Genet. 27: 117-120

Brenner, M., Lampel, K., Nakatani, Y., Mill, J., Nanner, C., Mearow, K., Dohadwala, M., Lipsky, R., and Freese, E. (1990) Characterization of human cDNA and genomic clones for glial fibrillary acidic protein. Mol. Brain Res. 7: 277-288

Brockmann, K., Meins, M., Taubert, A., Trappe, R., Grond, M., and Hanefeld, F. (2003) A novel GFAP mutation and disseminated white matter lesions: adult Alexander disease? Eur. Neurol. 50: 100-105

Brown, C. A., Lanning, R. W., McKinney, K. Q., Salvino, A. R., Chemiske, E., Crowe, C. A., Darras, B. T., Gominak, S., Greenberg, C. R., Grosmann, C., Heydemann, P., Mendel, J. R., Pober, B. R., Sasaki, T., Shapiro, F., Simpson, D. A., Suchowersky, O., and Spence, J. E. (2001) Novel and recurrent mutations in lamin A/C in patients with Emery-Dreifuss muscular dystrophy. Am. J. Med. Genet. 102: 359-367

Burkhard, P., Stetefeld, J., and Strelkov, S. V. (2001) Coiled coils: a highly versatile protein folding motif. Trends Cell Biol. 11: 82-88

Butterfield, D. A., and Lauderback, C. M. (2002) Lipid peroxidation and protein oxidation in Alzheimer's disease brain: potential causes and consequences involving amyloid beta-peptide-associated free radical oxidative stress. Free Radic. Biol. Med. 32(11): 1050-1060

Byun, Y., Chen, F., Chang, R., Trivedi, M., Green, K. J., and Cryns, V. L. (2001) Caspase cleavage of vimentin disrupts intermediate filaments and promotes apoptosis. Cell Death Differ. 8: 443-450

Caceres-Marzal, C., Vaquerizo, J., Galan, E., and Fernandez, S. (2006) Early mitochondrial dysfunction in an infant with Alexander disease. Pediatr. Neurol. 35: 293-296

Calne, D, B. (1994) Neurodegenerative diseases, ed. WB Saunders, Philadelphia

Carballido-Lopez, R. (2006) The bacterial actin-like cytoskeleton. Microbiol. Mol. Biol. Rev. 70: 888-909

Carlsson, L., Li, Z., Paulin, D., and Thornell, L. E. (1999) Nestin is expressed during development and in myotendinous and neuromuscular junctions in wild type and desmin knock-out mice. Exp. Cell Res. 251: 213-223

Caroli, F., Biancheri, R., Seri, M., Rossi, A., Pessagno, A., Bugiani, M., Corsolini, F., Savasta, S., Romano, S., Antonelli, C., Romano, A., Pareyson, D., Gambero, P., Uziel, G., Ravazzolo, R., Ceccherini, I., and Filocamo, M. (2007) GFAP mutations and polymorphisms in 13 unrelated Italian patients affected by Alexander disease. Clin. Genet. 72: 427-433

Carter, J.M., Hutcheson, A. M., and Quinlan, R. A. (1995) In vitro studies on the assembly properties of the lens proteins CP49, CP115: coassembly with alpha-crystallin but not with vimentin. Exp. Eye Res. 60: 181-192

Casanovas, O., Miró, F., Estanyol, J. M., Itarte, E., Agell, N., and Bachs, O. (2000) Osmotic stress regulates the stability of cyclin D1 in a p38^{SAPK2}-dependent manner. J. Biol. Chem. 275: 35091-35097

Castellani, R. J., Perry, G., Harris, P. L. R., Monnier, V. M., Cohen, M. L., and Smith, M. A. (1997) Advanced glycation modification of Rosenthal fibers in patients with Alexander disease. Neurosci. Lett. 231: 79-82

Castellani, R. J., Perry, G., Harris, P. L., Cohen, M. L., Sayre, L. M., Salomon, R. G., and Smith, M. A. (1998) Advanced lipid peroxidation end-products in Alexander's disease. Brain Res. 787: 15-18

Caulin, C., Ware, C. F., Magin, T. M., and Oshima, R. G. (2000) Keratin-dependent, epithelial resistance to tumor necrosis factor-induced apoptosis. J. Cell Biol. 149: 17-22

Cavestro, G. M., Frulloni, L., Nouvenne, A., Neri, T. M., Calore, B., Ferri, B., Bovo, P., Okolicsanyi, L., Di Mario, F., and Cavallini, G. (2003) Association of keratin 8 gene mutation with chronic pancreatitis. Dig. Liver Dis. 35: 416-420

Chain, D. G., Schwartz, J. H., and Hegde, A. N. (1999) Ubiquitin-mediated proteolysis in learning and memory. Mol. Neurobiol. 20: 125-142

Chang, C. S., Chen, W. N., Lin, H. H., Wu, C. C., and Wang, C. J. (2004) Increased oxidative DNA damage, inducible nitric oxide synthase, nuclear factor kappaB expression and enhanced antiapoptosis-related proteins in Helicobacter pylori-infected non-cardiac gastric adenocarcinoma. World J. Gastroenterol. 10(15): 2232-2240

Chang, L., and Goldman, R. D. (2004) Intermediate filaments mediate cytoskeletal crosstalk. Nat. Rev. Mol. Cell Biol. 5: 601-613

Chang, L., and Karin, M. (2001) Mammalian MAP kinase signalling cascades. Nature 410: 37-40

Chang, Y. C., Lee, Y. S., Tejima, T. Tanaka, K., Omura, S., Heintz, N. H., Mitsui, Y., and Magae, J. (1998) mdm2 and bax, downstream mediators of the p53 response, are degraded by the ubiquitin-proteasome pathway. Cell Growth Differ. 9: 79-84

Chapman, R., Sidrauski, C., and Walter, P. (1998) Intracellular signalling from the endoplasmic reticulum to the nucleus. Annu. Rev. Cell Dev. Biol. 14: 459-485

Chen, F., Chang, R., Trivedi, M., Capetanaki, Y., and Cryns, V. L. (2003) Caspase proteolysis of desmin produces a dominant-negative inhibitor of intermediate filaments and promotes apoptosis. J. Biol. Chem. 278: 6848-6853

Chen, J., Kelz, M. B., Zeng, G., Sakai, N., Steffen, C., Shockett, P. E., Picciotto, M. R., Duman, R. S., and Nestler, E. J. (1998) Transgenic animals with inducible, targeted gene expression in brain. Mol. Pharmacol. 54: 495-503

Chen, W. J., and Liem, R. K. (1994) The endless story of the glial fibrillary acidic protein. J. Cell Sci. 107 (Pt 8): 2299-2311

Chen, Y. R., Meyer, C. F., and Tan, T. H. (1996) Persistent activation of c-Jun N-terminal kinase 1 (JNK1) in gamma radiation-induced apoptosis. J. Biol. Chem. 271(2): 631-634

Chen, Z., Gibson, T. B., Robinson, F., Silvestro, L., Pearson, G. Xu, B., Wright, A., Vanderbilt, C., and Cobb, M. H. (2001) MAP kinase. Chem. Rev. 10: 2449-2476

Cheng, T. J., and Lai, Y. K. (1998) Identification of mitogen-activated protein kinase-activated protein kinase-2 as a vimentin kinase activated by okadaic acid in 9L rat brain tumor cells. J. Cell Biochem. 71: 169-181

Chopra, I., and Roberts, M. (2001) Tetracycline antibiotics: mode of action, applications, molecular biology, and epidemiology of bacterial resistance. Microbiol. Mol. Biol. Rev. 65: 232-260

Chopra, I., Hawkey, P. M., and Hinton, M. (1992) Tetracycline, molecular and clinical aspects. J. Antimicrob. Chemother. 29: 245-277

Chou, Y. H., Bischoff, J. R., Beach, D., and Goldman, R. D. (1990) Intermediate filament reorganization during mitosis is mediated by p34cdc2 phosphorylation of vimentin. Cell 62: 1063-1071

Cillekens, J. M., Belien, J. A., van der Valk, P., Faes, T. J., van Diest, P. J., Broeckaert, M. A., Kralendouk, J. H., and Kamphorst, W. (2000) A histopathological contribution to supratentorail glioma grading, definition of mixed gliomas and recognition of low grad glioma with Rosenthal fibers. J. Neurooncol. 46: 23-43

Colucci-D'Amato, L., Perrone-Capano, C., and di Porzio, U. (2003) Chronic activation of ERK and neurodegenerative disease. Bioessays 25: 1085-1095

Condorelli D. F., Nicoletti, V. G., Barresi, V., Conticello, S. G., Caruso, A., Tendi, E. A., and Giuffrida Stella, A. M. (1999) Structural features of the rat GFAP gene and identification of a novel alternative transcript. J. Neurosci. Res. 56: 219-228

Cooper, D. N., and Youssoufian, H. (1988) The CpG dinucleotide and human genetic disease. Hum. Genet. 78: 151-155

Correia, I., Chu, D., Chou, Y. H., Goldman, R. D., and Matsudaira, P. (1999) Integrating the actin and vimentin cytoskeletons, adhesion-dependent formation of fimbrin-vimentin complexes in macrophages. J. Cell Biol. 146: 831-842

Cowan, K., and Storey, K. B. (2003) Mitogen-activated protein kinases: new signalling pathways functioning in cellula response to environmental stress. J. Exp. Biol. 206: 1107-1115

Coyle, J. T., and Puttfarcken, P. (1993) Oxidative stress, glutamate, and neurodegenerative disorders. Science 262: 689-695

Crome, I. (1953) Megalencephaly associated with hyaline pan-neuropathy. Brain 76: 215-228

Cross, T., Griffiths, G., Deacon, E., Sallis, R., Gough, M., Watters, D., and Lord, J. M. (2000) PKC-delta is an apoptotic lamin kinase. Oncogene 19: 2331-2337

Cruts, M., Hendriks, L., and Van Broeckhoven, C. (1996) The presenilin genes: a new gene family involved in Alzheimer disease pathology. Hum Mol. Genet. 5: 1449-1455

Cuenda, A., Cohen, P., Buee-Scherrer, V., and Goedert, M. (1997) Activation of stress-activated protein kinase-3 (SAPK3) by cytokines and cellular stresses is mediated via

SAPKK3 (MKK6): comparison of the specificities of SAPK3 and SAPK2 (RK/p38). EMBO J. 16: 295-305

Cuenda, A., Rouse, J., Doza, Y. N., Meier, R., Cohen, P., Gollagher, T. F., Young, P. R., and Lee, J. C. (1995) SB203580 is a specific inhibitor of a MAP kinase homologue which is stimulated by cellular stresses and interleukin-1. FEBS Lett. 364: 229-233

D'Alessandro, M., Russell, D., Morley, S. M., Davies, A. M., and Lane, E. B. (2002) Keratin mutations of epidermolysi bullosa simplex alter the kinetics of stress response to osmotic shock. J. Cell Sci. 115: 4341-4351

da Silva, A. R., Viana, G. M., Varonil, C., Pires, B., Nascimento Mdo, D., and Costa J. M. (1997) |Visceral leishmaniasis (kala-azar) on Ilha de São Luís, Maranhão. Brazil: its evolution and outlook| Rev. Soc. Bras. Med. Trop. 30(5): 359-368

Daino, H., Matsumura, I., Takada, K., Odajima, J., Tanaka, H., Ueda, S., Shibayama, H., Ikeda, H., Hibi, M., Machii, T., Hirano, T., and Kanakura, Y. (2000) Induction of apoptosis by extracellular ubiquitin in human hematopoietic cells: possible involvement of STAT3 degradation by proteasome pathway in interleukin 6-dependent hematopoietic cells. Blood 95(8): 2577-2585

Dale, B. A., and Presland, R. B. (1999) Filaggrins. In "Guidebook to the cytoskeletal and motor proteins" (T. Kreis and R. Vale, Eds.), 333-337, Oxford University Press, New York

Dale, B. A., Holbrook, K. A., and Steinert, P. M. (1978) Assembly of stratum corneum basic protein and keratin filaments in macrofibrils. Nature 276: 729-731

Dalle-Donne, I., Rossi, R., Milzani, A., Di Simplicio, P., and Colombo, R. (2001) The actin cytoskeleton response to oxidants: from small heat shock protein phosphorylation to changes in the redox state of actin itself. Free Radic. Biol. Med. 31(12): 1624-1632

Das, A. T., Zhou, X., Vink, M., Klaver, B., Verhoef, K., Marzio, G., and Berkhout, B. (2004) Viral evolution as a tool to improve the tetracycline-regulated gene expression system. J. Biol. Chem. 279: 18776-18782

Davies, S. P., Reddy, H., Caivano, M., and Cohen, P. (2000) Specificity and mechanism of action of some commonly used protein kinase inhibitors. Biochem J. 351: 95-105

Davis, R. J. (2000) Signal transduction by the JNK group of MAP kinases. Cell 103: 239-252

Degenkolb, J., Takahashi, M., Ellestad, G. A., and Hillen, W. (1991) Structural requirements of tetracycline-Tet repressor interaction: determination of equilibrium binding constants for tetracycline analogs with the Tet repressor. Antimicrob. Agents Chemother. 35: 1591-1595

DePianto, D., and Coulombe, P. A. (2004) Intermediate filaments and tissue repair. Exp. Cell Res. 301: 68-76

Deprez, M., DíHooghe, M., Misson, J. P., de Leval, L., Ceurerick, C., Reznik, M., Martin, J. J., and DíHooge, M. (1999) Infantile and juvenile presentations of Alexander's disease: a report of two cases. Acta Neurol. Scand. 99: 158-165

Derijard, B., Hibi, M., Wu, I. H., Barrett, T., Su, B., Deng, T., Karin, M., and Davis, R. J. (1994) JNK1: a protein kinase stimulated by UV light and Ha-Ras that binds and phosphorylates the c-Jun activation domain. Cell 76: 1025-1037

Desagher, S., Glowinski, J., and Premont, J. (1996) Astrocytes protect neurons from hydrogen peroxide toxicity. J. Neurosci. 16(8): 2553-2562

Dhakshinamoorthy, S., and Jaiswal, A. K. (2001) Functional characterization and role of Nrf2 in antioxidant response element-mediated expression and antioxidant induction of NAD(P)H-quinone oxidoreductase1 gene. Oncogene 20: 3906-3917

DiColandrea, T., Karashima, T., Määttä, A., and Watt, F. M. (2000) Subcellular distribution of envoplakin and periplakin: insights into their role as precursors of the epidermal cornified envelope. J. Cell Biol. 151: 573-586

Diehl, J. A., Cheng, M., Roussel, M. F., and Sherr, C. J. (1998) Glycogen synthase kinase-3beta regulate cyclin D1 proteolysis and subcelluar localization. Genes Dev. 12: 3499-3511

Diehl, J. A., Zindy, F. and Sherr, C. J. (1997) Inhibition of cyclin D1 phosphorylation on threonine-286 prevents its rapid degradation via the ubiquitin-proteasome pathway. Genes Dev. 11: 957-972

Ding, M., Eliasson, C., Betsholtz, C., Hamberger, A., and Pekny, M. (1998) Altered taurine release following hypotonic stress in astrocytes from mice deficient for GFAP and vimentin. Brain Res. Mol. Brain Res. 62: 77-81

Dinkova-Kostova, A. T., Holtzclaw, W. D., Cole, R. N., Itoh, K., Wakabayashi, N., Katoh, Y., Yamamoto, M., and Talalay, P. (2002) Direct evidence that sulfhydryl groups of Keap1 are the sensors regulating induction of phase 2 enzymes that protect against carcinogens and oxidants. Proc. Natl. Acad. Sci. U. S. A. 99: 11908-11913

Dinsdale, D., J. Lee, C., Dewson, G., Cohen, G. M., and Peter, M. E. (2004) Intermediate filaments control the intracellular distribution of caspases during apoptosis. Am. J. Pathol. 164: 395-407

Djabali, K., de Nechaud, B., Landon, F., and Portier, M. M. (1997) AlphaB-crystallin interacts with intermediate filaments in response to stress. J. Cell Sci. 110 (Pt 21): 2759-2769

Dou, Q. P., McGuire, T. F., Peng, Y., and An, B. (1999) Proteasome inhibition leads to significant reduction of Bcr-Abl expression and subsequent induction of apoptosis in K562 human chronic myelogenous leukemia cells. J. Pharmacol. Exp. Ther. 289: 781-790

Dougherty, C. J., Kubasiak, L. A., Prentice, H., Andreka, P., Bishopric, N. H., and Webster, K. A. (2002) Activation of c-Jun N-terminal kinase promotes survival of cardiac myocytes after oxidative stress. Biochem. J. 362: 561-571

Duckett, S., Schwartzman, R. J., Osterholm, J., Rorke, L. B., Friedman, D., and McLellan, T. L. (1992) Biopsy diagnosis of familial Alexander's disease. Pediatr. Neurosurg. 18: 134-138

Easwaran, V., Song, V., Polakis, P., and Byers, S. (1999) The ubiquitin-proteasome pathway and serine kinase activity modulate adenomatous polyposis coli protein-mediated regulation of beta-catenin-lymphocyte enhancer-binding factor signalling. J. Biol. Chem. 274: 16641-16645

Eckelt, A., Herrmann, H., and Franke, W. W. (1992) Assembly of a tail-less mutant of the intermediate filament protein, vimentin, in vitro and in vivo. Eur. J. Cell Biol. 58: 319-330

Eckes, B., Dogic, D., Colucci-Guyon, E., Wang, N., Maniotis, A., Ingber, D., Merckling, A., Langa, F., Aumailley, M., Delouvee, A., Koteliansky, V., Babinet, C., and Krieg, T. (1998) Impaired mechanical stability, migration and contractile capacity in vimentin-deficient fibroblasts. J. Cell Sci. 111: 1897-1907

Eddleston, M., and Mucke, L. (1993) Molecular profile of reactive astrocytes – implications for their role in neurologic disease. Neuroscience 54: 15-36

Eggert, M., Radomski, N., Linder, D., Tripier, D., Traub, P., and Jost, E. (1993) Identification of novel phosphorylation sites in murine A-type lamins. Eur. J. Biochem. 213: 659-671

Ekholm, S. V., and Reed, S. I. (2000) Regulation of G(1) cyclin-dependent kinases in the mammalian cell cycle. Curr. Opin. Cell Biol. 12: 676-684

Eliasson, C., Sahlgren, C., Berthold, C. H., Stakeberg, J., Celis, J. E., Betsholtz, C., Eriksson, J. E., and Pekny, M. (1999) Intermediate filament protein partnership in astrocytes. J. Biol. Chem. 274: 23996-24006

Elobeid, A., Bongcam-Rudloff, E., Westermark, B., and Nistér, M. (2000) Effects of inducible glial fibrillary acidic protein on glioma cell motility and proliferation. J. Neurosci. Res. 60: 245-256

Emsley, J. G., Arlotta, P., and Macklis, J. D. (2004) Star-cross'd neurons: astroglial effects on neural repair in the adult mammalian CNS. Trends Neurosci. 27: 238-240

Eng, L. F. (1982) The glial fibrillary acidic protein: the major protein constituent of glial filaments. Scand. J. Immunol. Suppl. 9: 41-51

Eng, L. F., and Ghirnikar, R. S. (1994) GFAP and astrogliosis. Brain Pathol. 4: 229-237

Eng, L. F., and Lee, Y. L. (1998) Glial response to injury, disease, and aging. In astrocytes in brain aging and neurodegeneration, pp. 71-89. H. M. Schipper, ed. R. G. Landes Co., Georgetown, TX

Eng, L. F., Gerstl, B., and Vanderhaeghen, J. J. (1970) A study of proteins in old multiple sclerosis plaques. Trans. Am. Soc. Neurochem. 1: 42

Eng, L. F., Ghirnikar, R. S., and Lee, Y. (2000) Glial fibrillary acidic protein: GFAP-thirty-one years (1969-2000). Neurochem. Res. 251: 1439-1451

Eng, L. F., Kettenmann, H., and Ransom, B. R. (1995) Intermediate filaments in astrocytes. In: Neuroglia Oxford University Press, New York 650-667

Eng, L. F., Lee, Y. L., Kwan, H., Brenner, M., and Messing, A. (1998) Astrocytes cultured from transgenic mice carrying the added human glial fibrillary acidic protein gene contain Rosenthal fibers. J. Neurosci. Res. 53: 353-360

Eng, L. F., Vanderhaeghen, J. J., Bignami, A., and Gerstl, B. (1971) An acidic protein isolated from fibrous astrocytes. Brain Res. 18: 351-354

Epe, B., and Woolley, P. (1984) The binding of 6-demethylchlortetracycline to 70S, 50S, and 30S ribosomal particles: a quantitative study by fluorescence anisotrophy. EMBO J. 3: 121-126

Eriksson, J. E., Brautigan, D. L., Vallee, R., Olmsted, J., Fujiki, H., and Goldman, R. D. (1992) Cytoskeletal integrity in interphase cells requires protein phosphatase activity. Proc. Natl. Acad. Sci. U. S. A. 89: 11093-11097

Eriksson, J. E., He, T., Trejo-Skalli, A. V., Harmala-Brasken, A. S., Hellman, J., Chou, Y. H., and Goldman, R. D. (2004) Specific in vivo phosphorylation sites determine the assembly dynamics of vimentin intermediate filaments. J. Cell Sci. 117: 919-932

Escourolle, R., de Baecque, C., Gray, F., Baumann, N., and Hauw, J. J. (1979) Electron microscopic and neurochemical study of Alexander's disease. Acta Neuropathol. 45: 133-140

Escurat, M., Djabali, K., Gumpel, M., Gros, F., and Portier, M. M. (1990) Differential expression of two neuronal intermediate-filament proteins, peripherin and the low-molecular-mass neurofilament protein (NF-L), during the development of the rat. J. Neurosci. 10: 764-784

Farrell, K., Chuang, S., and Becker, L. E. (1984) Computed tomography in Alexander's disease. Ann. Neurol. 15: 605-607

Feinstein, D. L., Weinmaster, G. A., and Milner, R. J. (1992) Isolation of cDNA clones encoding rat glial fibrillary acidic protein: Expression in astrocytes and in Schwann cells. J. Neurosci. 32: 1-14

Feng, L., Zhou, X., Liao, J. and Omary, M. B. (1999) Pervanadate mediated tyrosine phosphorylation keratin 8 and 19 via a p38 mitogen-activated protein kinase-dependent pathway. J. Cell Sci. 112: 2081-2090

Ferrer, I., Blanco, R., Carmona, M., Puig, B., Barrachina, M., Gómez, C., and Ambrosio, S. (2001) Active, phosphorylation-dependent mitogen-activated protein kinase (MAPK/ERK), stress-activated protein kinase/c-Jun N-terminal kinase (SAPK/JNK), and p38 kinase expression in Parkinson's disease and Dementia with Lewy bodies. J. Neural Transm. 108(12): 1383-1396

Fischer, R. S., Quinlan, R. A., and Fowler, V. M. (2003) Tropomodulin binds to filensin intermediate filaments. FEBS Lett. 547: 228-232

Foisner, R., Leichtfried, F. E., Herrmann, H., Small, J. V., Lawson, D., and Wiche, G. (1988) Cytoskeleton-associated plectin: in situ localization, in vitro reconstitution, and binding to immobilized intermediate filament proteins. J. Cell Biol. 106: 723-733

Fontao, L., Favre, B., Riou, S., Geerts, D., Jaunin, F., Saurat, J. H., Green, K. J., Sonnenberg, A., and Borradori, L. (2003) Interaction of the bullous pemphigoid antigen 1 (BP230) and

desmoplakin with intermediate filaments is mediated by distinct sequences within their COOH terminus. Mol. Biol. Cell 14: 1978-1992

Franck, E., Madsen, O., van Rheede, T., Ricard, G., Huynen, M. A., and de Jong, W. W. (2004) Evolutionary diversity of vertebrate small heat shock proteins. J. Mol. Evol. 59: 792-805

Frappier, T., Stetzkowski-Marden, F., and Pradel, L. A. (1991) Interaction domains of neurofilament light chain and brain spectrin. Biochem. J. 275 (Pt 2): 521-527

Freshney, N. W., Rawlinson, L., Guesdon, F., Jones, E., Cowley, S., Hsuan, J., and Saklatvala, J. (1994) Interleukin-1 activates a novel protein kinase cascade that results in the phosphorylation of Hsp27. Cell 78: 1039-1049

Friede, R. (1964) Alexander's disease. Arch. Neurol. 11: 4414-4422

Friedman, J. H., and Ambler, M. (1992) Progressive parkinsonism associated with Rosenthal fibers. Neurology 42: 1733-1735

Frisen, J., Johansson, C. B., Torok, C., Risling, M., and Lendahl, U. (1995) Rapid, widespread, and longlasting inductin of nestin contributes to the generation of glial scar tissue after CNS injury. J. Cell Biol. 131: 453-464

Frodin, M., and Gammeltoft, S. (1999) Role and regulation of 90 kDa ribosomal S6 kinase (RSK) in signal transduction. Mol. Cell. Endocrinol. 151: 65-77

Fuchs, E., and Cleveland, D. W. (1998) A structural scaffolding of intermediate filaments in health and disease. Science 279: 514-519

Fuchs, E., and Weber, K. (1994) Intermediate filaments: structure, dynamics, function, and disease. Annu. Rev. Biochem. 63: 345-382

Furth, P. A. Onge, L. St., Böger, H., Gruss, P., Gossen, M., Kistner, A., Bujard, H., and Henninghausen, L. (1994) Temporal control of gene expression in transgenic mice by a tetracycline responsive promoter. Proc. Natl. Acad. Sci. U. S. A. 91: 9302-9306

Gabai, V. L., and Sherman, M. Y. (2002) Invited review: Interplay between molecular chaperones and signaling pathways in survival of heat shock. J. Appl. Physiol. 92:1743-1748

Galea, F., Dupouey, P., and Feinstein, D. L. (1995) Glial fibrillary acidic protein mRNA isotypes: expression in vitro and in vivo. J. Neurosci. Res. 41: 452-461

Gallia, G. L., and Khalili, K. (1998) Evaluation of an autoregulatory tetracycline regulated system. Oncogene 16: 1879-1884

Gallo, K. A., and Johnson, G. L. (2002) Mixed-lineage kinase control of JNK and p38 MAPK pathways. Nat. Rev. Mol. Cell Biol. 3: 663-672

Galloway, P. G., Mulvihill, P., and Perry, G. (1992) Filaments of Lewy bodies contain insoluble cytoskeletal elements. Am. J. Pathol. 140: 809-822

Galou, M. E., Colucci-Guyon, D., Ensergueix, J.-L., Rider, M., Gimenez y Tibotta, M., Privat, A., Babinet, C., and Dupouey, P. (1996) Disrupted glial fibrillary acidic protein network in astrocytes from vimentin knockout mice. J. Cell Biol. 133: 853-863

Garcia, L., Gascon, G., Ozand, P., and Yaish, H. (1992) Increased intracranial pressure in Alexander disease: A rare presentation of white-matter disease. J. Child Neurol. 7: 168-171

Garcia-Mata, R., Bebök, Z., Sorscher, E. J., and Sztul, E. S. (1999) Characterization and dynamics of aggresome formation by a cytosolic GFP-chimera. J. Cell Biol. 146: 1239-1254

Geisler, N., and Weber, K. (1982) The amino acid sequence of chicken muscle desmin provides a common structural model for intermediate filament proteins. EMBO J. 1: 1649-1656

Germain, D., Russell, A., Thompson, A., and Hendley, J. (2000) J. Biol. Chem. 275: 12074-12079

Giasson, B. I., and Mushynski, W. E. (1996) Aberrant stress-induced phosphorylation of perikaryal neurofilaments. J. Biol. Chem. 271: 30404-30409

Giasson, B. I., and Mushynski, W. E. (1997) Study of proline-directed protein kinases involved in phosphorylation of the heavy neurofilament subunit. J. Neurosci. 17: 9466-9472

Giasson, B. I., and Mushynski, W. E. (1998) Intermediate filament disassembly in cultured dorsal root ganglion neurons is associated with amino-terminal head domain phosphorylation of specific subunits. J. Neurochem. 70: 1869-1875

Gilbert, S., Loranger, A., and Marceau, N. (2004) Keratins modulate c-Flip/extracellular signal-regulated kinase 1 and 2 antiapoptotic signaling in simple epithelial cells. Mol. Cell. Biol. 24: 7072-7081

Gingold, M. K., Bodensteiner, J. B., Schochet, S. S., and Jaynes, M. (1999) Alexander's disease: unique presentation. J. Child Neurol. 14: 325-329

Gluszez, A. (1964) Disseminated cerebral gliomatosis with fibrillary degeneration of the glia with Rosenthal fibers. Acta Neuropathol. 4: 212-217

Goebel, H. H., Bode, G., Caesar, R., and Koblschutter, A. (1981) Bulbar palsy with Rosenthal fiber formation in the medulla of a 15-year-old girl, localized form of Alexander's disease? Neuropediatrics 12: 382-391

Goedert, M., Cuenda, A., Craxton, M., Jakes, R., and Cohen, P. (1997) Activation of the novel stress-activated protein kinase SAPK4 by cytokine and cellular stresses is mediated by SKK3 (MKK6); comparison of its substrate specificity with that of other SAP kinases. EMBO J. 16: 3563-3571

Goldman, J. E., and Corbin, E. (1991) Rosenthal fibers contain ubiquitinated alpha B-crystallin. Am. J. Pathol. 139: 933-938

Goldman, R. D., Gruenbaum, Y., Moir, R. D., Shumaker, D. K., and Spann, T. P. (2002) Nuclear lamins: building blocks of nuclear architecture. Genes Dev. 16: 533-547

Golub, L. M., Ciancio, S., Ramamurthy, N. S., Leung, M., and McNamara, T. F. (1990) Low-dose doxycycline therapy: effect on gingival and crevicular fluid collagenase activity in humans. J. Periodont. Res. 25: 321-330

Golub, L. M., Lee, H. M., Greenwald, R. A., Ryan, M. E., Salo, T., and Giannobile, W. V. (1997) A matrix metalloproteinase inhibitor reduces bone-type collagen degradation fragments and specific collegenases in gingival crevicular fluid during adult periodontitis. Inflamm. Res. 46: 310-319

Golub, L. M., Sorsa, T., Lee, H. M., Ciancio, S., Sorbi, D., Ramamurthy, N. S., Gruber, B., Salo, T., and Konttinen, Y. T. (1995) Doxycycline inhibits neutrophil (PMN)-type matrix metalloproteinases in human adult periodontitis gingiva. J. Clin. Periodontol. 22: 100-109

Gomes, F. C., Maia, C. G., de Menezes, J. R., and Neto, V. M. (1999) Cerebellar astrocytes treated by thyroid hormone modulate neuronal proliferation. Glia 25: 247-255

Gomi, H., Yokoyama, T., Fujimoto, K., Ikeda, T., Katoh, A., Itoh, T., and Itohara, S. (1995) Mice devoid of the glial fibrillary acidic protein develop normally and are susceptible to scrapie prions. Neuron 14: 29-41

Gorospe, J. R., Naidu, S., Johnson, A. B., Puri, V., Raymond, G. V., Jenkins, S. D., Pedersen, R. C., Lewis, D., Knowles, P., Fernandez, R., De Vivo, D., van der Knaap, M. S., Messing, A., Brenner, M., and Hoffman, E. P. (2002) Molecular findings in symptomatic and pre-symptomatic Alexander disease patients. Neurology 58: 1494-1500

Goss, V. L., Hocevar, B. A., Thompson, L. J., Stratton, C. A., Burns, D. J., and Fields, A. P. (1994) Identification of nuclear beta II protein kinase C as a mitotic lamin kinase. J. Biol. Chem. 269: 19074-19080

Gossen, M., and Bujard, H. (1992) Tight control of gene expression in mammalian cells by tetracycline response promoters. Proc. Natl. Acad. Sci. U. S. A. 89: 5547-5551

Gossen, M., and Bujard, H. (1993) Anhydrotetracycline: a novel effector for tetracycline controlled gene expression systems in higher eukaryotic cells. Nucleic Acids Res. 21: 4411-4412

Gossen, M., and Bujard, H. (1995) Efficacy of tetraycycline-controlled gene expression is influenced by cell type. BioTechniques 89: 213-215

Gossen, M., Bonin, A., and Bujard, H. (1993) Control of gene activity in higher eukaryotic cells by prokaryotic regulatory elements. Trends Biochem. Sci. 18: 471-475

Gossen, M., Freundlieb, S., Bender, G., Müller, G., Hillen, W., and Bujard, H. (1995) Transcriptional activation by tetracyclines in mammalian cells. Science 268: 1766-1769

Goto, H., Yasui, Y., Kawajiri, A., Nigg, E. A., Terada, Y., Tatsuka, M., Nagata, K., and Inagaki, M. (2003) Aurora-B regulates the cleavage furrow-specific vimentin phosphorylation in the cytokinetic process. J. Biol. Chem. 278: 8526-8530

Granger, B. L., and Lazarides, E. (1980) Synemin: a new high molecular weight protein associated with desmin and vimentin filaments in muscle. Cell 22: 727-738

Grcevic, N., and Yates, P. O. (1957) Rosenthal fibers in tumors of the central nervous system. J. Pathol. Bacteriol. 73: 467-472

Green, K. J., Bohringer, M., Gocken, T., and Jones, J. C. (2005) Intermediate filament associated proteins. Adv. Protein Chem. 70: 143-202

Gross-Mesilaty, S., Reinstein, E., Bercovich, B. Tobias, K. E., Schwartz, A. L., Kahana, C., and Ciechanover, A. (1998) Basal and human papillomavirus E6 oncoprotein-induced degradation of Myc proteins by the ubiquitin pathway. Proc. Natl. Acad. Sci. U. S. A. 95: 8058-8063

Guerin, C. J., Anderson, D. H., and Fisher, S. K. (1990) Changes in intermediate filament immunolabeling occur in response to retinal detachment and reattachment in primates. Invest. Ophthalmol. Vis. Sci. 31: 1474-1482

Gullotta, F., and Fliedner, E. (1972) Spongioblastomas, astrocytomas, and Rosenthal fibers: Ultrastructural, tissue culture and enzyme histochemical investigations. Acta Neuropathol. (Berl) 22: 68-78

Gupta, S., Barrett, T., Whitmarch, A. J., Cavanagh, J., Sluss, H. K., Derijard, B., and Davis, R. J. (1996) Selective interaction of JNK protein kinase isoforms with transcription factors. EMBO J. 15: 2760-2770

Guthrie, S. O., Burton, E. M., Knowles, P., and Marshall, R. (2003) Alexander's disease in a neurologically normal child: a case report. Pediatr. Radiol. 33: 47-49

Guyton, K. Z., Liu, Y., Gorospe, M., Xu, Q., and Holbrook, N. J. (1996) Activation of mitogen-activated protein kinase by H2O2. J. Biol. Chem. 271: 4138-4142

Hagemann, T. L., Gaeta, S. A., Smith, M. A., Johnson, D. A., Johnson, J. A., and Messing, A. (2005) Gene expression analysis in mice with elevated glial fibrillary acidic protein and Rosenthal fibers reveals a stress response followed by glial activation and neuronal dysfunction. Hum. Mol. Genet. 14: 2443-2458

Hallpike, J. F., Adams, C. W. M., and Tourtellote, W. W. (1983) Multiple sclerosis pathology. Diagnosis and management. Chapman and Hall, London

Hampton, R. Y., Gardner, R. G., and Rine, J. (1996) Role of 26S proteasome and Hrd genes in the degradation of 3-hydroxy-3-methylglutaryl-CoA reductase, an integral endoplasmic reticulum membrane protein. Mol. Biol. Cell 7: 2029-2044

Han, J., Lee, J. D., Bibbs, L., and Ulevitch, R. J. (1994) A MAP kinase targeted by endotoxin and hyperosmolarity in mammalian cells. Science 265: 808-811

Hansen, A., Jorgensen, O. S., Bolwig, T. G., and Barry, D. I. (1990) Hippocampal kindling alters the concentration of glial fibrillary acidic protein and other marker proteins in rat brain. Brain Res. 531: 307-311

Hara, A., Sakai, N., Yamada, H., Niikawa, S., Ohno, T., Tanaka, T., and Mori, H. (1991) Proliferative assessment of GFAP-positive and GFAP-negative glioma cells by nucleolar organizer region staining. Sur. Neurol. 36: 190-194

Harris, K. F., Shoji, I., Cooper, E. M., Kumar, S., Oda, H., and Howley, P. M. (1999) Ubiquitin-mediated degradation of active Src tyrosine kinase. Proc. Natl. Acad. Sci. U. S. A. 96: 13738-13743

Hartmann, H., Herchenbach, J., Stephani, U., Ledaal, P., Donnerstag, F., Lücke, T., Das, A. M., Christen, H. J., Hagedorn, M., and Meins, M. (2007) Novel mutations in exon 6 of the GFAP gene affect a highly conserved if motif in the rod domain 2B and are associated with early onset infantile Alexander disease. Neuropediatirics 38: 143-147

Hashimoto, R., Nakamura, Y., Komai, S., Kashiwagi, Y., Tamura, K., Goto, T., Aimoto, S., Kaibuchi, K., Shiosaka, S., and Takeda, M. (2000) Site-specific phosphorylation of neurofilament-L is mediated by calcium/calmodulin-dependent protein kinase II in the apical dendrites during long-term potentiation. J. Neurochem. 75: 373-382

Hatten, M. E., Liem, R. K., Shelanski, M. L., and Mason, C. A. (1991) Astroglia in CNS injury. Glia 4: 233-243

Hatzfeld, M., and Franke, W. W. (1985) Pair formation and promiscuity of cytokeratins: formation in vitro of heterotypic complexes and intermediate-sized filaments by homologous and heterologous recombinations of purified polypeptides. J. Cell Biol. 101: 1826-1841

Hatzfeld, M., Dodemont, H., Plessmann, U., and Weber, K. (1992) Truncation of recombinant vimentin by ompT. Identification of a short motif in the head domain necessary for assembly of type III intermediate filament proteins. FEBS Lett. 302: 239-242

Hatzfeld, M., Haffner, C., Schulze, K., and Vinzens, U. (2000) The function of plakophilin I in desmosome assembly and actin filament organization. J. Cell Biol. 149: 209-222

Hawrylak, N., Chang, F. L., and Greenough, W. T. (1993) Astrocytic and synaptic response to kindling in hippocampal subfield CA1: II. Synaptogenesis and astrocytic process increases to in vivo kindling. Brain Res. 603: 309-316

He, F., and Sun, Y. E. (2006) Glial cells more than support cells? Int. J. Biochem. Cell Biol. 39: 661-665

He, H. L., Qi, X. M., Grossmann, J., and Distelhorst, C. W. (1998) C-Fos degradation by the proteasome-an early, Bcl-2-regulated step in apoptosis. J. Biol. Chem. 273: 25015-25019

He, T., Stepulak, A., Holmstrom, T. H., Omary, M. B., and Eriksson, J. E. (2002) The intermediate filament protein keratin 8 is a novel cytoplasmic substrate for c-Jun N-terminal kinase. J. Biol. Chem. 277: 10767-10774

Head, M. W., Corbin, E., and Goldman, J. E. (1994) Coordinate and independent regulation of alpha B-crystallin and hsp27 expression in response to physiological stress. J. Cell Physiol. 159: 41-50

Hecht, B., Muller, G., and Hillen, W. (1993) Noninducible Tet repressor mutations map from the operator binding motif to the C terminus. J. Bacteriol. 175: 1206-1210

Helfand, B. T., Chang, L., and Goldman, R. D. (2003) The dynamic and motile properties of intermediate filaments. Annu. Rev. Cell Dev. Biol. 19: 445-467

Hemken, P. M., Bellin, R. M., Sernett, S. W., Becker, B., Huiatt, T. W., and Robson, R. M. (1997) Molecular characteristics of the novel intermediate filament protein paranemin. Sequence reveals EAP-300 and IFAPa-400 are highly homologous to paranemin. J. Biol. Chem. 272: 32489-32499

Herndon, R. M., Rubinstein, L. J., Freeman, J. M., and Mathieson, G. (1970) Light and electron microscopic observations of Rosenthal fibers in Alexander's disease and in multiple sclerosis. J. Neuropathol. Exp. Neurol. 29: 524-551

Herrmann, H., and Aebi, U. (1998) Intermediate filament assembly: fibrillogenesis is driven by decisive dimer-dimer interactions. Curr. Opin. Struct. Biol. 8: 177-185

Herrmann, H., and Aebi, U. (2000) Intermediate filaments and their associates: multi-talented structural elements specifying cytoarchitecture and cytodynamics. Curr. Opin. Cell Biol. 12: 79-90

Herrmann, H., Haner, M., Brettel, M., Ku, N. O., and Aebi, U. (1999) Characterization of distinct early assembly units of different intermediate filament proteins. J. Mol. Biol. 286: 1403-1420

Herrmann, H., Haner, M., Brettel, M., Muller, S. A., Goldie, K. N., Fedtke, B., Lustig, A., Franke, W W., and Aebi, U. (1996) Structure and assembly properties of the intermediate filament protein vimentin: the role of its head, rod and tail domains. J. Mol. Biol. 264: 933-953

Herrmann, H., Hesse, M., Reichenzeller, M., Aebi, U., and Magin, T. M. (2003) Functional complexity of intermediate filament cytoskeletons: from structure to assembly to gene ablation. Int. Rev. Cytol. 223: 83-175

Herrmann, H., Wedig, T., Porter, R. M., Lane, E. B., and Aebi, U. (2002) Characterization of early assembly intermediates of recombinant human keratins. J. Struct. Biol. 137: 82-96

Hershko, A., and Ciechanover, A. (1998) The ubiquitin system. Annu. Rev. Biochem. 67: 425-479

Hertz, L. (1965) Possible role of neuroglia: a potassium-mediated neuronal-neuroglial-neuronal impuse transmission system. Nature 206: 1091-1094

Hess, D. C., Fischer, A. Q., Yaghmai, F., Figuera, R., and Akamatsu, Y. (1990) Comparative neuroimaging with pathological correlates in Alexander's disease. J. Child Neurol. 5: 248-252

Hess, P., Pihan, G., Sawyers, C. L., Flavell, R. A., and Davis, r. J. (2002) Survival signaling mediated by c-Jun NH(2)-terminal kinase in transformed B lymphoblasts. Nat. Genet. 32: 201-205

Hesse, M., Magin, T. M., and Weber, K. (2001) Genes for intermediate filament proteins and the draft sequence of the human genome: novel keratin genes and a surprisingly high number of pseudogenes related to keratin genes 8 and 18. J. Cell Sci. 114: 2569-2575

Hijikata, T., Murakami, T., Imamura, M., Fujimaki, N., and Ishikawa, H. (1999) Plectin is a linker of intermediate filaments to Z-discs in skeletal muscle fibers. J. Cell Sci. 112 (Pt 6): 867-876

Hillen, W., and Berens, C. (1994) Mechanisms underlying expression of Tn10 encoded tetracycline resistance. Annu. Rev. Microbiol. 48: 345-369

Hinttala, R., Karttunen, V., Karttunen, A., Herva, R., Uusimaa, J., and Remes, A. M. (2007) Alexander disease with occipital predominance and a novel c.799G>C mutation in the GFAP gene. Acta Neuropathol. (Berl) 114: 543-545

Hirosumi, I., Tuncman, G., Chang, L., Gorgun, C. Z., Uysal, K. T., Maeda, K., Karin, M., and Hotamisligil, G. S. (2002) A central role for JNK in abesity and insulin resistance. Nature 420: 333-336

Ho, C. L., Martys, J. L., Mikhailov, A., Gundersen, G. G., and Liem, R. K. (1998) Novel features of intermediate filament dynamics revealed by green fluorescent protein chimeras. J. Cell Sci. 111 (Pt 13): 1767-1778

Hofmann, I., and Franke, W. W. (1997) Heterotypic interactions and filament assembly of type I and type II cytokeratins in vitro: viscometry and determinations of relative affinities. Eur. J. Cell Biol. 72: 122-32

Hofmann, I., Mertens, C., Brettel, M., Nimmrich, V., Schnolzer, M., and Herrmann, H. (2000) Interaction of plakophilins with desmoplakin and intermediate filament proteins: an in vitro analysis. J. Cell Sci. 113 (Pt 13): 2471-2483

Hol, E. M., Roelofs, R. F., Moral, E., Sonnemans, M. A., Sluijs, J. A., Proper, E. A., De Graan P. N., Fischer, D. F., and Van Leeuwen, F. W. (2003) Neuronal expression of GFAP in patients with Alzheimer pathology and identification of novel GFAP splice forms. Mol. Psychiatry 8(9): 786-796

Holwell, T. A., Schweitzer, S. C., and Evans, R. M. (1997) Tetracycline regulated expression of vimentin in fibroblasts derived from vimentin null mice. J. Cell Sci. 110: 1947-1956

Honnorat, J., Flocard, F., Ribot, C., Saint-Pierre, G., Pineau, D., and Peysson, P., and Kopp, N. (1993) Alexander's disease in adults and diffuse cerebral gliomatosis in 2 members of the same family. Rev. Neurol. 149: 781-787

Hopwood, D., Moitra, S., Vojtesek, B., Johnston, D. A., Dillon, J. F., Hupp, T. R. (1997) Biochemical analysis of the stress protein response in human oesophageal epithelium. Gut 41: 156-163

Hornbeck, P., Huang, K. P., and Paul, W. E. (1988) Lamin B is rapidly phosphorylated in lymphocytes after activation of protein kinase C. Proc. Natl. Acad. Sci. U. S. A. 85: 2279-2283

Horoupian, D. S., Kress, Y., Yen, S-H, and Gaskin, F. (1982) Nickel-induced changes and reappraisal of Rosenthal fibers in focal CNS lesions. J. Neuropathol. Exp. Neurol. 41: 664-675

Hotamisligil, G. S. (2005) Role of endoplasmic regiculum stress and c-Jun NH2-terminal kinase pathways in inflammation and origin of obesity and diabetes. Diabetes 54: S73-S78

Houle, J. D., and Reier, P. J. (1989) Regrowth of calcitonin gene-related peptide (CGRP) immunoreactive axons from the chronically injured rat spinal cord into fetal spinal cord tissue transplants. Neurosci. Lett. 103: 253-258

Howard, K. L., Hall, D. A., Moon, M., Agarwal, P., Newman, E., and Brenner, M. (2007) Adult-onset Alexander disease with progressive ataxia and palatal tremor. Mov Disord. 23: 118-122

Howard, R. S., Greenwood, R., Gawler, J., Scaravilli, F., Marsden, C. D., and Harding, A. E. (1993) A familial disorder associated with palatal myoclonus, other brainstem signs, tetraparesis, ataxia and rosenthal fibre formation. J. Neurol. Neurosurg. Psychiatry 56: 977-981

Howe, C. J., Lahair, M. M., McCubrey, J. A., and Franklin, R. A. (2004) Redox regulation of the calcium/calmodulin-dependent protein kinases. J. Biol. Chem. 279(43): 44573-44581

Hsiao, V. C., Tian, R., Long, H., Der Perng M., Brenner, M., Quinlan, R. A., and Goldman, J. E. (2005) Alexander-disease mutation of GFAP causes filament disorganization and decreased solubility of GFAP. J. Cell Sci. 118(9): 2057-2065

Hu, G., Zhang, S., Vidal, M., Baer, J. L., Xu, T., and Hearon, E. R. (1997) Mammalian homologs of seven in absentia regulate DCC via the ubiquitin-proteasome pathway. Genes Dev. 11: 2701-2714

Huang, H. C., Nguyen, T., and Pickett, C. B. (2002) Phosphorylation of Nrf2 at Ser-40 by protein kinase C regulates antioxidant response element-mediated transcription. J. Biol. Chem. 277: 42769-42774

Huang, H., Joazeiro, C. A., Bonfoco, E., Kamada, S., Leverson, J. D., and Hunter, T. (2000) The inhibitor of apoptosis, cIAP2, functions as an ubiquitin-protein ligase and promotes in vitro mono-ubiquitination of caspases 3 and 7. J. Biol. Chem. 27: 26661-26664

Huen, A. C., Park, J. K., Godsel, L. M., Chen, X., Bannon, L. J., Amargo, E. V., Hudson, T. Y., Mongiu, A. K., Leigh, I. M., Kelsell, D. P., Gumbiner, B. M., and Green, K. J. (2002) Intermediate filament-membrane attachments function synergistically with actin-dependent contacts to regulate intercellular adhesive strength. J. Cell Biol. 159: 1005-1017

Huot, J., Houle, F., Rousseau, S., Deschesnes, R. G., Shah, G. M., and Landry, J. (1998) SAPK2/p38-dependent F-actin reorganization regulates early membrane blebbing during stress-induced apoptosis. J. Cell Biol. 143(5): 1361-1373

Igarashi, K., and Kaji, A. (1970) Relationship between sites 1, 2 and acceptor, donor sites for the binding of aminoacyl tRNA to ribosomes. Eur. J. Biochem. 14: 41-46

Imamura, A., Orii, K. E., Mizuno, S., Hoshi, H., and Kondo, T. (2002) MR imaging and H-MR spectroscopy in a case of juvenile Alexander disease. Brain & Development 24: 723-726

Inada, H., Izawa, I., Nishizawa, M., Fujita, E., Kiyono, T., Takahashi, T., Momoi, T., and Inagaki, M. (2001) Keratin attenuates tumor necrosis factor-induced cytotoxicity through association with TRADD. J. Cell Biol. 155: 415-426

Inagaki, M., Nakamura, Y., Takeda, M., Nishimura, T., and Inagaki, N. (1994) Glial fibrillary acidic protein: dynamic property and regulation by phosphorylation. Brain Pathol. 4: 239-243

Ireland, M., and Maisel, H. (1983) Identification of native actin filaments in chick lens fiber cells. Exp. Eye Res. 36: 531-536

Ireland, M., and Maisel, H. (1984) A cytoskeletal protein unique to lens fiber cell differentiation. Exp. Eye Res. 38: 637-645

Ishida, N., Tanaka, K., Tamura, T. Nishizawa, M., Okazaki, K., Sagata, N., and Ichihara, A. (1993) Mos is degraded by the 26S proteasome in an ubiquitin-dependent fashion. FEBS Lett. 324: 345-348

Ishigaki, K., Ito, Y., Sawaishi, Y., Kodaira, K., Funatsuka, M., Hattori, N., Nakano, K., Saito, K., and Osawa, M. (2006) TRH therapy in a patient with juvenile Alexander disease. Brain Dev. 28: 663-667

Ishikawa, H., Bischoff, R., and Holtzer, H. (1968) Mitosis and intermediate-sized filaments in developing skeletal muscle. J. Cell Biol. 38: 538-555

Ito, H., Okamoto, K., Nakayama, H., Isobe, T., and Kato, K. (1997) Phosphorylation of αB-crystallin in response to various types of stress. J. Biol. Chem. 272: 29934-29941

Itoh, K., Wakabayashi, N., Katoh, Y., Ishii, T., Igarashi, K., Engel, J. D., and Yamamoto, M. (1999) Keap1 represses nuclear activation of antioxidant responsive elements by Nrf2 through binding to the amino-terminal Neh2 domain. Genes Dev. 13: 76-86

Iwaki, A., Iwaki, T., Goldman, J. E., Ogomori, K., Tateishi, J., and Sakaki, Y. (1992) Accumulation of B-crystallin in brains of patients with Alexander's disease is not due to an abnormality of the 5'-flanking and coding sequence of the genomic DNA. Neurosci. Lett. 140: 89-92

Iwaki, T., Iwaki, A., Tateishi, J., Sakaki, Y., and Goldman, J. E. (1993) Alpha B-crystallin and 27-kd heat shock protein are regulated by stress conditions in the central neuvous system and accumulate in Rosenthal fibers. Am. J. Pathol. 143: 487-495

Iwaki, T., Iwaki, A., Tateishi, J., Sakaki, Y., and Goldman, J. E. (1993) Alpha B-crystallin and 27-kd heat shock protein are regulated by stress conditions in the central nervous system and accumulate in Rosenthal fibers. Am. J. Pathol. 143: 487-495

Iwaki, T., Kume-Iwaki, A., Liem, R. K. H., and Goldman, J. E. (1989) Alpha B-crystallin is expressed in non-lenticular tissues and accumulates in Alexander's disease brain. Cell 57(1): 71-78

Iwaki, T., Kume-Iwaki, A., Liem, R. K., and Goldman, J. E. (1989) Alpha B-crystallin is expressed in non-lenticular tissues and accumulates in Alexander's disease brain. Cell 57: 71-78

Izawa, I., and Inagaki, M. (2006) Regulatory mechanisms and functions of intermediate filaments: a study using site- and phosphorylation state-specific antibodies. Cancer Sci. 97: 167-174

Izawa, I., Nishizawa, M., Ohtakara, K., Ohtsuka, K., Inada, H., and Inagaki, M. (2000) Identification of Mrj, a DnaJ/Hsp40 family protein, as a keratin 8/18 filament regulatory protein. J. Biol. Chem. 275: 34521-34527

Jacob, J., Robertson, N. J., and Hilton, D. A. (2003) The clinicopathological spectrum of Rosenthal fibre encaphalopathy and Alexander's disease: a case report and review of the literature. J Neurol. Neurosurg. Psychiatry. 74: 807-810

Janig, E., Stumptner, C., Fuchsbichler, A., Denk, H., and Zatloukal, K. (2005) Interaction of stress proteins with misfolded keratins. Eur. J. Cell Biol. 84: 329-339

Janknecht, R., and Hunter, T. (1997) Convergence of MAP kinase pathways on the ternary complex factor Sap-la. EMBO J. 16: 1620-1627

Janmey, P. A., Shah, J. V., Janssen, K. P., and Schliwa, M. (1998) Viscoelasticity of intermediate filament networks. Subcell. Biochem. 31: 381-397

Janosch, P., Kieser, A., Eulitz, M., Lovric, J., Sauer, G., Reichert, M., Gounari, F., Buscher, D., Baccarini, M., Mischak, H., and Kolch, W. (2000) The Raf-1 kinase associates with vimentin kinases and regulates the structure of vimentin filaments. FASEB J. 14: 2008-2021

Jantzie, L. L., Cheung, P.-Y., and Todd, K. G. (2005) Doxycycline reduces cleaved caspase-3 and microglial activation in an animal model of neonatal hypoxia-ischemia. J. Cereb. Blood Flow Metabol. 25: 314-324

Janzer, R. C., and Raff, M. C. (1987) Astrocytes induce blood-brain barrier properties in endothelial cells. Nature 325: 253-257

Jefferson, J. J., Leung, C. L., and Liem, R. K. (2004) Plakins: goliaths that link cell junctions and the cytoskeleton. Nat. Rev. Mol. Cell. Biol. 5: 542-553

Jensen, T. J., Loo, M. A., Pind, S., Williams, D. B., Goldberg, A. L. and Riordan, J. R. (1995) Multiple proteolytic systems, including the proteasome, contribute to CFTR processing. Cell 83: 129-135

Jessen, K. R., and Mirsky, R. (1980) Glial cells in the enteric nervous system contain glial fibrillary acidic protein. Nature 286: 736-737

Jessen, K. R., Morgan, L., Stewart, H. J., and Mirsky, R. (1990) Three markers of adult non-myelin-forming Schwann cells, 217c(Ran-1), A5E3 and GFAP: development and regulation by neuron-Schwann cell interactions. Development 109: 91-103

Jiang, Y., Chen, C., Li, Z., Guo, W., Gegner, J. A., Lin, S., and Han, J. (1996) Characterization of the structure and function of a new mitogen-activated protein kinase (p38β). J. Biol. Chem. 271: 17920-17926

Johnson, A. B. and Bettica, A. (1989) On-grid immunogold labeling of glial intermediate filaments in epoxy-embedded tissue. Am. J. Anat. 185: 335-341

Johnson, A. B., and Bettica, A. (1986) Rosenthal fibers in Alexander's disease show glial fibrillary acidic protein (GFAP) immunoreactivity with the immunogold staining method, abstract. J. Neuropathol. Exp. Neurol. 45: 349

Johnson, C. E., and Englund, P. T. (1998) Changes in organization of crithidia fasciculata kinetoplast DNA replication proteins during the cell cycle. J. Cell Biol. 143: 911-919

Johnson, G. L., and Lapadat, R. (2002) Mitogen-activated protein kinase pathways mediated by ERK, JNK, and p38 protein kinases. Science 298: 1911-1912

Johnson, S. A., and Hunter, T. (2005) Kinomic: methods for deciphering the kinome. Nat. Methods 2: 17-25

Jonak, C., Klosner, G., Kokesch, C., Fodinger, D., Honigsmann, H., and Trautinger, F. (2002) Subcorneal colocalization of the small heat shock protein, hsp27, with keratins and proteins of the cornified cell envelope. Br. J. Dermatol. 147: 13-19

Kajiwara, K., Orita, T., Nishizaki, T., Kamiryo, T., Nakayama, H., and Ito, H. (1992) Glial fibrillary acidic protein (GFAP) expression and nucleolar organizer regions (NORs) in human gliomas. Brain Res. 572: 314-318

Kamradt, M. C., Chen, F., Sam, S., and Cryns, V. L. (2002) The small heat shock protein alpha B-crystallin negatively regulates apoptosis during myogenic differentiation by inhibiting caspase-3 activation. J. Biol. Chem. 277: 38731-38736

Kamradt, M. C., Lu, M., Werner, M. E., Kwan, T., Chen, F., Strohecker, A., Oshita, S., Wilkinson, J. C., Yu, C., Oliver, P. G., Duckett, C. S., Buchsbaum, D. J., LoBuglio, A. F., Jordan, V. C., and Cryns, V. L. (2005) The small heat shock protein alpha B-crystallin is a

novel inhibitor of TRAIL-induced apoptosis that suppresses the activation of caspase-3. J. Biol. Chem. 280: 11059-11066

Kaplowitz, N. (2002) Biochemical and cellular mechanisms of toxic liver injury. Semin Liver Dis. 22: 137-144

Kapprell, H. P., Owaribe, K., and Franke, W. W. (1988) Identification of a basic protein of Mr 75,000 as an accessory desmosomal plaque protein in stratified and complex epithelia. J. Cell Biol. 106: 1679-1691

Karashima, T., and Watt, F. M. (2002) Interaction of periplakin and envoplakin with intermediate filaments. J. Cell Sci. 115: 5027-5037

Karin, M., and Gallagher, E. (2005) From Jnk to pay dirt: jun kinases, their biochemistry, physiology and clinical importance. IUBMB Life 57: 283-295

Karin, M., Lawrence, T., and Nizet, V. (2006) Innate immunity gone away: linking microbial infections to chronic inflammation and cancer. Cell 124: 823-835

Kato, K., Inaguma, Y., Ito, H., Iida, K., Iwamoto, I., Kamei, K., Ochi, N., Ohta, H., and Kishikawa, M. (2001) Ser-59 is the major phophorylatio site in αB-crystallin accumulated in the brains of patients with Alexander's disease. J. Neurochem. 76: 730-736

Kaufman, S. J., and Foster, R. F. (1988) Replicating myoblasts express a muscle-specific phenotype. Proc. Natl. Acad. Sci. U. S. A. 85: 9606-9610

Kaufmann, E., Weber, K, and Geisler, N. (1985) Intermediate filament forming ability of desmin derivatives lacking either the amino-terminal 67 or the carboxy-terminal 27 residues. J. Mol. Biol. 185: 733-742

Kawai, M., Sakai, N., Miyake, S., Tsukamoto, H., Akagi, M., Inui, K., Mushiake, S., Taniike, M., and Ozono, K. (2006) Novel mutation of gene coding for glial fibrillary acidic protein in a Japanese patient with Alexander disease. Brain Dev. 28: 60-62

Kazerounian, S., Uitto, J., and Aho, S. (2002) Unique role for the periplakin tail in intermediate filament association: specific binding to keratin 8 and vimentin. Exp. Dermatol. 11: 428-438

Kepes, J. J., and Ziegler, D. K. (1972) Alexander's disease in an adult (leukodystrophy with Rosenthal fibers). Mod. Med. 69(suppl): 23-25

Khurgel, M., Racine, R. J., and Ivy, G. O. (1992) Kindling causes changes in the composition of the astrocytic cytoskeleton. Brain Res. 592: 338-342

Kierszenbaum, A. L. (2000) The 26S proteasome: ubiquitin-mediated proteolysis in the tunnel. Mol. Reprod. Dev. 57: 109-110

Kim, S., and Coulombe, P. A. (2007) Intermediate filament scaffolds fulfill mechanical, organizational, and signaling functions in the cytoplasm. Genes Dev. 21: 1581-1597

King, R. J., Finley, J. R., Coffer, A. I., Millis, R. R., and Rukens, R. D. (1987) Characterization and biological relevance of a 29-kDa, oestrogen receptor-related protein. J. Steroid Biochem. 27: 471-475

Kinoshita, T., Imaizumi, T., Miura, Y., Fujimoto, H., Ayabe, M., Shoji, H., Okamoto, Y., Takashima, H., Osame, M., and Nakagawa, M. (2003) A case of adult-onset Alexander disease with Arg416Trp human glial fibrillary acidic protein gene mutation. Neurosci. Lett. 350: 169-172

Kinouchi, R., Takeda, M., Yang, L., Wilhelmsson, U., Lundkvist, A., Pekny, M., and Chen, D. F. (2003) Robust neural integration fromrtinal transplants in mice deficient in GFAP and vimentin. Nat. Neurosci. 6: 863-868

Kistner, A., Gossen, M., Zimmermann, F., Jerecic, J., Ullmer, C., Lübbert, H., and Bujard, H. (1996) Doxycycline-mediated quantitative and tissue-specific control of gene expression in transgenic mice. Proc. Natl. Acad. Sci. U. S. A. 93: 10933-10938

Klein, H. (1970) Alexanderísche Krankheit bei einerErwaschsenen. Zentralblges Neurol. Psychiat. 197: 338

Klemenz, R., Frohli, E., Steiger, R. H., Schafer, R., and Aoyama, A. (1991) Alpha B-crystallin is a small heat shock protein. Proc. Natl. Acad. Sci. U. S. A. 88: 3652-3656

Koepp, D. M., Harper, J. W., and Elledge, S. J. (1999) How the cyclin became a cyclin: regulated proteolysis in the cell cycle. Cell 97: 431-434

Kong, A. N., Owuor, E., Yu, R., Hebbar, V., Chen, C., Hu, R., and Mandlekar, S. (2001) Induction of xenobiotic enzymes by the MAP kinase pathway and the antioxidant or electrophile response element (ARE/EpRE). Drug Metab. Rev. 33: 255-271

Kopito, R. R., and Sitia, R. (2000) Aggresomes and Russell bodies. Symptoms of cellular indigestion? EMBO Rep. 1: 225-231

Kosako, H., Amano, M., Yanagida, M., Tanabe, K., Nishi, Y., Kaibuchi, K., and Inagaki, M. (1997) Phosphorylation of glial fibrillary acidic protein at the same sites by cleavage furrow kinase and Rho-associated kinase. J. Biol. Chem. 272: 10333-10336

Kosako, H., Goto, H., Yanagida, M., Matsuzawa, K., Fujita, M., Tomono, Y., Okigaki, T., Odai, H., Kaibuchi, K., and Inagaki, M. (1999) Specific accumulation of Rho-associated kinase at the cleavage furrow during cytokinesis: cleavage furrow-specific phosphorylation of intermediate filaments. Oncogene 18: 2783-2788

Kouklis, P. D., Hutton, E., and Fuchs, E. (1994) Making a connection: direct binding between keratin intermediate filaments and desmosomal proteins. J. Cell Biol. 127: 1049-1060

Kouklis, P. D., Papamarcaki, T., Merdes, A., and Georgatos, S. D. (1991) A potential role for the COOH-terminal domain in the lateral packing of type III intermediate filaments. J. Cell Biol. 114: 773-786

Koyama, Y., and Goldman, J. E. (1999) Formation of GFAP cytoplasmic inclusions in astrocytes and their disaggregation by alphaB-crystallin. Am. J. Pathol. 154: 1563-1572

Kreis, T. E., Geiger, B., Schmid, E., Jorcano, J. L., and Franke, W. W. (1983) De novo synthesis and specific assembly of keratin filaments in nonepithelial cells after microinjection of mRNA for epidermal keratin. Cell 32: 1125-1137

Kress, Y., Gaskin, F., Horoupoan, D. S., and Brosnan, C. (1981) Nickel induction of Rosenthal fibers in rat brain. Brain Res. 210: 419-425

Ku, N. O., Michie, S., Resurreccion, E. Z., Broome, R. L., and Omary, M. B. (2002b) Keratin binding to 14-3-3 proteins modulates keratin filaments and hepatocyte mitotic progression. Proc. Natl. Acad. Sci. U. S. A. 99: 4373-4378

Ku, N. O., and Omary, M. B. (2000) Keratins turn over by ubiquitination in a phosphorylation-modulated fashion. J. Cell Biol. 149: 547-552

Ku, N. O., and Omary, M. B. (2006) A disease- and phosphorylation-related nonmechanical function for keratin 8. J. Cell Biol. 174: 115-125

Ku, N. O., Azhar, S., and Omary, M. B. (2002a) Keratin 8 phosphorylation by p38 kinase regulates cellular keratin filament reorganization: modulation by a keratin 1-like disease causing mutation. J. Biol. Chem. 277: 10775-10782

Ku, N. O., Darling, J. M., Krams, S. M., Esquivel, C. O., Keeffe, E. B., Sibley, R. K., Lee, Y. M., Wright, T. L., and Omary, M. B. (2003) Keratin 8 and 18 mutations are risk factors for developing liver disease of multiple etiologies. Proc. Natl. Acad. Sci. U. S. A. 100: 6063-6068

Ku, N. O., Liao, J., Chou, C. F., and Omary, M. B. (1996a) Implications of intermediate filament protein phosphorylation. Cancer Metastasis Rev. 15: 429-444

Ku, N. O., Lim, J. K., Krams, S. M., Esquivel, C. O., Keeffe, E. B., Wright, T. L., Parry, D. A., and Omary, M. B. (2005) Keratins as susceptibility genes for end-stage liver disease. Gastroenterology 129: 885-893

Ku, N. O., Michie, S. A., Soetikno, R. M., Resurreccion, E. Z., Broome, R. L., Oshima, R. G., and Omary, M. B. (1996b) Susceptibility to hepatotoxicity in transgenic mice that express a dominant-negative human keratin 18 mutant. J. Clin. Invest. 98: 1034-1046

Ku, N. O., Michie, S., Oshima. R. G., and Omary, M. B. (1995) Chronic hepatitis, hepatocyte fragility, and increased soluble phosphoglycokeratins in transgenic mice expressing a keratin 18 conserved arginine mutant. J. Cell Biol. 131: 1303-1314

Ku, N.O., Fu, H., and Omary, M. B. (2004) Raf-1 activation disrupts its binding to keratins during cell stress. J. Cell Biol. 166: 479-485

Kuechle, M. K., Presland, R. B., Lewis, S. P., Fleckman, P., and Dale, B. A. (2000) Inducible expression of filaggrin increases keratinocyte susceptibility to apoptotic cell death. Cell Death Differ. 7: 566-573

Kühnel, F., Fritsch, C., Krause, S., Mundt, B., Wirth, T., Paul, Y., Malek, N. P., Zender, L., Manns, M. P., and Kubicka, S. (2004) Doxycycline regulation in a single retroviral vector by an autoregulatory loop facilitates controlled gene expression in liver cells. Nucleic Acids Res. 32: e30

Kuma, Y., Sabio, G., Bain, J., Shpiro, N., Marquez, R., and Cuenda, A. (2005) BIRB796 inhibits all p38 MAPK isoforms in vitro and in vivo. J. Biol. Chem. 280: 19472-19479

Kuroiwa, T., Ohta, T., and Tsutsumi, A. (1999) Malignant pilocytic astrocytoma in the medulla oblongata: case report. Brain Tumor Pathol. 16: 81-85

Kyriakis, J. M., and Avruch, J. (2001) Mammalian mitogen-activated protein kinases signal transduction pathways activated by stress and inflammation. Physiol. Rev. 81: 807-869

Kyriakis, J. M., Banerjee, P., Nikolakaki, E., Dai, T., Rubie, E. A., Ahmad, M. F., Avruch, J., and Woodgett, J. R. (1994) The stress-activated protei kinase subfamily of c-Jun kinases. Nature 369: 156-160

Lam, Y. A., Xu, W., DeMartino, G. N., and Cohen, R. E. (1997) Editing of ubiquitin conjugates by an isopeptidase in the 26S proteasome. Nature 385: 737-740

Lane, E. B., and Pekny, M. (2004) Stress models for the study of intermediate filament function. Methods Cell Biol. 78: 229-264

Lane, E. B., Hogan, B. L., Kurkinen, M., and Garrels, J. I. (1983) Co-expression of vimentin and cytokeratins in parietal endoderm cells of early mouse embryo. Nature 303: 701-704

Lang, D. M., Lommel, S., Jung, M., Ankerhold, R., Petrausch, B., Laessing, U., Wiechers, M. F., Plattner, H., and Stuermer, C. A. (1998) Identification of reggie-1 and reggie-2 as plasmamembrane-associated proteins which cocluster with activated GPI-anchored cell adhesion molecules in non-caveolar micropatches in neurons. J Neurobiol. 37(4): 502-523

Langley, R. C., Jr., and Cohen, C. M. (1986) Association of spectrin with desmin intermediate filaments. J. Cell Biochem. 30: 101-109

Langley, R. C., Jr., and Cohen, C. M. (1987) Cell type-specific association between two types of spectrin and two types of intermediate filaments. Cell Motil. Cytoskeleton. 8: 165-173

Lariviere, R. C., and Julien, J. P. (2004) Functions of intermediate filaments in neuronal development and disease. J. Neurobiol. 58: 131-148

Lavoie, J. N., Gingras-Breton, G., Tanguay, R. M., and Landry, J. (1993) Induction of Chinese hamster HSP27 gene expression in mouse cells confers resistance to heat shock. HSP27 stabilization of the microfilament organization. J. Biol. Chem. 268: 3420-3429

Lavoie, J. N., L'Allemain, G., Brunet, A., Muller, R., and Pouyssegur, J. (1996) A temporal and biochemical link between growth factor-activated MAP kinase, cyclin D1 induction and cell cycle entry. J. Biol. Chem. 271: 20608-10616

Lechner, C., Zahalka, M. A., Giot, J.-F., Moler, N. P. H., and Ullrich, A. (1996) ERK6, a mitogen-activated protei kinase involved in C2C12 myoblast differentiation. Proc. Natl. Acad. Sci. U. S. A. 93: 4355-4359

Lederer, T., Kintrup, M., Takahashi, M., Sum, P. E., Ellestad, G. A., and Hillen, W. (1996) Tetracycline analogs affecting binding to Tn10-Encoded Tet repressor trigger the same mechanism of induction. Biochemistry 35: 7439-7446

Lee, J. C., Schickling, O., Stegh, A. H., Oshima, R. G., Dinsdale, D., Cohen, G. M., and Peter, M. E. (2002) DEDD regulates degradation of intermediate filaments during apoptosis. J. Cell Biol. 158: 1051-1066

Lee, J. M., Hanson, J. M., Chu, W. A., and Johnson, J. A. (2001) Phosphatidylinositol 3-kinase, not extracellular signal regulated kinase, regulates activation of the antioxidant-responsive element in IMR-32 human neuroblastoma cells. J. Biol. Chem. 276: 20011-20016

Lee, J. M., Kim, A. S., Lee, S. J., Cho, S. M., Lee, D. S., Choi, S. M., Kim, D. K., Ki, C. S., and Kim, J. W. (2006) A case of infantile Alexander disease accompanied by infantile spasms diagnosed by DNA analysis. J. Korean Med. Sci. 21: 954-957

Lee, J. S., Zhang, M. H., Yun, E. K., Geum, D., Kim, K., Kim, T. H., Lim, Y. S., and Seo, J. S. (2005) Heat shock protein 27 interacts with vimentin and prevents insolubilization of vimentin subunits induced by cadmium. Exp. Mol. Med. 37: 427-435

Lee, K. Y., and Johnston, R. N. (1997) Neurofilaments are part of the high molecular weight complex containing neuronal cdc2-like kinase (nclk). Brain Res. 773: 197-202

Lee, M. K., and Cleveland, D. W. (1996) Neuronal intermediate filaments. Annu. Rev. Neurosci. 19: 187-217

Lee, P., Morley, G., Huang, Q., Fischer, A., Seiler, S., Horner, J. W., Factor, S., Vaidya, D., Jalife, J., and Fishman, G. I. (1998) Conditional lineage ablation to model human diseases. Proc. Natl. Acad. Sci. U. S. A. 95: 11371-11376

Lefrançois, T., Fages, C., Peschanski, M., and Tardy, M. (1997) Neuritic outgrowth associated with astroglial phenotypic changes induced by antisense glial. 17: 4121-4128

Lemin, A. J., Saleki, K., van Lith, M., and Benham, A. M. (2007) Activation of the unfolded protein response and alternative splicing of ATF6α in HLA-B27 positive lymphocytes. FEBS Lett. 581: 1819-1824

Lendahl, U., Zimmerman, L. B., and McKay, R. D. (1990) CNS stem cells express a new class of intermediate filament protein. Cell 60: 585-595

Lenormand, P., Sardet, C., Pages, G., L'Allemain, G., Brunet, A., and Pouyssegur, J. (1993) Growth factors induce nuclear translocation of MAP kinase ($p42^{mapk}$ and $p44^{mapk}$) but not of their activator MAP kinase ($p45^{mapk}$) in fibloblasts. J. Cell Biol. 122: 1079-1088

Lepekhin, E. A., Eliasson, C., Berthold, C. H., Berezin, V., Bock, E., and Pekny, M. (2001) Intermediate filaments regulate astrocyte motility. J. Neurochem. 79: 617-625

Leung, C. L., Sun, D., and Liem, R. K. (1999) The intermediate filament protein peripherin is the specific interaction partner of mouse BPAG1-n (dystonin) in neurons. J. Cell Biol. 144: 435-446

Leung, C. L., Zheng, M., Prater, S. M., and Liem, R. K. (2001) The BPAG1 locus: Alternative splicing produces multiple isoforms with distinct cytoskeletal linker domains, including predominant isoforms in neurons and muscles. J. Cell Biol. 154: 691-697

Lew, J., Winkfein, R. J., Paudel, H. K., and Wang, J. H. (1992) Brain proline-directed protein kinase is a neurofilament kinase which displays high sequence homology to p34cdc2. J. Biol. Chem. 267: 25922-25926

Lewis, G.P., Erickson, P. A., Guerin, C. J., Anderson, D. H., and Fisher, S. K. (1992) Basic fibroblast growth factor: a potential regulator of proliferation and intermediate filament expression in the retina. J. Neurosci. 12: 3968-3978

Lewis, S. A., Balcarek, J. M., Krek, V., Shelanski, M. L., and Cowan, N. J. (1984) Sequence of a cDNA clone encoding mouse glial fibrillary acidic proteins: Structural conservation of intermediate filaments. Proc. Natl. Acad. Sci. U. S. A. 81: 2743-2746

Lewis, T. S., Shapiro, P. S., and Ahn, N. G. (1998) Signal transduction through MAP kinse cascades. Adv. Cancer Res. 74: 49-139

Li, B. S., Veeranna, Gu, J., Grant, P., and Pant, H. C. (1999) Activation of mitogen-activated protein kinases (Erk1 and Erk2) cascade results in phosphorylation of NF-M tail domains in transfected NIH 3T3 cells. Eur. J. Biochem. 262: 211-217

Li, H., Guo, Y., Teng, J., Ding, M., Yu, A. C., and Chen, J. (2006) 14-3-3gamma affects dynamics and integrity of glial filaments by binding to phosphorylated GFAP. J. Cell Sci. 119: 4452-4461

Li, L., Lundkvist, A., Andersson, D., Wilhelmsson, U., Nagai, N., Pardo, A. C., Nodin, C., Stahlberg, A., Aprico, K., Larsson, K., Yabe, T., Moons, L., Fotheringham, A., Davies, I., Carmeliet, P., Schwartz, J. P., Pekna, M., Kubista, M., Blomstrand, F., Maragakis, N., Nilsson, M., and Pekny, M. (2007) Protective role of reactive astrocytes in brain ischemia. J. Cereb. Blood Flow Metab. 27: 1043-1054

Li, R., Johnson, A. B., Salomons, G., Goldman, J. E., Naidu, S., Quinlan, R., Cree, B., Ruyle, S. Z., Banwell, B., D'Hooghe, M., Siebert, J. R., Rolf, C. M., Cox, H., Reddy, A., Gutierrez-Solana, L. G., Collns, A., Weller, R. P., Messing, A., van der Knaap, M. S., and Brenner M. (2005) Glial fibrillary acidic protein mutations in infantile, juvenile, and adult form of Alexander disease. Ann. Neurol. 57(3): 310-326

Li, R., Messing, A., Goldman, J. E., and Brenner, M. (2002) GFAP mutations in Alexander disease. Int. J. Dev. Neurosci. 20: 259-268

Li, W., Jain, M. R., Chen, C., Yue, X., Hebbar, V., Zhou, R., et al (2005) Nrf2 possesses a redox-insensitive nuclear export signal overlapping with the leucine zipper motif. J. Biol. Chem. 280: 28430-28438

Liao, J., Lowthert, L. A., Ghori, N., and Omary, M. B. (1995) The 70-kDa heat shock proteins associate with glandular intermediate filaments in an ATP-dependent manner. J. Biol. Chem. 270: 915-922

Liao, J., Price, D., and Omary, M. B. (1997) Association of glucose-regulated protein (grp78) with human keratin 8. FEBS Lett. 417: 316-320

Liedtke, W., Edelmann, W., Bieri, P. L., Chiu, F. C., Cowan, N. J., Kucherlapati, R., and Raine, C. S. (1996) GFAP is necessary for the integrity of CNS white matter architecture and long-term maintenance of myelination. Neuron 17: 607-615

Lin, A. (2003) Activation of the JNK signalling pathway: breaking the break on apoptosis. Bioessays 25: 1-8

Lindsey Rose, K. M., Gourdie, R. G., Prescott, A. R., Quinlan, R. A., Crouch, R. K., and Schey, K. L. (2006) The C terminus of lens aquaporin 0 interacts with the cytoskeletal proteins filensin and CP49. Invest. Ophthalmol. Vis. Sci. 47: 1562-1570

Liovic, M., Mogensen, M. M., Prescott, A. R., and Lane, E. B. (2003) Observation of keratin particles showing fast bidirectional movement colocalized with microtubules. J. Cell Sci. 116: 1417-1427

Lommel, L., Ortolan, T., Chen, L., Madura, K., and Sweder, K. S. (2002) Proteolysis of a nucleotide excision repair protein by the 26S proteasome. Curr. Genet. 42: 9-20

Loranger, A., Duclos, S., Grenier, A., Price, J., Wilson-Heiner, M., Baribault, H., and Marceau, N. (1997) Simple epithelium keratins are required for maintenance of hepatocyte integrity. Am. J. Pathol. 151: 1673-1683

Lowe, J., McDermott, H., Pike, I., Spendlove, I., Landon, M., and Mayer, R. J. (1992) alpha B crystallin expression in non-lenticular tissues and selective presence in ubiquitinated inclusion bodies in human disease. J. Pathol. 166: 61-68

Lu, Z., Liu, D., Hornia, A., Devonish, W., Pagano, M., and Foster, D. A. (1998) Activation of protein kinase C triggers its ubiquitination and degradation. Mol. Cell. Biol. 18: 839-845

Lundkvist, A., Reichenbach, A., Betsholtz, C., Carmeliet, P., Wolburg, H., and Pekny, M. (2004) Under stress, the absence of intermediate filaments from Muller cells in the retina has structural and functional consequences. J. Cell Sci. 117: 3481-3488

Ma, H. W., Lu, J. F., Jiang, J., Chen, L. Y., Niu, G. H., Wu, B. M., Kanazawa, N., and Tsujino, S. (2005) Glial fibrillary acidic protein mutation in a Chinese girl with infantile Alexander disease. Zhonghua Yi Xue Yi Chuan Xue Za Zhi 22: 79-81

Mabuchi, K., Li, B., Ip, W., and Tao, T. (1997) Association of calponin with desmin intermediate filaments. J. Biol. Chem. 272: 22662-22666

Madsen, J. R., Partington, M. D., Hay, T. C., and Tyson, R. W. (1999) A 2-month-old female infant with progressive macrocephaly and irritability. Pediatr. Neurosurg. 30: 157-163

Mairesse, N., Horman, S., Mosselmans, R., and Galand, P. (1996) Antisense inhibition of the 27 kDa heat shock protein production affects growth rate and cytoskeletal organization in MCF-7 cells. Cell Biol. Int. 20: 205-212

Maisel, H., and Perry, M. M. (1972) Electron microscope observations on some structural proteins of the chick lens. Exp. Eye Res. 14: 7-12

Makarova, I., Carpenter, D., Khan, S., and Ip, W. (1994) A conserved region in the tail domain of vimentin is involved in its assembly into intermediate filaments. Cell Motil. Cytoskeleton 28: 265-277

Maki, C. G, Huibregtse, J. M., and Howley, P. M. (1996) In vivo ubiquitination and proteaosme-mediated degradation of p53(1). Cancer Res. 56: 2649-2654

Manet, V., Prieto, M., Privat, A., and Giménez y Ribotto, M. (2003) Axonal plasticity and functional recovery after spinal cord injury in mice deficient in both glial fibrillary acidic protein and vimentin genes. Proc. Natl. Acad. Sci. U. S. A. 100: 8999-9004

Mann, E., McDermott, M. J., Goldman, J., Chiesa, R., and Spector, A. (1991) Phoshporylation of α-crystallin B in Alexander's disese brain. FEBS Lett. 294: 133-136

Mansbridge, J. N., and Knapp, A. M. (1987) Changes in keratinocyte maturation during wound healing. J. Invest. Dermatol. 89: 253-263

Marceau, N., Schutte, B., Gilbert, S., Loranger, A., Henfling, M. E., Broers, J. L., Mathew, J., and Ramaekers, F. C. (2007) Dual roles of intermediate filaments in apoptosis. Exp. Cell Res. 313: 2265-2281

Marshall, C. J. (1995) Specificity of receptor tyrosine kinas signalling: transient versus sustained extracellular signal-regulated kianse activaton. Cell 80: 179—185

Martidis, A., Yee, R. D., Azzarelli, B., and Biller, J. (1999) Neuro-ophthalmic, radiographic, and pathologic manifestations of adult-onset Alexander disease. Arch. Ophthalmol. 117: 265-267

Martys, J. L., Ho, C. L., Liem, R. K., and Gundersen, G. G. (1999) Intermediate filaments in motion: observations of intermediate filaments in cells using green fluorescent protein-vimentin. Mol. Biol. Cell 10: 1289-1295

Mastri, A. R., and Sung, J. H. (1973) Diffuse Rosenthal fiber formation in the adult: A report of four cases. J. Neuropathol. Exp. Neurol. 32: 424-436

Masui, S., Shimosato, D., Toyooka, Y., Yagi, R., Takahashi, K., and Niwa, H. (2005) An efficient system to establish multiple embryonic stem cell lines carrying an inducible expression unit. Nucleic Acids Res. 33: e43

Matej, R., Dvoráková, L., Mrázová, L., Houst'ková, H., and Elleder, M. (2008) Early onset Alexander disease: a case report with evidence for manifestation of the disorder in neurohypophyseal pituicytes. Clin. Neuropathol. 27: 64-71

Maxwell, P. H., Wiesener, M. S., Chang, G. W., Clifford, S. C., Vaux, E. C., Cockman, M. E., Wykoff, C. C., Pugh, C. W., Maher, E. R., and Ratcliffe, P. J. (1999) The tumour suppressor protein VHL targets hypoxia-inducible factors for oxygen-dependent proteolysis. Nature 399: 271-275

McCall, M. A., Gregg, R. G., Behringer, R. R., Brenner, M., Delaney, C. L., Galbreath, E. J., Zhang, C. L, Perace, R. A., Chiu, S. Y., and Messing, A. (1996) Targeted deletion in astrocyte

intermediate filament (Gfap) alters neuronal physiology. Proc. Natl. Acad. Sci. U. S. A. 93: 6361-6366

McCormick, M. B., Kouklis, P., Syder, A., and Fuchs, E. (1993) The roles of the rod end and the tail in vimentin IF assembly and IF network formation. J. Cell Biol. 122: 395-407

McMahon, M., Thomas, N., Itoh, K., Yamamoto, M., and Hayes, J. D. (2006) Dimerization of substrate adaptors can facilitate cullin-mediated ubiquitylation of proteins by a "tethering" mechanism: a two-site interaction model for the Nrf2-Keap1 complex. J. Biol. Chem. 281: 24756-24768

Mehlen, P., Preville, X., Chareyron, P., Briolay, J., Klemenz, R., and Arrigo, A. P. (1995) Constitutive expression of human hsp27, Drosophila hsp27, or human alpha B-crystallin confers resistance to TNF- and oxidative stress-induced cytotoxicity in stably transfected murine L929 fibroblasts. J. Immunol. 154: 363-374

Meins, M., Brockmann, K., Yadav, S., Haupt, M., Sperner, J., Stephani, U., and Hanefeld, F. (2002) Infantile Alexander disease: a GFAP mutation in monozygotic twins and novel mutations in two other patients. Neuropediatrics 33: 194-198

Meng, J. J., Bornslaeger, E. A., Green, K. J., Steinert, P. M., and Ip, W. (1997) Two-hybrid analysis reveals fundamental differences in direct interactions between desmoplakin and cell type-specific intermediate filaments. J. Biol. Chem. 272: 21495-21503

Meng, L., Mohan, R., Kwok, B. H., Elofsson, M., Sin, N., and Crews, C. M. (1999) Epoxomicin, a potent and selective proteasome inhibitor, exhibits in vivo antiinflammatory activity. Proc. Natl. Acad. Sci. U. S. A. 96: 10403-10408

Merdes, A., Brunkener, M., Horstmann, H., and Georgatos, S. D. (1991) Filensin: a new vimentin-binding, polymerization-competent, and membrane-associated protein of the lens fiber cell. J. Cell Biol. 115: 397-410

Meriane, M., Mary, S., Comunale, F., Vignal, E., Fort, P., Gauthier-Rouviére, C. (2000) Cdc42Hs and Rac1 GTPases induce the collapse of the vimentin intermediate filament network. J. Biol. Chem. 275: 33046-33052

Mertens, S., Craxton, M., and Goedert, M. (1996) SAP kinase-3, a new member of the family of mammalian stress-activated protein kinases. FEBS Lett. 383: 273-276

Messing, A., Head, M. W., Galles, K., Galbreath, E. J., Goldman, J. E., and Brenner, M. (1998) Fatal encephalopathy with astrocyte inclusions in GFAP transgenic mice. Am. J. Pathol. 152: 391-398

Messing, A., and Goldman, J. (2004) Alexander disease. Elsevier, Amsterdam

Millecamps, S., Gowing, G., Corti, O., Mallet, J., and Julien, J.-P. (2007) Conditional NF-L transgene expression in mic for in vivo analysis of turnover and transport rate of neurofilaments. J. Neurosci. 27: 4947-4956

Miller, R. K., Khuon, S., and Goldman, R. D. (1993) Dynamics of keratin assembly: exogenous type I keratin rapidly associates with type II keratin in vivo. J. Cell Biol. 122: 123-135

Miller, R. K., Vikstrom, K., and Goldman, R. D. (1991) Keratin incorporation into intermediate filament networks is a rapid process. J. Cell Biol. 113: 843-855

Minamino, T., Yujiri, T., Papst, P. J., Chan, E. D., Johnson, G. L., and Terada, N. (1999) MEKK1 suppresses oxidative stress-induced aoptosis of embryonic stem cell-derived acardiac mocytes. Proc. Natl. Acad. Sci. U. S. A. 96: 15127-15132

Mizuguchi, H., and Hayakawa, T. (2002) The tet-off system is more effective than the tet-on system for regulating transgene expression in a single adenovirus vector. J. Gene Med. 4: 240-247

Mizuno, Y., Thompson, T. G., Guyon, J. R., Lidov, H. G., Brosius, M., Imamura, M., Ozawa, E., Watkins, S. C., and Kunkel, L. M. (2001) Desmuslin, an intermediate filament protein that interacts with alpha-dystrobrevin and desmin. Proc. Natl. Acad. Sci. U. S. A. 98: 6156-6161

Mochida, K., Tres, L. L., and Kierszenbaum, A. L. (2000) Structural features of the 26S proteasome complex isolated from rat testis and sperm tail. Mol. Reprod. Dev. 57: 176-184

Mohammadi, S., Alvarez-Vallina, L, Achworth, L. J., and Hawkins, R. E. (1997) Delay in resumption of the activity of tetracycline-regulatable promoter following removal of tetracycline analogues. Gene Ther. 4: 993-997

Monteiro, M. J., and Cleveland, D. W. (1989) Expression of NF-L and NF-M in fibroblasts reveals coassembly of neurofilament and vimentin subunits. J. Cell Biol. 108: 579-593

Motohashi, H., and Yamamoto, M. (2004) Nrf2-Keap1 defines a physiologically important stress response mechanism. Trends Mol. Med. 10: 549-557

Mouser, P. E., Head, E., Ha, K. H., and Rohn, T. T. (2006) Caspase-mediated cleavage of glial fibrillary acidic protein within degenerating astrocytes of the Alzheimer's disease brain. Am. J. Pathol. 168: 936-946

Muchowski, P. J., Bassuk, J. A., Lubsen, N. H., and Clark, J. I. (1997) Human alphaB-crystallin. Small heat shock protein and molecular chaperone. J. Biol. Chem. 272: 2578-2582

Müller, H. W., Junghans, U., and Kappler, J. (1995) Astroglial neurotrophic and neurite-promoting factors. Pharmacol. Ther. 65: 1-18

Mumby, M. C., and Walter, G. (1993) Protein serine/threonine phosphatases: structure, regulation, and functions in cell growth. Physiol. Rev. 73: 673-699

Murakami, N., Tsuchiya, T., Kanazawa, N., Tsujino, S., and Nagai, T. (2008) Novel deletion mutation in GFAP gene in an infantile form of Alexander disease. Pediatr. Neurol. 38: 50-52

Murakami, Y., Matsufuji, S., Kameji, T., Hayashi, S., Igarashi, K., Tamura, T., Tanaka, K., and Ichihara, A. (1992) Ornithine decarboxylase is degraded by the 26S proteasome without ubiquitination. Nature 360: 597-599

Muranyi, W., Haas, J., Wagner, M., Krohne, G., and Koszinowski, U. H. (2002) Cytomegalovirus recruitment of cellular kinases to dissolve the nuclear lamina. Science 297: 854-857

Murti, K. G., Kaur, K., and Goorha, R. M. (1992) Protein kinase C associates with intermediate filaments and stress fibers. Exp. Cell Res. 202: 36-44

Musi, N., and Goodyear, L. J. (2006) Insulin resistane and improvements in signal transduction. Endocrine 29: 73-80

Nagata, K., Izawa, I., and Inagaki, M. (2001) A decade of site- and phosphorylation state-specific antibodies: recent advances in studies of spatiotemporal protein phosphorylation. Genes Cells 6: 653-664

Nakagawa, H., Ishihara, M., and Ohashi, K. (1993) 33-kDa peptides prepared from chicken gizzard smooth muscle bundle both actin and desmin filaments in vitro. J. Biochem. (Tokyo) 114: 623-626

Nakamura, Y., Hashimoto, R., Kashiwagi, Y., Aimoto, S., Fukusho, E., Matsumoto, N., Kudo, T., and Takeda, M. (2000) Major phosphorylation site (Ser55) of neurofilament L by cyclic AMP-dependent protein kinase in rat primary neuronal culture. J. Neurochem. 74: 949-959

Namekawa, M., Takiyama, Y., Aoki, Y., Takayashiki, N., Sakoe, K., Shimazaki, H., Taguchi, T., Tanaka, Y., Nishizawa, M., and Saito, K. (2002) Identification of GFAP gene mutation in hereditary adult-onset Alexander's disease. Ann. Neurol. 52: 779-785

Naujokat, C., and Hoffmann, S. (2002) Role and function of the 26S proteasome in proliferation and apoptosis. Lab. Invest. 82: 965-980

Nawashiro, H., Messing, A., Azzam, N., and Brenner, M. (1998) Mice lacking GFAP are hypersensitive to traumatic cerebrospinal injury. Neuroreport 9: 1691-1696

Newey, S. E., Howman, E. V., Ponting, C. P., Benson, M. A., Nawrotzki, R., Loh, N. Y., Davies, K. E., and Blake, D. J. (2001) Syncoilin, a novel member of the intermediate filament

superfamily that interacts with alpha-dystrobrevin in skeletal muscle. J. Biol. Chem. 276: 6645-6655

Nguyen, M. D., Lariviere, R. C., and Julien, J. P. (2001) Deregulation of Cdk5 in a mouse model of ALS: toxicity alleviated by perikaryal neurofilament inclusions. Neuron 30: 135-147

Nguyen, M. D., Shu, T., Sanada, K., Lariviere, R. C., Tseng, H. C., Park, S. K., Julien, J. P., and Tsai, L. H. (2004) A NUDEL-dependent mechanism of neurofilament assembly regulates the integrity of CNS neurons. Nat. Cell Biol. 6: 595-608

Nguyen, T., Sherratt, P. J., Huang, H. C., Yang, C. S., and Pickett, C. B. (2003) Increased protein stability as a mechanism that enhances Nrf2-mediated transcriptional activation of the antioxidant response element. Degradation of Nrf2 by the 26 S proteasome. J. Biol. Chem. 278: 4536-4541

Nicholl, I. D., and Quinlan, R. A. (1994) Chaperone activity of alpha-crystallins modulates intermediate filament assembly. EMBO J. 13: 945-953

Nichols, N. R., Day, J. R., Laping, N. J., Johnson, S. A., and Finch, C. E. (1993) GFAP mRNA increase with age in rat and human brain. Neurobiol. Aging 14: 421-429

Nielesen, A. L., Holm, I. E., Johansen, M., Bonven, B., JØrgensen, P., and JØrgensen, A. L. (2002) A new splice variant of glial fibrillary acidic protein, GFAPε, interacts with the presenilin proteins. J. Biol. Chem. 277: 29983-29991

Nikolic, B., Mac Nulty, E., Mir, B., and Wiche, G. (1996) Basic amino acid residue cluster within nuclear targeting sequence motif is essential for cytoplasmic plectin-vimentin network junctions. J. Cell Biol. 134: 1455-1467

Nobuhara, Y., Nakahara, K., Higuchi, I., Yoshida, T., Fushiki, S., Osame, M., Arimura, K., and Nakagawa, M. (2004) Juvenile form of Alexander disease with GFAP mutation and mitochondrial abnormality. Neurology 63: 1302-1304

Noetzel, M. J. (2004) Diagnosing "undiagnosed" leukodystrophies: the role of molecular genetics. Neurology 62: 847-848

Nonomura, Y., Shimizu, K., Nishimoro, H., Matsubara, Y., and Nakano, I. (2002) Scoliosis in a patient with Alexander disease. J. Spinal Disord. Techn. 15: 261-264

Ochi, N., Kobayashi, K., Maehara, M., Nakayama, A., Negoro, T., Shinohara, H., Watanabe, K., Nagatsu, T., and Kato, K. (1991) Increment of alpha B-crystallin mRNA in the brain of patients with infantile type Alexander's disease. Biochem. Biophys. Res. Commun. 179: 1030-1035.

Ogasawara, N. (1965) Multiple Sklerose mit Rosenthalschen Fasern. Acta Neuropathol. (Berl) 5: 61-68

Ohnari, K., Yamano, M., Uozumi, T., Hashimoto, T., Tsuji, S., and Nakagawa, M. (2007) An adult form of Alexander disease: a novel mutation in glial fibrillary acidic protein. J. Neurol. 254: 1390-1394

Okamoto, Y., Mitsuyama, H., Jonosono, M., Hirata, K., Arimura, K., Osame, M., and Nakagawa, M. (2002) Autosomal dominant palatal myoclonus and spinal cord atrophy. J. Neurol. Sci. 195: 71-76

Oliva B, Gordon, G., McNicholas, P., Ellestad, G., and Chopra, I. (1992) Evidence that tetracycline analog whose primary target is not the bacterial ribosome cause lysis of Escherichia coli. Antimicrob. Agents Chemother. 36: 913-919

Omary, M. B., Baxter, G. T., Chou, C. F., Riopel, C. L., Lin, W. Y., and Strulovici, B. (1992) PKC epsilon-related kinase associates with and phosphorylates cytokeratin 8 and 18. J. Cell Biol. 117: 583-593

Omary, M. B., Coulombe, P. A., and McLean, W. H. (2004) Intermediate filament proteins and their associated diseases. N. Engl. J. Med. 351: 2087-2100

Omary, M. B., Ku, N. O., Liao, J., and Price, D. (1998) Keratin modifications and solubility properties in epithelial cells and in vitro. Subcell. Biochem. 31: 105-140

Omary, M. B., Ku, N. O., Tao, G. Z., Toivola, D. M., and Liao, J. (2006) "Heads and tails" of intermediate filament phosphorylation: multiple sites and functional insights. Trends Biochem. Sci. 31: 383-394

Orkand, R. K., Nicholls, J. G., and Kuffler, S. W. (1966) Effect of nerve impulses on the membrane potential of glial cells in the central nervous system of amphibia. J. Neurophysiol. 29: 788-806

Orth, P., Schnappinger, D., Hillen, W., Saenger, W., and Hinrichs, W. (2000) Structural basis of gene regulation by the tetracycline inducible Tet repressor-operator system. Nat. Struct. Biol. 7: 215-219

Osborn, M., and Weber, K. (1989) Keratins, transglutaminase, and Mallory bodies--the really insoluble stuff. Lab. Invest. 61: 585-587

Oshima, R. G. (2002) Apoptosis and keratin intermediate filaments. Cell Death Differ. 9: 486-492

Otth, C., Mendoza-Naranjo, A., Mujica, L., Zambrano, A., and Concha II Maccioni, R. B. (2003) Modulation of the JNK and p38 pathways by cdk5 protein kinase in a transgenic mouse model of Alzheimer's disease. Neuroreport 14(18): 2403-2409

Owen, P. J., Johnson, G. D., and Lord, J. M. (1996) Protein kinase C-delta associates with vimentin intermediate filaments in differentiated HL60 cells. Exp. Cell Res. 225: 366-373

Pachter, J. S., and Liem, R. K. (1985) alpha-Internexin, a 66-kD intermediate filament-binding protein from mammalian central nervous tissues. J. Cell Biol. 101: 1316-1322

Pagano, M., Tam, S. W., Theodoras, A. M., Beer-Romero, P., Del Sal, G., Chau, V., Yew, P. R., Draetta, G. F., and Rolfe, M. (1995) Role of the ubiquitin-proteasome pathway in regulating abundance of the cyclin-dependent kinase inhibitor p27. Science 269: 682-685

Pallari, H. M., and Eriksson, J. E. (2006) Intermediate filaments as signaling platforms. Sci. STKE. e53

Palombella, V. J., Conner, E. M., Fuseler, J. W., Destree, A., Davis, J. M., Laroux, F. S., Eolf, R. E., Huang, J., Brand, S., Elliott, P. J., Lazarus, D., McCormack, T., Parent, L., Stein, R., Adams, J., and Grisham, M. B. (1998) Role of the proteasome and NF-kappaB in streptococcal cell wall-induced polyarthritis. Proc. Natl. Acad. Sci. U. S. A. 95: 15671-15676

Papa, F. R., and Hochstrasser, M. (1993) The yeast DOA4 gene enode a deubiquitinating enzyme related to a product of the human Tre-2 oncogene. Nature 366: 313-319

Papachristou, D. J., Batistatou, A., Sykiotis, G. P., Varakis, I., and Papavassiliou, A. G. (2003) Activation of the JNK-AP-1 signal transduction pathway is asosociated with pathogenesis and progression of human osteosarcomas. Bone 32: 364-371

Paramio, J. M., and Jorcano, J. L. (2002) Beyond structure: do intermediate filaments modulate cell signalling: Bioessays 24: 836-844

Paramio, J. M., Segrelles, C., Ruiz, S., and Jorcano, J. L. (2001) Inhibition of protein kinase B (PKB) and PKCzeta mediates keratin K10-induced cell cycle arrest. Mol. Cell. Biol. 21: 7449-7459

Parcellier, A., Schmitt, E., Gurbuxani, S., Seigneurin-Berny, D., Pance, A., Chantome, A., Plenchette, S., Khochbin, S., Solary, E., and Garrido, C. (2003) HSP27 is a ubiquitin-binding protein involved in I-kappaBalpha proteasomal degradation. Mol. Cell. Biol. 23: 5790-5802

Parry, D. A., and Steinert, P. M. (1999) Intermediate filaments: molecular architecture, assembly, dynamics and polymorphism. Q. Rev. Biophys. 32: 99-187

Pasantes-Morales, H., Moran, J., and Schousboe, A. (1990) Volume-sensitive release of taurine from cultured astrocytes: properties and mechanism. Glia 3: 427-432

Paul, C., Manero, F., Gonin, S., Kretz-Remy, C., Virot, S., and Arrigo, A. P. (2002) Hsp27 as a negative regulator of cytochrome C release. Mol. Cell. Biol. 22: 816-834

209

Pearl-Yafe, M., Halperin, D., Scheuerman, O., and Fabian, I. (2004) The p38 pathway partially mediates caspase-3 activation induced by reactive oxygen species in Fanconi anemia C cells. Biochem. Pharmacol. 67(3): 539-546

Pekny, M. (2001) Astrocytic intermediate filaments: lessons from GFAP and vimentin knockout mice. Prog. Brain Res. 132: 23-30

Pekny, M., and Lane, E. B. (2007) Intermediate filaments and stress. Exp. Cell Res. 313: 2244-2254

Pekny, M., and Nilsson, M. (2005) Astrocyte activation and reactive gliosis. Glia 50(4): 427-434

Pekny, M., and Pekna, M. (2004) Astrocyte intermediate filaments in CNS pathologies and regeneration. J. Pathol. 204: 428-437

Pekny, M., Eliasson, C. Chien, C.-L., Kindblom, L. G., Liem, R., Hamberger, A., and Betsholtz, C. (1998) GFAP-deficient astrocytes are capable of stellation in vitro when cocultured with neurons and exibit a reduced amount of intermediate filament sand an increase cell saturation density. Exp. Cell Res. 239: 332-343

Pekny, M., Johansson, C. B., Eliasson, C., Stakeberg, J., Wallen, A., Perlmann, T, Lendahl, U., Betsholtz, C., Berthold, C. H., and Frisen, J. (1999) Abnormal reaction to central nervous system injury in mice lacking glial fibrillary acidic protein and vimentin. J. Cell Biol. 145: 503-514

Pekny, M., Leveen, P., Pekna, M., Eliasson, C., Berthold, C. H., Westermark, B., and Betsholtz, C. (1995) Mice lacking GFAP display astrocytes devoid of intermediate filaments but develop and reproduce normally. EMBO J. 14: 1590-1598

Pekny, M., Pekna, M., Wilhelmsson, U., and Chen, D. F. (2004) Response to Quinlan and Nilsson: Astroglia sitting at the controls? Trends Neurosci. 27: 243-244

Perez-Olle, R., Leung, C. L., and Liem, R. K. (2002) Effects of Charcot-Marie-Tooth-linked mutations of the neurofilament light subunit on intermediate filament formation. J. Cell Sci. 115: 4937-4946

Perlson, E., Hanz, S., Ben-Yaakov, K., Segal-Ruder, Y., Seger, R., and Fainzilber, M. (2005) Vimentin-dependent spatial translocation of an activated MAP kinase in injured nerve. Neuron 45: 15-26

Perng, M. D., and Quinlan, R. A. (2005) Seeing is believing! The optical properties of the eye lens are dependent upon a functional intermediate filament cytoskeleton. Exp. Cell Res. 305: 1-9

Perng, M. D., Cairns, L., van den Issel, I. P., Prescott, A., Hutcheson, A. M., and Quinlan, R. A. (1999) Intermediate filament interactions can be altered by HSP27 and alphaB-crystallin. J. Cell Sci. 112 (Pt 13): 2099-2112

Perng, M. D., Su, M., Wen, S. F., Li, R., Gibbon, T., Prescott, A. R., Brenner, M., and Quinlan, R. A. (2006) The Alexander disease-causing glial fibrillary acidic protein mutant, R416W, accumulates into Rosenthal fibers by a pathway that involves filament aggregation and the association of alpha B-crystallin and HSP27. Am. J. Hum. Genet. 79: 197-21

Perng, M. D., Wen, S. F., van den Issel, P., Prescott, A. R., and Quinlan, R. A. (2004) Desmin aggregate formation by R120G alphaB-crystallin is caused by altered filament interactions and is dependent upon network status in cells. Mol. Biol. Cell 15: 2335-2346

Pixley, S. K., and de Vellis, J. (1984) Transition between immature radial glia and mature astrocytes studied with a monoclonal antibody to vimentin. Brain Res. 317: 201-209

Poon, E., Howman, E. V., Newey, S. E., and Davies, K. E. (2002) Association of syncoilin and desmin: linking intermediate filament proteins to the dystrophin-associated protein complex. J. Biol. Chem. 277: 3433-3439

Porter, R. M., and Lane, E. B. (2003) Phenotypes, genotypes and their contribution to understanding keratin function. Trends Genet. 19: 278-285

Portier, M. M., de Nechaud, B., and Gros. F. (1983) Peripherin, a new member of the intermediate filament protein family. Dev. Neurosci. 6: 335-344

Prahlad, V., Yoon, M., Moir, R. D., Vale, R. D., and Goldman, R. D. (1998) Rapid movements of vimentin on microtubule tracks: kinesin-dependent assembly of intermediate filament networks. J. Cell Biol. 143: 159-710

Presland, R. B., and Fleckman, P. (2005) Tetracycline-regulated gene expression in epidermal keratinocytes. Methods Mol. Biol. 289: 273-286

Presland, R. B., Coulombe, P. A., Eckert, R. L., Mao-Qiang, M., Feingold, K. R., and Elias, P. M. (2004) Barrier function in transgenic mice overexpressing K16, involucrin, and filaggrin in the suprabasal epidermis. J. Invest. Dermatol. 123: 603-606

Presland, R. B., Kuechle, M. K., Lewis, S. P., Fleckman, P., and Dale, B. A. (2001) Regulated expression of human filaggrin in keratinocytes results in cytoskeletal disruption, loss of cell-cell adhesion, and cell cycle arrest. Exp. Cell Res. 270: 199-213

Price, M.G., and E. Lazarides. (1983) Expression of intermediate filament-associated proteins paranemin and synemin in chicken development. J. Cell Biol. 97: 1860-1874

Pridmore, C. L., Baraitser, M., Harding, B., Boyd, S. G., Kendall, B., and Brett, E. M. (1993) Alexander's disease: clues to diagnosis. J. Child Neurol. 8: 134-144

Privat, A. (2003) Astrocytes as support for axonal regeneration in the central nervous system of mammals. Glia 43: 91-93

Probst, E. N., Hagel, C., Weisz, V., Nagel, S., Wittkugel, O., Zeumer, H., and Kohlschutter, A. (2003) Atypical focal MRI lesions in a case of juvenile Alexander's disease. Ann. Neurol. 53: 118-120

Pulverer, B. J., Kyriakis, J. M., Avruch, J., Nikolakaki, E., and Woodgett, J. R. (1991) Phosphorylation of c-jun mediated by MAP kinases. Nature 353: 670-674

Qi, Z., D. Tang, X. Zhu, D.J. Fujita, and J.H. Wang. (1998) Association of neurofilament proteins with neuronal Cdk5 activator. J. Biol Chem. 273: 2329-2335

Qu, D., Teckman, J. H., Omura, S., and Perlmutter, D. H. (1996) Degradation of a mutant secretory protein, alpha 1-antitrypsin Z, in the endoplasmic reticulum requires proteasome activity. J. Biol. Chem. 271: 22791-22795

Quinlan, R. (2001) Cytoskeletal catastrophe causes brain degeneration. Nat. Genet. 27: 10-11

Quinlan, R. A., Brenner, M., Goldman, J. E., and Messing, A. (2007) GFAP and its role in Alexander disease. Exp. Cell Res. 313: 2077-2087

Quinlan, R., and Nilsson, M. (2004) Reloading the retina by modifying the glial matrix. Trends Neurosci. 27(5): 241-242

Quinlan, R., Hutchison, C., and Lane, B. (1995) Intermediate filament proteins. Protein Profile 2(8): 795-952

Raats, J.M., F.R. Pieper, W.T. Vree Egberts, K.N. Verrijp, F.C. Ramaekers, and H. Bloemendal. (1990) Assembly of amino-terminally deleted desmin in vimentin-free cells. J. Cell Biol. 111: 1971-1985

Racine, R. J., Ivy, G. O., and Milgram, N. W. (1989) Kindling: clinical relevance and anatomical substrates, in: T. G. Bolwig, M. R. Trimble (Eds.) The Clinical Relevance of Kindling, Wiley, Chichester. pp. 15-34

Raingeaud, J., Gupta, S., Rogers, J. S., Dickens, M., Han, J., Ulevitch, R. J., and Davis, R. J. (1995) Pro-inflammatory cytokines and environmental stress cause p38 mitogen-activated protein kinase activation by dual phosphorylation on tyrosine and threonine. J. Biol. Chem. 270: 7420-7426

Rajasekaran, N. S., Connell, P., Christians, E. S., Yan, L. J., Taylor, R. P., Orosz, A., Zhang, X. Q., Stevenson, T. J., Peshock, R. M., Leopold, J. A., Barry, W. H., Loscalzo, J., Odelberg, S. J., and Benjamin, I. J. (2007) Human alpha B-crystallin mutation causes oxido-reductive stress and protein aggregation cardiomyopathy in mice. Cell 130: 427-439

Ramamurthy, N., Bain, S. Liang, C. T., Barnes, J., Llavaneras, A., Liu, Y., Puemer, D., Strachan, M. J., and Golub, L. M. (2001) A combination of subtherapeuric dose of chemically modified doxycycline (CMT-8) and a bisphosphonate (clodronate) inhibits bone loss in the ovariectomized rat: a dynamic histomorphometric and gene expression study. Curr. Med. Chem. 8: 295-303

Reeves, S. A., Helman, L. J., Allison, A, and Israel, M. A. (1989) Molecular cloning and primary structure of human glial fibrillary acidic protein. Proc. Natl. Acad. Sci. U. S. A. 86: 5178-5182

Reichard, E. A. P., Ball, W. S., and Bove, K. E. (1996) Alexander disease: a case report and a review of the literature. Pediatr. Pathol. Lab. Med. 16: 327-343

Resnitzky, D., Gossen, M., Bujard, H., and Reed, S. I. (1994) Acceleration of the G1/S phase transition by expression of cyclins D1 and E using an inducible system. Mol. Cell. Biol. 14: 1669-1679

Ricci, R., Sumara, G., Sumara, I., Rozenberg, I., Kurrer, M., Akhmedov, A., Hersberger, M., Eriksson, U., Eberli, F. R., Becher, B., Boren, J., Chen, M., Cybulsky, M. I., Moore, K. J., Freeman, M. W., Wagner, E. F., Matter, C. M., and Luscher, T. F. (2004) Requirement of Jnk2 for scavenger receptor A-mediated foam cell formation in atherogenesis. Science 306: 1558-1561

Ridet, J. L., Malhotra, S. K., Privat, A., and Gage, F. H. (1997) Reactive astrocytes: cellular and molecular cues to biological function. Trends Neurosci. 20: 570-577

Ridge, K. M., Linz, L., Flitney, F. W., Kuczmarski, E. R., Chou, Y. H., Omary, M. B., Sznajder, J. I., and Goldman, R. D. (2005) Keratin 8 phosphorylation by protein kinase C delta regulates shear stress-mediated disassembly of keratin intermediate filaments in alveolar epithelial cells. J. Biol. Chem. 280: 30400-30405

Riggs, J. E., Schochet, S. S. S. Jr., and Nelson, J. (1988) Asymptomatic adult Alexander's disease: entity or nosological misconception? Neurology 38: 152-154

Robb, S. J., and Connor, J. R. (1998) An in vitro model for analysis of oxidative death in primary mouse astrocytes. Brain Res. 788: 125-132

Robertson, A., Perea, J., Tolmachova, T., Thomas, P. K., and Huxley, C. (2002) Effects of mouse strain, position of integration and tetracycline analogue on the tetracycline conditional system in transgenic mice. Gene 282: 65-74

Rock, K. L., and Goldberg, A. L. (1999) Degradation of cell proteins and generation of MHC class I-presented peptides. Annu. Rev. Immunol. 17: 739-779

Rodriguez, D., Gauthier, F., Bertini, E., Bugiani, M., Brenner, M., Níguyen, S., Goizet, C., Gelot, A., Surtees, R., Pedespan, J.-M., Hernandorena, X., Troncoso, M., Uziel, G., Messing, A., Ponsot, G., Pham-Dinh, D., Dautigny, A., and Boespflug-Tanguy, O. (2001) Infantile Alexander disease: Spectrum of GFAP mutations and genotype-phenotype correlation. Am. J. Hum. Genet. 69: 1134-1140

Roelofs, R. F., Fischer, D. F., Houtman, S. H., Sluijs, J. A., Van Haren, W., Van Leeuwen, F. W., and Hol, E. M. (2005) Adult human subventricular, subgranular, and subpial zones contain astrocytes with a specialized intermediate filament cytoskeleton. Glia 52: 289-300

Rosenthal, W. (1898) Uber eine eigenthumliche, mit syringomyelie complicirte geschwulst des ruckenmarks. Bietr. Pathol. Anat. 23: 111-143

Rouse, J., Cohen, P., Trigon, S., Morange, M., Alonso-Llamazares, A., Zamanillo, D., Hunt, T., and Nebreda, A. R. (1994) A novel kinase cascade triggered by stress and heat shock that stimulates MAPKAP kinase-2 and phosphorylation of the small heat shock proteins. Cell 78: 1027-1037

Ruchaud, S., N. Korfali, P. Villa, T.J. Kottke, C. Dingwall, S.H. Kaufmann, and W.C. Earnshaw. (2002) Caspase-6 gene disruption reveals a requirement for lamin A cleavage in apoptotic chromatin condensation. EMBO J. 21: 1967-1977

Rudge, J. S., Alderson, R. F., Pasnikowski, E., McClain, J., Ip, N. Y., and Lindsay, R. M. (1992) Expression of Ciliary Neurotrophic Factor and the Neurotrophins-Nerve Growth Factor, Brain-Derived Neurotrophic Factor and Neurotrophin 3-in Cultured Rat Hippocampal Astrocytes. Eur. J. Neurosci. 4: 459-471

Russo, L. S. Jr., Aron, A., and Anderson, P. J. (1976) Alexander's disease: A report and reappraisal. Neurology 26: 607-614

Rutka, J. T., and Smith, S. L. (1993) Transfection of human astrocytoma cells with glial fibrillary acidic protein complementary DNA: Analysis of expression, proliferation, and tumorigenicity. Cancer Res. 53: 3624-3631

Rutka, J. T., Murakami, M., Dirks, P. B., Hubbard, S. L., Becker, L. E., Fukuyama, K., Jung, S., Tsugu, A., and Matsuzawa, K. (1997) Role of glial filaments in cells and tumors of glial origin: a review. J. Neurosurg. 87: 420-430

Sacher, M. G., Athlan, E. S., and Mushynski, W. E. (1992) Okadaic acid induces the rapid and reversible disuption of the neurofilament network in rat dorsal root ganglion neurons. Biochem. Biophys. Res. Commun. 186: 524-530

Sahlgren, C. M., Mikhailov, A., Hellman, J., Chou, Y. H., Lendahl, U., Goldman, R. D., and Eriksson, J. E. (2001) Mitotic reorganization of the intermediate filament protein nestin involves phosphorylation by cdc2 kinase. J. Biol. Chem. 276: 16456-16463

Sahlgren, C. M., Mikhailov, A., Vaittinen, S., Pallari, H. M., Kalimo, H., Pant, H. C., and Eriksson, J. E. (2003) Cdk5 regulates the organization of Nestin and its association with p35. Mol. Cell. Biol. 23: 5090-5106

Sakakibara, A., Aoki, E., Hashizume, Y., Mori, N., and Nakayama, A. (2007) Distribution of nestin and other stem cell-related molecules in developing and diseased human spinal cord. Pathol. Int. 57: 358-368

Salmaggi, A., Botturi, A., Lamperti, E., Grisoli, M., Fischetto, R., Ceccherini, I., Caroli, F., and Boiardi, A. (2007) A novel mutation in the GFAP gene in a familial adult onset Alexander disease. J. Neurol. 254: 1278-1280

Salvi, F., Aoki, Y., Della Nave, R., Vella, A., Pastorelli, F., Scaglione, C., Matsubara, Y., and Mascalchi, M. (2005) Adult Alexander's disease without leukoencephalopathy. Ann. Neurol. 58: 813-814

Santos, M., Perez, P., Segrelles, C., Ruiz, S., Jorcano, J. L., and Laramio, J. M. (2003) Impaired NF-Kappa B activation and increased production of tumor necrosis factor alpha in transgenic mice expressing keratin K10 in the basal layer of the epidermis. J. Biol. Chem. 278: 13422-13430

Sasaki, T., Taoka, M., Ishiguro, K., Uchida, A., Saito, T., Isobe, T., and Hisanaga, S. (2002) In vivo and in vitro phosphorylation at Ser-493 in the glutamate (E)-segment of neurofilament-H subunit by glycogen synthase kinase 3beta. J. Biol. Chem. 277: 36032-36039

Satoh, J., Yamamura, T., and Arima, K. (2004) The 14-3-3 protein epsilon isoform expressed in reactive astrocytes in demyelinating lesions of multiple sclerosis binds to vimentin and glial fibrillary acidic protein in cultured human astrocytes. Am. J. Pathol. 165: 577-592

Sawada, K., Agata, K., Eguchi, G. (1992) Crystallin gene expression in the process of lentoidogenesis in cultures of chicken lens epithelial cells. Exp. Eye Res. 55: 879-887

Sawada, K., Agata, Y., Koshiki, A., and Eguchi, G. (1993) A set of anti-crystallin monoclonal antibodies for detecting lense speficities: beta-crystallin as a specific marker for detecting lentoidogenesis in cultures of chicken lens epithelial cells. Jpn. J. Ophthalmol. 37: 355-368

Sawaishi, Y., Yano, T., Takaku, I., and Takada, G. (2002) Juvenile Alexander disease with a novel mutation in glial fibrillary acidic protein gene. Neurology 58: 1541-1543

Schaumburg, H. H., Powers, J. M., Raine, C. S., Suzuki, K., and Richardson, E. P. (1975) Adrenoleukodystrophy. A clinical and pathological study of 17 cases. Arch. Neurol. 33: 577-591

Schietke, R., Brohl, D., Wedig, T., Mucke, N., Herrmann, H., and Magin, T. M. (2006) Mutations in vimentin disrupt the cytoskeleton in fibroblasts and delay execution of apoptosis. Eur. J. Cell Biol. 85: 1-10

Schnappinger, D., and Hillen, W. (1996) Tetracycline antibiotic action, uptake and resistance mechanisms. Arch. Microbiol. 165: 359-369

Schochet, S. S. Jr., Lampert, P. W., and Earle, K. M. (1968) Alexander's disease. A case report with electron microscopic observations. Neurology 18: 543-549

Schubert, U., Anton, L. C., Gibbs, J., Norbury, C. C., Yewdell, J. W., and Bennink, J. R. (2000) Rapid degradation of a large fraction of newly synthesized proteins by proteasomes. Nature 404: 770-774

Schulte, T. W., An, W. G., and Neckers, L. M. (1997) Geldanamycin-induced destabilization of Raf-1 involves the proteasome. Biochem. Biophys. Res. Commun. 239: 655-659

Schuster, V., Horwitz, A. E., and Kreth, H. W. (1991) Alexander's disease: cranial MRI and ultrasound findings. Pediatr. Radiol. 21: 133-134

Schutte, B., Henfling, M., and Ramaekers, F. C. (2006) DEDD association with cytokeratin filaments correlates with sensitivity to apoptosis. Apoptosis 11: 1561-1572

Schwankhaus, J. D., Parisi, J. E., Gulledge, W. R., Chin, L., and Currier, R. D. (1995) Hereditary adult-onset Alexander's disease with palatal myoclonus, spastic paraparesis and cerebellar ataxia. Neurology 45: 2266-2271

Schweitzer, S. C., Klymkowsky, M. W., Bellin, R. M., Robson, R. M., Capetanaki, Y., and Evans, R. M. (2001) Paranemin and the organization of desmin filament networks. J. Cell Sci. 114: 1079-1089

Scott, C., Keating, L., Bellamy, M., and Baines, A. J. (2001) Protein 4.1 in forebrain postsynaptic density preparations: enrichment of 4.1 gene products and detection of 4.1R binding proteins. Eur. J. Biochem. 268: 1084-1094

Segnitz, B., and Gehring, U. (1997) The function of steroid hormone receptors is inhibited by the hsp90-specific compound geldanamycin. J. Biol. Chem. 272: 18694-18701

Seil, F. J., Schochet, S. S. Jr., and Earle, J. M. (1968) Alexander's disease in an adult: report of a case. Arch. Neurol. 19: 494-502Schwankhaus, J. D., Parisi, J. E., Gulledge, W. R., Chin, L., and Currier, R. D. (1995) Hereditary adult-onset Alexander's disease with palatal myoclonus, spastic paraparesis and cerebellar ataxia. Neurology 45: 2266-2271

Sekhar, K. R., Yan, X. X., and Freeman, M. I. (2002) Nrf2 degradation by the ubiquitin-proteasome pathway is inhibited by K1AA0132, the human homolog to INrf2. Oncogene 21: 6829-6834

Sevcik, J., Urbanikova, L., Kost'an, J., Janda, L., and Wiche, G. (2004) Actin-binding domain of mouse plectin. Crystal structure and binding to vimentin. Eur. J. Biochem. 271: 1873-1884

Sharma, M., Sharma, P., and Pant, H. C. (1999) CDK-5-mediated neurofilament phosphorylation in SHSY5Y human neuroblastoma cells. J. Neurochem. 73: 79-86

Shearman, M. S. (1999) Toxicity of protein aggregates in PC12 cells: 3-(4,5-dimethylthiazol-2-yl)-2,5-diphenyltetrazolium bromide assay. Methods Enzymol. 309: 716-723

Sherman, M. Y., and Goldberg, A. L. (2001) Cellular defenses against unfolded proteins: a cell biologist thinks about neurodegenerative diseases. Neuron 29: 15-32

Sherr, C. J., and Roberts, J. M. (1999) CDK inhibitors: positive and negative r egulators of G1-phase progression. Genes Dev. 13: 1501-1512

Shibuki, K., Gomi, H., Chen, L., Bao, S., Kim, J. J., Wakatsuki, H., Fujisaki, T., Fujimoto, K., Katah, A., Ikeda, T., Chen, C., Thompson, R. F., and Itobara, S. (1996) Deficient cerebellar

long-term depression, impaired eye blink conditioning and normal motor coordination in GFAP mutant mice. Neuron 16: 587-599

Shibuya, S., Miyamoto, O., Auer, R. N., Itano, T., Mori, S., and Norimatsu, H. (2002) Embryonic intermediate filament, nestin, expression following traumatic spinal cord injury in adult rats. Neuroscience 114: 905-916

Shiihara, T., Sawaishi, Y., Adachi, M., Kato, M., and Hayasaka, K. (2004) Asymptomatic hereditary Alecander's disease caused by a novel mutation in GFAP J. Neurol. Sci. 225: 125-127

Shimizu, T., Cao, C. X., Shao, R. G., and Pommier, Y. (1998) Lamin B phosphorylation by protein kinase calpha and proteolysis during apoptosis in human leukemia HL60 cells. J. Biol. Chem. 273: 8669-8674

Shin, A. H., Kil, I. S., Yang, E. S., Huh, T. L., Yang, C. H., and Park, J. W. (2004) Regulation of high glucose-induced apoptosis by mitochondrial NADP+-dependent isocitrate dehydrogenase. Biochem. Biophys. Res. Commun. 325(1): 32-38

Shiroma, N., Kanazawa, N., Kato, Z., Shimozawa, N., Imamura, A., Ito, M., Ohtani, K., Oka, A., Wakabayashi, K., Iai, M., Sugai, K., Sasaki, M., Kaga, M., Ohta, T., and Tsujino, S. (2003) Molecular genetic study in Japanese patients with Alexander disease: a novel mutation, R79L. Brain Dev. 25: 116-121

Sihag, R. K., and Nixon, R. A. (1991) Identification of Ser-55 as a major protein kinase A phosphorylation site on the 70-kDa subunit of neurofilaments. Early turnover during axonal transport. J. Biol. Chem. 266: 18861-18867

Sihag, R. K., Inagaki, M., Yamaguchi, T., Shea, T. B., and Pant, H. C. (2007) Role of phosphorylation on the structural dynamics and function of types III and IV intermediate filaments. Exp. Cell Res. 313: 2098-2109

Skaper, S. D. (2007) The brain as a target for inflammatory proceses and neuroprotective strategies. Ann. N. Y. Acad. Sci. 1122: 23-34

Smith, S. J. (1992) Do astrocytes process neural information? Prog. Brain Res. 94: 119-136

Smith, T. W., Tyler, H. R., and Schoene, W. C. (1975) Atypical astrocytes and Rosenthal fibers in a case of amyotrophic lateral sclerosis associated with a cerebral glioblastoma multiforme. Acta Neuropathol. 31: 29-34

Soellner, P., Quinlan, R. A., and Franke, W. W. (1985) Identification of a distinct soluble subunit of an intermediate filament protein: tetrameric vimentin from living cells. Proc. Natl. Acad. Sci. U. S. A. 82: 7929-7933

Soffer, D., and Horoupian, D. A. (1979) Rosenthal fibers formation in the central neuvous system. Its relation to Alexander's disease. Acta Neuropathol. (Berl) 47: 81-84

Spalke, G., and Mennel, M. D. (1982) Alexander's disease in an adult: Clinicopathologic study of a case and review of the literature. Clin. Neuropathol. 1: 106-112

Sprengel, R., and Hasan, M. T. (2007) Tetracycline-controlled genetic switches. Handb. Exp. Pharmacol. 178: 49-72

Springer, S., Erlewein, R., Naegele, T., Becker, I., Auer, D., Grodd, W., and Krägeloh-Mann, I. (2000) Alexander disease—Classification revisited and isolation of a neonatal form. Neuropediatrics 31: 86-92

Spudich, A., Meyer, T., and Stryer, L. (1992) Association of the beta isoform of protein kinase C with vimentin filaments. Cell Motil. Cytoskeleton 22: 250-256

Staba, M. J., Goldman, S., Johnson, F. L., and Huttenlocher, P. R. (1997) Allogeneic bone marrow transplantation for Alexander's disease. Bone Marrow Transplant 20: 247-249

Stappenbeck, T. S., and Green, K. J. (1992) The desmoplakin carboxyl terminus coaligns with and specifically disrupts intermediate filament networks when expressed in cultured cells. J. Cell Biol. 116: 1197-1209

Stappenbeck, T. S., Bornslaeger, E. A., Corcoran, C. M., Luu, H. H., Virata, M. L., and Green, K. J. (1993) Functional analysis of desmoplakin domains: specification of the interaction with keratin versus vimentin intermediate filament networks. J. Cell Biol. 123: 691-705

Stappenbeck, T. S., Lamb, J. A., Corcoran, C. M., and Green, K. J. (1994) Phosphorylation of the desmoplakin COOH terminus negatively regulates its interaction with keratin intermediate filament networks. J. Biol. Chem. 269: 29351-29354

Steffan, J. S., Kazantsev, A., Spasic-Boskovic, O., Greenwald, M., Zhu, Y. Z., Gohler, H., Wanker, E. E., Bates, G. P., Housman, D. E., and Thompson, L. M. (2000) The Huntington's disease protein interacts with p53 and CREB-binding protein and represses transcription. Proc. Natl. Acad. Sci. U. S. A. 97(12): 6763-6768

Steinbock, F. A., Nikolic, B., Coulombe, P. A., Fuchs, E., Traub, P., and Wiche, G. (2000) Dose-dependent linkage, assembly inhibition and disassembly of vimentin and cytokeratin 5/14 filaments through plectin's intermediate filament-binding domain. J. Cell Sci. 113 (Pt 3): 483-491

Steinert, P. M., Chou, Y. H., Prahlad, V., Parry, D. A., Marekov, L. N., Wu, K. C., Jang, S. I., and Goldman, R. D. (1999) A high molecular weight intermediate filament-associated protein in BHK-21 cells is nestin, a type VI intermediate filament protein. Limited co-assembly in vitro to form heteropolymers with type III vimentin and type IV alpha-internexin. J. Biol. Chem. 274: 9881-9890

Steinert, P. M., Idler, W. W., and Zimmerman, S. B. (1976) Self-assembly of bovine epidermal keratin filaments in vitro. J. Mol. Biol. 108: 547-567

Steinert, P. M., Idler, W. W., Cabral, F., Gottesman, M. M., and Goldman, R. D. (1981) In vitro assembly of homopolymer and copolymer filaments from intermediate filament subunits of muscle and fibroblastic cells. Proc. Natl. Acad. Sci. U. S. A. 78: 3692-3696

Steinert, P. M., Parry, D. A., and Marekov, L. N. (2003) Trichohyalin mechanically strengthens the hair follicle: multiple cross-bridging roles in the inner root shealth. J. Biol. Chem. 278: 41409-41419

Steward, O., Torre, E. R., Tomasulo, R., and Lothman, E. (1991) Neuronal activity up-regulates astroglial gene expression. Proc. Natl. Acad. Sci. U. S. A. 88: 6819-6823

Stewart, D., Killeen, E., Naquin, R., Alan, S., and Alam, J. (2003) Degradation of transcription factor Nrf2 via the ubiquitin-proteasome pathway and stabilization by cadmium. J. Biol. Chem. 278: 2396-2402

Stieber, A., Gonatas, J. O., and Gonatas, N. K. (2000) Aggregates of mutant protein appear progressively in dendrites, in periaxonal processes of oligodendrocytes, and in neuronal and astrocytic perikarya of mice expressing the SOD1(G93A) mutation of familial amyotrophic lateral sclerosis. J. Neurol. Sci. 177(2): 114-123

Stokoe, D., Engel, K., Campbell, D. G., Cohe, P., and Gaestel, M. (1992) Identification of MAPKAP kinase 2 as a major enzyme responsible for the phosphorylation of the small mammalian heat shock proteins. FEBS Lett. 313: 307-313

Strelkov, S. V., Herrmann, H., and Aebi, U. (2003) Molecular architecture of intermediate filaments. Bioessays 25: 243-251

Stumpf, E., Masson, H., Duquette, A., Berthelet, F., McNabb, J., Lortie, A., Lesage, J., Montplaisir, J., Brais, B., and Cossette, P. (2003) Adult Alexander disease with autosomal dominant transmission: a distinct entity caused by mutation in the glial fibrillary acid protein gene. Arch. Neurol. 60: 1307-1312

Stuurman, N., Heins, S., and Aebi, U. (1998) Nuclear lamins: their structure, assembly, and interactions. J. Struct. Biol. 122: 42-66

Styers, M. L., Salazar, G., Love, R., Peden, A. A., Kowalczyk, A. P., and Faundez, V. (2004) The endo-lysosomal sorting machinery interacts with the intermediate filament cytoskeleton. Mol. Biol. Cell 15: 5369-5382

Sumara, G., Belwal, M., and Ricci, R. (2005) "Jnking" atherosclerosis. Cell Mol. Life Sci. 62: 2487-2494

Sun, Y., and MacRae, T. H. (2005) The small heat shock proteins and their role in human disease. FEBS J. 272: 2613-2627

Suzuki, Y., Kanazawa, N., Takenaka, J., Okumura, A., Negoro, T., and Tsujino, S. (2004) A case of infantile Alexander disease with a milder phenotype and a novel GFAP mutation, L90P. Brain Dev. 26: 206-208

Suzuki, Y., Nakabayashi, T., and Takahashi, R. (2001) Ubiquitin-protein ligase activity of X-linked inhibitor of apoptosis protein promotes proteasomal degradation of caspase-3 and enhances its anti-apoptotic effect in Fas-induced cell death. Proc. Natl. Acad. Sci. U. S. A. 98: 8662-8667

Sweder, K., and Madura, K. (2002) Regulation of repair by the 26S proteasome. J. Biomed. Biotechnol. 2: 94-105

Szebenyi, G., Smith, G. M., Li, P., and Brady, S. T. (2002) Overexpression of neurofilament H disrupts normal cell structure and function. J. Neurosci. Res. 68: 185-198

Takahashi, M., Altschmied, L., and Hillen, W. (1986) Kinetic and equilibrium characterization of the Tet repressor-tetracycline complex by fluorescence measurements. Evidence for divalent metal ion requirement and energy transfer. J. Mol. Biol. 187: 341-348

Takai, Y., Ogawara, M., Tomono, Y., Moritoh, C., Imajoh-Ohmi, S., Tsutsumi, O., Taketani, Y., and Inagaki, M. (1996) Mitosis-specific phosphorylation of vimentin by protein kinase C coupled with reorganization of intracellular membranes. J. Cell Biol. 133: 141-149

Takanashi, J., Sugita, K., Tanabe, Y., and Niimi, H. (1998) Adolescent case of Alexander disease: MR imaging and MR spectroscopy. Pediatr. Neurol. 18: 67-70

Tan, Y., Rouse, J., Zhang, A., Cariati, S., Cohen, P., and Comb, M. J. (1996) FGF and stress regulate CREB and ATF-1 via a pathway involving p38 MAP kinase and MAPKAP kinase-2. EMBO J. 15: 4629-4642

Tang, G., Xu, Z., and Goldman, J. E. (2006) Synergistic effects of the SAPK/JNK and the proteasome pathway on glial fibrillary acidic protein (GFAP) accumulation in Alexander disease. J. Biol. Chem. 281: 38634-38643

Tarcsa, E., Szymanska, G., Lecker, S., Oíconnor, C. M., and Goldberg, A. L. (2000) Ca2+-free calmodulin and calmodulin damaged by in vitro aging are selectively degraded by 26S proteasomes without ubiquitination. J. Biol. Chem. 275: 20295-20301

Tardy, M., Fages, C., Riol, H., LePrince, G., Rataboul, P., Charriere-Bertrand, C., and Nunez, J. (1989) Developmental expression of the glial fibrillary acidic protein mRNA in the central nervous system and in cultured astrocytes. J. Neurochem. 52: 162-167

Taylor, R. P., and Benjamin, I. J. (2005) Small heat shock proteins: a new classification scheme in mammals. J. Mol. Cell Cardiol. 38: 433-444

Thompson, L. J., and Fields, A. P. (1996) betaII protein kinase C is required for the G2/M phase transition of cell cycle. J. Biol. Chem. 271: 15045-15053

Thyagarajan, D., Chataway, T., Li, R., Gai, W. P., and Brenner, M. (2004) Dominantly-inherited adult-onset leukodystrophy with palatal tremor caused by a mutation in the glial fibrillary acidic protein gene. Mov. Disord. 19: 1244-1248

Tihen, W. S. (1972) Central pontine myelinolysis and Rosenthal fibers of the brain stem: association with emaciation and prolonged intravenous hyperalimentation. Neurology 22: 710-716

Tikka, T., Fiebich, B. L., Goldsteins, G., Keinanen, R., and Koistinaho, J. (2001) Minocycline, a tetracycline derivative, is neuroprotective against excitotoxicity by inhibiting activation and proliferation of microglia. J. Neurosci. 21: 2580-2588

Toda, M., Miura, M., Asou, H., Toya, S., and Uyemura, K. (1994) Cell growth suppression of astrocytoma C6 cells by glial fibrillary acidic protein cDNA transfection. J. Neurochem. 63: 1975-1978

Toivola, D. M., Goldman, R. D., Garrod, D. R., and Eriksson, J. E. (1997) Protein phosphatases maintain the organization and structural interactions of hepatic keratin intermediate filaments. J. Cell Sci. 110: 23-33

Toivola, D. M., Omary, M. B., Ku, N. O., Peltola, O., Baribault, H., and Eriksson, J. E. (1998) Protein phosphatase inhibition in normal and keratin 8/18 assembly-incompetent mouse strains supports a functional role of keratin intermediate filaments in preserving hepatocyte integrity. Hepatology 28: 116-128

Toivola, D. M., Zhou, Q., English, L. S., and Omary, M. B. (2002) Type II keratins are phosphorylated on a unique motif during stress and mitosis in tissues and cultured cells. Mol. Biol. Cell. 13: 1857-1870

Tomokane, N., Iwaki, T., Tateishi, J., Iwaki, A., and Goldman, J. E. (1991) Rosenthal fibers share epitopes with alpha B-crystallin, glial fibrillary acidic protein, and ubiquitin, but not with vimentin. Immunoelectron microscopy with colloidal gold. Am. J. Pathol. 138: 875-885

Townsend, J. J., Wilson, J. F., Harris, T., Coulter, D., and Fife, R. (1985) Alexanderís disease. Acta Neuropathol. (Berl) 67: 163-166

Trimmer, P. A., Reier, P. J., Oh, T. H., and Eng, L. F. (1982) An ultrastructural and immunocytochemical study of astrocytic differentiation n vitro: changes in the composition and distribution of the cellular cytoskeleton. J. Neuroimmunol. 2: 235-260

Triolo, D., Dina, G., Lowenzetti, I., Malaguti, M., Morana, P., Del Carro, U., Comi, G., Messing, A., Quattrini, A., and Previtali, S. C. (2006) Loss of glial fibrillary acidic protein (GFAP) impairs Schwann cell proliferation and delays nerve regeneration after damage. J. Cell Sci. 119: 3981-3993

Tsugu, A., Sakai, K., Dirks, P. B., Jung, S., Weksberg, R., Fei, Y.-L., Mondal, S., Ivanchuk, S., Ackerley, C., Hamel, P. A., and Rutka, J. T. (2000) Expression of p57KIP2 potently blocks the growth of human astrocytomas and induces cell senescence. Am. J. Pathol. 157: 919-932

Turner, G. C., Du, F., and Varshavsky, A. (2000) Peptides accelerate their uptake by activating an ubiquitin-dependent proteolytic pathway. Nature 405: 579-583

Tzivion, G., Luo, Z. J., and Avruch, J. (2000) Calyculin A-induced vimentin phosphorylation sequesters 14-3-3 and displaces other 14-3-3 partners in vivo. J. Biol. Chem. 275: 29772-29778

Umeoka, S., Miyamoto, O., Nakagawa, T., Janjua, N. A., Nagao, S., and Itano, T. (2001) Expression of an embryonic intermediate filament protein in amygdaloid kindled rats. Epilepsy Res. 43: 249-253

Urlinger, S., Baron, U., Thellmann, M., Hasan, M. T., Bujard, H., and Hillen, W. (2000) Exploring the sequence space for tetracycline-dependent transcriptional activators: novel mutations yield epanded range and sensitivity. Proc. Natl. Acad. Sci. U. S. A. 97: 7963-7968

Vaittinen, S., Lukka, R., Sahlgren, C., Hurme, T., Rantanen, J., Lendahl, U., Eriksson, J. E., and Kalimo, H. (2001) The expression of intermediate filament protein nestin as related to vimentin and desmin in regenerating skeletal muscle. J. Neuropathol. Exp. Neurol. 60: 588-597

Valgeirsdóttir, S., Claesson-Welsh, L., Bongcam-Rudloff, E., Hellman, U., Westermark, B., and Heldin, C. H. (1998) PDGF induces reorganization of vimentin filaments. J. Cell Sci. 111: 1973-1980

van der Knaap, M. S., Naidu, S., Breiter, S. N., Blaser, S., Stroink, H., Springer, S., Begger, J. C., van Coster, R., Barth, P. G., Thomas, N. H., Valk, J., and Powers, J. M. (2001) Alexander disease: diagnosis with MRI imaging. Am. J. Neuroradiol. 22: 541-552

van der Knaap, M. S., Ramesh, V., Schiffmann, R., Blaser, K., Kyllerman, M., Gholkar, A., Ellison, D. W., van der Voorn, J. P., can Dooren, S. J., Jakobs, C., Barkhof, F., and Salomons, G. S. (2006) Alexander disease: ventricular garlands and abnormalities of the medulla and spinal cord. Neurology 66(4): 494-498

van der Knaap, M. S., Salomons, G. S., Li, R., Franzoni, E., Gutierrez-Solana, L. G., Smit, L. M., Robinson, R., Ferrie, C. D., Cree, B., Reddy, A., Thomas, N., Banwell, B., Barkhof, F., Jakobs, C., Johnson, A., Messing, A., and Brenner, M. (2005) Unusual variants of Alexander's disease. Ann. Neurol. 57: 327-338

van Rossum, G. S., Drummen, G. P., Verkleij, A. J., Post, J. A., and Boonstra, J. (2004) Activation of cytosolic phospholipase A2 in Her14 fibroblasts by hydrogen peroxide: a p42/44(MAPK)-dependent and phosphorylation-independent mechanism. Biochim. Biophys. Acta 1636: 183-195

Vaughan, D. K., Erickson, P. A., and Fisher, S. K. (1990) Glial fibrillary acidic protein (GFAP) immunoreactivity in rabbit retina: effect of fixation. Exp. Eye Res. 50: 385-392

Veeranna, Amin, N. D., Ahn, N. G., Jaffe, H., Winters, C. A., Grant, P., and Pant, H. C. (1998) Mitogen-activated protein kinases (Erk1,2) phosphorylate Lys-Ser-Pro (KSP) repeats in neurofilament proteins NF-H and NF-M. J. Neurosci. 18: 4008-4021

Venugopal, R., and Jaiswal, A. K. (1996) Nrf1 and Nrf2 positively and c-Fos and Fra1 negatively regulate the human antioxidant response element-mediated expression of NAD(P)H:quinone oxidoreductase1 gene. Proc. Natl. Acad. Sci. U. S. A. 93: 14960-14965

Vessal, M., Dugani, C. B., Solomon, D. A., Burnham, W. M., and Ivy, G. O. (2004) Astrocytic proliferation in the piriform cortex of amygdala-kindled subjects: a quantitative study in partial versus fully kindled brains. Brain Res. 1022: 47-53

Vikstrom, K. L., Lim, S. S., Goldman, R. D., and Borisy, G. G. (1992) Steady state dynamics of intermediate filament networks. J. Cell Biol. 118: 121-129

Virtanen, I., Lehto, V. P., Lehtonen, E., Vartio, T., Stenman, S., Kurki, P., Wager, O., Small, J. V., Dahl, D., and Badley, R. A. (1981) Expression of intermediate filaments in cultured cells. J. Cell Sci. 50: 45-63

Voutsinos-Porche, B., Bonvento, G., Tanaka, K., Steiner, P., Welker, E., Chatton, J. Y., Magistretti, P. J., and Pellerin, L. (2003) Glial gluatamate transporters mediate a functional metabolic crosstalk between neurons and astrocytes in the mouse developing cortex. Neuron 37: 275-286

Wakabayashi, K., Lai, M., Masuko, K., Yamashita, S., Yamada, M., Iwamoto, H., Aida, N., Shiroma, N., Kanazawa, N., and Tsujino, S. (2005) A case of long-term survival of a patient with infantile Alexander disease diagnosed by DNA analysis. No To Hattatsu 37: 55-59

Walls, T. J., Jones, R. A., Cartlidge, N., Jones, R. A., Cartlidge, N., and Saunders, M. (1984) Alexander's disease with Rosenthal fibre formation in an adult. J. Neurol. Neurosurg. Psychiatry. 47: 399-403

Walz, W. (1989) Role of glial cells in the regulation of the brain ion microenvironment. Prog. Neurobiol. 33: 309-333

Wang, P., and Gusev, N. B. (1996) Interaction of smooth muscle calponin and desmin. FEBS Lett. 392: 255-258

Wang, S., Ghosh, R. N., and Chellappan, S. P. (1998) Raf-1 physically interacting protein, BAG-1, binds to and activates the kinase Raf-1. Proc. Natl. Acad. Sci. U. S. A. 93: 7063-7068

Ward, C. L., Omura, S., and Kopito, R. R. (1995) Degradation of CFTR by the ubiquitin-proteasome pathway. Cell 83: 121-127

Weber, K., and Geisler, N. (1985) Intermediate filaments: structural conservation and divergence. Ann. N. Y. Acad. Sci. 455: 126-143

Weinstein, D. E., Shelanski, M. L., and Liera, R. K. (1991) Suppression by antisense mRNA demonstrates a requirement for the glial fibrillary acidic protein in the formation of stable astrocytic processes in response to neurons. J. Cell Biol. 112: 1205-1213

Welch, W. J. (1992) Mammalian stress response: cell physiology, structure/function of stress proteins, and implications for medicine and disease. Physiol. Rev. 72: 1063-1081

Welch, W. J., Feramisco, J. R., and Blose, S. H. (1985) The mammalian stress response and the cytoskeleton: alterations in intermediate filaments. Ann. N. Y. Acad. Sci. 455: 57-67

Welihinda, A. A., Tirasophon, W., and Kaufman, R. J. (1999) The cellular response to protein misfolding in the endoplasmic reticulum. Gene Expression 7: 293-300

Whelton, A., Schach von Wittenaia, M., Twomey, T. M., Walker, W. G., and Bianchine, J. R. (1974) Doxycycline pharmacokinetics in the absence of renal function. Kidney Int. 5: 365-371

Wiche, G., Gromov, D., Donovan, A., Castanon, M. J., and Fuchs, E. (1993) Expression of plectin mutant cDNA in cultured cells indicates a role of COOH-terminal domain in intermediate filament association. J. Cell Biol. 121: 607-619

Wilhelmsson, U., Li, L., Pekna, M., Berthold, C. H, Blom, S., Eliasson, C., Renner, O., Bushong, E., Morgan, T. E., and Pekny, M. (2004) Absence of glial fibrillary acidic protien and vimentin prevents hypertoryphy of astrocytic processes and improves post-traumatic regeneration. J. Neurosci. 24: 5016-5021

Wilson, S. P., Al-Sarraj, S., and Bridges, L. R. (1996) Rosenthal fiber encephalopathy presenting with demyelination and Rosenthal fibers in a solvent abuser: adult Alexander's disease? Clin. Neuropathol. 15: 13-16

Windmann, C., Gibson, S., Jarpe, M. B., and Johnson, G. L. (1999) Mitogen-activated protein kinase: conservation of a three-kinase module from yeast to human. Physiol. Rev. 79: 143-180

Windoffer, R., Woll, S., Strnad, P., and Leube, R. E. (2004) Identification of novel principles of keratin filament network turnover in living cells. Mol. Biol. Cell 15: 2436-2448

Wippold, F. J., Perry, A., and Lennerz. J. (2006) Neuropathology for the neuroradiologist: Rosenthal fibers. Am. J. Neuroradiol. 27: 958-961

Wohlwill, F. J., Bernstein, J., and Yakovlev, P. I. (1959) Dysmyelinogenic leukodystrophy. Report of a case of a new, presumably familial type of leukodystrophy with megalobarencephaly. J. Neuropathol. Exp. Neurol. 18: 359-383

Wu, Y., Gu, Q., Wang, J., Yang, Y., Wu, X., and Jiang, Y. (2008) Clinical and genetic study in Chinese patients with Alexander disease. J. Child Neurol. 23: 173-177

Wyttenbach, A., Sauvageot, O., Carmichael, J., Diaz-Latoud, C., Arrigo, A. P., and Rubinsztein, D. C. (2002) Heat shock protein 27 prevents cellular polyglutamine toxicity and suppresses the increase of reactive oxygen species caused by huntingtin. Hum. Mol. Genet. 11: 1137-1151

Xia, Y., and Karin, M. (2004) The control of cell motility and epithelial morphogenesis by Jun kinses. Trends Cell Biol. 14: 94-101

Xia, Z., Dickens, M., Raingeaud, J., Davis, R. J., and Greenberg, M. E. (1995) Opposing effects of ERK and JNK-p38 MAP kinases on apoptosis. Science 270: 1326-1331

Xu, G. M., Sikaneta, T., Sullivan, B. M., Zhang, Q., Andreucci, M., Stehle, T., Drummond, I., and Arnaout, M. A. (2001) Polycystin-1 interacts with intermediate filaments. J. Biol. Chem. 276: 46544-46552

Yamaguchi, A., Udagawa, T., and Sawai, T. (1990) Transport of divalent cations with tetracycline as mediated by the transposon Tn10-encoded tetracycline resistance protein. J. Biol. Chem. 265: 4809-4813

Yamaguchi, T., Goto, H., Yokoyama, T., Sillje, H., Hanisch, A., Uldschmid, A., Takai, Y., Oguri, T., Nigg, E. A., and Inagaki, M. (2005) Phosphorylation by Cdk1 induces Plk1-mediated vimentin phosphorylation during mitosis. J. Cell Biol. 171: 431-436

Yang, D. D., Kuan, C. Y., Whitmarsh, A. J., Rincon, M., Zheng, T. S., Davis, R. J., Rakic, P., and Flavell, R. A. (1997) Absence of excitotoxicity-induce apoptosis in the hippocampus of mice lacking the Jnk3 gene. Nature 389: 865-870

Yang, Y. M., Bost, F., Charbono, W., Dean, N., McKay, R., Rhim, J. S., Depatie, C., and Mercola, D. (2003) C-Jun NH(2)-terminal kiinase mediates proliferation and tumor growth of human prostate carcinoma. Clin. Can. Res. 9: 391-401

Yang, Y., Dowling, J., Yu, Q. C., Kouklis, P., Cleveland, D. W., and Fuchs, E. (1996) An essential cytoskeletal linker protein connecting actin microfilaments to intermediate filaments. Cell 86: 655-665

Yew, P. R. (2001) Ubiqitin-mediated proteolysis of vertebrate G1- and S-phase regulators. J. Cell Physiol. 187: 1-10

Yoneda, K., Furukawa, T., Zheng, Y. J., Momoi, T., Izawa, I., Inagaki, M., Manabe, M., and Inagaki, N. (2004) An autocrine/paracrine loop linking keratin 14 aggregates to tumor necrosis factor alpha-mediated cytotoxicity in a keratinocyte model of epidermolysis bullosa simplex. J. Biol. Chem. 279: 7296-7303

Yoon, K. H., Yoon, M., Moir, R. D., Khuon, S., Flitney, F. W., and Goldman, R. D. (2001) Insights into the dynamic properties of keratin intermediate filaments in living epithelial cells. J. Cell. Biol. 153: 503-516

Yoon, M., Moir, R. D., Prahlad, V., and Goldman, R. D. (1998) Motile properties of vimentin intermediate filament networks in living cells. J. Cell Biol. 143: 147-157

Yoshimura, S., Banno, Y., Nakashima, S., Takenaka, K., Sakai, H., Nishimura, Y., Sakai, N., Shimizu, S., Eguchi, Y., Tsujimoto, Y., and Nozawa, Y. (1998) Ceramide formation leads to caspase-3 activation during hypoxic PC12 cell death. Inhibitory effects of Bcl-2 on ceramide formation and caspase-3 activation. J. Biol. Chem. 273: 6921-6927

Yrjanheikki, J., Keinanen, R., Pellikka, M., Hokfelt, T., and Koistinaho, J. (1998) Tetracyclines inhibit microglial activation and are neuroprotective in global brain ischemia. Proc. Natl. Acad. Sci. U. S. A. 95: 15769-15774

Yrjanheikki, J., Tikka, T., Keinanen, R., Goldsteins, G., Chan, P. H., and Koistinaho, J. (1999) A tetracycline derivative, minocycline, reduces inflammation and protects against focal cerebral ischemia with a wide therapeutic window. Proc. Natl. Acad. Sci. U. S. A. 96: 13496-13500

Zackroff, R. V., and Goldman, R. D. (1979) In vitro assembly of intermediate filaments from baby hamster kidney (BHK-21) cells. Proc. Natl. Acad. Sci. U. S. A. 76: 6226-6230

Zatloukal, K., French, S. W., Stumptner, C., Strnad, P., Harada, M., Toivola, D. M., Cadrin, M., and Omary, M. B. (2007) From Mallory to Mallory-Denk bodies: what, how and why? Exp. Cell Res. 313: 2033-2049

Zatloukal, K., Stumptner, C., Lehner, M., Denk, H., Baribault, H., Eshkind, L. G., and Franke, W. W. (2000) Cytokeratin 8 protects from hepatotoxicity, and its ratio to cytokeratin 18 determines the ability of hepatocytes to form Mallory bodies. Am. J. Pathol. 156: 1263-1274

Zelenika, D., Grima, B., Brenner, M., and Pessac, B. (1995) A novel glial fibrillary acidic protein mRNA lacking exon 1. Brain Res. Mol. Brain Res. 30: 251-258

Zenz, R., and Wagner, E. F. (2006) Jun signaling in the epidermis: From developmental defects to psoriasis and skin tumors. Int. J. Biochem. Cell Biol. 38: 1043-1049

Zhang, D. D., Lo, S. C., Cross, J. V., Templaeton, D. J., and Hannink, M. (2004) Keap1 is a redox-regulated substrate adaptor protein for a cul3-dependent ubiquitin ligase complex. Mol. Cell. Biol. 24: 10941-10953

Zhao, Y., and Davis, H. W. (1998) Hydrogen peroxide-induced cytoskeletal rearrangement in cultured pulmonary endothelial cells. J. Cell Physiol. 174(3): 370-379

Zheng, Y. L., Li, B. S., Veeranna, and Pant, H. C. (2003) Phosphorylation of the head domain of neurofilament protein (NF-M): a factor regulating topographic phosphorylation of NF-M tail domain KSP sites in neurons. J. Biol. Chem. 278: 24026-24032

Zonta, M., Angulo, M. C., Gobbo, S., Rosengarten, B., Hossmann, K. A., Pozzan, T., and Carmignoto, G. (2003) Neuron-to-astrocyte signalling is central to the dynamic control of brain microcirculation. Nat. Neurosci. 6: 43-50

Zourlidou, A., Payne Smith, M. D., and Latchman, D. S. (2004) HSP27 but not HSP70 has a potent protective effect against alpha-synuclein-induced cell death in mammalian neuronal cells. J. Neurochem. 88: 1439-1448

Appendix 1. Protein kinases involved in IF phosphorylation

IF protein	In vivo Kinases	Binding to IFs	In vitro Kinases	Reference
K8	PKC	Yes	Yes	[1]
	PKCδ			[2]
	JNK	Yes	Yes	[3]
	p38	Yes	Yes	[4]
K18	Raf-1	Yes	Yes	[5]
GFAP	Rho-kinase	Yes	Yes	[6, 7]
Desmin	Rho-kinase		Yes	[8]
Peripherin	PKA		Yes	[9]
Vimentin	Cdk1	Yes	Yes	[8, 10]
	PKA		Yes	[11]
	PKC		Yes	[8, 12]
	CaMK II		Yes	[8]
	Aurora-B		Yes	[13]
	Rho-kinase		Yes	[8]
	MAPKAP-2		Yes	[14]
	Plk-1		Yes	[15]
NF-H	GSK3β	Yes	Yes	[16]
	Erk 1/2			[17]
	Cdk 5	Yes	Yes	[18-20]
	SAPK			[21]
NF-M	PKA			[22]
	Erk 1/2		Yes	[17, 23]
	Cdk 5		Yes	[18]
NF-L	PKA	Yes	Yes	[24, 25]
	CaMK II	Yes	Yes	[26]
Lamin A/C	Cdk1		Yes	[27]
	PKC	Yes	Yes	[27, 28]
Lamin B	PKC		Yes	[29]
	PKCα		Yes	[30]
	PKCβII	Yes	Yes	[31, 32]
	PKCδ	Yes	Yes	[33]
Nestin	Cdk1		Yes	[34]
	Cdk5	Yes	Yes	[35]

References:

1. Omary, M. B., Ku, N. O., Liao, J., and Price, D. (1998) Keratin modifications and solubility properties in epithelial cells and in vitro. Subcell. Biochem. 31: 105-140
2. Ridge, K. M., Linz, L., Flitney, F. W., Kuczmarski, E. R., Chou, Y. H., Omary, M. B., Sznajder, J. I., and Goldman, R. D. (2005) Keratin 8 phosphorylation by protein kinase C delta regulates shear stress-mediated disassembly of keratin intermediate filaments in alveolar epithelial cells. J. Biol. Chem. 280: 30400-30405
3. He, T., Stepulak, A., Holmstrom, T. H., Omary, M. B., and Eriksson, J. E. (2002) The intermediate filament protein keratin 8 is a novel cytoplasmic substrate for c-Jun N-terminal kinase. J. Biol. Chem. 277: 10767-10774
4. Ku, N. O., Azhar, S., and Omary, M. B. (2002) Keratin 8 phosphorylation by p38 kinase regulates cellular keratin filament reorganization: modulation by a keratin 1-like disease causing mutation. J. Biol. Chem. 277: 10775-10782
5. Ku, N. O., Fu, H., and Omary, M. B. (2004) Raf-1 activation disrupts its binding to keratins during cell stress. J. Cell Biol. 166: 479-485
6. Kosako, H., Amano, M., Yanagida, M., Tanabe, K., Nishi, Y., Kaibuchi, K., and Inagaki, M. (1997) Phosphorylation of glial fibrillary acidic protein at the same sites by cleavage furrow kinase and Rho-associated kinase. J. Biol. Chem. 272: 10333-10336
7. Kosako, H., Goto, H., Yanagida, M., Matsuzawa, K., Fujita, M., Tomono, Y., Okigaki, T., Odai, H., Kaibuchi, K., and Inagaki, M. (1999) Specific accumulation of Rho-associated kinase at the cleavage furrow during cytokinesis: cleavage furrow-specific phosphorylation of intermediate filaments. Oncogene 18: 2783-2788
8. Nagata, K., Izawa, I., and Inagaki, M. (2001) A decade of site- and phosphorylation state-specific antibodies: recent advances in studies of spatiotemporal protein phosphorylation. Genes Cells 6: 653-664
9. Giasson, B. I., and Mushynski, W. E. (1998) Intermediate filament disassembly in cultured dorsal root ganglion neurons is associated with amino-terminal head domain phosphorylation of specific subunits. J. Neurochem. 70: 1869-1875
10. Chou, Y. H., Bischoff, J. R., Beach, D., and Goldman, R. D. (1990) Intermediate filament reorganization during mitosis is mediated by p34cdc2 phosphorylation of vimentin. Cell 62: 1063-1071
11. Eriksson, J. E., He, T., Trejo-Skalli, A. V., Harmala-Brasken, A. S., Hellman, J., Chou, Y. H., and Goldman, R. D. (2004) Specific in vivo phosphorylation sites determine the assembly dynamics of vimentin intermediate filaments. J. Cell Sci. 117: 919-932
12. Takai, Y., Ogawara, M., Tomono, Y., Moritoh, C., Imajoh-Ohmi, S., Tsutsumi, O., Taketani, Y., and Inagaki, M. (1996) Mitosis-specific phosphorylation of vimentin by protein kinase C coupled with reorganization of intracellular membranes. J. Cell Biol. 133: 141-149
13. Goto, H., Yasui, Y., Kawajiri, A., Nigg, E. A., Terada, Y., Tatsuka, M., Nagata, K., and Inagaki, M. (2003) Aurora-B regulates the cleavage furrow-specific vimentin phosphorylation in the cytokinetic process. J. Biol. Chem. 278: 8526-8530

14. Cheng, T. J., and Lai, Y. K. (1998) Identification of mitogen-activated protein kinase-activated protein kinase-2 as a vimentin kinase activated by okadaic acid in 9L rat brain tumor cells. J. Cell Biochem. 71: 169-181

15. Yamaguchi, T., Goto, H., Yokoyama, T., Sillje, H., Hanisch, A., Uldschmid, A., Takai, Y., Oguri, T., Nigg, E. A., and Inagaki, M. (2005) Phosphorylation by Cdk1 induces Plk1-mediated vimentin phosphorylation during mitosis. J. Cell Biol. 171: 431-436

16. Sasaki, T., Taoka, M., Ishiguro, K., Uchida, A., Saito, T., Isobe, T., and Hisanaga, S. (2002) In vivo and in vitro phosphorylation at Ser-493 in the glutamate (E)-segment of neurofilament-H subunit by glycogen synthase kinase 3beta. J. Biol. Chem. 277: 36032-36039

17. Veeranna, Amin, N. D., Ahn, N. G., Jaffe, H., Winters, C. A., Grant, P., and Pant, H. C. (1998) Mitogen-activated protein kinases (Erk1,2) phosphorylate Lys-Ser-Pro (KSP) repeats in neurofilament proteins NF-H and NF-M. J. Neurosci. 18: 4008-4021

18. Lew, J., Winkfein, R. J., Paudel, H. K., and Wang, J. H. (1992) Brain proline-directed protein kinase is a neurofilament kinase which displays high sequence homology to p34cdc2. J. Biol. Chem. 267: 25922-25926

19. Sharma, M., Sharma, P., and Pant, H. C. (1999) CDK-5-mediated neurofilament phosphorylation in SHSY5Y human neuroblastoma cells. J. Neurochem. 73: 79-86

20. Lee, K. Y., and Johnston, R. N. (1997) Neurofilaments are part of the high molecular weight complex containing neuronal cdc2-like kinase (nclk). Brain Res. 773: 197-202

21. Giasson, B. I., and Mushynski, W. E. (1997) Study of proline-directed protein kinases involved in phosphorylation of the heavy neurofilament subunit. J. Neurosci. 17: 9466-9472

22. Zheng, Y. L., Li, B. S., Veeranna, and Pant, H. C. (2003) Phosphorylation of the head domain of neurofilament protein (NF-M): a factor regulating topographic phosphorylation of NF-M tail domain KSP sites in neurons. J. Biol. Chem. 278: 24026-24032

23. Li, B. S., Veeranna, Gu, J., Grant, P., and Pant, H. C. (1999) Activation of mitogen-activated protein kinases (Erk1 and Erk2) cascade results in phosphorylation of NF-M tail domains in transfected NIH 3T3 cells. Eur. J. Biochem. 262: 211-217

24. Sihag, R. K., and Nixon, R. A. (1991) Identification of Ser-55 as a major protein kinase A phosphorylation site on the 70-kDa subunit of neurofilaments. Early turnover during axonal transport. J. Biol. Chem. 266: 18861-18867

25. Nakamura, Y., Hashimoto, R., Kashiwagi, Y., Aimoto, S., Fukusho, E., Matsumoto, N., Kudo, T., and Takeda, M. (2000) Major phosphorylation site (Ser55) of neurofilament L by cyclic AMP-dependent protein kinase in rat primary neuronal culture. J. Neurochem. 74: 949-959

26. Hashimoto, R., Nakamura, Y., Komai, S., Kashiwagi, Y., Tamura, K., Goto, T., Aimoto, S., Kaibuchi, K., Shiosaka, S., and Takeda, M. (2000) Site-specific phosphorylation of neurofilament-L is mediated by calcium/calmodulin-dependent

protein kinase II in the apical dendrites during long-term potentiation. J. Neurochem. 75: 373-382

27. Eggert, M., Radomski, N., Linder, D., Tripier, D., Traub, P., and Jost, E. (1993) Identification of novel phosphorylation sites in murine A-type lamins. Eur. J. Biochem. 213: 659-671

28. Muranyi, W., Haas, J., Wagner, M., Krohne, G., and Koszinowski, U. H. (2002) Cytomegalovirus recruitment of cellular kinases to dissolve the nuclear lamina. Science 297: 854-857

29. Hornbeck, P., Huang, K. P., and Paul, W. E. (1988) Lamin B is rapidly phosphorylated in lymphocytes after activation of protein kinase C. Proc. Natl. Acad. Sci. U. S. A. 85: 2279-2283

30. Shimizu, T., Cao, C. X., Shao, R. G., and Pommier, Y. (1998) Lamin B phosphorylation by protein kinase calpha and proteolysis during apoptosis in human leukemia HL60 cells. J. Biol. Chem. 273: 8669-8674

31. Thompson, L. J., and Fields, A. P. (1996) betaII protein kinase C is required for the G2/M phase transition of cell cycle. J. Biol. Chem. 271: 15045-15053

32. Goss, V. L., Hocevar, B. A., Thompson, L. J., Stratton, C. A., Burns, D. J., and Fields, A. P. (1994) Identification of nuclear beta II protein kinase C as a mitotic lamin kinase. J. Biol. Chem. 269: 19074-19080

33. Cross, T., Griffiths, G., Deacon, E., Sallis, R., Gough, M., Watters, D., and Lord, J. M. (2000) PKC-delta is an apoptotic lamin kinase. Oncogene 19: 2331-2337

34. Sahlgren, C. M., Mikhailov, A., Hellman, J., Chou, Y. H., Lendahl, U., Goldman, R. D., and Eriksson, J. E. (2001) Mitotic reorganization of the intermediate filament protein nestin involves phosphorylation by cdc2 kinase. J. Biol. Chem. 276: 16456-16463

35. Sahlgren, C. M., Mikhailov, A., Vaittinen, S., Pallari, H. M., Kalimo, H., Pant, H. C., and Eriksson, J. E. (2003) Cdk5 regulates the organization of Nestin and its association with p35. Mol. Cell Biol. 23: 5090-5106

Appendix 2. Cellular functions and associated substrates in the ubiquitin-proteosome system

Function	Substrate	Reference
Cell Cycle Progression	cyclins	[1]
	cdks and their inhibitors	[2]
	p21	[3]
Signal Transduction	Protein kinase C	[4]
	Src	[5]
Oncogenesis	p27^{Kip1}	[6]
	p53	[7]
	DCC	[8]
	retinoblastoma protein	[9]
	Myc	[10]
	c-Myb	[11]
	Mos	[12]
	Bcr-Abl	[13]
	Raf-1	[14]
	β-catenin	[15]
	HIF-1	[16]
Regulation of gene expression	p53	[7]
	c-Jun, E2F1, IκB, NF-κB, c-Myc, HIF-1α, MATα2, β-catenin	[17]
	c-Fos	[18]
	STAT3	[19]
	Glucocorticoid receptors	[20]
DNA repair	RAD4	[21]
	RAD23	[22]
	Xeroderma pigmentosum B protein	
Apoptosis	Mdm2 and bax	[23]
	cIAP	[24]
	Bid	[25]
	caspase 3	[26]
Regulation of Metabolic Pathways	Ornithine decarboxylase	[27]
	HMG-CoA reductase	[28]
	Cup9	[29]
Protein quality Control	CFTRΔF508	[30],[31]
	α1-antitrypsin (Z-variant)	[32]
	aged calmodulin	[33]
Inflammation	IκB	[34]
	p105 precursor of NF-κB	[35]
Long-term memory	Protein kinase A (regulatory subunit)	[36]
Immune surveillance	Most cytosolic and nuclear proteins	[37]

References:

1. Koepp, D. M., Harper, J. W., and Elledge, S. J. (1999) How the cyclin became a cyclin: regulated proteolysis in the cell cycle. Cell 97: 431-434

2. Yew, P. R. (2001) Ubiqitin-mediated proteolysis of vertebrate G1- and S-phase regulators. J. Cell Physiol. 187: 1-10

3. Naujokat, C., and Hoffmann, S. (2002) Role and function of the 26S proteasome in proliferation and apoptosis. Lab. Invest. 82: 965-980

4. Lu, Z., Liu, D., Hornia, A., Devonish, W., Pagano, M., and Foster, D. A. (1998) Activation of protein kinase C triggers its ubiquitination and degradation. Mol. Cell. Biol. 18:839-845

5. Harris, K. F., Shoji, I., Cooper, E. M., Kumar, S., Oda, H., and Howley, P. M. (1999) Ubiquitin-mediated degradation of active Src tyrosine kinase. Proc. Natl. Acad. Sci. U. S. A. 96: 13738-13743

6. Pagano, M., Tam, S. W., Theodoras, A. M., Beer-Romero, P., Del Sal, G., Chau, V., Yew, P. R., Draetta, G. F., and Rolfe, M. (1995) Role of the ubiquitin-proteasome pathway in regulating abundance of the cyclin-dependent kinase inhibitor p27. Science 269: 682-685

7. Maki, C. G., Huibregtse, J. M., and Howley, P. M. (1996) In vivo ubiquitination and proteaosme-mediated degradation of p53(1). Cancer Res. 56: 2649-2654

8. Hu, G., Zhang, S., Vidal, M., Baer, J. L., Xu, T., and Hearon, E. R. (1997) Mammalian homologs of seven in absentia regulate DCC via the ubiquitin-proteasome pathway. Genes Dev. 11: 2701-2714

9. Boyer, S. N., Wazer, D. E., and Band, V. (1996) E7 protein of human papilloma virus-induces degradation of retinoblastoma protein through the ubiquitin-proteasome pathway. Cancer Res. 56: 4620-4624

10. Gross-Mesilaty, S., Reinstein, E., Bercovich, B. Tobias, K. E., Schwartz, A. L., Kahana, C., and Ciechanover, A. (1998) Basal and human papillomavirus E6 oncoprotein-induced degradation of Myc proteins by the ubiquitin pathway. Proc. Natl. Acad. Sci. U. S. A. 95: 8058-8063

11. Bies, J., and Wolff, L. (1997) Oncogenic activation of c-Myb by carboxyl-terminal truncation leads to decreased proteolysis by the ubiquitin-26S proteasome pathway. Oncogene 14: 203-212

12. Ishida, N., Tanaka, K., Tamura, T. Nishizawa, M., Okazaki, K., Sagata, N., and Ichihara, A. (1993) Mos is degraded by the 26S proteasome in an ubiquitin-dependent fashion. FEBS Lett. 324: 345-348

13. Dou, Q. P., McGuire, T. F., Peng, Y., and An, B. (1999) Proteasome inhibition leads to significant reduction of Bcr-Abl expression and subsequent induction of apoptosis in K562 human chronic myelogenous leukemia cells. J. Pharmacol. Exp. Ther. 289: 781-790

14. Schulte, T. W., An, W. G., and Neckers, L. M. (1997) Geldanamycin-induced destabilization of Raf-1 involves the proteasome. Biochem. Biophys. Res. Commun. 239: 655-659

15. Easwaran, V., Song, V., Polakis, P., and Byers, S. (1999) The ubiquitin-proteasome pathway and serine kinase activity modulate adenomatous polyposis coli protein-mediated regulation of beta-catenin-lymphocyte enhancer-binding factor signalling. J. Biol. Chem. 274: 16641-16645

16. Maxwell, P. H., Wiesener, M. S., Chang, G. W., Clifford, S. C., Vaux, E. C., Cockman, M. E., Wykoff, C. C., Pugh, C. W., Maher, E. R., and Ratcliffe, P. J. (1999) The tumour suppressor protein VHL targets hypoxia-inducible factors for oxygen-dependent proteolysis. Nature 399: 271-275

17. Hershko, A., and Ciechanover, A. (1998) The ubiquitin system. Annu. Rev. Biochem. 67: 425-479

18. He, H. L., Qi, X. M., Grossmann, J., and Distelhorst, C. W. (1998) C-Fos degradation by the proteasome-an early, Bcl-2-regulated step in apoptosis. J. Biol. Chem. 273: 25015-25019

19. Daino, H., Matsumura, I., Takada, K., Odajima, J., Tanaka, H., Ueda, S., Shibayama, H., Ikeda, H., Hibi, M., Machii, T., Hirano, T., and Kanakura, Y. (2000) Induction of apoptosis by extracellular ubiquitin in human hematopoietic cells: possible involvement of STAT3 degradation by proteasome pathway in interleukin 6-dependent hematopoietic cells. Blood 95(8): 2577-2585

20. Segnitz, B., and Gehring, U. (1997) The function of steroid hormone receptors is inhibited by the hsp90-specific compound geldanamycin. J. Biol. Chem. 272: 18694-18701

21. Sweder, K., and Madura, K. (2002) Regulation of repair by the 26S proteasome. J. Biomed. Biotechnol. 2: 94-105

22. Lommel, L., Ortolan, T., Chen, L., Madura, K., and Sweder, K. S. (2002) Proteolysis of a nucleotide excision repair protein by the 26S proteasome. Curr. Genet. 42: 9-20

23. Chang, Y. C., Lee, Y. S., Tejima, T. Tanaka, K., Omura, S., Heintz, N. H., Mitsui, Y., and Magae, J. (1998) mdm2 and bax, downstream mediators of the p53 response, are degraded by the ubiquitin-proteasome pathway. Cell Growth Differ. 9: 79-84

24. Huang, H., Joazeiro, C. A., Bonfoco, E., Kamada, S., Leverson, J. D., and Hunter, T. (2000) The inhibitor of apoptosis, cIAP2, functions as an ubiquitin-protein ligase and promotes in vitro mono-ubiquitination of caspases 3 and 7. J. Biol. Chem. 27: 26661-26664

25. Breitshopf, K., Zeiher, A. M., and Dimmeler, S. (2000) Ubiquitin-mediated degradation of the proapoptotic active form of bid. A functional consequence on apoptosis induction. J. Biol. Chem. 275: 21648-21652

26. Suzuki, Y., Nakabayashi, T., and Takahashi, R. (2001) Ubiquitin-protein ligase activity of X-linked inhibitor of apoptosis protein promotes proteasomal degradation of caspase-3 and enhances its anti-apoptotic effect in Fas-induced cell death. Proc. Natl. Acad. Sci. U. S. A. 98: 8662-8667

27. Murakami, Y., Matsufuji, S., Kameji, T., Hayashi, S., Igarashi, K., Tamura, T., Tanaka, K., and Ichihara, A. (1992) Ornithine decarboxylase is degraded by the 26S proteasome without ubiquitination. Nature 360: 597-599

28. Hampton, R. Y., Gardner, R. G., and Rine, J. (1996) Role of 26S proteasome and Hrd genes in the degradation of 3-hydroxy-3-methylglutaryl-CoA reductase, an integral endoplasmic reticulum membrane protein. Mol. Biol. Cell 7: 2029-2044

29. Turner, G. C., Du, F., and Varshavsky, A. (2000) Peptides accelerate their uptake by activating an ubiquitin-dependent proteolytic pathway. Nature 405: 579-583

30. Jensen, T. J., Loo, M. A., Pind, S., Williams, D. B., Goldberg, A. L. and Riordan, J. R. (1995) Multiple proteolytic systems, including the proteasome, contribute to CFTR processing. Cell 83: 129-135

31. Ward, C. L., Omura, S., and Kopito, R. R. (1995) Degradation of CFTR by the ubiquitin-proteasome pathway. Cell 83: 121-127

32. Qu, D., Teckman, J. H., Omura, S., and Perlmutter, D. H. (1996) Degradation of a mutant secretory protein, alpha 1-antitrypsin Z, in the endoplasmic reticulum requires proteasome activity. J. Biol. Chem. 271: 22791-22795

33. Tarcsa, E., Szymanska, G., Lecker, S., Oíconnor, C. M., and Goldberg, A. L. (2000) Ca2+-free calmodulin and calmodulin damaged by in vitro aging are selectively degraded by 26S proteasomes without ubiquitination. J. Biol. Chem. 275: 20295-20301

34. Meng, L., Mohan, R., Kwok, B. H., Elofsson, M., Sin, N., and Crews, C. M. (1999) Epoxomicin, a potent and selective proteasome inhibitor, exhibits in vivo antiinflammatory activity. Proc. Natl. Acad. Sci. U. S. A. 96: 10403-10408

35. Palombella, V. J., Conner, E. M., Fuseler, J. W., Destree, A., Davis, J. M., Laroux, F. S., Eolf, R. E., Huang, J., Brand, S., Elliott, P. J., Lazarus, D., McCormack, T., Parent, L., Stein, R., Adams, J., and Grisham, M. B. (1998) Role of the proteasome and NF-kappaB in streptococcal cell wall-induced polyarthritis. Proc. Natl. Acad. Sci. U. S. A. 95: 15671-15676

36. Chain, D. G., Schwartz, J. H., and Hegde, A. N. (1999) Ubiquitin-mediated proteolysis in learning and memory. Mol. Neurobiol. 20: 125-142

37. Rock, K. L., and Goldberg, A. L. (1999) Degradation of cell proteins and generation of MHC class I-presented peptides. Annu. Rev. Immunol. 17: 739-779

Appendix 3. Intermediate filaments and their associated proteins

IF interacting partner	IF protein	Reference
Anchoring proteins		
4.1R	Neurofilament-L and α-internexin	[1]
α-dystrobrevin	Synemin, syncoilin	[2, 3]
BPAG1e	Peripherin, neurofilament, keratins	[4-7]
Desmoplakin	Keratins, vimentin	[8-13]
Periplakin	Keratin 8, vimentin	[14-16]
Plakophilin	Keratins, vimentin, desmin	[17-20]
Plectin	Keratins, vimentin, GFAP, desmin	[21-26]
Spectrin	Desmin, neurofilament-L	[27-29]
Aquaporin	Filensin, CP49	[30]
Cytolinkers		
α-actinin	Synemin	[31]
Calponin	Desmin	[32-34]
Filaggrin	Keratins	[35]
Fimbrin	Vimentin	[36]
Nebulin	Desmin	[37]
Trichohyalin	Keratins	[38, 39]
Tropomodulin	Filensin	[40]
Chaperones		
αB-crystallin	GFAP, desmin, vimentin, filensin, CP49, keratins 8/18, peripherin	[41-46]
HSP27	GFAP, keratins 8/18, Vimentin	[41, 47-49]
HSP40 (Mrj)	Keratins 8/18	[50]
HSP70	GFAP, Keratins 8/18	[41, 47, 51]
GRP78	Keratins 8/18	[52]
Enzymes		
Akt/PKB	Keratin 10	[53]
Caspase 3/9	Keratins 8/18	[54]
Cdk5/p35	Nestin, neurofilaments	[55, 56]
JNK	Keratins 8/18	[57]
p38	Keratins 8/18	[58]
PKC	Vimentin, keratins 8/18	[59-62]
Raf1 kinase	Vimentin, keratins 8/18	[63, 64]
Receptors		
c-Flip	Keratins 8/18	[65]
Polycystin-1	Keratins 8/18, vimentin, desmin	[66]
TNFR2	Keratins 8/18	[67]
Adapters		
NUDEL	Neurofilaments	[68]
14-3-3	Keratins 8/18, GFAP, vimentin	[69-72]
AP-3	Vimentin	[73]
DEDD	Keratins 8/18	[54, 74, 75]
TRADD	Keratins 8/18	[76]

References:

1. Scott, C., Keating, L., Bellamy, M., and Baines, A. J. (2001) Protein 4.1 in forebrain postsynaptic density preparations: enrichment of 4.1 gene products and detection of 4.1R binding proteins. Eur. J. Biochem. 268: 1084-1094

2. Mizuno, Y., Thompson, T. G., Guyon, J. R., Lidov, H. G., Brosius, M., Imamura, M., Ozawa, E., Watkins, S. C., and Kunkel, L. M. (2001) Desmuslin, an intermediate filament protein that interacts with alpha -dystrobrevin and desmin. Proc. Natl. Acad. Sci. U. S. A. 98: 6156-6161.

3. Newey, S. E., Howman, E. V., Ponting, C. P., Benson, M. A., Nawrotzki, R., Loh, N. Y., Davies, K. E., and Blake, D. J. (2001) Syncoilin, a novel member of the intermediate filament superfamily that interacts with alpha-dystrobrevin in skeletal muscle. J. Biol. Chem. 276: 6645-6655

4. Leung, C. L., Sun, D., and Liem, R. K. (1999) The intermediate filament protein peripherin is the specific interaction partner of mouse BPAG1-n (dystonin) in neurons. J. Cell. Biol. 144: 435-446

5. Yang, Y., Dowling, J., Yu, Q. C., Kouklis, P., Cleveland, D. W., and Fuchs, E. (1996) An essential cytoskeletal linker protein connecting actin microfilaments to intermediate filaments. Cell 86: 655-665

6. Leung, C. L., Zheng, M., Prater, S. M., and Liem, R. K. (2001) The BPAG1 locus: Alternative splicing produces multiple isoforms with distinct cytoskeletal linker domains, including predominant isoforms in neurons and muscles. J. Cell Biol. 154: 691-157

7. Fontao, L., Favre, B., Riou, S., Geerts, D., Jaunin, F., Saurat, J. H., Green, K. J., Sonnenberg, A., and Borradori, L. (2003) Interaction of the bullous pemphigoid antigen 1 (BP230) and desmoplakin with intermediate filaments is mediated by distinct sequences within their COOH terminus. Mol. Biol. Cell 14: 1978-1992

8. Bornslaeger, E. A., Corcoran, C. M., Stappenbeck, T. S., and Green, K. J. (1996) Breaking the connection: displacement of the desmosomal plaque protein desmoplakin from cell-cell interfaces disrupts anchorage of intermediate filament bundles and alters intercellular junction assembly. J. Cell Biol. 134: 985-1001

9. Kouklis, P. D., Hutton, E., and Fuchs, E. (1994) Making a connection: direct binding between keratin intermediate filaments and desmosomal proteins. J. Cell Biol. 127: 1049-1060

10. Meng, J. J., Bornslaeger, E. A., Green, K. J., Steinert, P. M., and Ip, W. (1997) Two-hybrid analysis reveals fundamental differences in direct interactions between desmoplakin and cell type-specific intermediate filaments. J. Biol. Chem. 272: 21495-503

11. Stappenbeck, T. S., and Green, K. J. (1992) The desmoplakin carboxyl terminus coaligns with and specifically disrupts intermediate filament networks when expressed in cultured cells. J. Cell Biol. 116: 1197-1209

12. Stappenbeck, T. S., Bornslaeger, E. A., Corcoran, C. M., Luu, H. H., Virata, M. L., and Green, K. J. (1993) Functional analysis of desmoplakin domains: specification of the interaction with keratin versus vimentin intermediate filament networks. J. Cell Biol. 123: 691-705

13. Stappenbeck, T. S., Lamb, J. A., Corcoran, C. M., and Green, K. J. (1994) Phosphorylation of the desmoplakin COOH terminus negatively regulates its interaction with keratin intermediate filament networks. J. Biol. Chem. 269: 29351-29354

14. DiColandrea, T., Karashima, T., Maatta, A., and Watt, F. M. (2000) Subcellular distribution of envoplakin and periplakin: insights into their role as precursors of the epidermal cornified envelope. J. Cell Biol. 151: 573-586

15. Karashima, T., and Watt, F. M. (2002) Interaction of periplakin and envoplakin with intermediate filaments. J. Cell Sci. 115: 5027-5037

16. Kazerounian, S., Uitto, J., and Aho, S. (2002) Unique role for the periplakin tail in intermediate filament association: specific binding to keratin 8 and vimentin. Exp. Dermatol. 11: 428-438

17. Kapprell, H. P., Owaribe, K., and Franke, W. W. (1988) Identification of a basic protein of Mr 75,000 as an accessory desmosomal plaque protein in stratified and complex epithelia. J. Cell Biol. 106: 1679-1691

18. Bonne, S., Gilbert, B., Hatzfeld, M., Chen, X., Green, K. J., and van Roy, F. (2003) Defining desmosomal plakophilin-3 interactions. J. Cell Biol. 161: 403-416

19. Hofmann, I., Mertens, C., Brettel, M., Nimmrich, V., Schnolzer, M., and Herrmann, H. (2000) Interaction of plakophilins with desmoplakin and intermediate filament proteins: an in vitro analysis. J. Cell Sci. 113 (Pt 13): 2471-2483

20. Hatzfeld, M., Haffner, C., Schulze, K., and Vinzens, U. (2000) The function of plakophilin 1 in desmosome assembly and actin filament organization. J. Cell Biol. 149: 209-222

21. Nikolic, B., Mac Nulty, E., Mir, B., and Wiche, G. (1996) Basic amino acid residue cluster within nuclear targeting sequence motif is essential for cytoplasmic plectin-vimentin network junctions. J. Cell Biol. 134: 1455-1467

22. Foisner, R., Leichtfried, F. E., Herrmann, H., Small, J. V., Lawson, D., and Wiche, G. (1988) Cytoskeleton-associated plectin: in situ localization, in vitro reconstitution, and binding to immobilized intermediate filament proteins. J. Cell Biol. 106: 723-733

23. Sevcik, J., Urbanikova, L., Kost'an, J., Janda, L., and Wiche, G. (2004) Actin-binding domain of mouse plectin. Crystal structure and binding to vimentin. Eur. J. Biochem. 271: 1873-1884

24. Hijikata, T., Murakami, T., Imamura, M., Fujimaki, N., and Ishikawa, H. (1999) Plectin is a linker of intermediate filaments to Z-discs in skeletal muscle fibers. J. Cell Sci. 112 (Pt 6): 867-876

25. Wiche, G., Gromov, D., Donovan, A., Castanon, M. J., and Fuchs, E. (1993) Expression of plectin mutant cDNA in cultured cells indicates a role of COOH-terminal domain in intermediate filament association. J. Cell Biol. 121: 607-619

26. Steinbock, F. A., Nikolic, B., Coulombe, P. A., Fuchs, E., Traub, P., and Wiche, G. (2000) Dose-dependent linkage, assembly inhibition and disassembly of vimentin and cytokeratin 5/14 filaments through plectin's intermediate filament-binding domain. J. Cell Sci. 113 (Pt 3): 483-491

27. Langley, R. C., Jr., and Cohen, C. M. (1986) Association of spectrin with desmin intermediate filaments. J. Cell Biochem. 30: 101-109

28. Langley, R. C., Jr., and Cohen, C. M. (1987) Cell type-specific association between two types of spectrin and two types of intermediate filaments. Cell Motil. Cytoskeleton 8: 165-173

29. Frappier, T., Stetzkowski-Marden, F., and Pradel, L. A. (1991) Interaction domains of neurofilament light chain and brain spectrin. Biochem. J. 275 (Pt 2): 521-527

30. Lindsey Rose, K. M., Gourdie, R. G., Prescott, A. R., Quinlan, R. A., Crouch, R. K., and Schey, K. L. (2006) The C terminus of lens aquaporin 0 interacts with the

cytoskeletal proteins filensin and CP49. Invest. Ophthalmol. Vis. Sci. 47: 1562-1570

31. Bellin, R. M., Sernett, S. W., Becker, B., Ip, W., Huiatt, T. W., and Robson, R. M. (1999) Molecular characteristics and interactions of the intermediate filament protein synemin. Interactions with alpha-actinin may anchor synemin-containing heterofilaments. J. Biol. Chem. 274: 29493-29499

32. Mabuchi, K., Li, B., Ip, W., and Tao, T. (1997) Association of calponin with desmin intermediate filaments. J. Biol. Chem. 272: 22662-22666

33. Nakagawa, H., Ishihara, M., and Ohashi, K. (1993) 33-kDa peptides prepared from chicken gizzard smooth muscle bundle both actin and desmin filaments in vitro. J. Biochem. (Tokyo) 114: 623-626

34. Wang, P., and Gusev, N. B. (1996) Interaction of smooth muscle calponin and desmin. FEBS Lett. 392: 255-258

35. Dale, B. A., and Presland, R. B. (1999) Filaggrins. In "Guidebook to the cytoskeletal and motor proteins" (T. Kreis and R. Vale, Eds.), Oxford University Press, New York.

36. Correia, I., Chu, D., Chou, Y. H., Goldman, R. D., and Matsudaira, P. (1999) Integrating the actin and vimentin cytoskeletons. adhesion-dependent formation of fimbrin-vimentin complexes in macrophages. J. Cell Biol. 146: 831-842

37. Bang, M. L., Gregorio, C., and Labeit, S. (2002). Molecular dissection of the interaction of desmin with the C-terminal region of nebulin. J. Struct. Biol. 137: 119-127

38. Steinert, P. M., Parry, D. A., and Marekov, L. N. (2003) Trichohyalin mechanically strengthens the hair follicle: multiple cross-bridging roles in the inner root shealth. J. Biol. Chem. 278: 41409-41419

39. Dale, B. A., Holbrook, K. A., and Steinert, P. M. (1978) Assembly of stratum corneum basic protein and keratin filaments in macrofibrils. Nature 276: 729-731

40. Fischer, R. S., Quinlan, R. A., and Fowler, V. M. (2003) Tropomodulin binds to filensin intermediate filaments. FEBS Lett. 547: 228-232

41. Perng, M. D., Cairns, L., van den, I. P., Prescott, A., Hutcheson, A. M., and Quinlan, R. A. (1999) Intermediate filament interactions can be altered by HSP27 and alphaB-crystallin. J. Cell Sci. 112 (Pt 13): 2099-2112

42. Perng, M. D., Wen, S. F., van den, I. P., Prescott, A. R., and Quinlan, R. A. (2004) Desmin aggregate formation by R120G alphaB-crystallin is caused by altered filament interactions and is dependent upon network status in cells. Mol. Biol. Cell 15: 2335-2346

43. Nicholl, I. D., and Quinlan, R. A. (1994) Chaperone activity of alpha-crystallins modulates intermediate filament assembly. EMBO J. 13: 945-953

44. Muchowski, P. J., Bassuk, J. A., Lubsen, N. H., and Clark, J. I. (1997) Human alphaB-crystallin. Small heat shock protein and molecular chaperone. J. Biol. Chem. 272: 2578-2582

45. Carter, J. M., Hutcheson, A. M., and Quinlan, R. A. (1995) In vitro studies on the assembly properties of the lens proteins CP49, CP115: coassembly with alpha-crystallin but not with vimentin. Exp. Eye Res. 60: 181-192

46. Djabali, K., de Nechaud, B., Landon, F., and Portier, M. M. (1997) AlphaB-crystallin interacts with intermediate filaments in response to stress. J. Cell Sci. 110 (Pt 21): 2759-2769

47. Janig, E., Stumptner, C., Fuchsbichler, A., Denk, H., and Zatloukal, K. (2005) Interaction of stress proteins with misfolded keratins. Eur. J. Cell Biol. 84: 329-339

48. Jonak, C., Klosner, G., Kokesch, C., D, F. O., H, H. O., and Trautinger, F. (2002) Subcorneal colocalization of the small heat shock protein, hsp27, with keratins and proteins of the cornified cell envelope. Br. J. Dermatol. 147: 13-19

49. Lee, J. S., Zhang, M. H., Yun, E. K., Geum, D., Kim, K., Kim, T. H., Lim, Y. S., and Seo, J. S. (2005) Heat shock protein 27 interacts with vimentin and prevents insolubilization of vimentin subunits induced by cadmium. Exp. Mol. Med. 37: 427-435

50. Izawa, I., Nishizawa, M., Ohtakara, K., Ohtsuka, K., Inada, H., and Inagaki, M. (2000) Identification of Mrj, a DnaJ/Hsp40 family protein, as a keratin 8/18 filament regulatory protein. J. Biol. Chem. 275: 34521-34527

51. Liao, J., Lowthert, L. A., Ghori, N., and Omary, M. B. (1995) The 70-kDa heat shock proteins associate with glandular intermediate filaments in an ATP-dependent manner. J. Biol. Chem. 270: 915-922

52. Liao, J., Price, D., and Omary, M. B. (1997) Association of glucose-regulated protein (grp78) with human keratin 8. FEBS Lett. 417: 316-320

53. Paramio, J. M., Segrelles, C., Ruiz, S., and Jorcano, J. L. (2001) Inhibition of protein kinase B (PKB) and PKCzeta mediates keratin K10-induced cell cycle arrest. Mol. Cell Biol. 21: 7449-7459

54. Dinsdale, D., Lee, J. C., Dewson, G., Cohen, G. M., and Peter, M. E. (2004) Intermediate filaments control the intracellular distribution of caspases during apoptosis. Am. J. Pathol. 164: 395-407

55. Sahlgren, C. M., Mikhailov, A., Vaittinen, S., Pallari, H. M., Kalimo, H., Pant, H. C., and Eriksson, J. E. (2003) Cdk5 regulates the organization of Nestin and its association with p35. Mol. Cell Biol. 23: 5090-5106

56. Qi, Z., Tang, D., Zhu, X., Fujita, D. J., and Wang, J. H. (1998) Association of neurofilament proteins with neuronal Cdk5 activator. J. Biol. Chem. 273: 2329-2335

57. He, T., Stepulak, A., Holmstrom, T. H., Omary, M. B., and Eriksson, J. E. (2002) The intermediate filament protein keratin 8 is a novel cytoplasmic substrate for c-Jun N-terminal kinase. J. Biol. Chem. 277: 10767-10774

58. Ku, N. O., Azhar, S., and Omary, M. B. (2002) Keratin 8 phosphorylation by p38 kinase regulates cellular keratin filament reorganization: modulation by a keratin 1-like disease causing mutation. J. Biol. Chem. 277: 10775-10782

59. Owen, P. J., Johnson, G. D., and Lord, J. M. (1996) Protein kinase C-delta associates with vimentin intermediate filaments in differentiated HL60 cells. Exp. Cell Res. 225: 366-373

60. Murti, K. G., Kaur, K., and Goorha, R. M. (1992) Protein kinase C associates with intermediate filaments and stress fibers. Exp. Cell Res. 202: 36-44

61. Spudich, A., Meyer, T., and Stryer, L. (1992) Association of the beta isoform of protein kinase C with vimentin filaments. Cell Motil. Cytoskeleton 22: 250-256

62. Omary, M. B., Baxter, G. T., Chou, C. F., Riopel, C. L., Lin, W. Y., and Strulovici, B. (1992) PKC epsilon-related kinase associates with and phosphorylates cytokeratin 8 and 18. J. Cell Biol. 117: 583-593

63. Janosch, P., Kieser, A., Eulitz, M., Lovric, J., Sauer, G., Reichert, M., Gounari, F., Buscher, D., Baccarini, M., Mischak, H., and Kolch, W. (2000) The Raf-1 kinase associates with vimentin kinases and regulates the structure of vimentin filaments. FASEB J. 14: 2008-2021

64. Ku, N. O., Fu, H., and Omary, M. B. (2004) Raf-1 activation disrupts its binding to keratins during cell stress. J. Cell Biol. 166: 479-485

65. Gilbert, S., Loranger, A., and Marceau, N. (2004) Keratins modulate c-Flip/extracellular signal-regulated kinase 1 and 2 antiapoptotic signaling in simple epithelial cells. Mol. Cell Biol. 24: 7072-7081

66. Xu, G. M., Sikaneta, T., Sullivan, B. M., Zhang, Q., Andreucci, M., Stehle, T., Drummond, I., and Arnaout, M. A. (2001) Polycystin-1 interacts with intermediate filaments. J. Biol. Chem. 276: 46544-46552

67. Caulin, C., Ware, C. F., Magin, T. M., and Oshima, R. G. (2000) Keratin-dependent, epithelial resistance to tumor necrosis factor-induced apoptosis. J. Cell Biol. 149: 17-22

68. Nguyen, M. D., Shu, T., Sanada, K., Lariviere, R. C., Tseng, H. C., Park, S. K., Julien, J. P., and Tsai, L. H. (2004) A NUDEL-dependent mechanism of neurofilament assembly regulates the integrity of CNS neurons. Nat. Cell Biol. 6: 595-608

69. Ku, N. O., Michie, S., Resurreccion, E. Z., Broome, R. L., and Omary, M. B. (2002) Keratin binding to 14-3-3 proteins modulates keratin filaments and hepatocyte mitotic progression. Proc. Natl. Acad. Sci. U. S. A. 99: 4373-4378

70. Satoh, J., Yamamura, T., and Arima, K. (2004) The 14-3-3 protein epsilon isoform expressed in reactive astrocytes in demyelinating lesions of multiple sclerosis binds to vimentin and glial fibrillary acidic protein in cultured human astrocytes. Am. J. Pathol. 165: 577-592

71. Li, H., Guo, Y., Teng, J., Ding, M., Yu, A. C., and Chen, J. (2006) 14-3-3gamma affects dynamics and integrity of glial filaments by binding to phosphorylated GFAP. J. Cell Sci. 119: 4452-4461

72. Tzivion, G., Luo, Z. J., and Avruch, J. (2000) Calyculin A-induced vimentin phosphorylation sequesters 14-3-3 and displaces other 14-3-3 partners in vivo. J. Biol. Chem. 275: 29772-29778

73. Styers, M. L., Salazar, G., Love, R., Peden, A. A., Kowalczyk, A. P., and Faundez, V. (2004) The endo-lysosomal sorting machinery interacts with the intermediate filament cytoskeleton. Mol. Biol. Cell 15: 5369-5382

74. Lee, J. C., Schickling, O., Stegh, A. H., Oshima, R. G., Dinsdale, D., Cohen, G. M., and Peter, M. E. (2002) DEDD regulates degradation of intermediate filaments during apoptosis. J. Cell Biol. 158: 1051-1066

75. Schutte, B., Henfling, M., and Ramaekers, F. C. (2006) DEDD association with cytokeratin filaments correlates with sensitivity to apoptosis. Apoptosis 11: 1561-1572

76. Inada, H., Izawa, I., Nishizawa, M., Fujita, E., Kiyono, T., Takahashi, T., Momoi, T., and Inagaki, M. (2001) Keratin attenuates tumor necrosis factor-induced cytotoxicity through association with TRADD. J. Cell Biol. 155: 415-426

Appendix 4. GFAP mutations associated with Alexander disease

GFAP mutation	Type	Domain	Reference
P47L	Substitution	Head	[1]
K63Q	Substitution	Head	[2]
K63Q	Substitution	Head	[3]
R70W	Substitution	1A	[4]
R70Q	Substitution	1A	[5]
M73R	Substitution	1A	[6]
M73R	Substitution	1A	[2]
M73K	Substitution	1A	[5]
M74T	Substitution	1A	[7]
L76F	Substitution	1A	[8]
L76F	Substitution	1A	[2]
L76V	Substitution	1A	[2]
N77Y	Substitution	1A	[8]
N77S	Substitution	1A	[2]
D78E	Substitution	1A	[9]
R79C	Substitution	1A	[1]
R79G	Substitution	1A	[6]
R79C	Substitution	1A	[6]
R79C	Substitution	1A	[10]
R79L	Substitution	1A	[11]
R79C	Substitution	1A	[12]
R79C	Substitution	1A	[2]
R79H	Substitution	1A	[1]
R79H	Substitution	1A	[8]
R79H	Substitution	1A	[6]
R79H	Substitution	1A	[13]
R79H	Substitution	1A	[14]
R79P	Substitution	1A	[5]
Y83H	Substitution	1A	[37]
K86/V87- E86/F87	Deletion/insertion	1A	[3]
V87G	Substitution	1A	[15]
R88C	Substitution	1A	[8]
R88S	Substitution	1A	[8]
R88C	Substitution	1A	[6]
R88C	Substitution	1A	[16]
R88C	Substitution	1A	[17]
R88C	Substitution	1A	[2]
R88C	Substitution	1A	[18]
L90P	Substitution	1A	[19]
L97P	Substitution	1A	[2]
L97P	Substitution	1A	[13]
V115F	Substitution	1B	[2]
V115I	Substitution	1B	[3]
R126/L127	Duplication	1B	[18]

Appendix 4. (Continued)

GFAP mutation	Type	Domain	Reference
E207K	Substitution	1B	[2]
E207Q	Substitution	1B	[2]
E207K	Substitution	1B	[3]
E207Q	Substitution	1B	[3]
E210K	Substitution	1B	[2]
E210K	Substitution	1B	[3]
E223Q	Substitution	L12	[20]
L235P	Substitution	2A	[2]
L235P	Substitution	2A	[3]
R239C	Substitution	2A	[1]
R239C	Substitution	2A	[8]
R239C	Substitution	2A	[11]
R239C	Substitution	2A	[6]
R239C	Substitution	2A	[13]
R239C	Substitution	2A	[21]
R239C	Substitution	2A	[2]
R239C	Substitution	2A	[3]
R239H	Substitution	2A	[1]
R239H	Substitution	2A	[8]
R239H	Substitution	2A	[2]
R239H	Substitution	2A	[22]
R239P	Substitution	2A	[13]
R239P	Substitution	2A	[2]
R239P	Substitution	2A	[3]
R239L	Substitution	2A	[23]
Y242D	Substitution	2A	[6]
A244V	Substitution	2A	[24]
A244V	Substitution	2A	[2]
A244V	Substitution	2A	[3]
A253G	Substitution	L2	[2]
A253G	Substitution	L2	[3]
Y257C	Substitution	2B	[25]
R258P	Substitution	2B	[1]
A267P	Substitution	2B	[26]
R276L	Substitution	2B	[27]
K279E	Substitution	2B	[2]
R330G	Substitution	2B	[38]
R330G	Substitution	2B	[39]
L331P	Substitution	2B	[28]
E332K	Substitution	2B	[38]
E332K	Substitution	2B	[39]
L352P	Substitution	2B	[29]
L352P	Substitution	2B	[2]
L359V	Substitution	2B	[2]

Appendix 4. (Continued)

GFAP mutation	Type	Domain	Reference
L359P	Substitution	2B	[5]
D360V	Substitution	2B	[30]
E362D	Substitution	2B	[31]
A364P	Substitution	2B	[2]
A364V	Substitution	2B	[40]
Y366H	Substitution	2B	[2]
E371G	Substitution	2B	[32]
Y366C	Substitution	2B	[40]
E373K	Substitution	2B	[6]
E373K	Substitution	2B	[2]
E373K	Substitution	2B	[41]
E374G	Substitution	2B	[2]
Q386I	Substitution	Tail	[33]
S393I	Substitution	Tail	[34]
R416W	Substitution	Tail	[1]
R416W	Substitution	Tail	[6]
R416W	Substitution	Tail	[35]
R416W	Substitution	Tail	[36]
R416W	Substitution	Tail	[2]
R416W	Substitution	Tail	[18]
1247-1249GGG>GG	Deletion	Tail	[42]

References:

1. Brenner, M., Johnson, A. B., Boespflug-Tanguy, O., Rodriguez, D., Goldman, J. E., and Messing, A. (2001) Mutations in GFAP, encoding glial fibrillary acidic protein, are associated with Alexander disease. Nat. Genet. 27: 117-120

2. Li, R., Johnson, A. B., Salomons, G., Goldman, J. E., Naidu, S., Quinlan, R., Cree, B., Ruyle, S. Z., Banwell, B., D'Hooghe, M., Siebert, J. R., Rolf, C. M., Cox, H., Reddy, A., Gutierrez-Solana, L. G., Collins, A., Weller, R. O., Messing, A., van der Knaap, M. S., and Brenner, M. (2005) Glial fibrillary acidic protein mutations in infantile, juvenile, and adult forms of Alexander disease. Ann. Neurol. 57: 310-326

3. van der Knaap, M. S., Salomons, G. S., Li, R., Franzoni, E., Gutierrez-Solana, L. G., Smit, L. M., Robinson, R., Ferrie, C. D., Cree, B., Reddy, A., Thomas, N., Banwell, B., Barkhof, F., Jakobs, C., Johnson, A., Messing, A., and Brenner, M. (2005) Unusual variants of Alexander's disease. Ann. Neurol. 57: 327-338

4. Salvi, F., Aoki, Y., Della Nave, R., Vella, A., Pastorelli, F., Scaglione, C., Matsubara, Y., and Mascalchi, M. (2005) Adult Alexander's disease without leukoencephalopathy. Ann. Neurol. 58: 813-814

5. Caroli, F., Biancheri, R., Seri, M., Rossi, A., Pessagno, A., Bugiani, M., Corsolini, F., Savasta, S., Romano, S., Antonelli, C., Romano, A., Pareyson, D., Gambero, P., Uziel, G., Ravazzolo, R., Ceccherini, I., and Filocamo, M. (2007) GFAP mutations and polymorphisms in 13 unrelated Italian patients affected by Alexander disease. Clin. Genet. 72: 427-433

6. Gorospe, J. R., Naidu, S., Johnson, A. B., Puri, V., Raymond, G. V., Jenkins, S. D., Pedersen, R. C., Lewis, D., Knowles, P., Fernandez, R., De Vivo, D., van der Knaap, M. S., Messing, A., Brenner, M., and Hoffman, E. P. (2002) Molecular findings in symptomatic and pre-symptomatic Alexander disease patients. Neurology 58: 1494-1500

7. Ohnari, K., Yamano, M., Uozumi, T., Hashimoto, T., Tsuji, S., and Nakagawa, M. (2007) An adult form of Alexander disease: a novel mutation in glial fibrillary acidic protein. J. Neurol. 254: 1390-1394

8. Rodriguez, D., Gauthier, F., Bertini, E., Bugiani, M., Brenner, M., N'Guyen, S., Goizet, C., Gelot, A., Surtees, R., Pedespan, J. M., Hernandorena, X., Troncoso, M., Uziel, G., Messing, A., Ponsot, G., Pham-Dinh, D., Dautigny, A., and Boespflug-Tanguy, O. (2001) Infantile Alexander disease: spectrum of GFAP mutations and genotype-phenotype correlation. Am. J. Hum. Genet. 69: 1134-1140

9. Stumpf, E., Masson, H., Duquette, A., Berthelet, F., McNabb, J., Lortie, A., Lesage, J., Montplaisir, J., Brais, B., and Cossette, P. (2003) Adult Alexander disease with autosomal dominant transmission: a distinct entity caused by mutation in the glial fibrillary acid protein gene. Arch. Neurol. 60: 1307-1312

10. Probst, E. N., Hagel, C., Weisz, V., Nagel, S., Wittkugel, O., Zeumer, H., and Kohlschutter, A. (2003) Atypical focal MRI lesions in a case of juvenile Alexander's disease. Ann. Neurol. 53: 118-120

11. Shiroma, N., Kanazawa, N., Kato, Z., Shimozawa, N., Imamura, A., Ito, M., Ohtani, K., Oka, A., Wakabayashi, K., Iai, M., Sugai, K., Sasaki, M., Kaga, M., Ohta, T., and Tsujino, S. (2003) Molecular genetic study in Japanese patients with Alexander disease: a novel mutation, R79L. Brain Dev. 25: 116-121

12. Ma, H. W., Lu, J. F., Jiang, J., Chen, L. Y., Niu, G. H., Wu, B. M., Kanazawa, N., and Tsujino, S. (2005) Glial fibrillary acidic protein mutation in a Chinese girl with infantile Alexander disease. Zhonghua Yi Xue Yi Chuan Xue Za Zhi 22: 79-81

13. Meins, M., Brockmann, K., Yadav, S., Haupt, M., Sperner, J., Stephani, U., and Hanefeld, F. (2002) Infantile Alexander disease: a GFAP mutation in monozygotic twins and novel mutations in two other patients. Neuropediatrics 33: 194-198

14. Asahina, N., Okamoto, T., Sudo, A., Kanazawa, N., Tsujino, S., and Saitoh, S. (2006) An infantile-juvenile form of Alexander disease caused by a R79H mutation in GFAP. Brain Dev. 28: 131-133

15. Okamoto, Y., Mitsuyama, H., Jonosono, M., Hirata, K., Arimura, K., Osame, M., and Nakagawa, M. (2002) Autosomal dominant palatal myoclonus and spinal cord atrophy. J. Neurol. Sci. 195: 71-76

16. Guthrie, S. O., Burton, E. M., Knowles, P., and Marshall, R. (2003) Alexander's disease in a neurologically normal child: a case report. Pediatr. Radiol. 33: 47-49

17. Nobuhara, Y., Nakahara, K., Higuchi, I., Yoshida, T., Fushiki, S., Osame, M., Arimura, K., and Nakagawa, M. (2004) Juvenile form of Alexander disease with GFAP mutation and mitochondrial abnormality. Neurology 63: 1302-1304

18. van der Knaap, M. S., Ramesh, V., Schiffmann, R., Blaser, S., Kyllerman, M., Gholkar, A., Ellison, D. W., van der Voorn, J. P., van Dooren, S. J., Jakobs, C., Barkhof, F., and Salomons, G. S. (2006) Alexander disease: ventricular garlands and abnormalities of the medulla and spinal cord. Neurology 66: 494-498

19. Suzuki, Y., Kanazawa, N., Takenaka, J., Okumura, A., Negoro, T., and Tsujino, S. (2004) A case of infantile Alexander disease with a milder phenotype and a novel GFAP mutation, L90P. Brain Dev. 26: 206-208

20. Brockmann, K., Meins, M., Taubert, A., Trappe, R., Grond, M., and Hanefeld, F. (2003) A novel GFAP mutation and disseminated white matter lesions: adult Alexander disease? Eur. Neurol. 50: 100-105

21. Wakabayashi, K., Lai, M., Masuko, K., Yamashita, S., Yamada, M., Iwamoto, H., Aida, N., Shiroma, N., Kanazawa, N., and Tsujino, S. (2005) A case of long-term survival of a patient with infantile Alexander disease diagnosed by DNA analysis. No To Hattatsu 37: 55-59

22. Sakakibara, A., Aoki, E., Hashizume, Y., Mori, N., and Nakayama, A. (2007) Distribution of nestin and other stem cell-related molecules in developing and diseased human spinal cord. Pathol. Int. 57: 358-368

23. Lee, J. M., Kim, A. S., Lee, S. J., Cho, S. M., Lee, D. S., Choi, S. M., Kim, D. K., Ki, C. S., and Kim, J. W. (2006) A case of infantile Alexander disease accompanied by infantile spasms diagnosed by DNA analysis. J. Korean Med. Sci. 21: 954-957

24. Aoki, Y., Haginoya, K., Munakata, M., Yokoyama, H., Nishio, T., Togashi, N., Ito, T., Suzuki, Y., Kure, S., Iinuma, K., Brenner, M., and Matsubara, Y. (2001) A novel mutation in glial fibrillary acidic protein gene in a patient with Alexander disease. Neurosci. Lett. 312: 71-74

25. Howard, K. L., Hall, D. A., Moon, M., Agarwal, P., Newman, E., and Brenner, M. (2007) Adult-onset Alexander disease with progressive ataxia and palatal tremor. Mov. Disord. 23: 118-122

26. Hinttala, R., Karttunen, V., Karttunen, A., Herva, R., Uusimaa, J., and Remes, A. M. (2007) Alexander disease with occipital predominance and a novel c.799G>C mutation in the GFAP gene. Acta Neuropathol. (Berl) 114: 543-545

27. Namekawa, M., Takiyama, Y., Aoki, Y., Takayashiki, N., Sakoe, K., Shimazaki, H., Taguchi, T., Tanaka, Y., Nishizawa, M., Saito, K., Matsubara, Y., and Nakano, I. (2002) Identification of GFAP gene mutation in hereditary adult-onset Alexander's disease. Ann. Neurol. 52: 779-785

28. Shiihara, T., Sawaishi, Y., Adachi, M., Kato, M., and Hayasaka, K. (2004) Asymptomatic hereditary Alexander's disease caused by a novel mutation in GFAP. J. Neurol. Sci. 225: 125-127

29. Bassuk, A. G., Joshi, A., Burton, B. K., Larsen, M. B., Burrowes, D. M., and Stack, C. (2003) Alexander disease with serial MRS and a new mutation in the glial fibrillary acidic protein gene. Neurology 61: 1014-1015

30. Ishigaki, K., Ito, Y., Sawaishi, Y., Kodaira, K., Funatsuka, M., Hattori, N., Nakano, K., Saito, K., and Osawa, M. (2006) TRH therapy in a patient with juvenile Alexander disease. Brain Dev. 28: 663-667

31. Sawaishi, Y., Yano, T., Takaku, I., and Takada, G. (2002) Juvenile Alexander disease with a novel mutation in glial fibrillary acidic protein gene. Neurology 58: 1541-1543

32. Kawai, M., Sakai, N., Miyake, S., Tsukamoto, H., Akagi, M., Inui, K., Mushiake, S., Taniike, M., and Ozono, K. (2006) Novel mutation of gene coding for glial fibrillary acidic protein in a Japanese patient with Alexander disease. Brain Dev. 28: 60-62

33. Caceres-Marzal, C., Vaquerizo, J., Galan, E., and Fernandez, S. (2006) Early mitochondrial dysfunction in an infant with Alexander disease. Pediatr. Neurol. 35: 293-296

34. Salmaggi, A., Botturi, A., Lamperti, E., Grisoli, M., Fischetto, R., Ceccherini, I., Caroli, F., and Boiardi, A. (2007) A novel mutation in the GFAP gene in a familial adult onset Alexander disease. J. Neurol. 254: 1278-1280

35. Kinoshita, T., Imaizumi, T., Miura, Y., Fujimoto, H., Ayabe, M., Shoji, H., Okamoto, Y., Takashima, H., Osame, M., and Nakagawa, M. (2003) A case of adult-onset Alexander disease with Arg416Trp human glial fibrillary acidic protein gene mutation. Neurosci. Lett. 350: 169-172

36. Thyagarajan, D., Chataway, T., Li, R., Gai, W. P., and Brenner, M. (2004) Dominantly-inherited adult-onset leukodystrophy with palatal tremor caused by a mutation in the glial fibrillary acidic protein gene. Mov. Disord. 19: 1244-1248

37. Wu, Y., Gu, Q., Wang, J., Yang, Y., Wu, X., and Jiang, Y. (2008) Clinical and genetic study in Chinese patients with Alexander disease. J. Child Neurol. 23: 173-177

38. Bachetti, T., Caroli, F., Bocca, P., Prigione, I., Balbi, P., Biancheri, R., Filocamo, M., Mariotti, C., Pareyson, D., Razazzolo, R., and Ceccherini, I. (2008) Mild functional effects of a novel GFAP mutation allele identified in a familial case of adult-onset Alexander disease. Eur. J. Hum. Genet. 16: 462-470

39. Balbi, P., Seri, M., Ceccherini, I., Uggetti, C., Casale, R., Fundarò, C., Caroli, F., and Santoro, L. (2008) Adult-onset Alexander disease: report on a family. J. Neurol. 255: 24-30

40. Hartmann, H., Herchenbach, J., Stephani, U., Ledaal, P., Donnerstag, F., Lücke, T., Das, A. M., Christen, H. J., Hagedorn, M., and Meins, M. (2007) Novel mutations in exon 6 of the GFAP gene affect a highly conserved if motif in the rod domain 2B and are associated with early onset infantile Alexander disease. Neuropediatirics 38: 143-147

41. Matej, R., Dvoráková, L., Mrázová, L., Houst'ková, H., and Elleder, M. (2008) Early onset Alexander disease: a case report with evidence for manifestation of the disorder in neurohypophyseal pituicytes. Clin. Neuropathol. 27: 64-71

42. Murakami, N., Tsuchiya, T., Kanazawa, N., Tsujino, S., and Nagai, T. (2008) Novel deletion mutation in GFAP gene in an infantile form of Alexander disease. Pediatr. Neurol. 38: 50-52

The Alexander Disease–Causing Glial Fibrillary Acidic Protein Mutant, R416W, Accumulates into Rosenthal Fibers by a Pathway That Involves Filament Aggregation and the Association of αB-Crystallin and HSP27

Ming Der Perng,* Mu Su,* Shu Fang Wen, Rong Li, Terry Gibbon, Alan R. Prescott, Michael Brenner, and Roy A. Quinlan

Here, we describe the early events in the disease pathogenesis of Alexander disease. This is a rare and usually fatal neurodegenerative disorder whose pathological hallmark is the abundance of protein aggregates in astrocytes. These aggregates, termed "Rosenthal fibers," contain the protein chaperones αB-crystallin and HSP27 as well as glial fibrillary acidic protein (GFAP), an intermediate filament (IF) protein found almost exclusively in astrocytes. Heterozygous, missense GFAP mutations that usually arise spontaneously during spermatogenesis have recently been found in the majority of patients with Alexander disease. In this study, we show that one of the more frequently observed mutations, R416W, significantly perturbs in vitro filament assembly. The filamentous structures formed resemble assembly intermediates but aggregate more strongly. Consistent with the heterozygosity of the mutation, this effect is dominant over wild-type GFAP in coassembly experiments. Transient transfection studies demonstrate that R416W GFAP induces the formation of GFAP-containing cytoplasmic aggregates in a wide range of different cell types, including astrocytes. The aggregates have several important features in common with Rosenthal fibers, including the association of αB-crystallin and HSP27. This association occurs simultaneously with the formation of protein aggregates containing R416W GFAP and is also specific, since HSP70 does not partition with them. Monoclonal antibodies specific for R416W GFAP reveal, for the first time for any IF-based disease, the presence of the mutant protein in the characteristic histopathological feature of the disease, namely Rosenthal fibers. Collectively, these data confirm that the effects of the R416W GFAP are dominant, changing the assembly process in a way that encourages aberrant filament-filament interactions that then lead to protein aggregation and chaperone sequestration as early events in Alexander disease.

Alexander disease (MIM 203450) is a rare and often fatal neurological disorder, first described by W. S. Alexander.[1] On the basis of age at onset, the disorder has been divided into three subtypes: infantile, juvenile, and adult.[2] The infantile form, with onset between birth and age ~2 years, is the most common type and is characterized by extensive loss of white matter.[3-5] A striking neuropathological feature of all forms of Alexander disease is the presence of Rosenthal fibers, unique cytoplasmic inclusions within astrocytes that contain the major astrocytic intermediate filament (IF) protein glial fibrillary acidic protein (GFAP) and the chaperones αB-crystallin and HSP27.[6-8] Although the GFAP within Rosenthal fibers appears disorganized, astrocytes in Alexander disease also possess GFAP filaments with conventional 10-nm morphology.

Recently, missense point mutations in GFAP have been identified as a genetic basis for Alexander disease.[9] To date, all known mutations have been heterozygous, indicating that the mutant form of the protein is dominant over the wild type. This is consistent with the finding of autosomal

dominant mutations in 26 other IF genes that are linked to human disease,[10,11] summarized in the online Intermediate Filament Disease Mutation Database. The list of known mutations in GFAP now includes 32 nucleotide changes that affect 24 aa spread throughout the entire sequence[12] (see also the Alexander Disease Web site). The mutations usually arise spontaneously during spermatogenesis,[13] with familial cases being quite rare because of the high morbidity associated with the disease. The mutation studied in this report, R416W, is one of the four mutations reported in familial cases and is also found in sporadic cases.[12]

Like other IF family members, GFAP has a characteristic domain structure comprising a central α-helical rod domain flanked by non-α-helical N-terminal "head" and C-terminal "tail" domains.[14] The rod domain contains characteristic heptad repeats of hydrophobic residues, which are the underlying basis for the coiled-coil dimer in the filament, and the highly conserved LNDR and TYRK-LEGGE motifs that are present at the start and the end of

this central rod domain.[14] Both of these motifs are highly conserved throughout the whole IF family,[15] and those mutations in Alexander disease and other genetic IF protein disorders found within them usually correlate with the severest forms of the diseases.[10,11] The crystallization of regions containing these two motifs from vimentin, a closely related type III IF protein[16,17] that coassembles with GFAP, has provided the atomic structure of these particular highly conserved motifs. Our knowledge of the important higher order interactions within the filament, however, is still limited to low-resolution studies[18–20]; therefore, the full structural impact of most of these rod mutations has not yet been detailed.

One of the other common mutations outside the central rod domain of GFAP that causes Alexander disease is R416W. This mutation occurs in the tail domain within the RDG motif, which is conserved among all GFAP proteins from multiple species, as well as the related type III IF proteins vimentin and desmin. Here, we describe the effects of this mutation on GFAP assembly and use this R416W GFAP mutant to identify the early events in the development of Alexander disease.

Material and Methods

Plasmid Construction and Site-Directed Mutagenesis

Total RNA was extracted from human astrocytoma U373MG cells with the RNeasy kit (Qiagen). The complete human GFAP cDNA was amplified by RT-PCR, with the SuperScript RT-PCR system (Invitrogen), with use of oligonucleotides 5'-CATATGGAGAGGA-GACGCAT-3' and 5'-TCACATCACATCCTTGTGCT-3' as forward and reverse primers, respectively. The amplified PCR product was cloned into the pGEM-T Easy vector (Promega), to generate pGEM-T Easy-WTGFAP, and the entire sequence was confirmed against the GenBank database entry for GFAP (accession number J04569). The R416W mutation was introduced by QuickChange site-directed mutagenesis (Stratagene) with use of the pGEM-T Easy-WTGFAP vector as a template. The following mutagenic oligonucleotides that contained the desired C→T mutation at np 1246 were synthesized: 5'-GAAGACCGTGGAGATGTGGGATGG-AGAGGTCAT-3' and 5'-ATGACCTCTCCATCCCACATCTCCACG-GTCTTC-3'. The amplified PCR product containing the R416W mutation was cloned into the pGEM-T Easy vector, and the mutation sequence was confirmed by DNA sequencing. For expression in cultured mammalian cells, both the wild-type and R416W GFAP cDNA in the pGEM-T Easy vector were subcloned into the pcDNA3.1(−) vector (Invitrogen) with use of the XbaI and EcoRI restriction sites. The GFAP mutant R239C was also subcloned into pCDNA3.1 from the pRSVi vector[21] with use of the restriction enzyme HindIII. For expression in bacteria, wild-type and R416W GFAP cDNA samples were subcloned into the pET23b vector (Novagen) with use of the NdeI and EcoRI restriction sites.

Expression and Purification of Recombinant GFAPs

For bacterial expression of proteins, pET 23b vector containing either wild-type or mutant GFAP cDNA samples were transformed into Escherichia coli strain BL21(DE3) pLysS (Novagen). After transformation, cultures were grown in Luria Bertani medium supplemented with appropriate antibiotics to OD_{600} of 0.5–0.6, and pro-tein expression was induced by the addition of 0.5 mM isopropyl-1-thio-β-D-galactopyranoside for 3 h. Overexpressed GFAP formed inclusion bodies, which were prepared as described elsewhere.[22] The final pellets, consisting predominantly of GFAP, were solubilized in extraction buffer (8 M urea, 20 mM Tris-HCl [pH 7.4], 5 mM EDTA, 1 mM EGTA, 1 mM dithiothreitol [DTT], and 1 mM phenylmethylsulfonyl fluoride [PMSF]) at room temperature for 3 h, and any insoluble material was removed by centrifugation, at 100,000 g, in a benchtop Optima MAX Ultracentrifuge with use of an MLA-80 rotor (Beckman Coulter). GFAP was further purified by ion-exchange chromatography with use of a Merck-Hitachi Biochromatography system equipped with a Fractogel-EMD TMAE 650S column (Merck) pre-equilibrated in the column buffer (6 M urea, 10 mM Tris-HCl [pH 8.0], 5 mM EDTA, 1 mM EGTA, 1 mM DTT, and 1 mM PMSF). GFAP was eluted from the column with a linear gradient of 0–0.5 M NaCl in the same buffer over 1 h at a flow rate of 1 ml/min. The GFAP-enriched fractions were pooled, concentrated, and applied to a Fractogel EMD COO-650S column (Merck) and were pre-equilibrated with column buffer (6 M urea, 20 mM sodium formate [pH 4.0], 5 mM EDTA, 1 mM EGTA, 1 mM DTT, and 1 mM PMSF). After washing with buffer B, GFAP was eluted with a linear gradient of 0–0.5 M NaCl in the same buffer. Column fractions were analyzed by SDS-PAGE, and those containing purified GFAP were collected and stored at −80°C. Protein concentrations were determined by bicinchonic acid assay (BCA reagent [Perbio Science]) with use of BSA as standard.

In Vitro Assembly and Sedimentation Assay

Purified GFAP was diluted to 0.3 mg/ml in 6 M urea in a buffer of 10 mM Tris-HCl (pH 8.0), 5 mM EDTA, 1 mM EGTA, and 1 mM DTT and was dialyzed stepwise against 3 M urea in the same buffer for 4–6 h at room temperature and then against the same buffer without urea overnight at 4°C. Filament assembly was completed by dialyzing against assembly buffer (20 mM imidazole-HCl [pH 6.8], 100 mM NaCl, and 1 mM DTT) for 12–16 h at room temperature. The efficiency of in vitro assembly was assessed by sedimentation assay as described elsewhere.[23] In brief, the assembly mixture was layered onto a 0.85-M sucrose cushion in assembly buffer and was centrifuged at 80,000 g for 30 min. To investigate the effect of mutations on filament-filament interactions, assembled filaments were subjected to low-speed centrifugation at 3,000 g for 10 min in a bench-top centrifuge (Eppendorf). The supernatant and pellet fractions were analyzed by SDS-PAGE[24] and were visualized by Coomassie blue staining. In some instances, the proportion of GFAP distributed between pellet and supernatant fractions was measured using an image analyzer (LAS-1000plus [FujiFilm]). Coomassie blue signals for individual bands were quantified using the Image Gauge software (v. 4.0) (FujiFilm).

Electron Microscopy

GFAP was diluted in assembly buffer to 100 μg/ml and was negatively stained with 1% (w/v) uranyl acetate (Agar Scientific). Samples on carbon-coated copper grids were examined with a Phillips 400T transmission electron microscope, with use of an accelerating voltage of 80 kV. Images were acquired at a magnification of 17,000 × on Kodak 4489 film and then were digitized at 1,200 × 1,200–pixel resolution before being processed further in Adobe Photoshop 7 (Adobe Systems).

Cell Cultures and Transient Transfection

Human breast cancer epithelial MCF7 cells were obtained from the European Collection of Cell Cultures (Sigma). Human adrenal cortex carcinoma SW/cl.1 and SW13/cl.2 cells were kindly provided by Dr. Robert Evans (University of Colorado Health Sciences Center, Denver). The human astrocytoma cell line U343MG was a gift from Dr. Rutka (Toronto), and the cells were grown in αMEM (Invitrogen). These cells express vimentin and GFAP as well as HSP27 and αB-crystallin. Primary mouse astrocytes from wild-type and vimentin/GFAP double-knock littermates were a generous gift of Dr. Milos Pekny (Göteborg, Sweden). They were prepared and grown as described elsewhere.[25] Unless otherwise stated, cells were grown in Dulbecco's modified Eagle medium supplemented with 10% (v/v) fetal calf serum, 2 mM L-glutamine, 100 U/ml penicillin, and 0.1 mg/ml streptomycin (Sigma) and were maintained at 37°C in a humidified incubator of 95% (v/v) air and 5% (v/v) CO_2.

For transient transfection studies, cells grown on 13-mm coverslips at a density of 40%–50% confluency were transfected with pcDNA3.1(−) expressing either wild-type or R416W GFAP, with use of GeneJuice transfection reagent (Novagen) according to the manufacturer's protocol. In some experiments, the R239C GFAP[31] and myc-tagged ubiquitin (His₆-myc-Ubiquitin)[29] were used. Cells were analyzed by double-label immunofluorescence microscopy 48 h after transfection.

Antibody Production

Mouse monoclonal antibodies were made that specifically recognized human but not wild-type R416W GFAP. The immunogen was a peptide dodecamer centered on the mutation site, KTVEMWDGEVIK (Genemed Synthesis), which was linked to keyhole limpet hemocyanin. Monoclonal antibodies were produced by the UAB Epitope Recognition Core, which also performed an initial ELISA screen against purified recombinant wild-type and R416W mutant GFAP. The corresponding wild-type peptide, KTVEMRDGEVIK, failed to produce monoclonal antibodies specific to the wild-type sequence.

Immunostaining of Cells and Tissues and Immunofluorescence Microscopy

Immunocytochemistry of cultured cells was performed on coverslips washed twice with PBS, and the cells were fixed in either ice-cold methanol/acetone (1:1 [v/v]) for 20 min or in 4% (w/v) paraformaldehyde/PBS for 10 min. In the case of paraformaldehyde fixation, cells were subsequently permeabilized with 0.5% NP-40 in PBS for 10 min. After being washed twice with PBS containing 0.02% (w/v) sodium azide and 0.02% (w/v) BSA (PBS/BSA/azide), cells were blocked with 10% (v/v) goat serum in PBS/BSA/azide for 20 min and then were incubated with primary antibodies at room temperature for 1 h. The primary antibodies used in this study were mouse monoclonal anti-GFAP (G-A-5, 1:500 [Sigma]), rabbit polyclonal GFAP antibodies (Z0334, 1:500 [Dako]), monoclonal anti-human GFAP (SMI-21, 1:500 [Sternberger Monoclonals]), monoclonal anti-keratin 18 (LE41 [kindly provided by Prof. Birgit Lane, University of Dundee, Dundee, United Kingdom), monoclonal anti-R416W GFAP (19.2 and 1A3, described below, 1:500), rabbit polyclonal anti-GFAP (clone 3270, 1:200),[25] polyclonal anti-vimentin (clone 3052, 1:200),[28] and the myc-epitope monoclonal antibody (Clone 9E11, 1:10).[29] After cells were washed with PBS/BSA/azide, the primary antibodies

were detected using Alexa 488 (1:400 [Molecular Probes]) or Alexa 594 (1:600 [Molecular Probes]) conjugated secondary antibodies. All antibodies were diluted in PBS/BSA/azide buffer. The glass coverslips were mounted on slides with the fluorescent protecting agent Citifluor (Citifluor Labs) and were observed with a Zeiss LSM 510 confocal laser scanning microscope (Carl Zeiss). Optical sections were set to ~1.0 μm. Images were processed and prepared for figures with Adobe Photoshop 7 (Adobe Systems). Quantitation of the GFAP filament phenotypes was by visual assessment of the cells and by scoring cells for the presence or absence of GFAP-containing aggregates. Approximately 100–150 transfected cells were assessed, and each experiment was repeated at least three times.

Immunohistochemistry from normal human and Alexander disease brain sections was performed on 6 μm–thick paraffin sections kindly provided by Drs. Jim Goldman and Goumei Tang (Columbia Medical School, New York). Internal review board approval was obtained from Columbia Medical School for these studies. Archival material for the infantile R416W Alexander disease case used in this study was described elsewhere.[40] Primary antibodies were rabbit anti-cow GFAP (Z0334, 1:5,000 [Dako]), and mouse anti-R416W GFAP (19.2, described below, 1:2,000). Secondary antibody for the peroxidase method was peroxidase-conjugated donkey anti-mouse IgG (Jackson ImmunoResearch) (1:2,000), with staining visualized using 3,3'-diaminobenzidine tetrachloride (DAB, metal-enhanced Substrate Kit [Pierce]). Secondary fluorescent antibodies are described above. Some sections were counterstained with Hoechst 33258 (Sigma) to reveal nuclei.

Ultrastructural Analysis by Immunoelectron Microscopy

MCF7 cells grown on 10-cm² petri dishes (Greiner Bio-One) were transfected with either wild-type or R416W GFAP for 48 h. Cells were then fixed directly in 80 mM cacodylate buffer (pH 7.2) containing 1.25% (v/v) glutaraldehyde and 1% (w/v) paraformaldehyde for 30 min at room temperature. Cells were scraped off the dish by a rubber policeman, were pelleted by low-speed centrifugation, and were washed three times with cacodylate buffer. The cells were then postfixed with 1% (w/v) osmium tetroxide in cacodylate buffer. After several washes with distilled water, cells were subjected to a series of graded ethanol dehydration, followed by overnight incubation in 1:1 propylene oxide:epoxy resin (Durcupan [Sigma]). After two changes of 100% fresh resin, cell pellets were transferred to BEEM capsules (Agar Scientific) and were polymerized in fresh resin overnight at 60°C. Ultrathin sections were generated using a Leica Ultracut ultramicrotome and were collected on pioloform and carbon-coated nickel grids (Agar Scientific). The grid specimens were then etched with 1% periodic acid, and osmium was removed by 2% (w/v) sodium periodate before incubation with blocking solution consisting of 0.5% (w/v) fish skin gelatin (Sigma) in PBS. Subsequently, sections were incubated with polyclonal anti-GFAP antibodies (clone 3270) diluted 1:20 in blocking solution for 90 min, were washed three times in PBS, and then were incubated with protein A conjugated with 5-nm gold particles (British BioCell International) for 2 h. After several washes in distilled water, specimens were stained with saturated aqueous uranyl acetate (3% [w/v]) for 30 min, followed by staining with lead citrate for 30 min.[41] Stained samples were subsequently examined on an FEI Tecnai 12 transmission electron microscope (FEI).
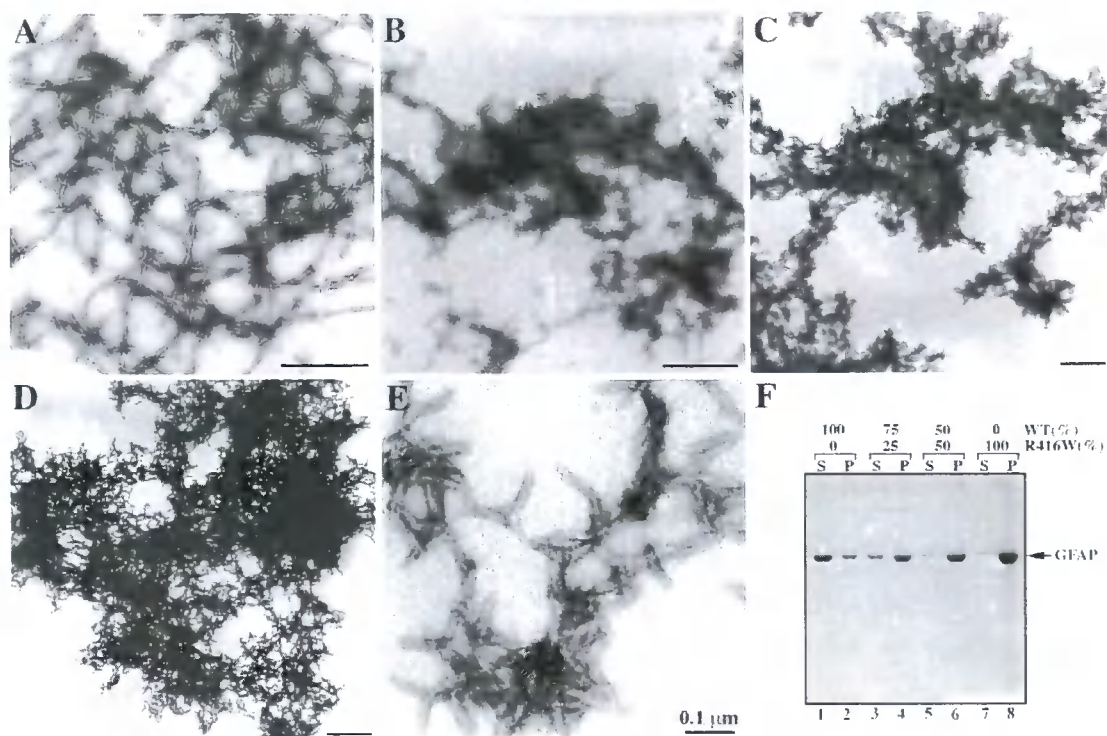
Figure 1. The dominant effect of R416W GFAP, revealed by in vitro assembly studies. Purified GFAP at a concentration of 0.3 mg/ml was assembled in vitro by stepwise dialysis into assembly buffer, as described in the "Material and Methods" section. Assembled filaments were negatively stained and were visualized by transmission electron microscopy. Under these assembly conditions, wild-type GFAP assembled into typical 10-nm filaments with length of several microns (*A*), whereas R416W GFAP alone and in different proportions with wild-type protein formed short filamentous intermediates that had a strong tendency to aggregate (*B–E*). It is difficult to see the structural detail of the aggregates formed by R416W GFAP (*D*) and mixtures thereof (*B* and *C*) when negatively stained with uranyl acetate. Sometimes, less aggregated material can be found, and then, at higher magnification (*E*), the filamentous structures that comprise the aggregates are clearly seen. Mixing wild-type GFAP in either 75:25 (*B*) or 50:50 (*C*) proportions with R416W GFAP failed to rescue intermediate filament formation, and similar aggregates were formed (*B* and *C*). A low-speed sedimentation assay was used to assess the extent of this aggregation. *F,* Wild-type (WT) (*lanes 1* and *2*) and R416W GFAP (*lanes 7* and *8*) were assembled, either individually or in mixtures of 75:25 (*lanes 3* and *4*) or 50:50 (*lanes 5* and *6*) WT:R416W GFAP. After assembly, the samples were subjected to low-speed centrifugation, and the resulting supernatant (S) and pellet (P) fractions were analyzed by SDS-PAGE and were visualized by Coomassie blue staining. Whereas only one-third of assembled wild-type GFAP was sedimented (*lane 1*), almost all the R416W mutant was found in the pellet fraction (*lane 8*). Mixing wild-type GFAP with the R416W mutant in different proportions did not dramatically increase the GFAP signal in either the supernatant fraction of the 50:50 mixture (*lane 5*) or the 75:25 mixture (*lane 3*). These data show that the effects of R416W GFAP on in vitro filament assembly is dominant over the wild-type protein. Bars = 1 μm, except in panel E, where it is 0.1μm.

Preparation of Cytoskeletal Fractions and Immunoblotting Analysis

Cells grown on 10-cm² petri dishes were transfected with control vector (pcDNA3.1) or vectors containing either wild-type or R416W GFAP cDNA. At 48 h after transfection, cells were lysed using two different extraction buffers, designed to test the resistance of GFAP filaments and aggregates to extraction. In the mild extraction protocol, cells were lysed on ice for 15 min in 1 ml mild extraction buffer (MEB; 20 mM Tris-HCl [pH 7.6], 140 mM NaCl, 5 mM EDTA, 1 mM EGTA, 0.5% [v/v] NP-40 supplemented with Complete protease inhibitor cocktail [Roche Diagnostics], and 1 mM PMSF). In the more severe extraction protocol, cells were lysed in 1 ml of a harsher extraction buffer (HEB) containing

deoxycholate (20 mM Tris-HCl [pH 7.6], 140 mM NaCl, 5 mM EDTA, 1 mM EGTA, 1% [v/v] NP-40, 0.5% [w/v] sodium deoxycholate supplemented with Complete protease inhibitor cocktail [Roche Diagnostics], and 1 mM PMSF). Cell lysates were collected, were homogenized in a Dounce homogenizer (Wheaton), and were centrifuged at 16,000 *g* for 15 min at 4°C. The pellet was resuspended in pelleting buffer (20 mM Tris-HCl [pH 8.0], 10 mM MgCl$_2$, and 1 mM PMSF) containing 250 U/ml benzonase nuclease (Novagen) and was incubated for 30 min at room temperature. After repelleting, the final pellets were washed in PBS containing 1 mM PMSF and then were resuspended in Laemmli's sample buffer,[24] in a volume that was equivalent to the supernatant. Supernatant and pellet fractions were then boiled for 5 min in
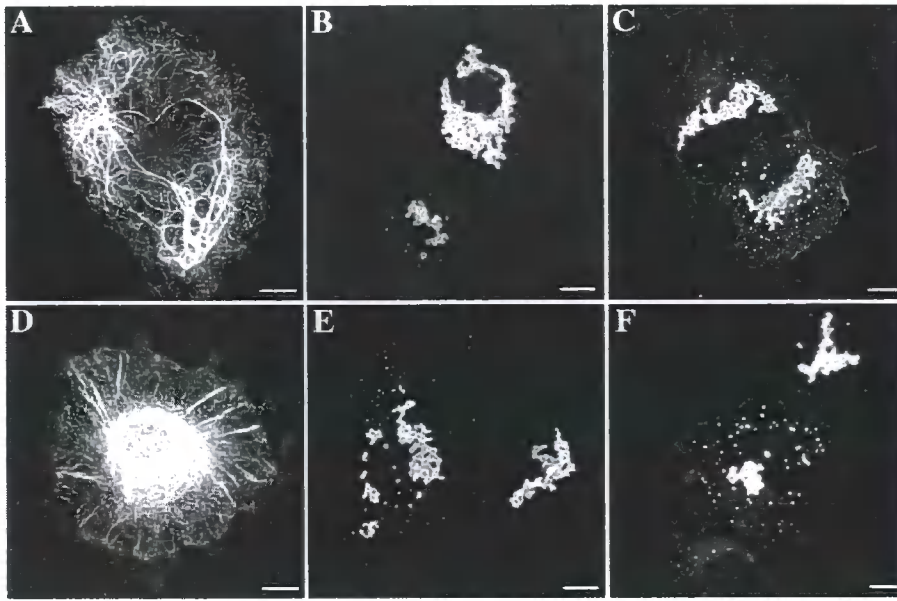
Figure 2. Effect of R416W and R239C mutations on the de novo GFAP IF network formation in IF-free cells. SW13/cl.2 (*A–C*) and primary astrocytes derived from GFAP/vimentin-null mice (*D-F*) were transiently transfected with either wild-type (*A* and *D*), R416W (*B* and *E*), or R239C (*C* and *F*) GFAP. At 48 h after transfection, the distribution of GFAP was assessed by confocal immunofluorescence microscopy with use of the rabbit polyclonal anti-GFAP antibody. When expressed in SW13/cl.2 cells, wild-type GFAP assembled into bundled filaments that extended throughout the cytoplasm (*A*). In contrast, cells transfected with either R416W (*B*) or R239C (*C*) GFAP-expression plasmids exhibited only GFAP-positive aggregates. In the IF-free mouse astrocytes, wild-type GFAP assembled into extended filaments at the cell periphery with some perinuclear accumulations (*D*), whereas R416W mutant GFAP formed punctuate aggregates scattered throughout the cytoplasm without any detectable filaments (*E*). Expression of R239C GFAP also induced numerous GFAP aggregates in the cytoplasm (*F*). For both R416W and R239C GFAP, all the transfected cells had aggregates. Bars = 10 μm.

Laemmli's sample buffer, and equal volumes were analyzed by SDS-PAGE and immunoblotting. Actin was used as a loading control for these samples.

Immunoblotting was performed using the semidry blotting method, according to the manufacturer's specifications (Bio-Rad Laboratories). After the blotting, protein-transfer efficiency was assessed by Ponceau S (Sigma) staining of the nitrocellulose membrane, followed by destaining in Tris-buffered saline (TBS; 20 mM Tris-HCl [pH 7.4], and 150 mM NaCl). Membranes were blocked for 2 h in blocking buffer containing 5% (w/v) BSA in either TTBS (TBS containing 0.2% [v/v] Tween 20) or PBST (5% [w/v] nonfat milk and 0.1% [v/v] Tween-20 in PBS) and were incubated for 2 h with mouse monoclonal anti-GFAP (GA-5), monoclonal anti-human GFAP (SMI-21), monoclonal anti-actin (AC-40 [Sigma]), or rabbit polyclonal anti-GFAP antibodies (3270) diluted by 1:5,000 in blocking buffer. In some experiments, the mouse monoclonal antibodies to the c-myc epitope (9E10, diluted by 1:100 in blocking buffer) were used to detect tagged ubiquitin after transfection. After several washes with TTBS, the membrane was incubated for 1 h with horseradish peroxidase–conjugated secondary antibodies (Dako) diluted by 1:2,000 in blocking buffer, followed by washing with TBS for 30 min. Antibody labeling was detected by enhanced chemiluminescence (ECL Plus [Amersham Biosciences]) with use of a luminescent image analyzer (LAS-1000plus [FujiFilm]). The strength of signal was quantified using the Image Gauge software (v. 4.0) (FujiFilm).

Immunoblotting of brain samples was performed using anon-

ymous, frozen tissues kindly provided by Drs. Jim Goldman and Goumei Tang (New York). The tissues were Dounce homogenized on ice in 10 mM Tris-HCl (pH 7.4), 2 mM β-mercaptoethanol, 0.1 M NaCl, 5 mM EDTA, and 1× protease inhibitor cocktail (Sigma) at a 10:1 (v/w) buffer:tissue ratio. The homogenate was centrifuged at 80,000 *g* for 1 h at 4°C, and the pellet was dissolved in ~15 volumes of the above buffer containing 2% (w/v) SDS. After determination of protein concentrations with the BCA reagent (Pierce), triplicate sets of 500-ng aliquots of each extract were run on a 10% (w/v) SDS-polyacrylamide gel, with 20-ng samples of purified recombinant wild-type and R416W GFAP. After transfer to Hybond ECL membranes (Amersham Pharmacia Biotech), the blots were probed with either anti-human GFAP monoclonal antibody SMI-21 (Sternberger Monoclonal) (1:2,000) or anti-R416W GFAP monoclonal antibodies 1A3 or 19.2 (1:1,000 dilution). Signals were detected by ECL (Amersham) and were visualized using a ChemImager 4400 (Alpha Innotech).

Results

Effect of R416W Mutation on In Vitro GFAP Assembly

In vitro assembly studies were performed to determine how the R416W mutation affects the structural properties of GFAP filaments. Purified recombinant wild-type and R416W GFAP, produced in *E. coli* with a pET-based expression system, were assembled in vitro by dialysis-based
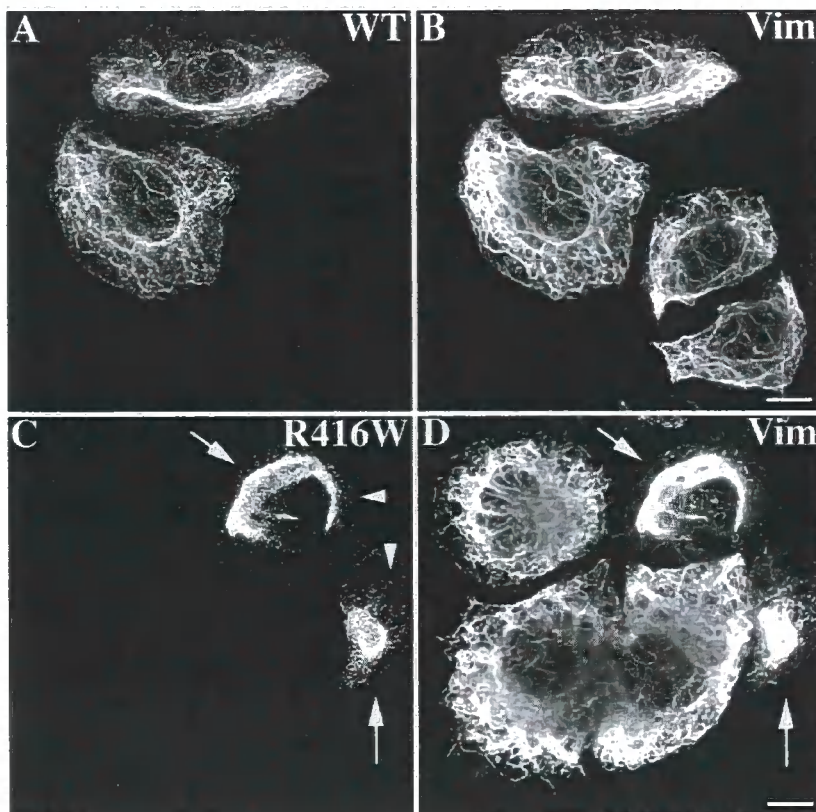
Figure 3. The network-forming abilities of the wild-type and R416W GFAP in SW13/cl.1 cells. SW13/cl.1 cells transiently transfected with either wild-type (A and B) or R416W (C and D) GFAP were fixed at 48 h after transfection and were processed for double-label confocal immunofluorescence microscopy. GFAP immunofluoresence is shown in panels A and C, whereas the counterstaining for vimentin is in panels B and D. Notice that wild-type GFAP (A) incorporated into endogenous vimentin (Vim) (B) networks, whereas this is not the case for R416W GFAP (C). Whereas some transfected cells exhibited one large inclusion with small aggregates at the cell periphery (*arrowheads* in C), other transfected cells displayed bundled filaments (*arrows* in C) that coaligned with the endogenous vimentin (*arrows* in D). Bars = 10 μm. (A color version of this figure is available in the online edition of the journal.)

assembly and were visualized by negative staining with uranyl acetate followed by electron microscopy. Whereas wild-type GFAP assembled into typical 10-nm filaments (fig. 1A), R416W GFAP on its own or in combination with mixtures of wild-type GFAP failed to form extended filaments (fig. 1B–1E). Instead, it formed short rod-like structures that looked like short filament pieces that had failed to elongate and compact properly into 10-nm filaments (fig. 1E). These had a strong tendency to laterally associate into aggregates (fig. 1D). Because the R416W mutation is heterozygous in patients with Alexander disease, we also assessed the assembly behavior of R416W mutant GFAP in the presence of increasing proportions of wild-type GFAP. At both 50:50 (fig. 1C) and 75:25 (fig. 1B) proportions of wild-type:R416W GFAP, normal filament assembly was disrupted, and aggregates similar to those made by R416W GFAP alone (fig. 1D) were formed instead. These data indicate that, in vitro, the R416W mutant GFAP acts in a

dominant manner over the wild-type protein. These data suggested that the assembled R416W GFAP filaments were prone to aggregation; therefore, we performed a low-speed centrifugation assay designed to monitor the extent of filament-filament interactions in the whole filament population.[32] With use of this assay, only approximately one-third of the wild-type GFAP was found in the supernatant fraction (fig. 1F; e.g., lanes 1 and 2). In contrast, when assembled on its own, nearly all of the R416W GFAP sedimented into the pellet fraction (fig. 1F; e.g., lanes 8 and 7). High-speed centrifugation assay confirmed that the wild-type GFAP had assembled efficiently, because >90% of the protein was sedimented under standard centrifugation conditions[24,27] (data not shown). Decreasing the proportion of mutant GFAP in mixtures with wild-type GFAP (fig. 1F; lanes 3–6) failed to markedly increase the proportion of soluble material. These data suggest that the R416W GFAP mutation promotes more interfilament in-
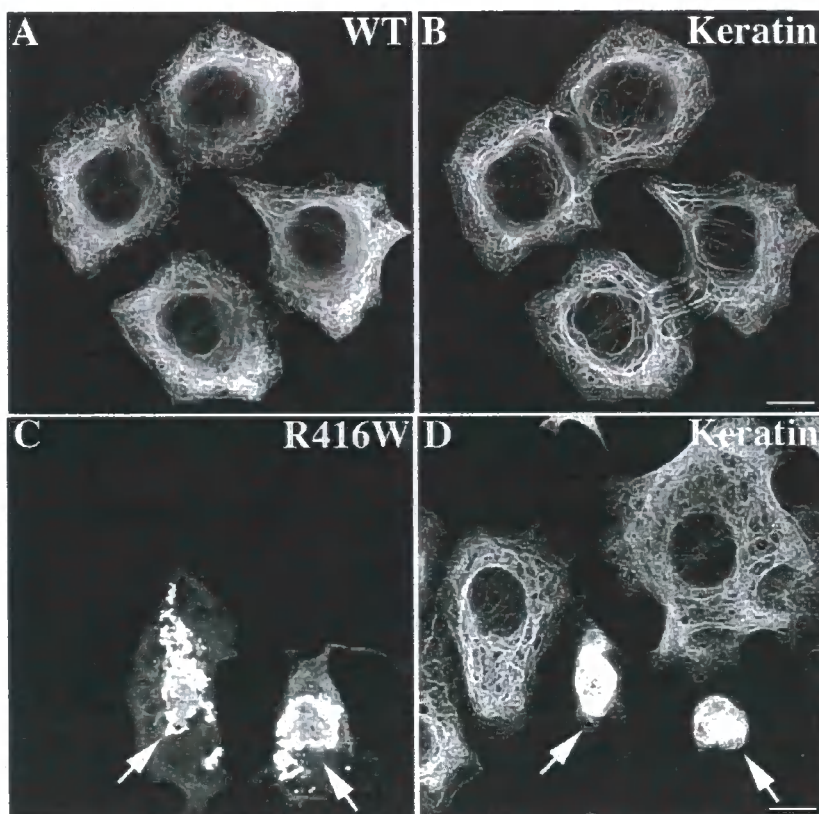
Figure 4. Expression of R416W mutant in MCF7 cells resulted in the formation of GFAP aggregates. MCF7 cells transfected with either wild-type (*A* and *B*) or R416W GFAP (*C* and *D*) were processed at 48 h after transfection for confocal double-label immunofluorescence microscopy with use of antibodies against GFAP (*A* and *C*) and keratin (*B* and *D*). When expressed in these cells, wild-type GFAP formed extended filaments as well as perinuclear filament bundles (*A*) that partially colocalized with keratin IF networks (*arrows* in *A* and *B*). In contrast, transfected cells expressing R416W GFAP exhibited large aggregates (*C*) that also cocollapsed the endogenous keratin IF networks (*arrows* in *C* and *D*). Bars = 10 μm. (A color version of this figure is available in the online edition of the journal.)

teractions and that this effect is again dominant over the wild-type protein.

Effect of R416W Mutation on GFAP Network Formation in Cells Lacking Endogenous GFAP

Transient transfection assays were used to investigate the effects of the R416W mutation on the formation of GFAP networks in a range of cell lines that have different IF compositions. To determine the effect of the R416W mutation on de novo IF network formation, we selected as the host cells the human adrenocarcinoma-derived SW13/cl.2 cell line, which does not contain any endogenous cytoplasmic IFs.[33] When expressed in SW13/cl.2 cells, wild-type GFAP formed filaments (fig. 2A), in agreement with previous studies.[34,35] In contrast, R416W GFAP failed to assemble into filaments but instead formed clusters of cytoplasmic aggregates (fig. 2B). Similar results were observed when wild-type (fig. 2D) and R416W plasmids (fig. 2E) were transiently transfected into primary astrocytes

derived from mice lacking GFAP and vimentin.[25] For comparison, R239C GFAP was also transfected into both these cell lines (fig. 2C and 2F), and, like R416W GFAP, it also formed numerous cytoplasmic aggregates when the cytomegalovirus promoter was used to drive mutant GFAP expression. Previous studies have already established that the R239C mutation in GFAP makes the filaments more stable and changes the organization of GFAP networks in transfected cells. Taken together, these data suggest that the R416W mutation, like the R239C mutation, affects the ability of GFAP to self-assemble into an extended filament network in IF-free primary cells and that this deficiency is independent of the cellular background.

Recent studies have revealed that two or more IF proteins are required for the formation of most normal IF networks in vivo, including those formed by the type III IF proteins GFAP, desmin, and vimentin. For instance, desmin requires paranemin to produce an extended IF network in nonmuscle-derived cell lines.[35] Vimentin requires

GFAP to form filaments in astrocytes,[46] whereas, in other cell types, vimentin coassembles with nestin.[47] Whereas GFAP is able to self-assemble into IFs within astrocytes lacking vimentin, vimentin is required for the correct spacing of the assembled filaments.[16] Therefore, it is important to assess the assembly behavior of GFAP in cells containing this key assembly partner.

For these experiments, SW13/cl.1 cells that express vimentin IFs were selected for transient transfection studies. In this cell line, wild-type GFAP assembled into filamentous networks (fig. 3A) that colocalized with the endogenous vimentin IFs (fig. 3B). In contrast, most of the cells transfected with R416W GFAP contained large aggregates (fig. 3C; arrows) with small clumps at the cell periphery (fig. 3C; arrowheads). These aggregates disrupted the endogenous vimentin IF networks, usually causing them to collapse into a large perinuclear aggregate (Fig. 3D; arrows).

The finding that R416W GFAP caused the collapse of the endogenous vimentin IF network led us to examine its effects on keratin networks, IF proteins that do not coassemble with GFAP. For these experiments, we used a human breast cancer epithelial MCF7 cell line that expresses only keratin IF proteins (K8, K18, and K19).[38] When transfected into this cell line, wild-type GFAP assembled into filaments that tended to bundle in most of the transfected cells (fig. 4A). The GFAP filament networks were found to partially coalign with the keratin IF networks (fig. 4B; arrows), which is consistent with previous observations.[22,27] In contrast, nearly all MCF cells expressing R416W mutant GFAP formed aggregates (fig. 4C; arrows) that often collapsed the endogenous keratin IF networks (fig. 4D; arrows). These results suggest that the R416W mutation not only impaired the ability of GFAP to form normal IF network but also revealed a dominant effect on endogenous keratin filament networks in the absence of any obvious coassembly.

The relative expression levels and solubility of the wild-type and the R416W GFAP were determined by immunoblotting of extracts from MCF7 cells prepared using a mild lysis buffer protocol. Analysis of both supernatant and pellet fractions revealed no endogenous GFAP expressed in nontransfected MCF7 cells (fig. 5A; lanes 1 and 2). In contrast, cells transfected with either wild-type (fig. 5A; lanes 3 and 4) or R416W (fig. 5A; lanes 5 and 6) GFAP generated proteins of the expected size at comparable levels, suggesting that aggregate formation is likely due to the mutation per se rather than elevated expression levels. Although a small fraction of wild-type GFAP remained in the supernatant fraction (fig. 5A; lane 3), R416W GFAP was found exclusively in the pellet fraction (fig. 5A; lane 6), consistent with its sequestration into cytoplasmic aggregates. Equal loading for the various supernatant and pellet fractions was verified using an anti-actin antibody (fig. 5B).
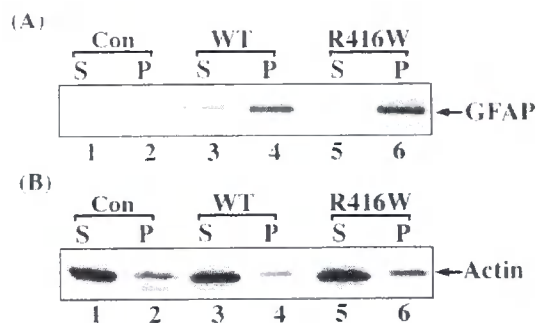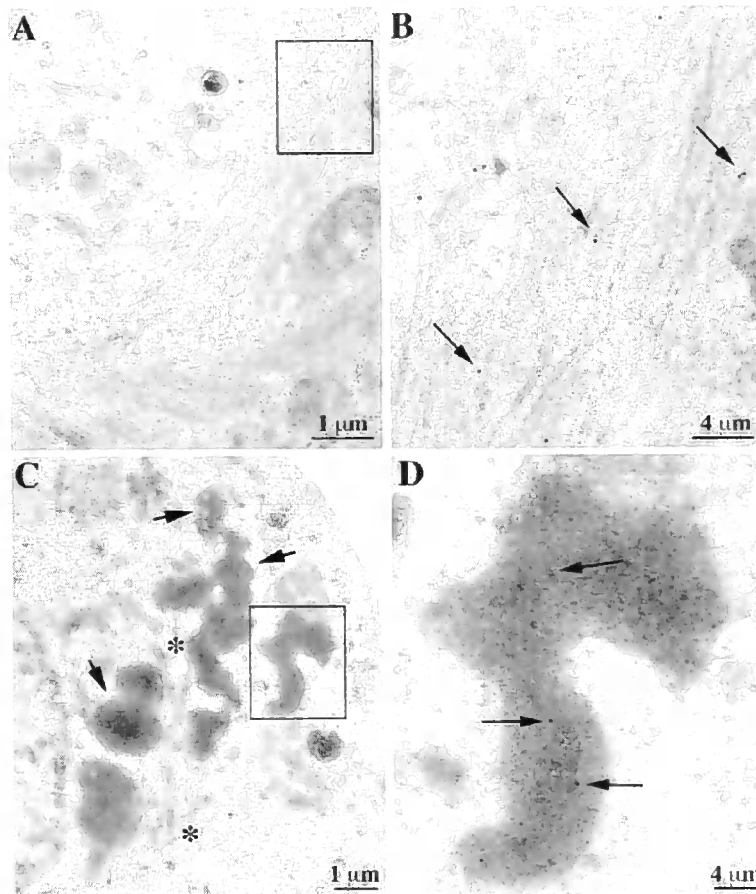

Figure 5. Analysis of wild-type and R416W GFAP expression in transfected MCF7 cells by immunoblotting. MCF7 cells were transfected with either wild-type (*lanes 3* and *4*) or R416W GFAP (*lanes 5* and *6*). Untransfected cells were used as a control (*lanes 1* and *2*). At 48 h after transfection, cells were collected, lysed with MEB, and centrifuged at 18,000 *g* for 15 min at 4°C. The resulting supernatant (S) and pellet (P) fractions were analyzed by SDS-PAGE, followed by immunoblotting using anti-GFAP (*A*) and anti-actin (*B*) antibodies. The blots were developed by the ECL system. Notice that, after transfection into MCF7 cells, both wild-type and mutant GFAP expressed at comparable levels, although proteolyzed GFAP fragments with slightly higher electrophoretic mobilities were also detected. Most of the wild-type GFAP was detected in the pellet fraction (*A, lane 4*) with a small proportion that remained soluble (*A, lane 3*), whereas the R416W GFAP was found exclusively in the pellet fraction (*A, lane 6*). Equal loading of each supernatant and pellet fractions was confirmed by probing with anti-actin antibody (*B*).

Analysis of R416W GFAP Aggregates in MCF7 Cells by Electron Microscopy

The high transfection efficiency of both wild-type and R416W GFAP in MCF7 cells allowed us to further analyze the ultrastructural organization of GFAP by immunoelectron microscopy. MCF7 cells transfected with plasmids expressing either the wild-type or the R416W GFAP were processed for immunogold labeling with anti-GFAP antibodies followed by protein A conjugated with 5-nm gold particles. In cells expressing wild-type GFAP, fibrous regions consisting of 10-nm filaments were observed (fig. 6A and 6B). These filaments were organized into bundles that traversed the cytoplasm (fig. 6A). At a higher magnification, individual filaments were decorated with gold particles (fig. 6B; arrows), confirming the presence of GFAP in these filaments. In contrast, cells expressing R416W GFAP displayed electron-dense aggregates, distributed throughout the cytoplasm (fig. 6C; arrows), that were often accompanied by IFs (fig. 6C; asterisks). At a higher magnification, these electron-dense aggregates appear as amorphous membrane-free structures composed of aggregated GFAP, as evidenced by the presence of gold particles (fig. 6D; arrows).

Figure 6. Ultrastructural analysis of wild-type and R416W GFAP in MCF7 cells by immunoelectron microscopy. MCF7 cells transfected with either wild-type (*A* and *B*) or R416W (*C* and *D*) GFAP were processed at 48 h after transfection for immunogold labeling, as described in the "Material and Methods" section. Immunogold labeling of ultrathin sections was stained and visualized by a transmission electron microscope. Wild-type GFAP assembled into filaments that were organized into parallel bundles (*A*). In contrast, cells expressing the R416W mutant formed membrane-free irregular-shaped structures composed of electron-dense aggregates at the perinuclear region (*C*), often in association with IFs (*asterisks* [*] in *C*). Panels B and D are higher magnification views of the boxed areas of panels A and C, respectively, showing that both the filaments (*B*) and aggregates (*D*) were decorated with 5-nm gold particles (*arrows* in *B* and *D*), confirming the identity of GFAP.

Effects of R416W GFAP on Endogenous GFAP Networks in Primary Astrocytes

The assembly behavior of R416W GFAP was also examined in mouse primary astrocytes, to test the effects of endogenous wild-type GFAP and vimentin IFs on the aggregation process. The distribution of transfected GFAP in relation to the endogenous GFAP was visualized by double-label immunofluorescence microscopy with use of monoclonal antibody SMI-21 (fig. 7*A* and 7*C*), which specifically recognizes human GFAP, and polyclonal anti-panGFAP antibody, which recognizes both the endogenous mouse GFAP and the transfected human GFAP (fig. 7*B* and 7*D*). Mouse astrocytes transiently transfected with wild-type GFAP mainly formed filaments (fig. 7*A*) that colocalized with the endogenous GFAP network (fig. 7*B*; arrows). In contrast, the effects of R416W GFAP expression in astrocytes were similar to those observed for the vimentin-containing SW13/cl.1 cells. Most of the transfected cells contained cytoplasmic aggregates with smaller particles at the cell periphery (fig. 7*C*), which colocalized with collapsed endogenous GFAP networks (fig. 7*C* and 7*D*; arrows). In some transfected cells, however, expressed R416W GFAP was incorporated into the endogenous GFAP networks without any apparent changes (fig. 7*C* and 7*D*; cell on the right). Careful examination revealed that there were small aggregates intermingled with the filaments (fig. 7*D*; arrowheads), which were immunopositive for the human R416W GFAP, indicative of perhaps an early change in the
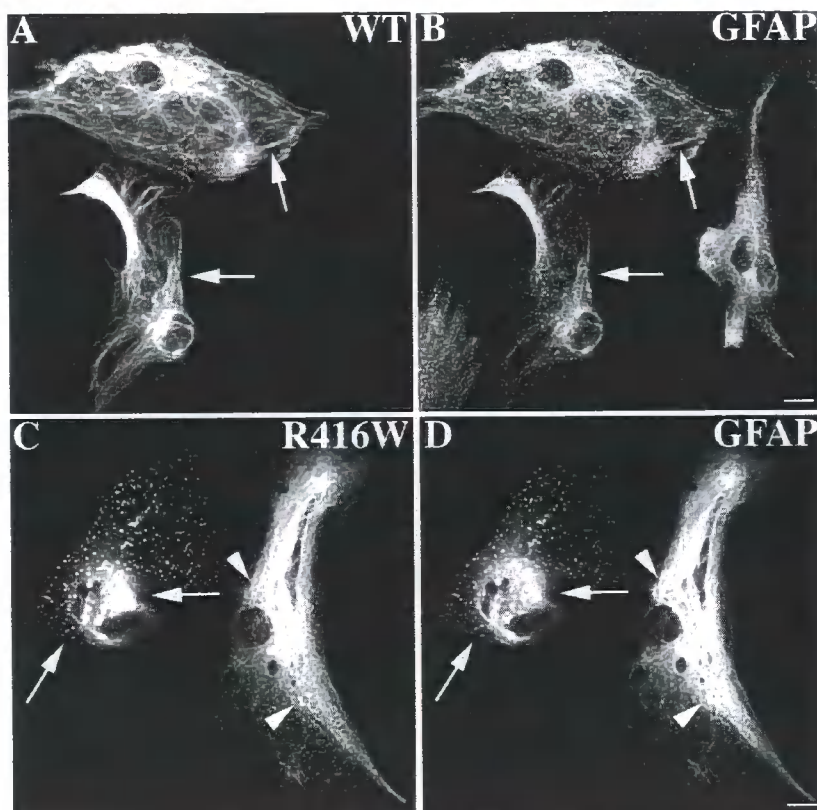
Figure 7. Transient expression of wild-type or R416W GFAP in primary mouse astrocytes. Primary mouse astrocytes were transfected with either human wild-type (*A* and *B*) or R416W (*C* and *D*) GFAP. At 48 h after transfection, cells were processed for double-label immunofluoresence microscopy with use of anti-human GFAP monoclonal antibody (SMI-21) and anti-panGFAP polyclonal antibodies (3270). When expressed in mouse primary astrocytes, wild-type GFAP formed filaments (*arrows* in *A*) that colocalized with the endogenous mouse GFAP (*arrows* in *B*). The expression of human R416W GFAP resulted in both filamentous (*arrowheads* in *C*) and aggregate staining patterns (*arrows* in *C*), which also costained with the endogenous mouse GFAP (*arrows* and *arrowheads*, respectively, in *D*). Bars = 10 μm. (A color version of this figure is available in the online edition of the journal.)

organization of the GFAP filaments preceding the eventual collapse of the network.

Detection of R416W GFAP in Alexander Disease Brain with Mutant-Specific Monoclonal Antibodies

The amino acid sequences of mouse and human GFAP are highly homologous, with 91% identity and 95% similarity,[39] but species differences could influence the assembly properties of the mutant human R416W GFAP in mouse astrocytes. To follow the fate of the human R416W GFAP in the presence of the endogenous wild-type human GFAP, we sought to develop mouse monoclonal antibodies that specifically recognized human R416W GFAP but not wild-type GFAP, and vice versa (see the "Material and Methods" section for details). The immunogen specific for the wild type failed to elicit any GFAP monoclonal antibodies. The R416W GFAP peptide, however, yielded two monoclonal antibodies, 19.2 and 1A3, that recognized R416W GFAP

but not wild-type GFAP, as judged by immunoblots of purified, recombinant proteins (fig. 8*A*). In addition, neither of these monoclonal antibodies crossreacted with a lysate from a normal brain or with a lysate from a brain containing another GFAP mutation commonly associated with Alexander disease, R239C, and both produced signals from lysates of R416W brain that were nearly identical to those of the control SMI-21 monoclonal antibody (fig. 8*A*). Suitability for immunohistochemistry was demonstrated by immunostaining SW13/cl2 cells transfected with vectors expressing either the mutant R416W or wild-type protein (data not shown).

The R416W GFAP–specific monoclonal antibodies then allowed us to determine whether R416W GFAP incorporated into Rosenthal fibers, normal-appearing filaments, or both. Staining of normal, control brain was first tested as a negative control. Control brain was readily stained by a standard, GFAP polyclonal antibody (fig. 8*B*), but no
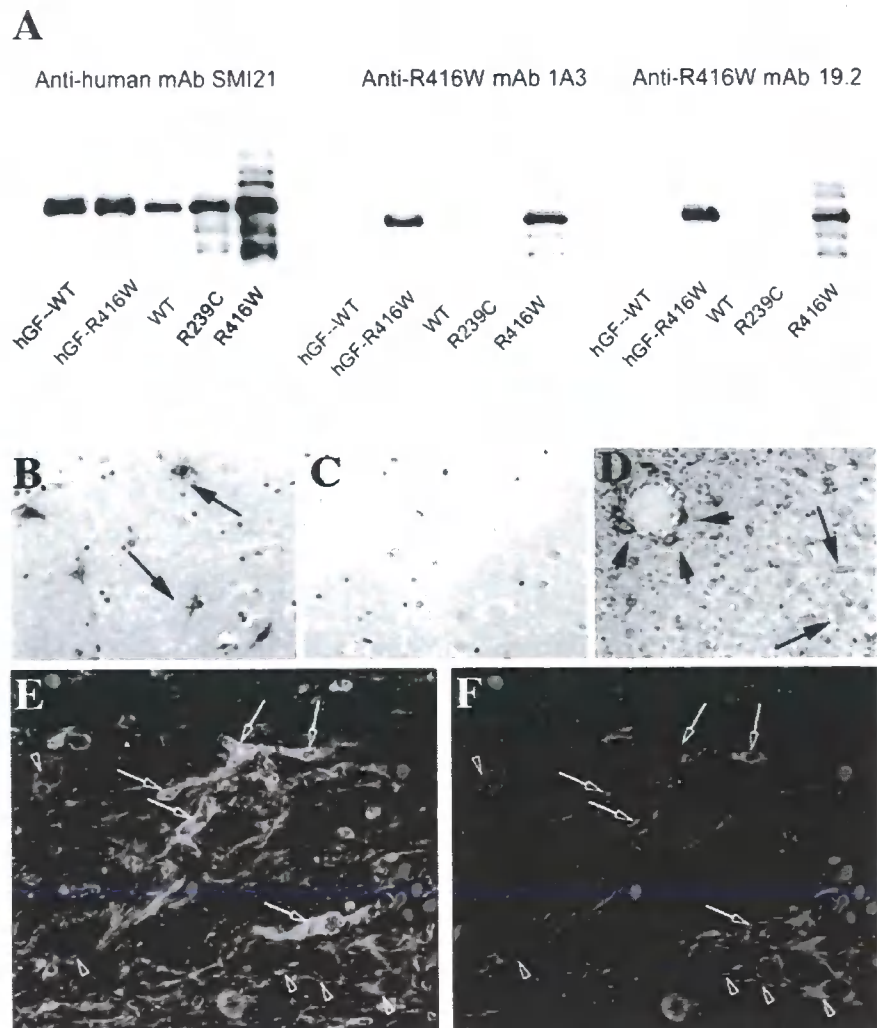
Figure 8. Characterization of R416W GFAP-specific antibodies and demonstration of its presence in Rosenthal fibers. *A,* Immunoblots, performed as described in the "Material and Methods" section, with use of purified, recombinant human wild-type (hGF-WT) and R416W (hGF-R416W) GFAP and lysates from brain samples taken from either control human (WT) or patients with Alexander disease that harbor either an R239C mutation (R239C) or an R416W mutation (R416W) in GFAP. The general anti-human GFAP monoclonal antibody (SMI-21) reacts with all samples, whereas the anti-R416W monoclonal antibodies (1A3 and 19.2) produce signals from R416W-containing samples only, with the pattern for the R416W patient lysate identical to that of SMI-21. The identity of the immunopositive bands above and below the prominent GFAP-positive band are as yet unknown. The lower bands most likely correspond to degradation products, since these are normally seen in control brain samples. The upper bands are common to both the R239C and R416W samples, suggesting these are a common feature of Alexander disease pathology, but, as yet, the reason for their slower electrophoretic mobility is unknown. Panels B and C are striatum in a control (normal) brain stained with standard polyclonal GFAP antibody (*B*) and by R416W monoclonal antibody 19.2 (*C*). Note that the R416W antibody does not crossreact with normal human brain tissue. Panels D–F are brain sections from a patient with the R416W GFAP mutation that are stained with the monoclonal 19.2 antibody and then are visualized by either peroxidase- (*D*) or rhodamine-tagged secondary antibodies (*F*) or are stained with the rabbit polyclonal GFAP antibody (Dako) and then are detected with FITC-tagged secondary antibodies (*E*). Nuclei are counterstained with Hoechst 33258 (*E* and *F* [see the "Material and Methods" section for procedure details]) to assist comparison of the panels E and F. Numerous Rosenthal fibers are stained around their periphery (*arrows* in *E* and *F*), a feature often reported for these aggregates (e.g., the work of Tomokane et al.[6]). Normal-looking GFAP filaments are also stained by the R416W-specific mAb (*arrowheads* in *F*) and can be detected by the diffuse staining in other parts of the section.

signal was produced with the R416W antibody (fig. 8C), confirming the immunoblot results that the R416W antibody does not crossreact with normal human brain GFAP. On the other hand, the R416W antibody strongly stained brain from a patient with Alexander disease who harbored an R416W mutation, with use of either peroxidase (fig. 8D) or fluorescent (fig. 8F) detection methods. This staining was apparent both along the periphery of the Rosenthal fibers and in normal-appearing filaments (fig. 8F) and largely colocalized with staining of total GFAP (fig. 8E). These data confirm the specificity of the R416W antibodies produced. Importantly, they also demonstrate, for the first time, that the mutant protein is stably expressed in patients with the R416W mutation and that it is incorporated into both filaments and Rosenthal fibers.

Assembly Properties of Mutant GFAP Expressed in Human Cells Containing Endogenous GFAP Filament Networks

These R416W GFAP-specific monoclonal antibodies also permitted us to follow the fate of R416W GFAP when transiently expressed in human astrocytoma U343MG cells. This cell system would be expected to better mimic the scenario of R416W GFAP being expressed in a human astrocyte cell background and removes potential species conflicts. In this model system, R416W GFAP induced the formation of GFAP-rich aggregates (fig. 9A and 9B; arrows). These data show that R416W GFAP is capable of disrupting the endogenous networks of wild-type GFAP filaments within the context of a human astrocytoma cell line and once again demonstrate the dominant negative potential of the mutant R416W GFAP on the endogenous IFs.

Similarities between the R416W-Induced Aggregates in Transfected Cells and Rosenthal Fibers

In previous studies of Alexander disease pathology, several other proteins were found to associate with Rosenthal fibers, including the small heat shock proteins (sHSPs) αB-crystallin[6] and HSP27.[40] We investigated whether these proteins would associate with the aggregates of R416W GFAP formed in the U343MG astrocytoma cells (fig. 9C–9F). Both αB-crystallin (fig. 9D; arrows) and HSP27 (fig. 9F; arrows) colocalized with the GFAP-containing aggregates in these cells (fig. 9C and 9E, respectively; arrows). Rosenthal fibers are also ubiquitinated.[6] That the GFAP aggregates in transfected cells are also ubiquitinated was demonstrated by cotransfection of His$_6$-myc tagged ubiquitin[26] along with R416W GFAP into the human astrocytoma cells (fig. 9G and 9H; arrows). Thus, the aggregates formed by R416W GFAP in the transiently transfected human astrocytoma cells have many features reported elsewhere and expected for Rosenthal fibers.[41]

To obtain biochemical evidence of the similarities between the Rosenthal fibers in patients and the R416W GFAP aggregates formed in the transfected U343MG cells, we extracted the cells and monitored the solubility of the GFAP and the associated protein chaperones (fig. 9I). With use of an extraction buffer containing deoxycholate, wild-type GFAP was almost completely extracted from both the untransfected (fig. 9I; Mock) and wild-type GFAP transfected cells (fig. 9I; WT), conditions that also extracted αB-crystallin, HSP27, and HSP70 (fig. 9I; Mock and WT). In contrast, R416W GFAP remained entirely in the pellet fraction of the extracted cells that had been transiently transfected with R416W GFAP (fig. 9I; R416W). Interestingly, when the immunoblots of the supernatant and pellet fractions were also probed with antibodies to αB-crystallin (fig. 9I; αB-cry), HSP27 (fig. 9I; HSP27), and HSP70 (fig. 9I; HSP70), a significant proportion of both αB-crystallin and HSP27—but not HSP70—remained in the pellet fractions of R416W GFAP–transfected cells (fig. 9I; R416W). These data show that a proportion of both sHSPs is associated with the insoluble R416W GFAP. Since HSP70[27] was completely extracted from the R416W GFAP–transfected cells under these conditions (fig. 9I; HSP70), the association of the sHSPs with R416W GFAP is specific and not a general property for all protein chaperones.

Discussion

The R416W Mutation in GFAP: A Dominant Mutation That Affects Interfilament Interactions

In this study, we investigated the properties of the common Alexander disease–causing R416W GFAP mutation to obtain insights into the initial stages of the disease process. We demonstrated that this R416W GFAP mutation dramatically alters assembly, both in vitro and in transfected cells (figs. 1, 2, 4, 7, and 9), and does so in a dominant manner. The mutant protein can also disturb endogenous IF networks in cultured cells, including those of vimentin (fig. 3D), keratin (fig. 4), and GFAP (figs. 7 and 9A). The effects of R416W GFAP are different in several respects from those of R239C, the only other Alexander disease–causing mutation that has been studied in detail.[21] When assembled in vitro, the R239C mutant formed IFs that appeared indistinguishable from wild-type filaments,[21] whereas the R416W GFAP formed short filament intermediates that associated laterally (fig. 1). Despite this difference, we show here that both the R239C and the R416W GFAP form aggregates when expressed in either the vimentin-negative SW13/cl.2 cell line or the primary mouse astrocytes lacking both vimentin and GFAP (fig. 2), confirming some of the results in a previous study.[21] When R239C GFAP was transiently expressed in primary rat astrocytes, however, its assembly properties were not radically different from those of transiently expressed wild-type GFAP.[21] In contrast, we found that the R416W mutant invariably formed aggregates when transiently overexpressed in several different cell lines, including primary mouse astrocytes (figs. 2 and 7) and human astrocytoma cells (fig. 9B). Despite these differences, both mutations were found to increase the resistance of GFAP to extraction (figs. 5 and 9I).[21] Taken together, these data indicate that, whereas the immediate structural consequences of differ-
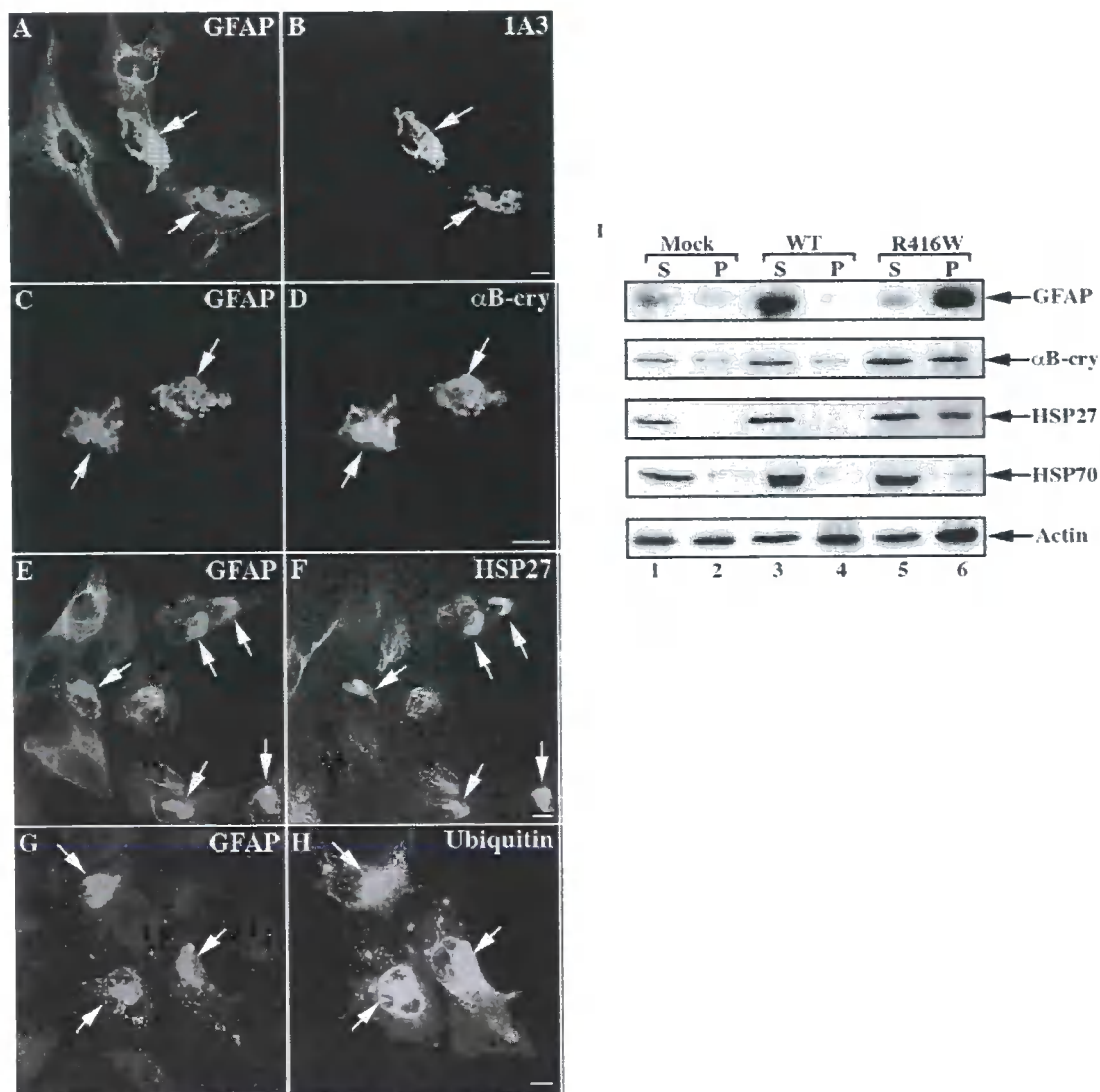
Figure 9. The similarity between Rosenthal fibers and GFAP aggregates formed in transfected human astrocytoma cells. U343MG cells were transiently transfected with R416W GFAP and were routinely stained with rabbit polyclonal antibodies (3270) to GFAP (*A, C, E,* and *G*) and then were double stained with mouse monoclonal antibodies specific to R416W GFAP (*B*), αB-crystallin (αB-cry) (*D*), or HSP27 (*F*). Notice that the GFAP containing aggregates are also positive for both αB-crystallin and HSP27 (*arrows* in *C–F*). To demonstrate the presence of ubiquitin in the GFAP aggregates, cells were cotransfected with His$_6$-myc ubiquitin as well as R416W GFAP and then were stained with rabbit polyclonal antibodies to GFAP (*G*) and the mouse monoclonal antibodies that recognize the myc epitope (*H*), showing that the GFAP aggregates contain ubiquitin. Bars = 10 μm. *I*, Wild-type and R416W GFAP (R416W) were transiently expressed in the human astrocyte cell line U343MG, and supernatant (S) and pellet (P) fractions were prepared from these culture and were compared with mock transfected cells. Cell fractionation used HEB, which almost completely solubilized wild-type GFAP. R416W GFAP, on the other hand, remained in the pellet fraction. Immunoblots of the cell fractions were probed with antibodies to GFAP, αB-crystallin, HSP27, HSP70, and finally actin, which was used as a loading control. Notice that, when cells were transfected with R416W GFAP, a significant proportion of the HSP27 and αB-crystallin but not HSP70 remained in the pellet fraction along with the R416W GFAP. Both the sHSPs and R416W GFAP were more resistant to extraction compared with these proteins in the wild-type GFAP transfected cells. (A color version of this figure is available in the online edition of the journal.)

ent GFAP mutations are likely to differ, as has been found for other intermediate filament proteins,[10,42,43] there will likely be common consequences that lead to Alexander disease.

## The RDG-Containing Motif and Its Role in Filament Assembly

The R416W mutation lies within the RDG motif that is conserved within the tail domain of nearly all of the type III IF proteins. Previous studies of GFAP had concluded that the RDG motif was important to filament assembly, but only in the context of the rest of the C-terminal domain.[44] Our assembly data, presented here, show that changing the precise sequence of this motif to WDG does have dramatic effects on GFAP assembly (figs. 1 and 2). Change of the equivalent arginine (R449) to proline in vimentin also severely disrupted the in vitro assembly and network formation in transiently transfected cells.[45] These combined data suggest that this arginine residue in the RDG motif within the C-terminal domain is very important for the assembly IF proteins with the motif.

Previous studies proposed that the C-terminal domain associates intramolecularly with the C-terminal end of the rod domain.[46] Crystallization of the helix IIB rod domain suggests that the two α helices fold away from the dimer axis,[17] which is consistent with the hypothesis that the C-terminal domain could form a surface-exposed loop structure and prevent inappropriate subunit interactions in the self-assembly process.[46] This offers an explanation of the altered width of vimentin filaments assembled from tail-truncated and deleted forms of vimentin[47] and the changed in vitro assembly characteristics of the R416W GFAP we report here (fig. 1).

Our studies also suggest that the RDG motif will contribute to interfilament interactions as well as subunit organization within the IF. We have demonstrated the increased tendency of R416W GFAP to aggregate in vitro (fig. 1) as well as in transfected cells (figs. 2, 4, 7, and 9). Studies of keratins also show that the C-terminal domain is very important in promoting filament-filament interactions.[48–50] Together with our data presented here, a consensus is thus beginning to emerge that C-terminal sequences of cytoplasmic IFs help regulate both intra- and interfilament associations.

The Mutant R416W GFAP: A Component of Rosenthal Fibers

The presence of Rosenthal fibers has been documented in two cases of Alexander disease caused by the R416W GFAP mutation.[6,9,51] For one of these cases, we show, for the first time for any Alexander disease case, that the mutant GFAP is present as the defining histopathological feature (fig. 8D and 8F). This is also the first time for any IF-based human disease that the link between the presence of the mutated protein and a characteristic histopathogical IF aggregate has been rigorously shown. In a case of epidermolysis bul-
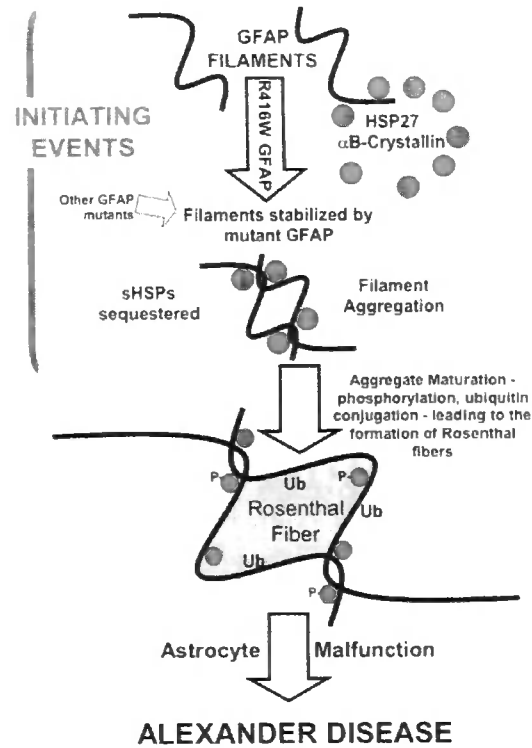
Figure 10. GFAP aggregation caused by the R416W mutation induces sHSP association and the association of ubiquitin as early events in the etiology of Alexander disease. The presence of the R416W GFAP mutation decreases the solubility of the GFAP filaments, probably by altering the filament-filament interactions in a manner that encourages aggregation. This is accompanied by the sequestration of the sHSP protein chaperones—αB-crystallin and HSP27 (*shaded circles*)—and GFAP into aggregates. Both proteins also localize to Rosenthal fibers, which also contain ubiquitin (Ub). The filament aggregates undergo a maturing process, with the additional posttranslational modification of integral components, such as the phosphorylation[64] and ubiquitination[8] of αB-crystallin to form the Rosenthal fibers. The model is not exclusive to R416W GFAP, since Rosenthal fibers are a characteristic diagnostic feature of Alexander disease.[12] Other GFAP mutations differ in the details of the mechanism by which they produce aberrant filament-filament interactions leading to the formation of stabilized aggregates, but, once formed, they then follow a common pathway to Rosenthal fiber formation. Increased GFAP filament stability and the specific association of sHSPs are predicted to be the earliest events in the development of Alexander disease. (A color version of this figure is available in the online edition of the journal.)

losa simplex, a keratin-blistering disease, the loss of an epitope was used to confirm the genotype of patients,[52] but this reagent was unable to demonstrate the presence of the mutant keratin 5 in the aggregates found in keratinocytes. Another study described the generation of a polyclonal antibody specific for a keratin 8 variant (R340H), which may predispose carriers to liver disease,[53] but these

antibodies were used only for immunblotting studies. Even in the case of Mallory bodies formed as a result of alcoholic hepatitis, where antibodies were developed that selectively stained the Mallory bodies and not the surrounding keratin filaments, the antibodies still detected wild-type keratins.[54] Our antibody reagents are therefore the first to specifically identify a mutant missense IF protein in the presence of its wild-type counterpart. These antibodies allowed us to demonstrate that the mutant protein is a component of Rosenthal fibers in human patient brain tissue (fig. 8D and 8F) and also in GFAP-containing aggregates of transfected human astrocytoma cells (fig. 9B).

Association of αB-Crystallin and HSP27 with R416W GFAP Aggregates

We also discovered that the protein chaperones αB-crystallin and HSP27 specifically associate with the GFAP aggregates that are formed in transfected cells that express R416W GFAP. Both chaperones are components of Rosenthal fibers found in patients, including those with the R416W mutation.[6,40] These chaperones normally minimize filament-filament associations,[27] and their overexpression can dissolve accumulations of wild-type GFAP filaments.[55] Their presence, however, in both brain astrocytes of patients with Alexander disease and in cultured cells does not prevent the changes in GFAP-filament solubility, filament aggregation, or the formation of Rosenthal fibers by R416W GFAP. The association of HSP27 and αB-crystallin with R416W GFAP and resistance to extraction is likely due to the altered filament properties induced by this mutation. Although other stresses have been shown to stimulate the association of both HSP27 and αB-crystallin with GFAP filaments,[27,40] those studies involved wild-type proteins. Our data show that it is specifically the presence of the R416W GFAP, and not wild-type GFAP, that both stabilizes GFAP and leads to the sequestration of sHSPs (figs. 9C–9F and 9I).

The sequestration of HSP27 and αB-crystallin could potentially compromise the astrocyte stress response and therefore contribute to the initiation of Alexander disease. For example, it has already been shown that either the reduction of HSP27 or the loss of αB-crystallin compromises cytoskeletal integrity and function[56] or induces muscular atrophy,[57] respectively. HSP27 is a key protein in protecting cells, including neurons,[58] against apoptosis by inhibiting caspase activity[59] and preserving mitochondrial function.[60] HSP27 has also been implicated in regulating the stress response through the ubiquitin-mediated proteosomal regulation of the key transcription factor, NFκB.[61] Importantly, HSP27 protects cells against other protein aggregation–based diseases caused by huntingtin[62] and α-synuclein.[63] Such studies identify diminution of sHSP levels as a potential Achilles' heel in the cellular response to protein aggregate–based diseases that require either upregulation[58] or overexpression[63] to ameliorate the disease phenotype. These observations suggest that the early sequestration of sHSPs into GFAP aggregates (this study) and Rosenthal fibers[6] is a key event at the onset of Alexander disease. Figure 10 incorporates these ideas into a diagram of the events that we believe to be important in the early stages of Alexander disease.

Web Resources

The accession number and URLs for data presented herein are as follows:

Alexander Disease Web site, http://www.waisman.wisc.edu/alexander/home.htmlx
GenBank, http://www.ncbi.nlm.nih.gov/Genbank/ (for GFAP [accession number J04569])
Intermediate Filament Disease Mutation Database, http://www.interfil.org/
Online Mendelian Inheritance in Man (OMIM), http://www.ncbi.nlm.nih.gov/Omim/ (for Alexander disease)

References

1. Alexander WS (1949) Progressive fibrinoid degeneration of fibrillary astrocytes associated with mental retardation in a hydrocephalic infant. Brain 72:373–381
2. Russo LS Jr, Aron A, Anderson PJ (1976) Alexander's disease: a report and reappraisal. Neurology 26:607–614
3. Neal JW, Cave EM, Singhrao SK, Cole G, Wallace SJ (1992) Alexander's disease in infancy and childhood: a report of two cases. Acta Neuropathol (Berl) 84:322–327
4. Deprez M, D'Hooghe M, Misson JP, de Leval L, Ceuterick C, Reznik M, Martin JJ, D'Hooge M (1999) Infantile and juvenile presentations of Alexander's disease: a report of two cases. Acta Neurol Scand 99:158–165
5. Rodriguez D, Gauthier F, Bertini E, Bugiani M, Brenner M, N'Guyen S, Goizet C, Gelot A, Surtees R, Pedespan J-M, Hernandorena X, Troncoso M, Uziel G, Messing A, Ponsot G, Pham-Dinh D, Dautigny A, Boespflug-Tanguy O (2001) Infantile Alexander disease: spectrum of GFAP mutations and genotype-phenotype correlation. Am J Hum Genet 69:1134–1140
6. Tomokane N, Iwaki T, Tateishi J, Iwaki A, Goldman JE (1991) Rosenthal fibers share epitopes with alpha B-crystallin, glial fibrillary acidic protein, and ubiquitin, but not with vimen-

tin: immunoelectron microscopy with colloidal gold. Am J Pathol 138:875–885

7. Johnson AB, Bettica A (1989) On-grid immunogold labeling of glial intermediate filaments in epoxy-embedded tissue. Am J Anat 185:335–341

8. Head MW, Corbin E, Goldman JE (1993) Overexpression and abnormal modification of the stress proteins alpha B-crystallin and HSP27 in Alexander disease. Am J Pathol 143:1743–1753

9. Brenner M, Johnson AB, Boespflug-Tanguy O, Rodriguez D, Goldman JE, Messing A (2001) Mutations in GFAP, encoding glial fibrillary acidic protein, are associated with Alexander disease. Nat Genet 27:117–120

10. Omary MB, Coulombe PA, McLean WH (2004) Intermediate filament proteins and their associated diseases. N Engl J Med 351:2087–2100

11. McLean WH, Smith FJ, Cassidy AJ (2005) Insights into genotype-phenotype correlation in pachyonychia congenita from the human intermediate filament mutation database. J Investig Dermatol Symp Proc 10:31–36

12. Li R, Johnson AB, Salomons G, Goldman JE, Naidu S, Quinlan R, Cree B, Ruyle SZ, Banwell B, D'Hooghe M, Siebert JR, Rolf CM, Cox H, Reddy A, Gutierrez-Solana LG, Collins A, Weller RO, Messing A, van der Knaap MS, Brenner M (2005) Glial fibrillary acidic protein mutations in infantile, juvenile, and adult forms of Alexander disease. Ann Neurol 57:310–326

13. Li R, Johnson AB, Salomons GS, van der Knaap MS, Rodriguez D, Boespflug-Tanguy O, Gorospe JR, Goldman JE, Messing A, Brenner M (2006) Propensity for paternal inheritance of de novo mutations in Alexander disease. Hum Genet 119:137–144

14. Herrmann H, Aebi U (2000) Intermediate filaments and their associates: multi-talented structural elements specifying cytoarchitecture and cytodynamics. Curr Opin Cell Biol 12:79–90

15. Herrmann H, Aebi U (2004) Intermediate filaments: molecular structure, assembly mechanism, and integration into functionally distinct intracellular scaffolds. Annu Rev Biochem 73:749–789

16. Strelkov SV, Herrmann H, Geisler N, Wedig T, Zimbelmann R, Aebi U, Burkhard P (2002) Conserved segments 1A and 2B of the intermediate filament dimer: their atomic structures and role in filament assembly. EMBO J 21:1255–1266

17. Strelkov SV, Herrmann H, Aebi U (2003) Molecular architecture of intermediate filaments. Bioessays 25:243–251

18. Wu KC, Bryan JT, Morasso MI, Jang SI, Lee JH, Yang JM, Marekov LN, Parry DA, Steinert PM (2000) Coiled-coil trigger motifs in the 1B and 2B rod domain segments are required for the stability of keratin intermediate filaments. Mol Biol Cell 11:3539–3558

19. Yamada S, Wirtz D, Coulombe PA (2002) Pairwise assembly determines the intrinsic potential for self-organization and mechanical properties of keratin filaments. Mol Biol Cell 13:382–391

20. Bernot KM, Lee CH, Coulombe PA (2005) A small surface hydrophobic stripe in the coiled-coil domain of type I keratins mediates tetramer stability. J Cell Biol 168:965–974

21. Hsiao VC, Tian R, Long H, Der Perng M, Brenner M, Quinlan RA, Goldman JE (2005) Alexander-disease mutation of GFAP causes filament disorganization and decreased solubility of GFAP. J Cell Sci 118:2057–2065

22. Ralton JE, Lu X, Hutcheson AM, Quinlan RA (1994) Identi-

fication of two N-terminal non-alpha-helical domain motifs important in the assembly of glial fibrillary acidic protein. J Cell Sci 107:1935–1948

23. Nicholl ID, Quinlan RA (1994) Chaperone activity of alpha-crystallins modulates intermediate filament assembly. EMBO J 13:945–953

24. Laemmli UK (1970) Cleavage of structural proteins during the assembly of the head of bacteriophage T4. Nature 227:680–685

25. Ding M, Eliasson C, Betsholtz C, Hamberger A, Pekny M (1998) Altered taurine release following hypotonic stress in astrocytes from mice deficient for GFAP and vimentin. Brain Res Mol Brain Res 62:77–81

26. Ward CL, Omura S, Kopito RR (1995) Degradation of CFTR by the ubiquitin-proteasome pathway. Cell 83:121–127

27. Perng MD, Cairns L, van den IJsse P, Prescott A, Hutcheson AM, Quinlan RA (1999) Intermediate filament interactions can be altered by HSP27 and alphaB-crystallin. J Cell Sci 112:2099–2112

28. Sandilands A, Prescott AR, Carter JM, Hutcheson AM, Quinlan RA, Richards J, FitzGerald PG (1995) Vimentin and CP49/filensin form distinct networks in the lens which are independently modulated during lens fibre cell differentiation. J Cell Sci 108:1397–1406

29. Evan GI, Lewis GK, Ramsay G, Bishop JM (1985) Isolation of monoclonal antibodies specific for human c-myc proto-oncogene product. Mol Cell Biol 5:3610–3616

30. Iwaki T, Wisniewski T, Iwaki A, Corbin E, Tomokane N, Tateishi J, Goldman JE (1992) Accumulation of alpha B-crystallin in central nervous system glia and neurons in pathologic conditions. Am J Pathol 140:345–356

31. Reynolds ES (1963) The use of lead citrate at high pH as an electron-opaque stain in electron microscopy. J Cell Biol 17:208–212

32. Pollard TD, Cooper JA (1982) Methods to characterize actin filament networks. Methods Enzymol 85:211–233

33. Hedberg KK, Chen LB (1986) Absence of intermediate filaments in a human adrenal cortex carcinoma-derived cell line. Exp Cell Res 163:509–517

34. Chen WJ, Liem RK (1994) The endless story of the glial fibrillary acidic protein. J Cell Sci 107:2299–2311

35. Schweitzer SC, Klymkowsky MW, Bellin RM, Robson RM, Capetanaki Y, Evans RM (2001) Paranemin and the organization of desmin filament networks. J Cell Sci 114:1079–1089

36. Eliasson C, Sahlgren C, Berthold CH, Stakeberg J, Celis JE, Betsholtz C, Eriksson JE, Pekny M (1999) Intermediate filament protein partnership in astrocytes. J Biol Chem 274:23996–24006

37. Steinert PM, Chou YH, Prahlad V, Parry DA, Marekov LN, Wu KC, Jang SI, Goldman RD (1999) A high molecular weight intermediate filament-associated protein in BHK-21 cells is nestin, a type VI intermediate filament protein: limited co-assembly in vitro to form heteropolymers with type III vimentin and type IV alpha-internexin. J Biol Chem 274:9881–9890

38. Moll R, Franke WW, Schiller DL, Geiger B, Krepler R (1982) The catalog of human cytokeratins: patterns of expression in normal epithelia, tumors and cultured cells. Cell 31:11–24

39. Brenner M, Lampel K, Nakatani Y, Mill J, Banner C, Mearow K, Dohadwala M, Lipsky R, Freese E (1990) Characterization of human cDNA and genomic clones for glial fibrillary acidic protein. Brain Res Mol Brain Res 7:277–286

40. Iwaki T, Iwaki A, Tateishi J, Sakaki Y, Goldman JE (1993) Alpha-b-crystallin and 27-kd heat-shock protein are regulated by stress conditions in the central-nervous-system and accumulate in rosenthal fibers. Am J Path 143:487–495

41. Iwaki A, Iwaki T, Goldman JE, Ogomori K, Tateishi J, Sakaki Y (1992) Accumulation of alpha B-crystallin in brains of patients with Alexander's disease is not due to an abnormality of the 5'-flanking and coding sequence of the genomic DNA. Neurosci Lett 140:89–92

42. Herrmann H, Hesse M, Reichenzeller M, Aebi U, Magin TM (2003) Functional complexity of intermediate filament cytoskeletons: from structure to assembly to gene ablation. Int Rev Cytol 223:83–175

43. Bar H, Mucke N, Kostareva A, Sjoberg G, Aebi U, Herrmann H (2005) Severe muscle disease-causing desmin mutations interfere with in vitro filament assembly at distinct stages. Proc Natl Acad Sci USA 102:15099–15104

44. Chen WJ, Liem RK (1994) Reexpression of glial fibrillary acidic protein rescues the ability of astrocytoma cells to form processes in response to neurons. J Cell Biol 127:813–823

45. McCormick MB, Kouklis P, Syder A, Fuchs E (1993) The roles of the rod end and the tail in vimentin IF assembly and IF network formation. J Cell Biol 122:395–407

46. Kouklis PD, Papamarcaki T, Merdes A, Georgatos SD (1991) A potential role for the COOH-terminal domain in the lateral packing of type III intermediate filaments. J Cell Biol 114:773–786

47. Herrmann H, Haner M, Brettel M, Muller SA, Goldie KN, Fedtke B, Lustig A, Franke WW, Aebi U (1996) Structure and assembly properties of the intermediate filament protein vimentin: the role of its head, rod and tail domains. J Mol Biol 264:933–953

48. Bousquet O, Ma L, Yamada S, Gu C, Idei T, Takahashi K, Wirtz D, Coulombe PA (2001) The nonhelical tail domain of keratin 14 promotes filament bundling and enhances the mechanical properties of keratin intermediate filaments in vitro. J Cell Biol 155:747–754

49. Gu LH, Coulombe PA (2005) Defining the properties of the nonhelical tail domain in type II keratin 5: insight from a bullous disease-causing mutation. Mol Biol Cell 16:1427–1438

50. Yamada S, Wirtz D, Coulombe PA (2003) The mechanical properties of simple epithelial keratins 8 and 18: discriminating between interfacial and bulk elasticities. J Struct Biol 143:45–55

51. Reichard EA, Ball WS Jr, Bove KE (1996) Alexander disease: a case report and review of the literature. Pediatr Pathol Lab Med 16:327–343

52. Lane EB, Rugg EL, Navsaria H, Leigh IM, Heagerty AH, Ishida-Yamamoto A, Eady RA (1992) A mutation in the conserved helix termination peptide of keratin 5 in hereditary skin blistering. Nature 356:244–246

53. Ku NO, Lim JK, Krams SM, Esquivel CO, Keeffe EB, Wright TL, Parry DA, Omary MB (2005) Keratins as susceptibility genes for end-stage liver disease. Gastroenterology 129:885–893

54. Hazan R, Denk H, Franke WW, Lackinger E, Schiller DL (1986) Change of cytokeratin organization during development of Mallory bodies as revealed by a monoclonal antibody. Lab Invest 54:543–553

55. Koyama Y, Goldman JE (1999) Formation of GFAP cytoplasmic inclusions in astrocytes and their disaggregation by alphaB-crystallin. Am J Pathol 154:1563–1572

56. Mairesse N, Horman S, Mosselmans R, Galand P (1996) Antisense inhibition of the 27 kDa heat shock protein production affects growth rate and cytoskeletal organization in MCF-7 cells. Cell Biol Int 20:205–212

57. Brady JP, Garland DL, Green DE, Tamm ER, Giblin FJ, Wawrousek EF (2001) AlphaB-crystallin in lens development and muscle integrity: a gene knockout approach. Invest Ophthalmol Vis Sci 42:2924–2934

58. Benn SC, Perrelet D, Kato AC, Scholz J, Decosterd I, Mannion RJ, Bakowska JC, Woolf CJ (2002) Hsp27 upregulation and phosphorylation is required for injured sensory and motor neuron survival. Neuron 36:45–56

59. Kamradt MC, Chen F, Sam S, Cryns VL (2002) The small heat shock protein alpha B-crystallin negatively regulates apoptosis during myogenic differentiation by inhibiting caspase-3 activation. J Biol Chem 277:38731–38736

60. Paul C, Manero F, Gonin S, Kretz-Remy C, Virot S, Arrigo AP (2002) Hsp27 as a negative regulator of cytochrome C release. Mol Cell Biol 22:816–834

61. Parcellier A, Schmitt E, Gurbuxani S, Seigneurin-Berny D, Pance A, Chantome A, Plenchette S, Khochbin S, Solary E, Garrido C (2003) HSP27 is a ubiquitin-binding protein involved in I-kappaBalpha proteasomal degradation. Mol Cell Biol 23:5790–5802

62. Wyttenbach A, Sauvageot O, Carmichael J, Diaz-Latoud C, Arrigo AP, Rubinsztein DC (2002) Heat shock protein 27 prevents cellular polyglutamine toxicity and suppresses the increase of reactive oxygen species caused by huntingtin. Hum Mol Genet 11:1137–1151

63. Zourlidou A, Payne Smith MD, Latchman DS (2004) HSP27 but not HSP70 has a potent protective effect against alpha-synuclein-induced cell death in mammalian neuronal cells. J Neurochem 88:1439–1448

64. Mann E, McDermott MJ, Goldman J, Chiesa R, Spector A (1991) Phosphorylation of alpha-crystallin B in Alexander's disease brain. FEBS Lett 294:133–136